University of Nottingham

School of Chemical, Environmental and Mining Engineering

Separation and Control of Gas-Liquid Flows at Horizontal T-junctions

by

Glen Baker M.Eng.

Thesis submitted to The University of Nottingham for the degree of Doctor of Philosophy

March 2003

Abstract

The separation of gas-liquid flows is an integral part of many industrial processes. Traditionally, such separations are performed in large vessels under the effect of gravity. However, such vessels can contain inherently large inventories of potentially flammable and/or toxic material. The main objective of this thesis is to combine the knowledge of partial phase separation at T-junctions with control strategies to enhance the development of continuous compact partial phase separators. Such applications would form an integral part of more intensive phase separation systems that allow for smaller downstream separator vessels. This would be especially beneficial to the petroleum industry where safety, space, weight and cost are all issues related to off-shore oil platforms. For such applications a simple definition for a partial phase separator would be one that produced two streams, one rich in gas and the other rich in liquid, each containing less than 10% v/v of the unwanted phase.

A series of optimisation experiments produced the final T-junction configuration. This comprised of two horizontal T-junctions placed in series, the first with a vertically upwards side-arm, the second with a vertically downwards one. The addition of control valves on the exit streams of the T-junctions extended previous fundamental studies, incorporating the concept of control and flexibility. An automatic liquid level control on the down leg provided a physical barrier against gas entrainment by maintaining a constant liquid presence within that pipe. A further control valve beyond the second junction then optimised the liquid hold-up above this down leg. Experiments showed that the run valve setting was only dependent on the approaching flow regime and independent of the inlet phase flowrates.

A simple active control strategy was developed based around these control valves such that for stratified flows the run arm control valve was set at 20% open, while for slug flows the valve was required to be 55% open. Under this control scheme it was possible to obtain a liquid only stream and a gas-rich stream which always satisfied the simple separation criterion of less than 10% v/v liquid-in-gas.

Within industrial situations it is rare to operate under steady-state flow conditions continuously and there will be at least one time dependent variable. Examples of general transient situations involve plant shutdown and start-up, changes in flowrates in response to planned operating conditions and emergency situations. Even more relevant to the petroleum industry however, is bringing an additional well on line. Within the petroleum industry the problem of multiphase transient flows has lead to the development of many commercially available prediction packages but none that handle branched pipe networks. A series of experiments were performed to compare the outlet phase mass flowrate responses for a straight pipe and the T-junction separator. The results indicate that in general the T-junction responses are analogous to those observed in a pipe. However, the existence of pipe branches adds another level of complexity as the flow splits exhibit a very non-linear nature.

Acknowledgments

I would first like to express my gratitude to my supervisors Prof. B. J. Azzopardi and Dr J. A. Wilson. Their insight and enthusiasm proved invaluable in the pursuit of new ideas and in the preparation of this thesis.

My appreciation also goes to the technical staff in the School Workshop, without their expertise and experience my conceptual ideas could never have been transformed into successful working realities.

I also gratefully acknowledge the EPSRC for the financial support that allowed me to undertake the research as well as UMIST and the IPSO consortium.

Huge thanks also go to my colleagues, both past and present, for making my postgraduate experience something I'll always want to remember. I make special mention of Wayne, who has been an invaluable help throughout, and Liz, for her counsel and companionship. I am privileged to be able to call them both *my friends*.

I also thank my church family, especially Steve and Stuart for their encouragement and understanding and William for his simple, but effective, help and advice.

Finally, I reserve the biggest thank you for my family who have supported me throughout this adventure, especially my wife, Clare, and two daughters, Koren and Lois. They have demonstrated immense patience, enduring through to the completion of this work, and continue to be an unending source of love and support.

God Bless

To Mum and Dad,

With love

I have fought well. I have finished the race, and I have been faithful

- 2 Timothy 4:7 (CEV)

Contents

List of Figures

List of Tables

Nomenclature

A	cross-sectional area of pipe	m^2
c	characteristic speed of an electromagnetic wave	m/s
C	capacitance	F
D	diameter of pipe	m
e_{rrf}	maximum error in calculated slug frequency	-
f	frequency	Hz
f_{max}	maximum calculate slug frequency	Hz
f_{min}	minimum calculated slug frequency	Hz
g	acceleration due to gravity	m/s^2
$F1$	total feed flowrate	kg/s
G'	fraction of inlet gas taken-off into side-arm	-
L'	fraction of inlet liquid taken-off into side arm	-
L'_{max}	maximum fraction of inlet liquid taken-off	-
M	total mass flux	kg/m^2 s
MG	mass flux of gas	kg/m^2 s
N	number of slugs	-
$\overline{N}$	average number of slugs	-
P	pressure	bar
Q	charge on electrode	C
r	radius	m
R	resistance	Ω
S_{eff}	Separation Effectiveness as defined in Equation 6.3	-
S_F	Separation Factor as defined in Equation 4.1	-
t	time	s
U_{gs}	gas superficial velocity	m/s
U_{ls}	liquid superficial velocity	m/s

$U_{ls,\,gas}$	liquid superficial velocity in gas-rich stream	m/s
V	control valve setting	(% open)
V_c	potential difference	V
V_{opt}	calculated optimum control valve setting	(% open)
WG	mass flow of gas	kg/s
WL	mass flow of liquid	kg/s
WL_{exit}	exit liquid mass flow	kg/s
WL^*	liquid mass flow perturbation	kg/s
$\overline{WL}_1$	mean steady-state inlet liquid mass flow	kg/s
x	stream quality	-
Xv	valve fraction open (simulation model)	-

Greek symbols

e	permittivity	F/m
l	wavelength	m
m	viscosity	kg/m s
r	density	kg/m^3
s	surface tension	N/m

Subscripts

G	gas
i	electrode
j	electrode
L	liquid
1	inlet stream
2	run arm, or connection stream for combined T-junction system
3	side-arm, or up arm for combined T-junction system
4	run arm for combined T-junction system
5	down arm for combined T-junction system

CHAPTER 1

Introduction

Throughout a wide range of industrial processes where gas-liquid flows occur there is an almost inevitable requirement to separate the different phases. Such separations are desirable to reduce the problems associated with handling two-phase mixtures, with the single phase streams produced being both safer and easier to transport. Current practice is to carry out such separations in large vessels, using gravity as the major means of separation. Such designs are based on providing sufficient residence time for the phases to separate and also giving adequate volume to contain the fluctuating liquid level caused by surges in the feed flowrates. Although such gravity separators are reliable and very efficient, they are large pieces of equipment, with the associated problems of weight and high capital and operating costs. Furthermore, they inherently contain a very large inventory of toxic and/or flammable material.

The problems of gravity separators are enhanced further when they are considered for off-shore oil platform applications, where space is limited and weight must be minimised. The presence of a large inventory of highly flammable materials is in direct conflict with the recommendations of the Cullen Report (1990), published following the inquiry into the Piper Alpha disaster. As the cost of off-shore drilling increases, due to the need to exploit smaller less accessible oil fields coupled with ever tightening safety regulations, the petroleum industry needs to explore alternative phase separation technologies. Research has indicated that a possible alternative may be provided by a simple pipe junction. It is known that when a gas-liquid stream

encounters a pipe T-junction it has the potential to undergo a partial phase separation. Thus, two different phase-rich streams are produced, one rich in gas the other rich in liquid. One of the main advantages of a junction is its size relative to a normal gravity separator. The small footprint enables it to be installed where space is at a premium, for instance on off-shore oil platforms. There is even the possibility of sub-sea deployment, since it would have a virtually zero maintenance requirement. Such a system would then feed the gas-rich and liquid-rich streams to a more conventional separator, designed for the reduced loading. This smaller separator would require less space, reducing the construction and installation costs.

Although this may sound like a very attractive concept, there are potential drawbacks that require consideration. Gravity separators may be large pieces of equipment but they have the capacity and the control system to handle sudden changes in the feed flowrates without compromising the separation performance. Transient flows are a common occurrence within most industrial processes, occurring during plant start-up and shutdown, or in the case of the petroleum industry, in response to a new oil well being brought online.

To make optimum use of a T-junction as a partial phase separator several key inter-related factors need to be considered. These inter-relationships are illustrated in Figure 1.1. The study of the flow split at T-junctions has been the focus of much research effort over the last twenty years. Although, the initial driving force behind the research was in the attempt to understand how to minimise the phase redistribution problem, it soon became apparent that this same phenomenon could be utilised in a positive way for partial phase separation. Nevertheless, there are still large gaps within the knowledge base. Since a T-junction can be considered to be essentially a branched pipe network, an understanding of transient flows through pipes will lead to a better appreciation of the behaviour of similar transient flows through a T-junction. Finally, by placing some method of control on the gas-liquid flow through the junction it should be possible to add flexibility to the system. Thus, the separation performance could be optimised over a much wider range of inlet flow conditions.

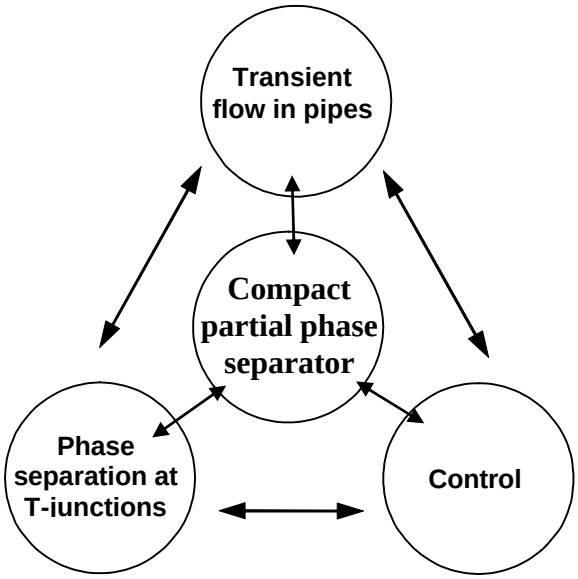

Figure 1.1: Inter-relationships that need consideration in the design of a compact partial phase separator

1.1 What are Multiphase Flows?

Before being able to discuss the potential applications of T-junctions as partial phase separators it is useful to give a brief introduction to the subject of multiphase flow. A good understanding of any gas-liquid system is crucial for the design of plant equipment and as been the subject of much research over many years. One key issue is the understanding and prediction of the two-phase flow regime present within given pipeline. Whereas such flows can occur within any pipe orientations the emphasis of this work is on horizontal co-current flows.

Throughout the chemical, power generation and hydrocarbon production industries there will be various flows that can be termed as *multiphase.* Such flows consist of at least two different, or immiscible, phases, solid, liquid or gas, flowing simultaneously inside of the same pipe. These flows can occur in a variety of situations. A common occurrence is vapour-liquid flows in condensers and reboilers, while pneumatic conveyance systems deal with gas-solid systems. Within the oil industry, multiphase

flows are associated with oil wells, where there is the potential to deal with the one of the most complex flows, a four-phase system of gas-oil-water and sand.

With so many variations the study of multiphase flows is a complex science. However, the industrial requirement to handle and process such flows has made multiphase flow a key area of research. This concentrated activity has produced a myriad of equations and correlations all attempting to adequately predict the dynamic behaviour of multiphase flow. The area of gas-liquid flow has probably received the most interest, attributed to its wide occurrence within industry and the unique complex issues related to such flows.

1.1.1 Gas-Liquid Flow in Horizontal Pipes

An important factor in the processing of two-phase gas-liquid flows is an understanding of how such flows behave within a pipe. Whenever a gas-liquid stream flows co-currently in a pipe, the two-phase mixture can adopt a number of different flow configurations related to the interface between the phases. The exact nature of this two-phase stream depends on the relative ratios and velocities of the gas and liquid present as well as the orientation of the pipe itself. A good understanding of these various flow regimes is crucial as they will have a large impact not only on the hydrodynamics of the flow but also on the momentum, heat and mass transfer of the system.

Over the years there have been many different definitions suggested for the various flow pattern observed. Recently however there has been some consolidation on such descriptions and there is now a general acceptance of standard definitions.

In the case of horizontal co-current gas-liquid flows gravity acts perpendicular to the direction of motion. Since gravity will have a much larger effect on the denser liquid phase, there will generally be a distinct gas-liquid boundary. The four major flow patterns that can be excepted are illustrated in Figure 1.2 and described below.

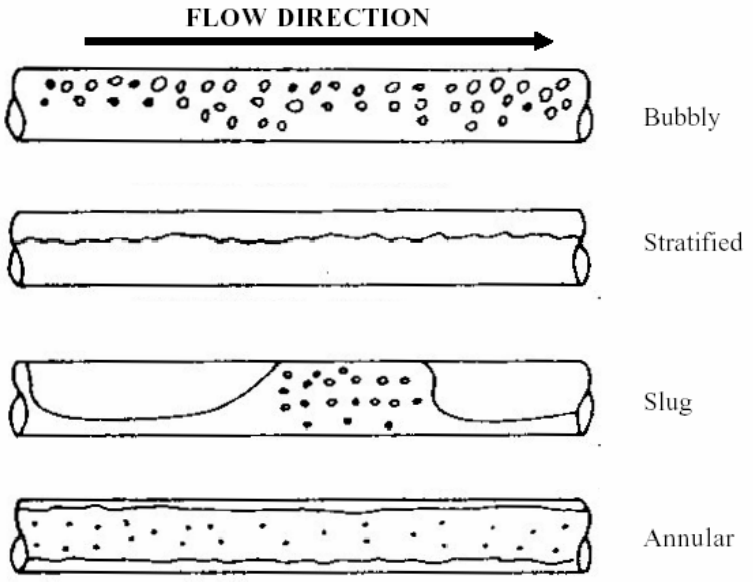

Figure 1.2: The major flow patterns observed in horizontal gas-liquid flow

Bubbly: Here non-uniformed size gas bubbles are distributed within a liquid continuum. These bubbles travel with a complex motion, and they are seen to coalesce and break-up as they travel along the pipe. Gravity will tend to make the gas bubbles accumulate at the top of the pipe, except at very high liquid velocities when turbulence disperses the bubbles about the entire pipe cross-section.

Stratified: In this flow regime there is a continuous liquid layer flowing along the lower section of the pipe, with the gas flow flowing above it. At low gas superficial velocities the interface between the phases will be smooth, but as the gas superficial velocity increases waves are seen to form, producing stratified-wavy flows.

Slug: As the liquid superficial is increased the waves present in the stratified-wavy regime become large enough to fill the pipe-cross section. Eventually, this leads to the intermittent flow pattern termed slug flow,

where the gas phase will travel in large pockets at the top of the pipe between fast moving liquid slugs, which may contain smaller gas bubbles. As the liquid slug travels along the pipe, new liquid is added at the front while old liquid is ejected at the rear.

Annular: At very high gas velocities some of the liquid is forced around the wall of the pipe while the rest travels as entrained droplets within the faster moving central gas core. Again, gravity will tend to force liquid to the bottom of the pipe making the liquid film thicker however, as the gas velocity is further increased the film becomes more uniform around the circumference. There is a constant exchange of liquid between the film and the core.

1.2 Introducing the T-junction

The *simple* T-junction can be considered to consist of one pipe branching off at right angles to another. While it is these types of junctions that are of interest to this work it should be noted that there are more complex geometries where, for example, the branch arms are not set at right-angles, classed as Y-junctions. In single phase flow there is sufficient knowledge and understanding to allow engineers to adequately predict the flow split and thus design efficient downstream networks. However, in the case of two-phase flows the number of variables increases and the problem becomes much more complex. Many studies have been carried out in an attempt to understand and ultimately predict the flow phenomena involved.

1.2.1 T-junction Parameters

The geometrical parameters of a T-junction can affect the flow split as well as the physical properties of the fluids flowing in the pipe. Figure 1.3 shows the many variables that must be considered when trying to predict the phase split at a junction.

To fully describe the geometry of a junction it is necessary to define all three pipe diameters and their associated angles. Although there are, in theory, three such diameters, the inlet, D_1, run arm, D_2, and side-arm or branch, D_3, in reality it is expected that at least two of these, usually the inlet and run, will be the same. For the case where all the diameters are equal, as for this current work, the junction is said to be *regular*. There are then three corresponding angles to consider – the angle of the main pipe from the horizontal, q; (where q equals 0° for a horizontal inlet); the angle of the side-arm from the main pipe, b, (when b equals 90° the junction is classed as a T); and the orientation of the side-arm, f, which can take any angle between -90°, for a vertically downwards side-arm, and +90°, for a vertically upwards one. A T-junction is termed *fully horizontal* if both the inlet and side-arm are positioned in the horizontal plane.

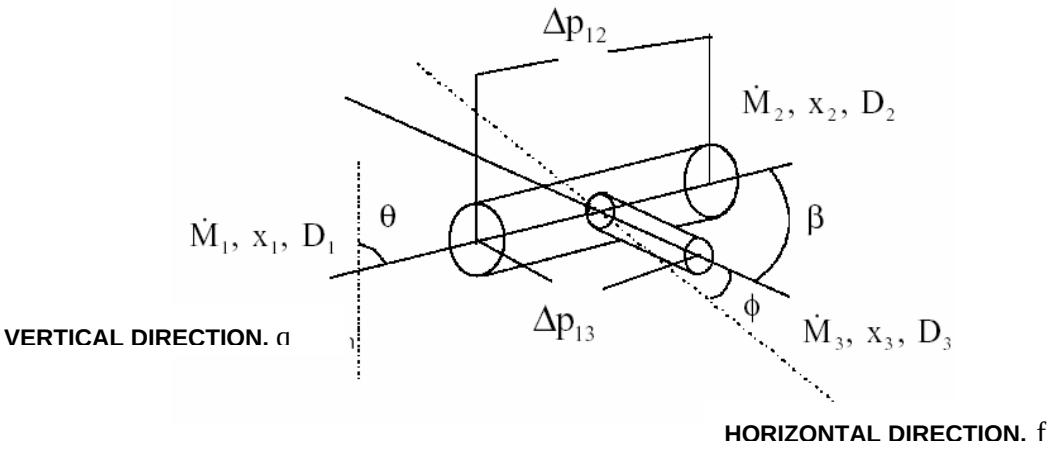

Figure 1.3: Parameters involved in the T-junction problem

There will then be eight more variables required to fully define the two-phase flow in a T-junction. These are the mass fluxes in each arm, $\dot{M}_1$, $\dot{M}_2$ and $\dot{M}_3$, the quality of these streams, x_1, x_2 and x_3, and the associated pressure drops, DP_{12} and DP_{13}. The suffixes 1, 2 and 3 indicate the inlet, run and branch arm, respectively.

For a given system, three of these above variables will be known leaving five unknown parameters requiring five equations to be solved. Mass balances over the system on either phase provide two of these equations, with energy, or momentum, balances for the branch and run arms providing two more. The remaining equation is then provided by the locus of the phase split at the junction. It is the requirement to adequately predict this relationship that has been the driving force behind much of the previous research in this field.

To begin to do this it is necessary to have an understanding of the dominant forces that will affect the phase split at a horizontal T-junction. These are considered to be:

Gravity: Gravitational acceleration will act predominantly on the liquid phase. This will tend to either encourage liquid displacement down the side-arm if it is orientated downwards, or help minimise the liquid taken off when the side-arm is angled upwards.

Inertia: The liquid phase will travel along the pipe with a much higher axial momentum than the gas due to its relatively higher mass. This will have the effect of forcing the liquid to continue along the pipe, bypassing the entrance to the side-arm. If the side-arm has a reduced diameter then this effect is even more pronounced since the liquid will have even less time to be influenced by gravity.

Pressure: Pressure drop measurements around a T-junction generally show a loss between the inlet and side-arm and a recovery into the run. This recovery is attributed to an affect similar to that of Bernoulli for single-phase flows, produced as a result of the decrease in the mixture velocity in the run. Figure 1.4 shows a typical pressure profile for a junction.

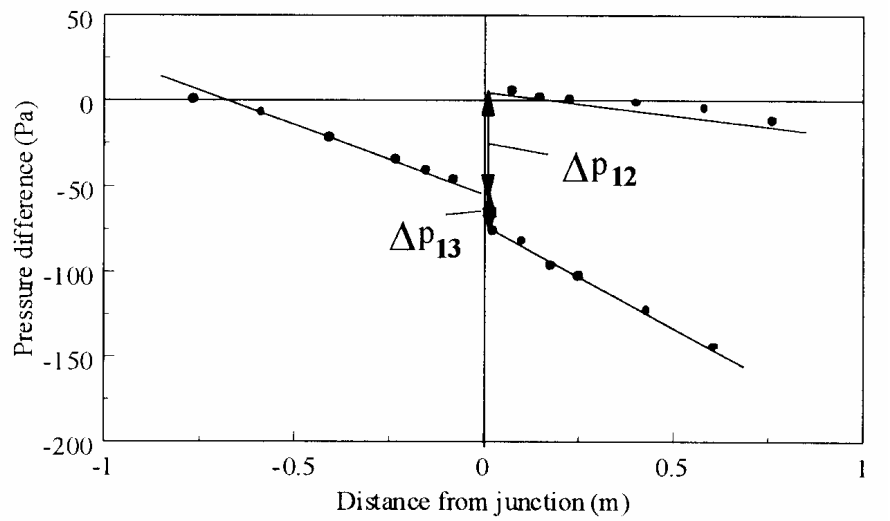

Figure 1.4: Pressure drop profiles across a junction

1.2.2 Representing Phase Split Data

As mentioned above, the locus of the phase split at the T-junction must be known in order to close the prediction problem. Traditionally this has been obtained through experimental methods and although various attempts at mathematical and empirical solutions have been suggested, experimental verification is still generally required.

A number of approaches have been suggested to illustrate the flow split data but they can all be considered to be variations of each other. One of the most useful methods of representing the phase split data is a plot of the fraction of the inlet liquid diverted into the branch arm, *L'*, against the fraction of the inlet gas diverted into the same branch, *G'*. Figure 1.5 illustrates this type of diagram, which allows quick identification of the zones of liquid or gas dominated flow split.

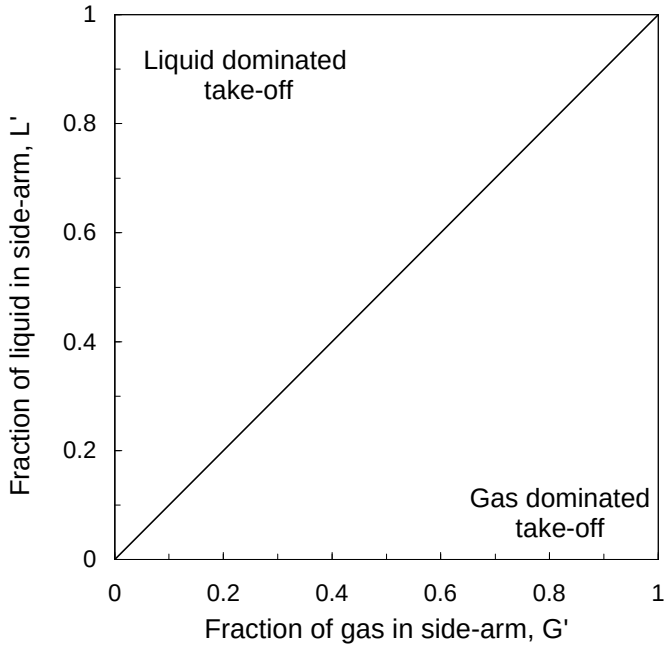

Figure 1.5: Graphical representation of phase split at a T-junction

The diagonal line, $y = x$, represents the line of equal flow split between the two exit streams. Above this line the take-off into the side-arm would be liquid dominated, while below this line the separation is gas dominated. Gas only extraction is represented by data lying on the x-axis, $L' = 0$, and similarly for liquid only extraction, the data would lie on the y-axis, $G' = 0$. Conversely complete gas and liquid removal into the branch is represented by the straight lines $G' = 1$ and $L' = 1$, respectively.

1.3 Thesis Objectives and Structure

Having highlighted the requirement to separate gas-liquid flows as well as the complex problem of two-phase flow and T-junctions, it is important to quantify the aims and objectives of the work. It is the drive to reduce costs, while still maintaining a high degree of separation efficiency, plus the added benefit of increasing operational safety that is the driving force behind this research.

Since this thesis is primarily concerned with the application of T-junctions as partial phase separators for gas-liquid flow it is useful to identify separation criteria to assess the performance of the system. In terms of partial phase separation, one possible criterion would be to define the separation in terms of the volumetric content of each of the exit streams. For the present work the proposed boundary limit on the unwanted phase volumetric content within one phase-rich stream is set at 10% v/v. Thus, after the T-junction separator, the two resultant streams must contain less than 10% v/v gas-in-liquid and less than 10% v/v liquid-in-gas. The lower this volumetric contamination is, the smaller the downstream secondary separator would have to be, and so there is the desire to reduce this volume ratio to be as small as possible.

1.3.1 Aims and Objectives

The aims and objectives that will be met by the work contained in this thesis are:

1. Apply knowledge of the flow split of gas-liquid flows at T-junctions to the development of a novel partial phase separator. This will be based on a unique combination of T-junctions, control valves and a method for identification of the flow pattern within a pipe.

2 To aid the development of a T-junction separator a feasibility study will be performed using a steady-state simulation of a T-junction based on existing flow split models. This will allow comparisons to be made between different phase split models and provide some indication of the potential for phase separation control at T-junctions.

3. The proposed T-junction separator will be evaluated, with respect to the separation criteria of less than 10% v/v gas-in-liquid and liquid-in-gas, over a wide range of steady-state gas and liquid flow conditions, spanning the stratified and slug flow regimes. This separation data will then be used to devise a control strategy based on the optimisation of the flow split over the widest range of flow conditions.

4. Very few studies have examined how transient flows behave at a T-junction. By applying step changes to both the gas and liquid inlet superficial velocities, the response of the T-junctions to such transient flows will be investigated. This will increase the knowledge and understanding of how transients behave at a T-junction.

5. To aid in the assessment of the separation performance new ways of representing and comparing the phase separation will be considered.

1.3.2 Thesis Structure

Having given a brief introduction to the subject of gas-liquid flow, the problem of its separation and the T-junction, the structure of the thesis required to fulfil the stated objectives is outlined here.

A critical review of the most relevant and important published material is presented in Chapter 2. This will include a review not only of T-junctions but also the subjects of flow pattern identification within a pipe and of transient behaviour of gas-liquid flows. Chapter 3 provides an overview of the experimental arrangements used in this study, including a detailed description of individual components of the flow facility, the properties of the fluids involved, operating procedures and a review of safety considerations. Preliminary studies based on simulated feasibility studies of a T-junction in combination with control valves are presented in Chapter 4. Chapter 5 will present the results from preliminary experimental investigations, and highlight the potential configuration for an effective T-junction separator. Steady-state phase separation results for the final T-junction separator design are presented in Chapter 6, along with an evaluation of the separation performance. Chapter 7 gives a comparison of transient experimental results for gas-liquid flows both through a straight pipe and the T-junctions. Finally, Chapter 8 summarises the findings of the research with conclusions and highlights possible areas for future work.

CHAPTER 2

Literature Survey

There are three main areas of discussion within the context of the work presented in this thesis. Since there is such a wealth and diversity of literature available on two-phase gas and liquid flows in pipes, throughout this literature survey only the most significant research work will be cited but where appropriate the reader will be directed to more rigorous discussion texts. Section 2.1 will introduce two-phase flow pattern maps and compare the alternative methods available for flow pattern identification within a pipe. This will concentrate on the potential applicability of these methods within active control schemes. The fundamental ideas behind the use of T-junctions as partial phase separators for gas-liquid flows will be addressed in Section 2.2. Here different pipe configurations and modifications will be examined. Such arrangements have been applied to the simple T-junction in an attempt to try and enhance or control the phase separation as much as possible. Within the petroleum industry the flow of gas-oil pipelines will undoubtedly involve transient flows, for example as a new well head is brought online. In view of this, Section 2.3 will discuss transient gas-liquid flows in pipes and through T-junctions.

2.1 Flow Pattern Identification

Knowledge, and possible identification, of the flow regime of an approaching gas-liquid mixture is crucial in the operation of many pieces of plant equipment. Experimental detection of flow patterns and transition boundaries has to be based on

the prerequisite knowledge of expectant flow patterns. Industrially, there is a requirement not just to understand the possible flow patterns but to also predict which flow regime exists within a given pipeline. Two-phase gas-liquid flows will assume various configurations as it travels along a horizontal pipe, as outlined in Chapter 1 of this thesis, all of which will have different characteristics. For example, because of the intermittent nature of slug flow vibration damage to equipment can be a problem, as it is continuously hit by a fast moving liquid slug followed by a gas pocket. For this reason such a flow regime is best avoided. However, the nature of bubbly flow gives it a very large mass transfer area that could be beneficial in certain situations.

To help to quantify the different flow regimes that may be expected within a pipe, the concept of using flow pattern maps was developed. The subject of flow pattern determination can be very subjective, especially when visual observations are used alone. Although with the use of high-speed video photography, in the right environment, visual inspections may be appropriate. In more industrial situations, where the pipelines will probably not be transparent, more instrumental-based techniques are required. Barnea and Taitel (1985) outline several possible methods for measuring void fractions or pressure fluctuations in two-phase flows.

Ultimately, of course, being able to detect the flow patterns within a pipe network is of little importance during the design stage of a process plant. Here prior knowledge of the expected flow patterns would be a useful tool. To address this issue the notion of using two-dimensional plots to display transition boundaries was developed. There are two basic types of coordinates used for mapping; one uses dimensional axes (e.g. superficial velocities, mass flow rates) while the other utilises dimensionless groups (e.g. Froude number, Reynolds number, gas-liquid mass ratios). These so called flow pattern maps are certainly useful tools but the inherent subjectivity in the description of flow patterns coupled with the relatively limited amount of experimental data makes them far from perfect. Nevertheless, industry accepts them as the only real method of trying to predict the gas-liquid flow regime within a pipeline.

Over many years there have been many different horizontal flow pattern maps suggested for various flow conditions. One of the earliest maps was created by Baker (1954). Being simple to use and based on industrially relevant data, it is still popular within the petroleum industry. However, later work has shown that some of the transition boundaries, which were determined only by visual observations, are poor. Noticing that the superficial velocities of the gas and liquid phases are the major influence on the flow pattern Mandhane *et al.* (1974) mapped a significant data base from various sources on to a coordinate system of superficial gas velocity and superficial liquid velocity, locating the transition lines. Later,Weisman *et al.* (1979) adapted that idea but included property correction factors for both axes as they mapped transition boundaries derived from correlated data. An unusual approach was followed by Spedding and Nguyen (1980), who produced maps based on four basic flow regimes types that do not conform to the standard method of flow pattern identification. They defined X type flow regimes, where both phases are continuous (stratified and annular);B type, in which the liquid phase is continuous (slug and bubbly); D type, where the gas phase is continuous with the liquid phase distributed as droplets; and finally M type flows, where both the phases are discontinuous. They then presented the transitions in terms of two dimensionless groups, a modified Froude number and the ratio of gas and liquid superficial velocities. The strange choice of flow identifiers makes this particular flow pattern map difficult to understand within the context of other two-phase flow work.

Although empirical based correlations are still being used, more effort has been focused on the development of theoretical approaches to flow pattern predictions. Taitel and Dukler (1976) produced a flow map based on the mechanisms of flow regime transitions. The analysis looked at the conditions for transition between five basic flow regimes; stratified smooth, stratified wavy, intermittent, annular and bubbly. All the analysis starts with stratified smooth flow as the initial flow pattern and examines the mechanisms by which a change from that regime could occur and the final flow pattern that would be expected. Although, stratified flow may not initially exist within the pipe they assumed that the final steady-state flow pattern

observed for set values of gas and liquid superficial velocities was independent of the path used to arrive at that condition.

Comparisons of the theoretical boundaries lines proposed by the method of Taitel and Dukler (1976) and those suggested by more empirical based flow pattern maps show very good agreement. Figure 2.1 shows a typical flow pattern map produced using the methodology of Taitel and Dukler (1976). The only criticism that could be noted is the distinction used to predict the transition between annular and slug flows. This is based solely on the liquid level in the pipe; if the pipe is less than half-full than it was assumed that annular flow would occur, else slug flow could be expected. Nevertheless, this methodical approach allows various flow pattern maps to be produced for a wide range of flow conditions and fluids.

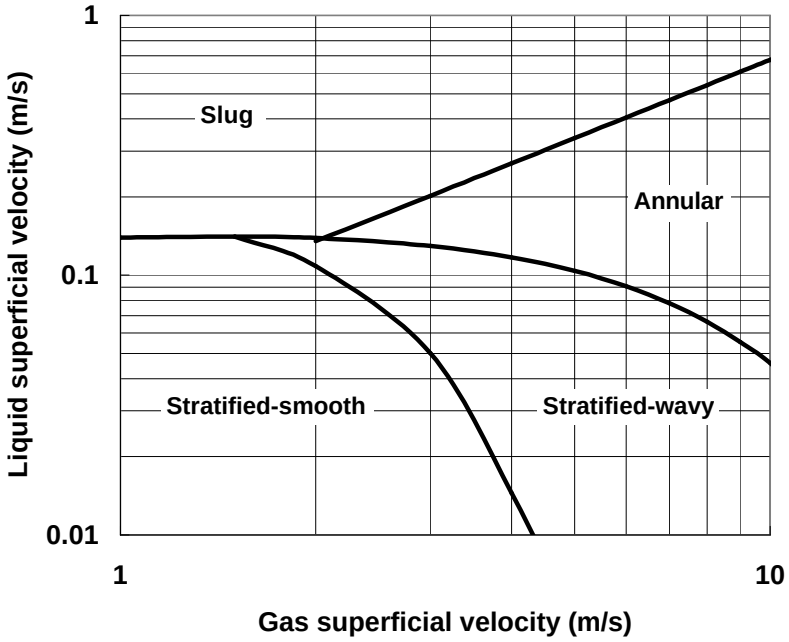

Figure 2.1: Typical horizontal flow pattern map based on methodology of Taitel and Dukler (1976)

The nature of two-phase flow, which can quite often be fast and chaotic, can lead to misinterpretation of the experimental data. In addition to this, the transition between defined flow patterns is a gradual process, making it impossible to define a sharp boundary. With such a difficult problem it is not surprising that there has been much research carried out on the subject of flow pattern detection within pipelines. The following Section aims not to provide a thorough review of every available flow detection method but will serve to highlight specific examples which demonstrate the suitability of each application as well as any potential limitations.

2.1.1 Visual Observations and Optical Techniques

The simplest method for the determination of gas-liquid flow patterns is to merely observe them flowing along transparent pipes. Where this is not feasible because of high gas and liquid flowrates, high speed photography is employed, such as that performed by, among others, Hewitt and Roberts (1969). Obviously such methods are of no use within a control system because industrial pipelines are generally not transparent and interpretation of visually obtained information, by image analysis techniques, within a computer control strategy is cumbersome. Nevertheless, such methods are relevant because they are the only practical method of verifying other instrument based techniques.

Persen (1984) developed an optical method, based on a light signal being affected by the gas-liquid interface conditions within the active space of a light sensor. The system he devised consisted of a light source and a light receiver positioned directly opposite the light beam. The resultant voltage signal generated was then a function of the intensity of the received light. Persen states that the variation in the light intensity, and hence the voltage signal, at the receiver is caused mainly by the scattering effects of the interface. These interfaces can be the surfaces of gas bubbles in the liquid or of liquid droplets in the gas. Observations of time traces of the voltage signal indicated that this technique did have the potential for flow pattern determination. However, as with all optical techniques they are limited to applications where there are at least some transparent sections in the pipes.

2.1.2 Photon Attenuation Technique

The photon attenuation technique has been widely applied and is based on the absorption of x-rays or γ-rays by the liquid phase and its relationship to the void fraction. The rays can either come along a single beam as used by Jones and Zuber (1975) or from an array of multiple beams across the flow path, as employed by Smith (1975). It was the significant work of Jones and Zuber (1975), using x-ray absorption, which highlighted the usefulness of statistical analysis techniques for flow pattern determination. Typical probability density functions of the void fraction variations they used to identify flow patterns are shown in Figure 2.2. Such probability density function techniques became the main tool in assessing various other measurable parameters for flow pattern determination.

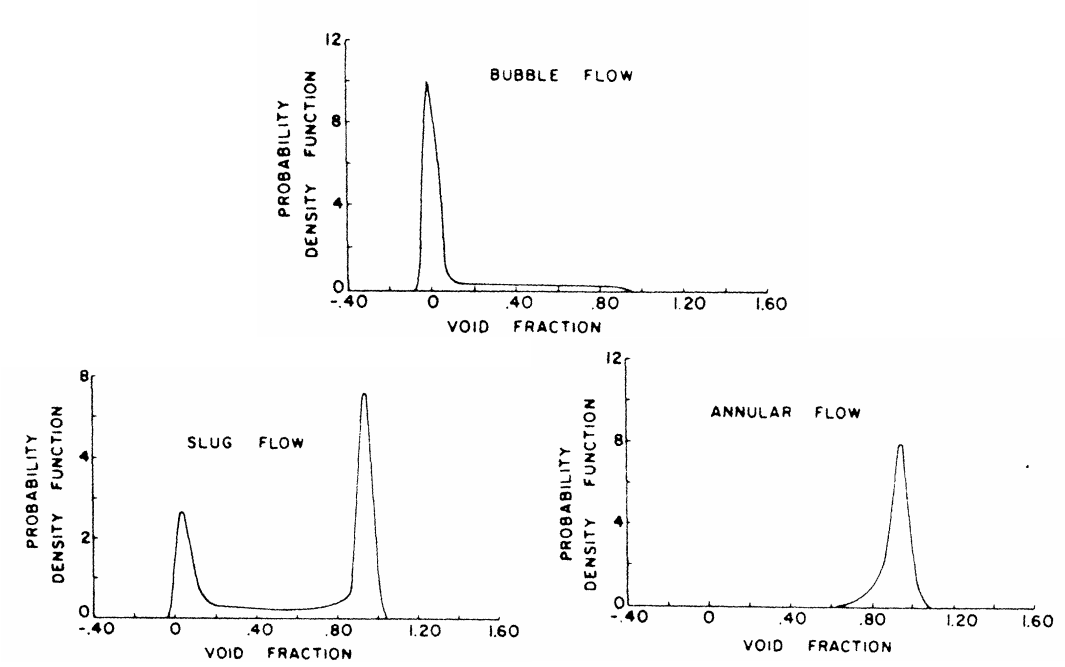

Figure 2.2: X-ray absorption probability density functions of void fractions by Jones and Zuber (1975)

2.1.3 Pressure Fluctuations

Hubbard and Dukler (1966) were the first researchers who analysed pressure fluctuations in an attempt to try and identify flow patterns. Using experimental data from a horizontal air-water flow facility they developed a method to determine the flow pattern from the spectral distribution of the wall pressure fluctuations. Figure 2.3 shows the three basic spectral distributions they observed.

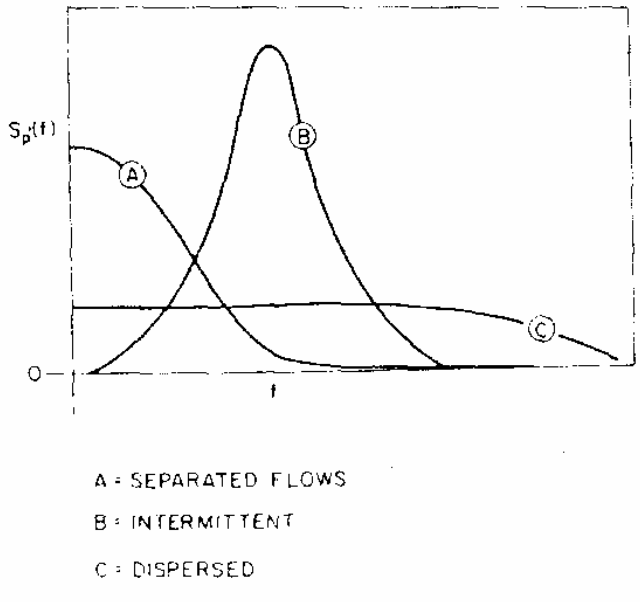

Figure 2.3: Power spectral density of wall pressure fluctuation from Hubbard and Dukler (1966)

Type *A* distributions, which are characteristic of turbulent flows with a maximum zero frequency, correspond to stratified and low entrainment annular flows, termed separated flows. Type *B* spectrum corresponds to intermittent flows, showing features typical of a periodic process. Finally, Type *C* distributions relate to bubbly or mist flows, with a spectral characteristic of white noise. It can be noted that more complex flow patterns can be considered to be superimposition of two basic patterns. Observations then showed that the corresponding spectra of these complex flows were

formed by the superimposition of the basic spectra. However, the authors could not use their method to discriminate between stratified and annular flows or dispersed liquid or dispersed gas flows.

A simple criterion for the determination of the flow pattern based on the pressure drop between two pressure taps 0.15 m apart was developed by Weisman *et al.* (1979). Here the criteria were primarily based on the ratio of amplitude of the pressure trace to the amplitude of a "standard slug". It is unclear whether the same frequency ratios that they suggest could be applied for systems with different diameter pipes and pressures.

More recently, Cai *et al.* (1996) have attempted to apply chaos theory to time traces of pressure fluctuation signals, with the aim of identifying flow pattern transitions. The conclusions of the authors were that although the software and algorithms required intensive development before they could be used practically, the random-like pressure fluctuations did have potential for flow pattern identification.

2.1.4 Conductance Probes

The next level of complexity for determining flow patterns is by measuring the conductance or the complimentary parameter, resistance, of the mixture. There are two distinct methods used for conductance probe measurements, either insertion into the flow or flush-mounted around the pipe wall. In all cases the current from the probes is measured and the generated time trace is then used to represent the distribution of the phases and therefore the flow pattern. Barnea and Taitel (1985) point out that such techniques were not necessarily applicable to all flow patterns but note that an improved conductance probe method by Barnea *et al.* (1980) did produce satisfactory characteristic profiles for all flow patterns.

The design of Barnea *et al.* (1980), which is applicable for vertical, horizontal and slightly inclined pipes, is shown in Figure 2.4. It is a combination of both inserted probes, labelled *A*, *B*, and *C*, and flush-mounted probes, *D* and *E*.

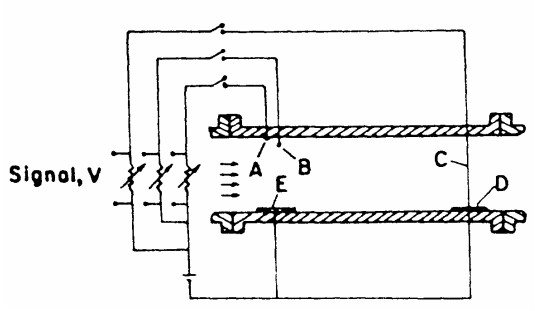

Figure 2.4: Electrode configuration for conductance method of Barnea *et al.* (1980)

Probe *A* is flat with the upper part of the wall and is designed to detect surface wetness around the pipes inner circumference. Probe *B* is designed to detect small bubbles at the top of the pipe. Probe *C* is designed to detect the liquid level under stratified conditions. For vertical flow, the symmetry of the system means that only two probes are required, *A*, which is used to detect wetness on the walls, and *B*, which is extended into the centre of the pipe to detect bubbles. For horizontal flows the various different flow regimes were then detected by examining the signals from all five probes.

Figure 2.5 gives typical timer traces for the conductance probes in a horizontal air-water flow for various flow regimes. Stratified flows would be detected by zero voltage outputs from probes *A* and *B*, while probe *C* allowed a distinction between stratified smooth and stratified wavy flows. Annular flow was detected by a voltage output from probe *A* but not from *B*. Intermittent or dispersed bubble flows were detected by a voltage output from both probes *A* and *B*, with the exact pattern detected by *B*. Dispersed bubble flow was characterised by high frequency uniform pulses. Intermittent flows are displayed as long, intermittent rectangular pulses, separated by zero voltage. The distinction between elongated bubble and slug flow is made by the detection of bubbles within the liquid slug zone.

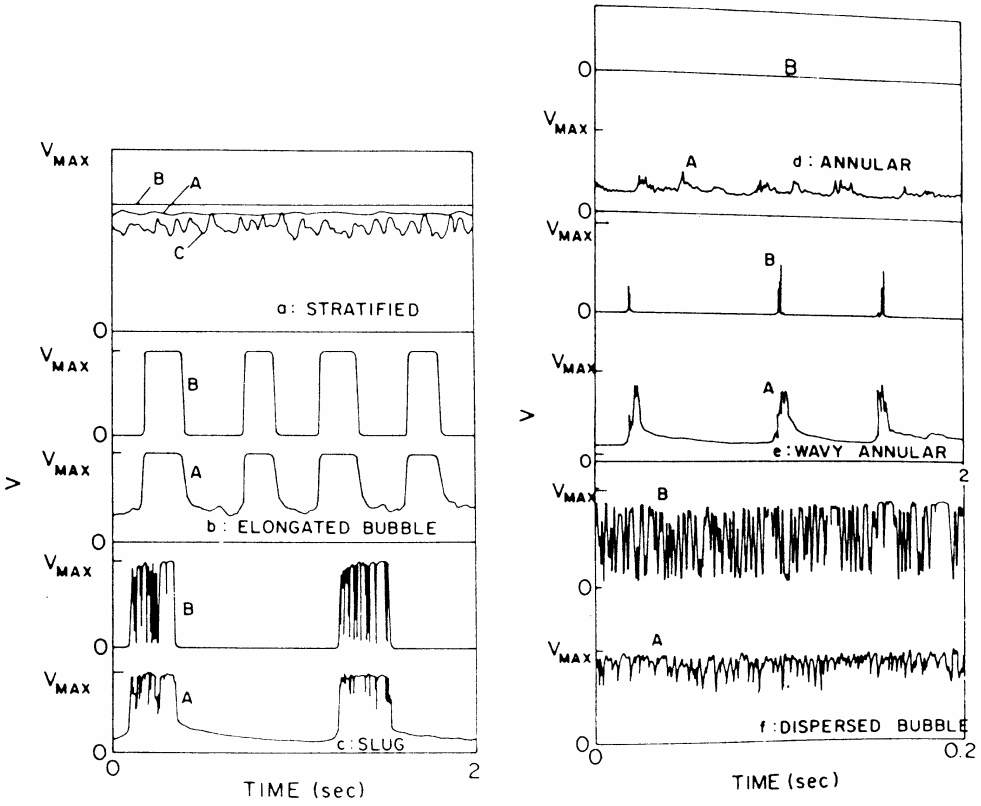

Figure 2.5: Horizontal air-water time traces from conductance probes of Barnea *et al.* (1980)

Obviously, conductance methods can only be applied where the liquid phase is electrically conductive, for example air-water systems and where contact with the operating fluids is acceptable. For non-conducting fluids, like the air-kerosene mixture used in this study, capacitance probes have to be used instead.

2.1.5 Tomographic Imaging

More recently the emphasis has moved from mere identification of the flow pattern to a desire to produce imaging of the two-phase flow within the pipe. This has lead to the development of more complex sensor designs coupled with more intensive algorithms to analyse the raw signals. These *tomographic sensors* are able to produce a graphical representation of the cross-sectional flow inside the pipe. The raw data

used in the image reconstruction can come from any number of measurement sources, for example, ultrasonic or acoustic techniques and electrical field interactions. Each individual measurement technique will have unique advantages and disadvantages in relation to the accuracy, frequency and resolution of the measured images produced. Figure 2.6 compares the imaging rate with the spatial resolution for various types of tomographic measurement techniques.

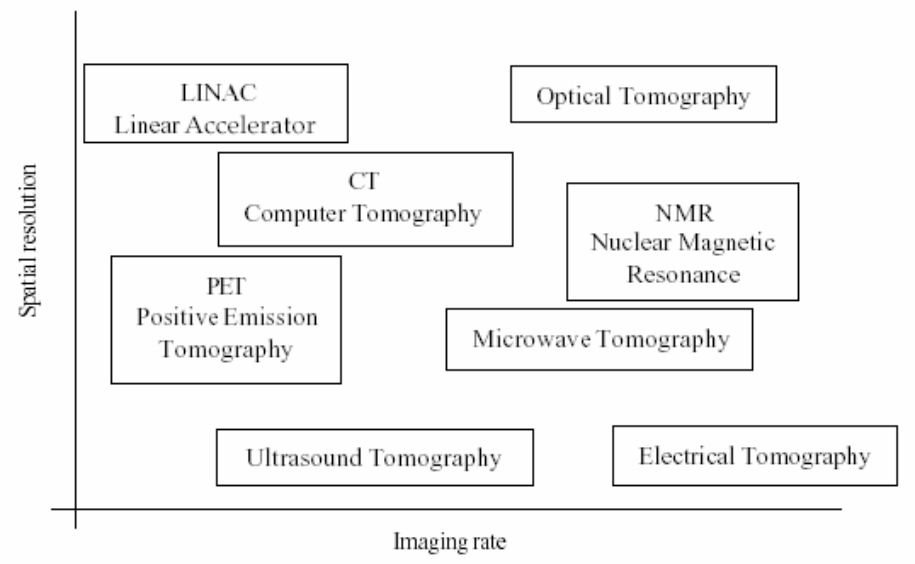

Figure 2.6: Qualitative comparisons of various tomographic measurement techniques as suggested by Jeanmeure (2001)

It should be noted that the classical medial tomography imaging systems, like x-ray, positron emission or nuclear magnetic resonance, have high image resolution but very poor time resolution, usually in the order of 1 to 600 seconds, and are disregarded because of the greater expense. The need in this work is to provide relatively low cost imaging of industrial processes for control purposes, termed as *process tomography*. The requirement for these sensors is to provide a fast time resolution with the consequence of much lower, but sufficient, image resolution. Thus it is expected that only two systems can be considered to fall within this criterion, namely, ultrasound

and electrical tomography. A typical layout of a process tomography system is shown schematically in Figure 2.7. Here the sensor takes the signals and passes them to a data acquisition module. These signals are then processed in a PC to produce a reconstructed image representing the cross-sectional phase distribution within the pipe. Typically this whole process can be achieved in less than 0.04 seconds.

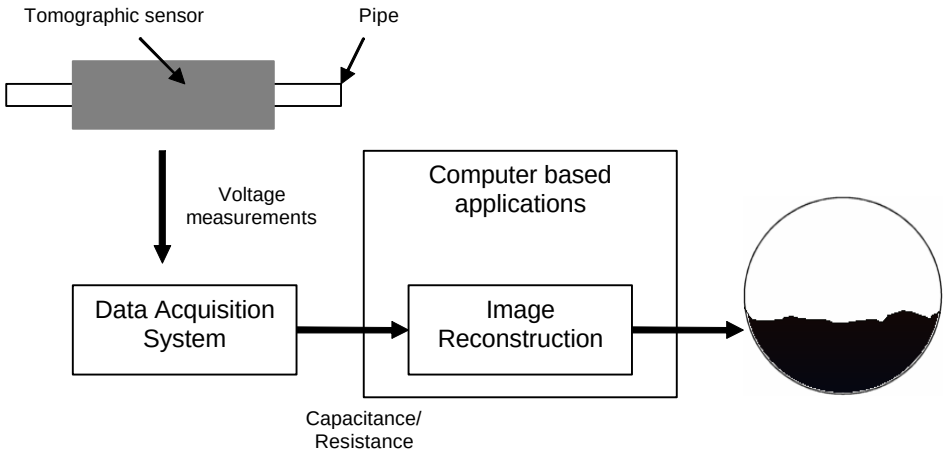

Figure 2.7: A typical layout for process tomography applications

2.1.5.1 Ultrasound Computerised Tomography

The technique of ultrasound tomography relies on the variation in transmitted acoustic waves as they pass through a gas-liquid flow. Xu *et al.* (1997) considered ultrasound computerised tomography (UCT) as an important technique available to reconstruct an image of a gas-liquid distribution inside of a pipe, receiving much interest from researchers since the 1980s. In their paper they give a brief outline of the developmental history of the technique and go on to highlight the major difficulties in applying UCT. Such problems include the lack of an adequate scattering model, which must account for multi-scattering and multiple reflections, and the issue of monitoring a moving flow, where the reflected waves may not occur in the required pipe cross-section, resulting in a loss of key information.

The system used by Xu *et al.* (1997) had a spatial resolution of 0.014 m within a 0.187 m diameter vessel. A single frame had a capture time of 1.5 ms but it took 24 ms to reconstruct the associated image, corresponding to 667 and 42 frames/s, respectively. The authors note that all these frame rates would increase as the diameter of the pipe increased. Tests were conducted on the ultrasound sensor to try and establish the effectiveness of the system in the identification of different gas-liquid flow patterns using simple fabricated models to simulate annular, slug, bubbly and stratified flows. The resultant tomographic images from these tests clearly indicate the apparent success in identifying the different flow patterns studied however there has been no reported online experimental testing of such sensors.

2.1.5.2 Electrical Tomography

The field of electrical tomography can be separated into two distinct regions based on the method by which the electrical field is produced, either conductance or capacitance. The choice will be based primarily on the electrical properties of the fluids, whether they conduct or not. The other major difference between the two approaches is that conductance probes need to be in contact with the fluids while capacitances probes can positioned on the exterior of the pipe. This has obvious implications for sensor applicability within real process situations. The capacitance sensor, in theory, could be a portable device capable of being attached to the outside of an existing pipeline. To use conductance methods specially constructed pipework, with embedded probes, need to be inserted in the pipe section under study. Being in contact with the fluids also raises questions of the probes long term use, with the potential of deposits, especially in oil field applications, and natural degradation of the probes over time, both being major causes of concern. With capacitance probes located on the outside of the pipe, there are not the same issues for concern. In view of these points, the subject of conductive tomography will only be briefly mentioned for completeness, before considering capacitance tomography in greater depth.

Conductance Tomography

Conductance tomography is in some way an extension of the conductance probe approach mentioned earlier but with multiple probes flush-mounted and evenly distributed around the entire pipe interior. There are essentially two methods of measurement, using either a constant current and measuring the resulting potential at the other electrodes, or applying a constant potential between two electrodes and measuring the induced current. Since there is a need for the electrodes to be in direct electrical contact with the conducting fluid, tomographic imaging of certain flow patterns, for example slug flow, cannot be achieved with this flush-mounted method.

To overcome this shortfall Reinecke *et al.* (1998) proposed an extension of the conductance approach that used wire-mesh electrodes. Their arrangement, shown schematically in Figure 2.8, consisted of three planes of 29 thin wires each with a diameter of 0.1 mm. The planes are set 3 mm apart and the wires of two successive planes form an angle of 60°. With a distance of 2 mm between parallel wires the total free cross-sectional area through the sensor is greater than 95%. It is assumed that since the wires are so small the flow is not disturbed and the associated pressure drop can be neglected.

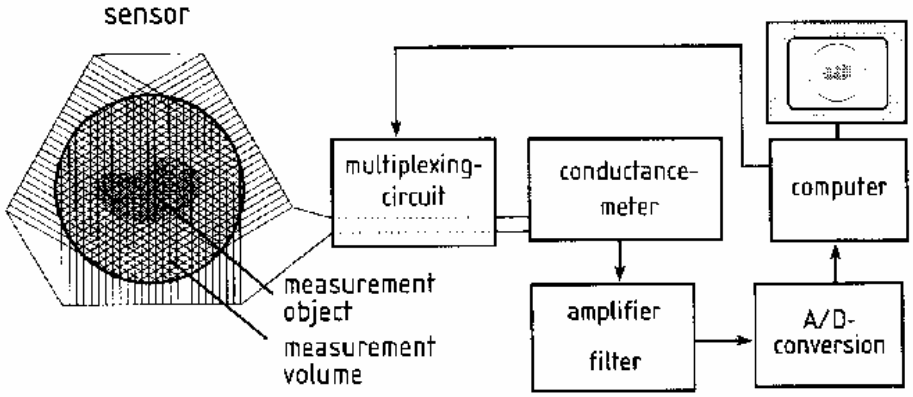

Figure 2.8: Schematic representation of the measuring chain for wire-mesh tomographic measurement technique by Reinecke *et al.* (1998)

By measuring the impedance between all pairs of adjacent wires in the same plane a projection of the conductivity distribution along the direction of the wires is obtained. For each plane, the impedance measurement is carried out with a high frequency (1000 Hz) alternating current, with the sampling of the individual electrode pairs performed by a multiplex unit. This process results in three independent projections, which are then transformed into the conductivity distribution and then further interpreted as the void fraction distribution. The overall system offers a sampling rate of 112 frames/s and a spatial resolution equivalent to 0.1% of the cross-sectional area.

The main disadvantage of the approach of Reinecke *et al.* (1998) was, according to Prasser *et al.* (1998), the image reconstruction step, both in terms of the time overhead and the underdetermined nature of the equations needed to be solved. In view of this Prasser *et al.* (1998) presented a new wire-mesh sensor for fast tomographic imaging without the need for time consuming and potentially inaccurate image reconstruction procedures. The sensor, shown schematically in Figure 2.9, used two electrode planes 1.5 mm apart, one for transmitting and the other for receiving signals

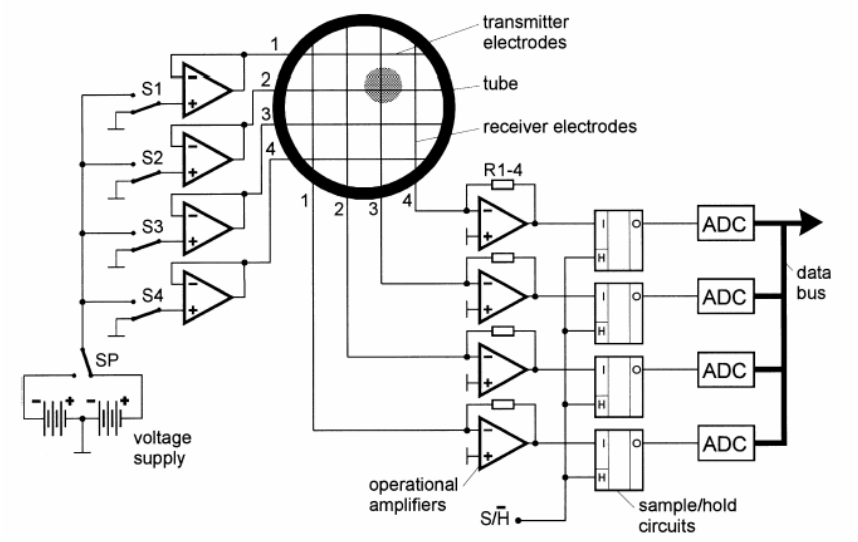

Figure 2.9: Simplified scheme of the two-plane electrode-mesh device used by Prasser *et al.* (1998)

Each plane consisted of sixteen 0.12 mm diameter electrode wires, producing a grid of 16 × 16 measurement points evenly distributed across the pipe cross-section. The grid had a free area of approximately 96%, with a negligible pressure drop. In one measurement cycle, the transmitter electrodes are activated by a multiplex circuit in successive order. The data acquisition for the imaging was achieved by replacing the binary signal integration by an evaluation of the analogue current signals from the receiver electrodes. These currents are then transformed into voltages by operational amplifiers and sampled by individual sample/hold circuits. This procedure is repeated for all transmitter electrodes and each signal is separately stored for every individual receiver electrode. The distribution of the electrical conductivity over the cross-section area of the sensor is thus obtained row by row. This raw data is then processed, by relating the measured conductivity to the local void fraction, to produce a virtual cross-section of the pipe. A typical sequence of frames is shown in Figure 2.10.

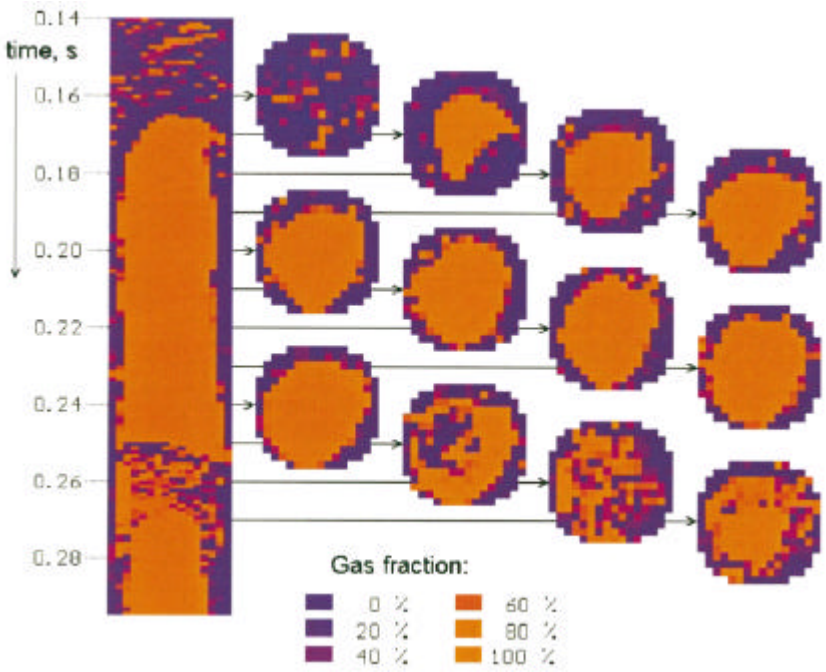

Figure 2.10: Typical tomographic sequence of frames for vertical slug flow using the 16 x 16 wire-mesh sensor of Prasser *et al.* (1998)

This system offers a data capture rate of 1024 frames/s but can only display a limited number of online images, typically 20 per second, depending on the speed of the interface and PC. The spatial resolution of 3 mm is determined from the pitch of the electrodes. Although no attempt is made to use this mesh approach has a means for flow pattern identification, it is clear that the potential for such applications does exist. More recent work by Prasser *et al.* (2001) has improved the data capture rate to 10,000 frames/s, applying it to the study of flow structures within vertical air-water annular flows.

Regardless of the positive results obtained, both in terms of speed and spatial resolution, in terms of the application within the flow identification of gas-oil flows there are two major drawbacks. The first, and most significant, is the non-conducting nature of the fluids involved within this study and the petroleum industry, while the second is a desire to keep the sensing electrodes out of physical contact with the fluids. Placing them on the exterior of the pipe would provide a greater flexibility as well as an increased lifespan to the sensors. Thus, a more realistic option could be the use of capacitance techniques.

Capacitance Tomography

Electrical capacitance tomography (ECT) is a truly non-invasive technique since the sensing electrodes are not in contact with the medium under observation but are positioned peripherally around the pipe exterior. The imaging parameter, the permittivity, is the dielectric property of each of the phases in the two-phase system. Isaksen (1996) has shown that an ECT image can be reconstructed based on the permittivity distribution obtained from the measurements of the electrical capacitance taken between all possible pairs of electrodes. Figure 2.11 shows a cross-sectional view of the measurement principle for an eight electrode ECT sensor.

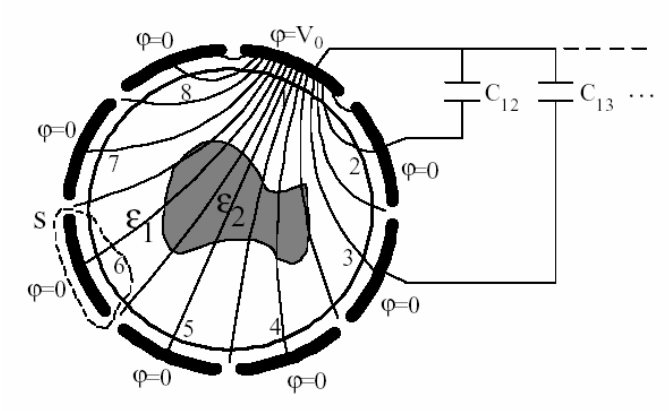

Figure 2.11: Measurement principle for an eight electrode ECT sensor system

Recent work by Ostrowski *et al.* (2000) on the application of electrical capacitance tomography within liquid-solid environments highlighted the possibility of flow pattern analysis using tomography data. In an attempt to provide a method of distinguishing different types of dense flow online they selected several statistical estimators that could be applied in the data processing step. Although they give no definite methodology for flow pattern detection, the authors do conclude that such techniques are promising. They acknowledge further development of the sensor systems and process control systems is necessary but still expect industrial examples to emerge in the near future.

Initially the focus of electrical tomography capacitance is to provide cross-sectional images across the pipe interior. The traditional approach of flow pattern analysis using tomography would rely on taking a control decision based on the reconstructed image. However, where it is relatively simple to collect the capacitance data and form the associated image it is not so easy to then process that image for control purposes. There would be several extra time intensive steps required to obtain a decision from an image, which would have to be subject to image analysis as well as further quantifiable steps.

Investigations by Jingabo *et al.* (2000) combined an eight electrode capacitance sensor with an artificial neural network that was trained to recognise the flow patterns based on a comparison of the capacitance measurements. The system was tested using 3 mm plastic pellets in a pipe to simulate the major flow patterns. Overall, the average recognition rate was found to be nearly 88% but the authors do note that training a neural network is a very time consuming process.

Further work carried out by Jeanmeure *et al.* (2001a, 2001b) has highlighted the use of electrical capacitance tomography has a means of direct flow pattern identification again without the requirement for image reconstruction. Such an approach would have the advantage of reducing the computer overhead time and would be better suited for implementation within a control loop situation. Since the image is reconstructed from raw capacitance data it seems reasonable that there must be fundamental geometrical properties, related to the flow pattern, hidden within the data set of measurements. The capacitance sensor employed in their studies, which is the same one as used for the studies presented in this thesis, consisted of eight electrodes distributed evenly around the pipe, operating at a maximum data collection speed of 100 frames/s and a maximum online image output rate of 50 frames/s.

Jeanmeure (2001) proposed two principal identifiers based on the geometrical nature of the flow pattern. For annular flow, where the liquid film is distributed around the pipe wall, adjacent electrode pairs are expected to give similar capacitance measurements. While for stratified flows, where the liquid flows along the bottom of the pipe, the balance between the electrode pair measurements for the upper and lower pipe sections is considered. A more detailed account of the methodology and work undertaken to identify these critical identification parameters is given in the work of Jeanmeure (2001). Essentially, to check that a parameter linked to a set of capacitance values, idealised flow patterns were simulated. From the capacitance data sets obtained it was then possible to identify the best electrode pair measurements associated with each distinct flow pattern. This process produced three distinct parameters for the determination of the flow pattern within a pipe. Using the same

numerical notation for the electrodes as given in Figure 2.11, these parameters were as follows:

Stratified flow:

$$Ratio\ top/bottom = (C_{35}+C_{46}+C_{36})/(C_{17}+C_{28}+C_{27})$$

Annular flow:

$$Variance\ parameter = var(C_{13}+C_{24}+C_{35}+C_{46}+C_{57}+C_{68}+C_{71}+C_{82})$$

Phase fraction indicator:

$$Average\ facing\ electrode\ pairs = (C_{15}+C_{26}+C_{37}+C_{48})/4$$

Based on these values a decision tree, shown in Figure 2.12, was then compiled to allow the flow pattern to be identified from the capacitance data.

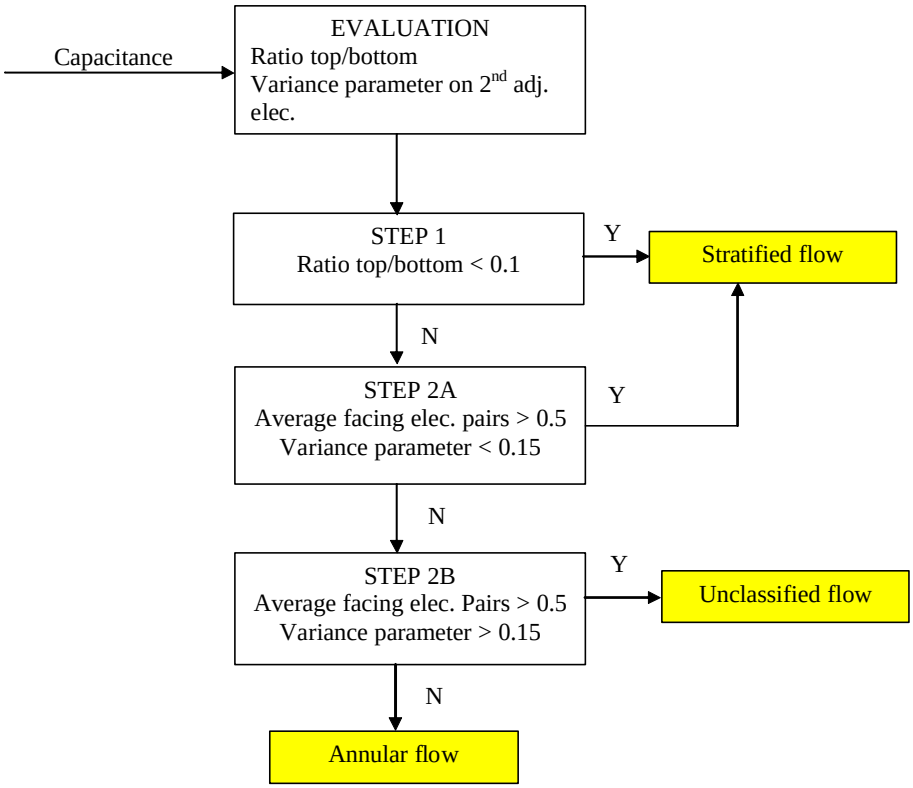

Figure 2.12: ECT decision tree for flow pattern identification based on the work of Jeanmeure (2001)

The remaining flow pattern that is of great interest to this research is that of slug flow. A positive recognition of slug flow could be delivered by monitoring the liquid phase fraction in the pipe. If this value, determined from the average facing electrode pair measurements, was to rise above a certain level, say 0.8, then slug flow would be identified. Jeanmeure *et al.* (2001a) gives details of six reconstructed tomographic images and the equivalent classification obtained using the selected parameters. The images and the classification are shown in Figure 2.13. These clearly show that all three flow regimes are correctly identified.

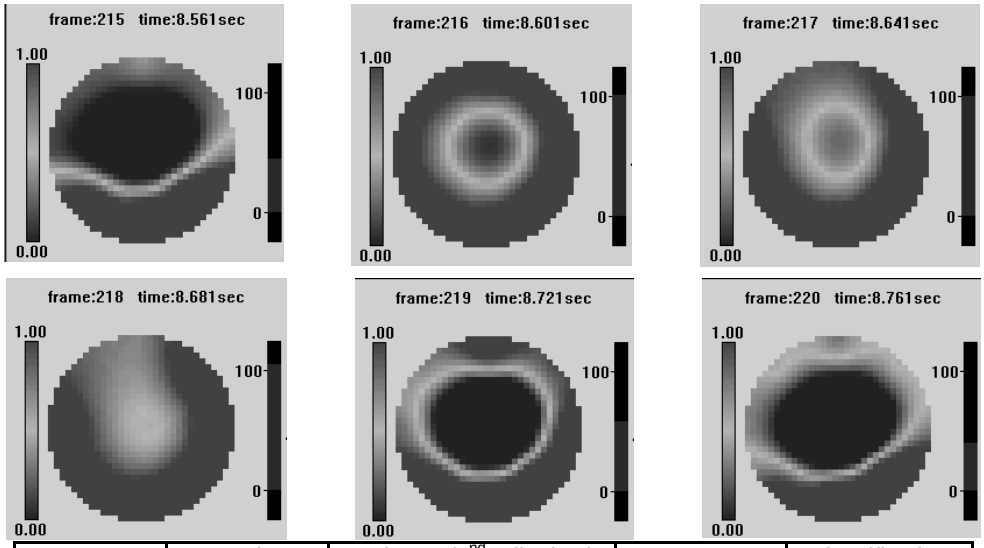

Image	Ratio Top/Bottom	Variance (2nd adj. elec.)	Average facing elec.	Classification
Frame 215	0	0.164	0.203	Stratified
Frame 216	0.790	0.006	0.872	Slug
Frame 217	0.734	0.015	0.907	Slug
Frame 218	0.904	0.004	0.967	Slug
Frame 219	0.172	0.103	0.219	Annular
Frame 200	0.046	0.115	0.116	Stratified

Figure 2.13: Electrical capacitance tomography reconstructed images and parametric classification of Jeanmeure *et al.* (2001a)

2.1.6 Summary of Flow Pattern Identification Techniques

A concise review by Keska and Williams (1999) compares four techniques, of what they thought were the possible options, for flow pattern identification. These were pressure, optical, conductance and capacitance methods. They carried out simultaneous comparative studies of these techniques using eight different flow patterns and analysed the responses from each method. In summarising their findings they found that the measurement of pressure fluctuations had the lowest potential for flow pattern determination and noted that the optical methods would only apply to non-opaque situations. The final two options they examined, the capacitance and conductance techniques, were considered to be of similar nature, both demonstrating a high potential for flow pattern determination.

The final selection of the flow pattern identification technique has to be based on only one constraint, the electrical properties of the fluids under study. For electrical conductive liquids, with a corresponding high electrical permittivity, capacitance techniques cannot be applied, leaving conductance probes as the only option. Such probes seem to be able to provide better time and spatial resolution than capacitance alternatives at the expense for the requirement for direct electrical contact.

In the context of the application considered within this thesis, namely the control of a T-piece separator for oil-gas applications, conduction methods are not applicable. This leaves the capacitance techniques as the only viable method. Since they do not need to be in direct contact with the fluids under study, they are intrinsically safe and could be flexible enough to be positioned around any pipe section. The novel approach of identifying the flow pattern without the overhead of image reconstruction, as suggested by Jeanmeure (2001), is the most suitable for implementation into the control scheme required for the separator system envisaged in this work.

2.2 T-Junctions as Partial Phase Separators

The effect of geometry, fluid properties and flow pattern on the phase split of a gas-liquid flow at a T-junction has already been highlighted in Chapter 1. Over the years, the full range of possible flow regimes has been studied for various T-junction systems. The majority of the work has focused on stratified, slug and annular flow patterns, as they are considered most relevant to industry. Within the petroleum industry, which is the main focus for this research, the expected flow patterns for the incoming gas-oil mixture would be either stratified or, more predominately, slug. With such a significant difference between annular flow and the other two regimes, the associated T-junction separators would potentially have to take very different forms and so this work focuses on separation of only stratified and slug flows.

Before discussing the results of this study it is important to gain an understanding of the previous research carried out on T-junctions and applications for separation systems. It is worth remembering that this thesis deals with an application of T-junctions and does not necessarily focus on improving fundamental knowledge of two-phase flow at junctions. This Section will summarise and review the important published material, highlighting the key points where appropriate. The vast number of studies on T-junctions is a testament to the complexity and seriousness of the problem. As there has been so much research activity investigating the many aspects that affect phase split at junctions only the relevant literature will be cited in this review. Over the years, there have been a number of comprehensive reviews on the subject of T-junctions published, most notably by Lahey (1986), Muller and Reimann (1991), Azzopardi and Hervieu (1994) and Azzopardi (1999b).

2.2.1 Effect of Main Pipe Orientation on Phase Split

Two-phase gas-liquid flows in pipes can be divided into two main groups, dependent on the orientation of the pipe. This classification system can also be applied to T-junctions, in terms of the orientation of the inlet, producing, what are then termed, *horizontal* or *vertical* T-junctions.

Since the influence of gravity will be so different on the phases for the two cases, it may be expected that for the same flowrates the resultant phase separation would also be different. However several authors, including Seeger *et al.* (1986) and Hwang *et al.* (1988), have noted that the orientation of this main pipe does not appear to have such a strong influence on the flow split. They both based their conclusions on the comparisons between the phase split data of Honan and Lahey (1981), taken for a vertical inlet regular T-junction, and Saba and Lahey (1984), for a fully horizontal regular T-junction. Wren (2001) recorded the same phenomena in a comparison of the horizontal T-junction data of Azzopardi *et al.* (1988) and the vertical data of Hewitt *et al.* (1990), for similar inlet parameters.

Regardless of the apparent similarities between vertical and horizontal junctions they are nearly always treated independently within the literature. The work in this thesis deals exclusively with a horizontal inlet system and the rest of this review examines the progression of the knowledge in this area.

2.2.2 Geometrical Improvements to Increase Phase Separation

Once the concept of trying to use T-junctions as a means to separate gas-liquid flows was established the emphasis of research moved to find ways of enhancing the natural phenomena. For a horizontal main pipe there are a number of possible approaches suggested to increase the phase separation performance. Some of the most widely investigated areas include, reducing the diameter of the branch arm, changing the orientation of the branch arm, introducing inserts at the junction or combining two, or more, junctions together.

2.2.2.1 Reduction of Side-arm Diameter

The initial focus for studying the phase separation at junctions with a reduced side-arm diameter was for industrial situations, where the branch arm of a conduit system could well have a smaller diameter than the main pipe. Table 2.1 details the sources of phase split data for horizontal T-junctions where the influence of side-arm diameter on the phase split has been investigated. Typically it can be found that less

liquid is taken-off, for a fixed gas take-off, when the diameter of the side-arm is reduced.

Table 2.1: Sources of phase split data where the effect of side-arm diameter has been investigated for fully horizontal T-junctions

Source	Main pipe diameter (m)	Side-arm/Main pipe diameter ratio	Flow patterns
Ballyk *et al.* (1991)	0.0257	0.5 0.82 1.0	Annular
Azzopardi *et al.* (1988) Azzopardi and Memory (1989) Azzopardi and Smith (1992) Azzopardi (1999a)	0.038	0.33 0.67 1.0	Stratified Annular
Buell *et al.* (1994) Walters *et al.* (1998) Van Gorp *et al.* (2001)	0.038	0.206 0.5 1.0	Stratified Annular
Reimann *et al.* (1988)	0.05	0.084 0.2 0.52 1.0	Stratified Slug Annular
Shoham *et al.* (1987) Shoham *et al.* (1989)	0.051	0.5 1.0	Stratified Annular
Peng (1994) Peng *et al.* (1998)	0.076	0.33 1.0	Stratified Annular
Azzopardi (1999a) Wren (2001)	0.127	0.6 1.0	Stratified Annular

A reduction in the side-arm diameter will have two distinct effects, namely, the associated pressure drop and the axial distance available for take-off. It is well known that the division of the phases at a T-junction depends not only on the system geometry and approaching flow pattern but also on the two downstream pressures and the pressure drop across the junction itself. The outlet with the lower pressure, or greater suction, has a stronger influence on the passing fluids, thus more will be diverted in that direction. Studies undertaken by Walters *et al.* (1998) and later by Van Gorp *et al.* (2001) have compared the pressure drops for both a regular and reduced fully horizontal T-junction with similar inlet flowrates. As shown in Figure 2.14 the pressure drop between the inlet and the run arm, DP_{12}, is relatively

small and unaffected by the diameter of the side-arm. However, the inlet to side-arm pressure drop, DP_{13}, increases significantly with a decrease in the side-arm diameter ratio. So, for the same inlet conditions, a higher pressure drop is associated with the reduced T-junction. This is due to the higher gas velocities within the reduced diameter pipe for the same mass fraction extracted through the branch, as demonstrated by Bernoulli's equation. If the side-arm/inlet diameter ratio is 2:1, the gas velocity in the reduced arm increases four times. This acceleration of the gas phase has a strong influence on the liquid, potentially drawing more liquid into the branch when compared to a regular T-junction system.

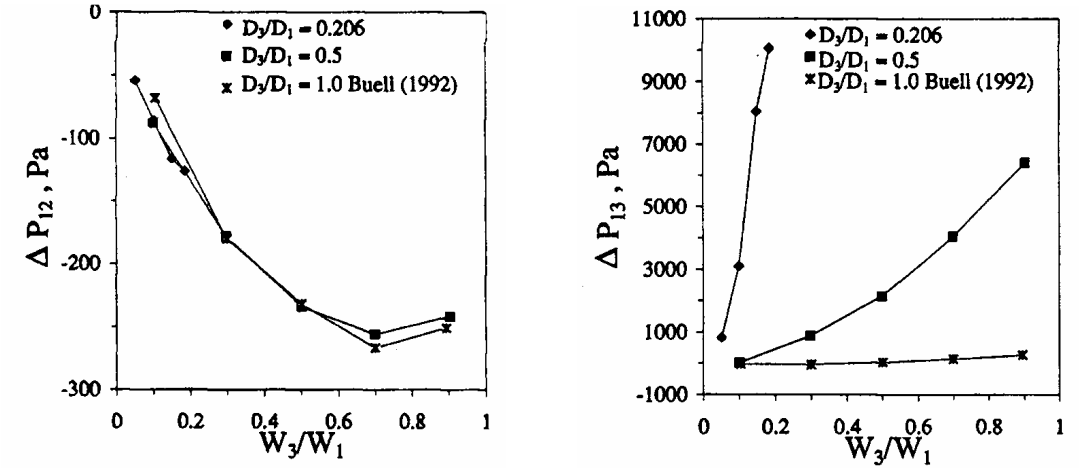

Figure 2.14: Pressure drop across a regular and a reduced horizontal T-junction as determined by Walters *et al.* (1988)

The second effect caused by a reduction in side-arm diameter, as first suggested by Azzopardi (1984), will be to reduce the axial distance available for phase take-off to occur. This reduces the liquid travel time, the time available for the liquid to flow into the side-arm instead of flowing straight into the run. As such there is less chance of the liquid that is dragged towards the side-arm by the gas leaving in the smaller opening has it hits the pipe wall instead and continues along the pipe into the run.

Hence, more liquid by-passes the branch, so for a given gas take-off, the corresponding liquid take-off should be less than for a regular T-junction. The final effect on the phase separation produced by a reduction in the side-arm would appear to be a combination of the two factors above coupled with the flow pattern approaching the junction.

For stratified flows, it has been observed (Azzopardi *et al.*, 1988; Reimann *et al.*, 1988; Shoham *et al.*, 1989; Peng *et al.*, 1998 and Wren, 2001) that a reduction in the side-arm diameter will generally result in an increased phase separation, with less liquid removed for a given gas take-off for horizontal junctions. This relates directly to the idea of the reduced travel time for the liquid for diversion into the branch above. As well as this, the phase separation will be influenced by the elevation difference between the bottom of the inlet pipe and the side-arm opening. Both Azzopardi *et al.* (1988) and Shoham *et al.* (1989) point out that the majority of the liquid, flowing along the bottom of the pipe, will not be directly influenced by the side-arm entrance and will need to "climb" the wall before being able to enter the branch. However, Azzopardi *et al.* (1988) also found that for high gas take-off the liquid take-off was unaffected by changes in diameter ratios. The same trend can be found in the comparison of the reduced side-arm studies of Wren (2001) and the regular side-arm work of Rea (1998), using the same experimental facility and flow conditions again with a fully horizontal T-junction. This could be attributed to a phenomenon termed *hydraulic jump*, as described by Azzopardi and Smith (1992). Here, beyond a critical gas take-off point the liquid height at the junction increases sharply, as the liquid momentum decreases, and is more readily diverted into the side-arm.

Azzopardi (1999a) has shown that the effect of reducing the side-arm diameter becomes much less pronounced for stratified flows. Indeed at certain flow conditions, with low gas flowrates, the phase separation achieved for a diameter ratio of 0.33 is closer to that for a regular T-junction and much worse than for a ratio of 0.67. This result mirrors the findings of Walters *et al.* (1998), who found that more liquid was extracted through the smallest side-arm/main pipe diameter ratio system for

increasing extraction rates. They explained this by the increased gas velocity in the smaller diameter pipe creating a strong Bernoulli Effect, associated with the pressure drop. This entrains more liquid into the branch than would be expected, counteracting the benefit of the reduced axial distance and the *wall-climbing* effect. Reimann *et al.* (1988) carried out a small number of studies on slug flow at a reduced T-junction, with the results following the same trends as for stratified flows.

In the case of annular flows the effect of the reduced side-arm is diminished as liquid take-off is dominated by centripetal forces. The results of Shoham *et al.* (1989) show negligible differences between regular and reduced T-junction phase split data, with the liquid preferentially entering the side-arm. In contrast, the results of Wren (2001) and Rea (1998), using a larger diameter system, show that a reduced side-arm has no noticeably effect on the phase separation but that the separation is gas dominated. These results are also consistent with those of Azzopardi *et al.* (1988) and the steam-water data of Ballyk *et al.* (1991). This is attributed to a similar mechanism as for stratified flow, where the circumferential liquid film flowing above or below the branch opening cannot be directly extracted without a vertical as well as a radial force.

The data of Ballyk *et al.* (1991) also shows that the effect of branch diameter becomes less pronounced as the diameter is decreased for a horizontal junction. The data for a branch-to-inlet diameter ratio of 0.82 is closer to the data for a ratio of 0.5 than it is to that of a regular junction (a ratio of 1.0). This is attributed to the increased gas velocity encountered in the side-arm, which increases both of the carry over mechanisms expected, pressure drop and entrainment. Azzopardi *et al.* (1988) observed similar trends, when under certain conditions the side-arm diameter had no influence on the liquid take-off. This was explained in terms of a phenomenon they termed *break point*, which is similar to the *film stop* mechanism described by Azzopardi (1988) for annular flow. Here the liquid film reacts to the increasing pressure present downstream of the junction in the main pipe, causing a reduction in momentum. This velocity decrease causes the local film thickness to increase, and this slower moving liquid is more susceptible to take-off.

2.2.2.2 Change in Orientation of Branch Arm

Since gravity has a strong affect on the phase distribution within a horizontal pipe, it is also expected to have an affect on the phase separation. Thus by rotating the branch arm around the main pipe axis it is possible to maximise both the gravity forces and the fluid density differences to increase the phase separation performance of the junction. So for a branch arm inclined downwards, more liquid can be drawn off and conversely with an upward inclined branch, a significant amount of gas has to be diverted before any liquid is extracted with it. Interestingly, work by Ottens *et al.* (1999) has shown that even the smallest side-arm inclination angle above the horizontal, in their case less than 0.5°, can have a significant influence on the phase separation of gas-liquid flows.

Much of the research into the effect of side-arm orientation has been coupled with investigations on reduced diameter T-junctions as well. These systematic changes on the same experimental facilities have helped to increase the understanding of the mechanisms taking place. Table 2.2 summarises the sources of phase split data at T-junctions where the affect of the branch inclination has been investigated. By convention an angle of 0° represents a fully horizontal T-junction, positive angles indicate the branch is raised above the horizontal and negative angles indicate downward inclinations of the branch. The extreme cases then become a vertically upwards branch, +90°, and a vertically downwards branch, -90°.

A systematic study on the effect of side-arm orientation is reported by Penmatcha *et al.* (1996). Although confined only to stratified flows it involved rotating the side-arm around the main horizontal pipe from angles of +35° above the horizontal to -60° below it. For downward side-arms the trends observed are as expected, the greater the incline angle the greater the liquid take-off. They found for their system and flow conditions that almost 100% of the liquid was diverted into the side-arm, achieving complete phase separation, when it was inclined downwards at an angle of -60°. In the case of upward inclined branches the phase splitting curves all show the same general characteristics.

Table 2.2: Sources of phase split data where the effect of side-arm inclination has been investigated for horizontal T-junctions

Source	Main pipe diameter (m)	Diameter ratio	Branch orientation (°)	Flow patterns
Hong (1978)	0.0095	1.0	0, ±(45, 90)	Stratified Annular
Ballyk *et al.* (1991) Peng *et al.* (1993) Peng *et al.* (1996)	0.0257	0.5 0.82 1.0	0, -(45, 90)	Annular
Smith and Azzopardi (1990) Azzopardi and Smith (1992)	0.038	0.67 1.0	0, +90	Stratified Annular
Seeger *et al.* (1986)	0.05	1.0	0, ±90	Slug Annular Bubbly
Reimann *et al.* (1988)	0.05	0.084 0.2 0.52 1.0	0, ±90	Stratified Slug Annular
Fouda and Rhodes (1974)	0.051	0.5	+90	Annular
Penmatcha *et al.* (1996) Marti and Shoham (1997)	0.051	0.5 1.0	0, +(1, 5, 10, 20, 35) -(5, 10, 25, 40, 60)	Stratified
Ottens *et al.* (1999)	0.051	1.0	0, +(0.1, 0.25, 0.5)	Stratified
Peng (1994) Peng and Shoukri (1997) Peng *et al.* (1998)	0.076	0.33 1.0	0, -(45, 90)	Stratified Annular
Wren (2001)	0.127	0.67 1.0	0, ±90	Stratified Annular
Maciaszek and Memponteil (1986)	0.135	0.15	0, ±90	Stratified
Katsaounis and Schultheiss (1985) Katsaounis (1987)	0.203	0.40	+90	Stratified Slug
Mudde *et al.* (1993)	0.23	0.43	+90	Stratified Bubbly

In all cases a significant amount of gas has be diverted into the side-arm before any liquid is extracted with it. However, once the liquid had started flowing, there needed to be only a relatively small increase in the gas take-off, usually much less than 10% extra, to get the majority of the liquid drawn off with it. As the inclination angle is increased the fraction of gas required to start liquid flowing into the side-arm also increases. So for an angle of +5°, the onset of liquid off-take occurs with a gas take-off of 50%, while with an angle of +35°, the gas split needs to be around 80%. It was also noted that the splitting ratios tended to become independent of the inlet liquid velocities as the upward inclination angle exceeded 5°. A mechanistic model

for the downward T-junction was developed based on the dividing streamline approach of Shoham *et al.* (1987). Although it predicted the general data trends, it tended to under predict the gas take-off for a given liquid extraction.

Following on from the work of Penmatcha *et al.* (1996), Marti and Shoham (1997) extended the experimental data for a reduced diameter side-arm. Comparisons between the two data sets for similar flow conditions for downward side-arms show that at low gas fraction extraction the branch liquid fractions are less for the reduced junction as compared to the regular one. For higher gas fractions both cases have an almost equal liquid fraction take-off for a given gas fraction diversion. This is explained as before for fully horizontal junctions, at low gas fractions travel time and inertia forces dominate, while at high gas take-off the pressure drop becomes important in determining the liquid take-off. Similar comparisons for the case of upward inclined side-arms, suggest that the reduced side-arm promotes liquid extraction into the branch, as compared to the regular tee. However, as the gas take-off fraction is increased the amount of liquid extracted, for a particular gas fraction, becomes essentially equal, for both junctions. The explanation for this is that the reduced tee has a higher pressure drop, due to the higher gas velocities within the smaller cross-section. This pressure drop is the dominate force affecting flow split at low gas extraction. As more gas is removed the combination of the pressure drop, gravity and inertia forces appear to be equal for both the regular and reduced tee cases resulting in similar separation characteristics. The model developed by Penmatcha *et al.* (1996) is extended for the reduced T-junction, with reasonable agreement between the experimental data and theoretical predictions.

An early study by Hong (1978), using a relatively small diameter system, shows the same expected trends. With the side-arm vertically upwards the gas-liquid split was almost equal, moving the side-arm towards -90° increased the liquid take-off. Total liquid take-off being achieved in the side-arm with 40% of the gas removed with it.

Both Seeger *et al.* (1986) and Reimann *et al.* (1988) note how the inlet flow pattern could influence the phase split for both vertically upwards and downwards regular

T-junctions. For upward branches it was found that the inlet flow pattern had a relatively small affect on the flow split, with the greatest deviations from total separation corresponding to the bubbly flow regime. This was accounted for by considering the void fraction in the upper part of the pipe. Within the bubbly flow regime there is a continuous liquid presence across the whole pipe cross-section. Since it is assumed that the fluids that enter the side-arm come from this upper part of the pipe, a low quality inlet will promote a low quality side-arm recovery. In the case of a downward branch there is critical liquid take-off point before which no gas enters the side-arm; the more stratified the flow, the higher this critical point becomes. As the flowrates of the fluids are increased, gravity becomes less of an influence on the flow split, since both the phases travel with a much higher momentum sufficient to traverse the branch opening without being affected by it. Changing the liquid velocity has less affect on the phase split than altering the gas velocity, due to the fact that the flow regime present depends more on gas phase flowrate than liquid.

For vertically upward side-arms, Azzopardi and Smith (1992) observed a phenomenon where at a critical gas take-off the amount of liquid extracted increased sharply. This is attributed to the *hydraulic jump* phenomenon as already discussed for the situation of a horizontal reduced side-arm. The value of this critical gas take-off was found to depend on both the gas and liquid inlet superficial velocities. The data of Smith and Azzopardi (1990) also highlighted the maximum gas fraction take-off without any liquid for a reduced diameter side-arm. The trend shows that as the gas inlet velocity increases the gas-only take-off limit decreases for constant liquid flow. These findings were confirmed by the results of Wren (2001), using a larger diameter system, the data was compared on the basis of similar phase momenta. Not only were the same trends observed but the absolute values for the critical gas fraction limit were also comparable.

Peng *et al.* (1998) considered the phase split of stratified flows at a vertically downwards side-arm. Similar to the upward side-arm situation where a critical gas take-off limit was observed before any liquid extraction occurred; the onset of vapour extraction in the downward side-arm only started once a certain liquid take-off had

already been achieved. Vapour extraction was only possible once it had been pulled through the liquid layer flowing along the bottom of the pipe. It was found that as the inlet vapour superficial increased this onset of vapour extraction began at lower flow split ratios. This was explained by the depth of the liquid layer depending strongly on the vapour velocity above it. The faster the vapour travels the thinner the layer will be and so the easier it becomes for the vapour to pass through it.

For annular flows, the studies of Ballyk *et al.* (1991) and Peng *et al.* (1996) show that having a downward side-arm significantly affects the phase separation. This is an affect of the asymmetrical distribution of the liquid film around the pipe wall, since gravity will cause the film to be thicker at the bottom of the pipe more liquid is available for extraction, increasing the liquid content in the branch.

The work of Wren (2001) highlighted the presence of a continuous liquid level above the valve within the downwards side-arm. This provided a barrier against gas passing the valve, up to a critical liquid take-off value. Beyond this there appeared to be a linear relationship between the gas and liquid take-off up to the point of total liquid extraction. A model was developed based on the concept of bubble rise velocity within the column of water above the valve in the outlet combined with a description of the phase split gradient in terms of the phase momentum relationship. A similar affect is reported by Reimann *et al.* (1988), who note the presence of rising bubbles within the liquid recirculation zone in a downwards side-arm.

While the vast amount of research has centred on small diameter systems, several studies have involved larger, more industrially relevant, pipe diameters (Katsaounis and Schultheiss, 1985; Maciaszek and Mempoteil, 1986; Mudde *et al.*, 1993). The general trends observed were consistent with the data colleted using smaller diameter systems, although the published models could not accurately predict the experimental data.

2.2.2.3 Physical Alterations to the T-junction

By affecting the internal dimensions of the T-junction it may be possible to improve the phase separation performance by the addition of baffles or inserts. Table 2.3 shows the relatively small number of studies that have been published based on this idea. Within the limited data, there are two distinct objective groups, those aiming to improve the separation or those trying to create a predictable flow divider.

Table 2.3: Sources of phase split data where the effect of altering the physical dimensions of the T-junction has been investigated

Source	Main pipe diameter (m)	Modifications	Flow patterns
Butterworth (1980)	0.038	45° rotational inserts protruding from side-arm into main pipe	Stratified Annular
Azzopardi and Smith (1992)	0.038	½*D* baffle plus a 90° bend downstream of T-junction	Stratified Annular
Fouda and Rhodes (1974)	0.051	¼*D*, ½*D*, ¾*D* baffles at T-junction	Annular
Wren (2001)	0.127	30° and 45° rotational inserts with ½*D*, ¾*D* protrusion depth into main pipe	Stratified Annular
Katsaounis and Schultheiss (1985) Katsaounis (1987)	0.203	0.052 m to 0.082 m diverging branch arm (in 0.125 m)	Stratified Slug

The simple modification of Katsaounis and Schulthesis (1985) involved the use of a diverging vertical upward side-arm, changing from a diameter of 0.052 m to 0.082 m over a 0.125 m length. Although they were interested in the pressure drop across the junction, it was reported that total gas separation was achieved for all flow patterns investigated. This modified T-junction was later incorporated into a dynamic slug catcher proposed by Katsaounis *et al.* (1997).

The use of baffles placed at a T-junction have been considered by both Fouda and Rhodes (1974) and Azzopardi and Smith (1992). The effect of these baffles was not

to enhance the phase separation but rather to homogenise the flow sufficiently to produce an acceptable flow divider. In the annular flow experiments of Fouda and Rhodes (1974) it was found that for a baffle height extending for three-quarters of the tube diameter the uneven two-phase flow split observed for the simple junction was significantly reduced. Smaller baffles were found to have only a relatively small affect on the separation. They also considered insertion of a ½*D* sized orifice upstream of the junction, again designed to homogenise the flow prior to reaching the junction. It was concluded that if equal flow division was required than a suitable orifice could evenly distribute the phases at the junction sufficiently.

The effect of inserts on the phase redistribution at a T-junction as been reported by both Butterworth (1980) and Wren (2001). Figure 2.15 shows a schematic of the position of the inserts. The early tests of Butterworth (1980), for a fully horizontal T-junction with a main pipe diameter of 0.038 m, a side-arm diameter of 0.025 m and an insert angle of 45°, were limited. However, it was found for annular flow that a forward facing insert (scooped section facing the flow direction) decreased the phase maldistribution, while a backward facing insert (scooped section opposing the flow direction) increased the phase distribution. For stratified flows, the backward facing insert was found to have little impact on the phase split, while the forward facing insert only reduced the phase maldistribution for low gas take-off.

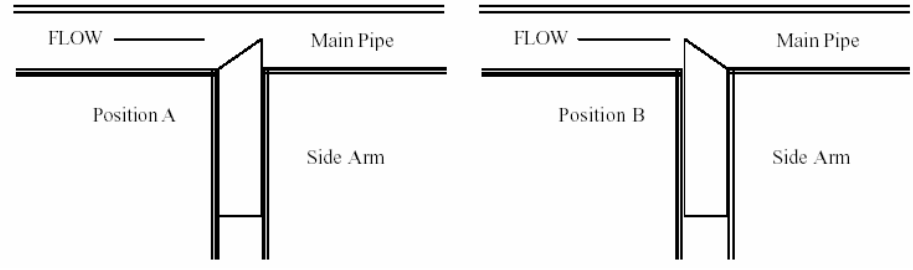

Figure 2.15: Schematic diagram showing insert positions used by Butterworth (1980) and Wren (2001)

Based on these initial findings, Wren (2001) undertook a more rigorous experimental program to determine the potential for inserts to act as phase split enhancers. The affect of the insert cut angle, the insert protrusion depth and the insert orientation were all considered for both regular and reduced fully horizontal T-junctions. The two insert cut angles investigated, 30° and 45°, were seen to behave in similar fashions, having exactly the same influence on the phase separation at the junction. This was attributed to the fact that the profiles for the two cases with respect to the oncoming flow were essentially the same regardless of the angle. Wren (2001) found that with the insert facing backwards the flow split was enhanced for both annular and stratified flows. However, with the insert facing forwards, so as to scoop the oncoming flow, the inserts acted more as equal flow dividers, significantly reducing the phase maldistribution for both annular and stratified flows.

2.2.2.4 Combining Junctions in Series

Early studies by Collier (1976) into gas-liquid route selectivity for horizontal systems found that multiple junctions behaved in a similar manner to single junctions. Here the gas is preferentially extracted through the branches while the liquid accumulates in the exit pipe furthest away from the inlet.

Recently there has been much attention focused on combining two, or more, junctions together in series in the hope of developing a compact, low inventory and economical partial phase separator. A study by Bevilacqua *et al.* (2000) highlighted the concept of combined junction phase separators. In their studies, they constructed various *comb separators* using combinations of simple T- and Y-junctions with vertically upwards side-arms. The favourable separation characteristics of such branched networks and the combined effect of multiple junctions in series produced a series of tests designed to optimise the geometrical configuration of the structure, see Figure 2.16.

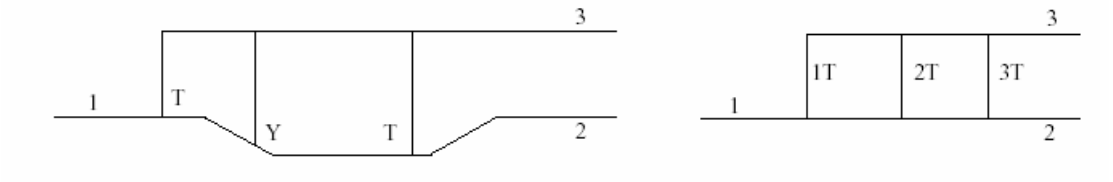

Figure 2.16: The comb separators proposed by Beveilacqua *et al.* (2000)

The efficiency of each arrangement was considered in terms of the number and height of the branches, as well as the available liquid capacity. A final selection of which configuration to use depended on the separation performance required from the system. When the requirement is to guarantee high void fractions in the combined branch stream, a combination of T- and Y-junctions (Figure 2.16 *left*) proved to be the most effective. Using three T-junctions in series reduces the void fraction in the main run, producing a more liquid-rich stream. Since the downstream pressures can have a significant influence on the phase separation performance of a junction, reducing the pressure in the combined branch arm can remove nearly all the gas from the inlet stream.

Since it is known that a vertically upward side-arm will promote gas take-off and a downward side-arm will encourage liquid take-off then a combination the two could have potential in a partial phase separation application. Such a partial separator design was proposed by Wren (2001). Here, a vertically upward T-junction was placed upstream of a vertically downward one. While experimentally such an arrangement would produce three outlets, in reality there would only be a requirement for two exit streams, one rich in gas the other in rich in liquid. However, the ability to examine all three outlets individually produced a theoretical design based on the separation requirements. This design involved combining the up and run arms of the system to form a gas-rich stream, while the down leg provided a liquid-rich stream. Analysis of the results indicates that while it is possible to achieve the required separation criterion performance of 10% v/v liquid-in-gas, it is not so easy to produce a liquid stream containing less than 10%v/v of gas.

The study of Wren (2001) also examined the effect of increasing the separation distance between the two junctions. Due to location limitations, only a small number of studies were conducted with the junctions placed 0.5 m (4*D*) and 1.2 m (10*D*) apart. The results indicate that the separation difference had negligible impact on the separation performance, although further studies over a much wider range could provide more substantial evidence.

2.2.2.5 Controlling the Flow Split at T-Junctions

Within any gas-liquid phase separator there will generally be a need to provide a method of control over the system, to maintain the liquid level in the separation vessel, preventing gas leaving through the liquid line. Traditionally this has been provided by control valves but recent advances in the field of power fluidics offers alternatives to this approach. Priestman and Tippetts (2000) present an application of a fluidic level control in a conventional gas-liquid separator vessel. Such fluidic valves are attractive devices as they have no moving parts, no power requirements and exhibit reliable, automatic fast responses. Using a similar fluidic device Priestman and Tippetts (2002) present an intensified gas-liquid T-junction separator. Figure 2.17 shows the arrangement of their proposed separator.

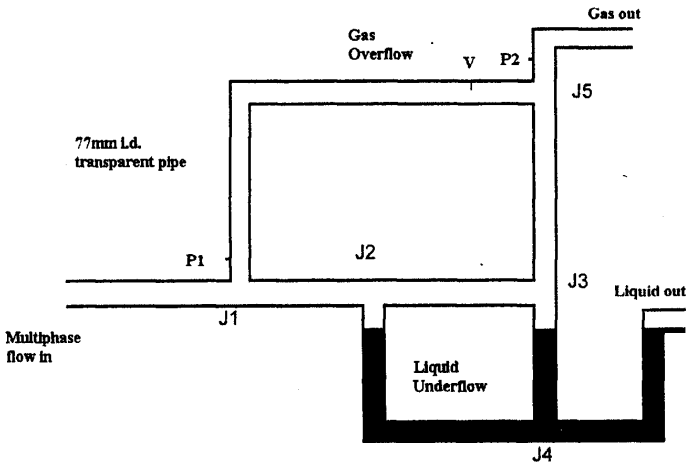

Figure 2.17: Arrangement of T-junction separator system of Priestman and Tippetts (2002)

The fluidic device, in this case a Symmetrical Turn-up Vortex Amplifier (STuVA), controls the level within the end vessel, with a diameter approximately 2.5 times that of the pipe. The design consisted of a gas overflow and a liquid underflow with the STuVA maintaining an interface between the two phases. In essence this provides a means to maintain a liquid barrier to the gas, preventing it from leaving in the liquid-rich stream, although there will some gas entrainment as bubbles.

Various adaptations were presented; including having a larger diameter ($1.3D_1$) downward branch, all designed to promote phase separation. Although many tests are reported with this system, the available data is incomplete. The only separation data given is for the gas split at the first upward junction and the liquid split at the first downward branch, with only a small mention of liquid carried over with the gas under certain flow conditions. There are no clear trends that can be determined from the given results. The gas split at the first upward junction appears to be independent of the gas velocity and generally increases with increasing liquid velocity. Likewise, the liquid flow split at the first downward junction seems to depend only on the liquid velocity, generally decreasing with increasing liquid flowrate.

2.2.3 Summary of Phase Separation at T-junctions

With the amount of research activity centred on the T-junction and its potential in partial separation of gas-liquid flows it is surprising that only recently has there been a reported case of an industrial application. The report of Azzopardi *et al.* (2002) outlines the design and installation of a T-junction partial phase separator within an operational plant. The final design proposed and installed within the plant is shown in Figure 2.18.

Essentially the problem faced by the plant operators was that only part of the liquid product from a reactor was flashed to vapour on passing through a valve before reaching a distillation column. That meant that within the column liquid was being carried upwards with the vapour, reducing the efficiency. A standard solution would be to install a conventional gravity separator, allowing the liquid and vapour to be fed

into different points of the column. This would have been expensive, time consuming and awkward within the confines of space available within an operational plant. The proposed geometry was based on knowledge of both T-junctions and the two-phase flow in pipes, especially at bends. The design is based on two principles, the idea that gas will preferentially enter the side-arm after the bend and the fact that when a two-phase flow travels around a bend, the gas tends to follow the curve, while the liquid will impinge on the bend wall. This will reduce the liquid entrainment within the gas stream, while the presence of the U-bend acts to prevent gas leaving in the liquid stream. The two streams, each rich in only one phase, are then introduced into the column at appropriate points, improving the efficiency of the column.

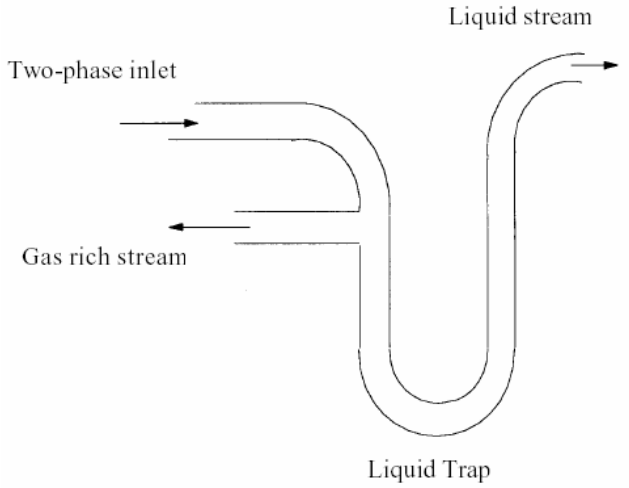

Figure 2.18: Proposed design of T-junction partial phase separator of Azzopardi *et al.* (2002)

From the onset it has been noted that the very different natures between stratified/slug and annular flows implies that the design on a compact T-junction separator would be influenced by the flow pattern encountered. The requirement of this work is to separate stratified and slugs flows, which have common phase distributions within a horizontal pipe. Interestingly, the design outlined above for the industrial plant

application, shows how the use of T-junctions could be adapted for the unique characteristics of annular flows.

The concept of utilising T-junctions as partial phase separators has produced a wide range of potential configurations and suggested improvements. The research effort that has been applied has gone some way to aid in the understanding of the phenomena of two-phase flows at T-junctions but nonetheless there are issues still to be resolved. In terms of improving the phase separation the above review highlights the main subjects for consideration. The reduction in the side-arm diameter in relation to the main pipe does provide better separation than a regular junction for fully horizontal geometries. However, in terms of achieving the set requirement of 10% v/v phase purities the most suitable option appears to utilise vertical side-arms. The lack of general models describing the phase split for such orientations highlights the amount of work still required in this area, although attempts at describing the downward problem are encouraging.

The inclusion of inserts and baffles, to try and divert the flow, have been shown to give some improvement of the phase split but their use is limited to specific ranges of flow conditions and flow regimes. So, while one insert configuration could aid the separation of stratified flows, it would adversely affect the T-junction performance under annular flow conditions. There are also other issues related to inserts, regarding the extra pressure drop and the difficulties in maintaining a clean pipe network, usually achieved by *pigging*.

Of all the improvements to phase separation, the combination of two, or more, junctions in series does provide the best solution to the problem. In a natural extension to the one junction problem it builds on previous knowledge and has been shown to be capable of handling a wide range of gas and liquid flowrates. However, as with most gas-liquid separation systems there is still a control issue to be addressed, which is inherently absent within T-junction systems. The inclusion of fluidic devices by Priestman and Tippetts (2002) to maintain a control level on the gas-liquid interface provides some indication of the possible route forward.

Industrially, however, the inclusion of fluidic devices could prove to be yet another factor counting against the embracement of T-junction technology. A more conservative approach to the issue of control would be to utilise standard control valves, as already widely used throughout industry. Although complicated separator designs have been suggested, combining several junctions, it is the simple case of vertically upward and downward T-junctions combined in series which is considered within this thesis. It is hoped that such a design, coupled with control valves, could go some way to promote the T-junction separator as a viable option within an intensified separation system.

2.3 Transient Two-phase Flow

The study of two-phase flow is a complex problem, which is further complicated when the flows are no longer considered to be at steady-state. Within industry there are many occasions when the flowrates will vary with time. Examples include start-up and shutdown of process equipment, changes in flowrates in response to planned operating conditions and emergency situations. Within the petroleum industry the problem of transient multiphase flow has lead to the development of many commercial numerical packages aimed at their prediction. Examples of such packages are TACITE™ developed by *Elf*, *Total* and *Institute Français du Pétrol*, or TRAFLOW from *Shell Research and Technology Amsterdam*. However, for obvious reasons these packages are not generally available, nevertheless researchers have developed less complicated methods of predicting two-phase flow transients. For comparison, two cases are considered here; transient flows in straight pipes and T-junctions.

2.3.1 Transient Flows in a Pipe

Transient two-phase flows can be considered in many cases. In general they can be thought of as a change from one steady-state flow condition to another steady-state condition. In most cases transient flows are introduced with an instantaneous change in either the gas or liquid flowrates, or possibly both simultaneously. However, it is

also viable to have a gradual increase/decrease in the relevant phase flowrate over a period of time. Depending on the production method of the transient, the characteristics of the resultant flow will be different.

For such an important aspect of industrial operations the subject of transient two-phase flow has received relatively attention in the literature. One of the first experimental investigations into transient flows was carried out by Sakaguchi *et al.* (1973). They used air and water in a transparent acrylic pipe with a diameter of 0.04 m and 8.1 m long with various sensors positioned to measure the liquid hold-up and depth and conductance probes to distinguish between the two phases at various points along the pipe. They examined the affect of air flowrate increases and decreases and liquid flowrate increases, paying particular attention to the flow pattern and flowrate variations. It was observed that for step increases in the air flowrate there was often a temporary transition flow pattern between the two final steady-state patterns. Thus for a sudden increase in the air flowrate where both the initial and final flows are within the stratified-wavy regimes a period of instantaneous slugging was seen to occur. This transitory effect was not observed for increases in liquid flowrate or for decreases in the air flow. It is the presence of these potentially unexpected intermediate flow patterns, especially slug flow, which are a concern to industry.

Following on from the results of Sakaguchi *et al*. (1973), Taitel *et al.* (1978) carried out their own experiments and developed a theoretical transient gas-liquid flow model for horizontal pipes by extending the steady-state analysis of Taitel and Dukler (1976). The approach was based on predicting a stable stratified liquid level which varied both with position along the pipe and time. The stability of this level to transient disturbances is explored according to four criteria, as defined previously in the steady-state model. The assumptions used in the model were that both phases are incompressible, the gas is at a quasi-steady-state, so that the axial flow is identical at every cross-section of pipe, and a negligible effect of surface tension. The authors go on to give detailed instructions on how to predict the intermediate transient flow patterns expected for changes in phase flowrate. They went on to test the theoretical

predictions against experimental data and found that the correct transition flow patterns were predicted and the transient time for the appearance of the first slug agreed within acceptable accuracy.

The main disadvantage in the use of theoretical equations for solving the transient flow problem is the need to solve simultaneous partial differential equations and the corresponding computational time overhead that entails. In view of this, there have been recent efforts to produce more simplified approaches to transient predictions. The first proposed simplified model was suggested by Taitel *et al.* (1989). They considered only the liquid continuity equation to be in a transient state, with the gas continuity equation and both phase momentum equations considered to be in a quasi-steady-state. This reduced the number of partial differential equations to one, for the liquid cross-sectional area as a function of time and space. It was assumed that for the relatively slow transient effects that occur in hydrocarbon pipelines, such simplifications were justified. The assumption of local momentum equilibrium allows the use of well accepted mechanistic models for the different flow patterns.

Taitel *et al.* (1989) selected which flow pattern equations to use within the transient model based on the steady-state flow pattern transition criteria for horizontal flow developed by Taitel and Dukler (1976). There are other possible approaches for detecting the local flow pattern in transient flow, for example, the use of the Kelvin-Holmhotz instability of liquid heights corresponding to the local liquid hold-up. Minami and Shoham (1994) suggested that the procedures for determination of the flow pattern boundaries within transient flow models were not adequate. They go on to propose a new approach based on the stability of slug flow. By assuming that slug flow is present within a pipe section, all the slug characteristics are determined from standard equations. Further analysis of these characteristics yields the actual flow pattern. For the stratified to annular boundary, the Kelvin-Helmhotz instability criterion is still used. This method, which could also be applied for steady-state situations, results in only one possible flow pattern for a given liquid hold-up and transitions occurring with minor liquid discontinuities.

Grolman and Fortuin (1996) elaborated further on the theoretical methodology of Taitel *et al.* (1978). In an attempt to improve the predictions they included the effects of changes in the gas phase dynamic pressure (Bernoulli effects), a liquid phase velocity profile and new equations for the frictional contributions to the loss of momentum. A typical output of the model for a decreasing gas transient is shown in Figure 2.19. The agreement between the simulation results and experimental data is very good, but the lack of comparative results for increasing gas transients or liquid transients is frustrating.

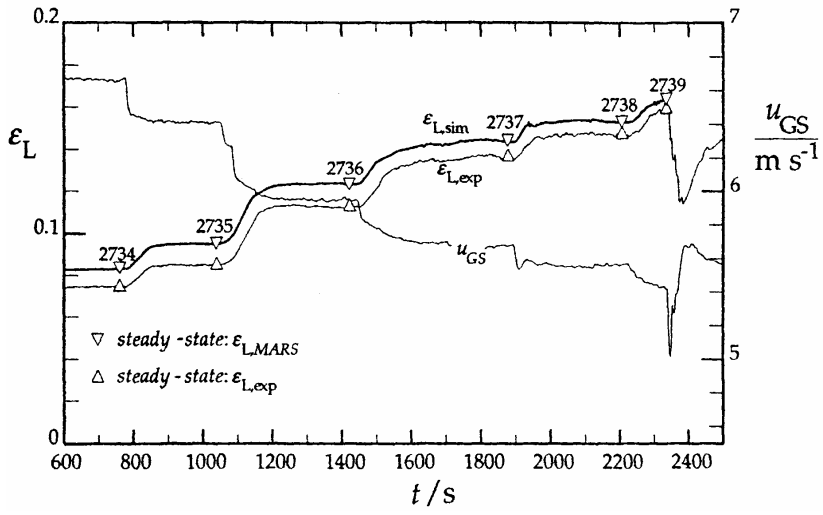

Figure 2.19: Sub critical gas transient model of Grolman and Fortuin (1996) comparing the simulated, $e_{L,sim}$, and measured, $e_{L,exp}$, liquid hold-up as a function of time

A later study by Taitel and Barnea (1997) highlights the poor treatment of the calculation of gas accumulation in the pipeline of the simplified methods of Taitel *et al.* (1989) and Minami and Shoham (1994). In their work a simplified numerical method is proposed that attempts to correctly treat the continuity equations for both the gas and liquid phases. The flow patterns are considered in terms of separated flow, for stratified and annular, and dispersed flows, for slug and bubble.

However, unlike the solution of Minami and Shoham (1994), there is the potential to obtain non-unique flow pattern determinations. In the decision process it is suggested that when two flow regimes are possible, one stable the other unstable, it is the unstable flow pattern that will occur. Thus in a choice between stratified and slug flow, it is slug flow that is considered dominant. Interestingly, the model also allows for hilly terrains, where the liquid can be considered to flow down the uphill slope against the direction of the flow.

An experimental study on the characteristics of transients within the slug flow regime has been carried out by King *et al.* (1998). The test section used was 36 m long with a diameter of 0.076 m using air and water. They performed experiments using various transient step changes in both the gas and liquid phases and considered four main transient effects, "up-gas", "down-gas", "up-liquid" and "down-liquid". For the case of gas transients they observed a pressure overshoot, for increasing flowrates, and a pressure undershoot, for decreasing transients. The magnitude of the overshoot was, unsurprisingly, a function of the magnitude of the gas flowrate change. For the inverse case of pressure undershoot, the results were less conclusive, because of the natural pressure variation present in slug flow, but similar trends to those observed for "up-gas" transients are evident. During the transient period it was observed that a larger slug developed, sweeping along the pipe at the new velocity, driven essentially by the gas flowrate. For "down-gas" transients a period of stratified flow was observed to exist as the liquid hold-up in the system adjusts to its new steady-state value and the slug frequency decayed over time. In both "up" and "down" liquid transient cases there are no changes in flow pattern and no evidence for large pressure fluctuations. The only change observed was either an increase, for "up-liquid" transients, or a decrease, for "down-liquid" transients, in the slug frequency, as predicted by standard slug models, for example Gregory and Scott (1969). Their study suggests that modelling slug transients using a series of quasi-steady-states may not be applicable because, unlike the liquid phase, some of the gas phase transient characteristics cannot be predicted using steady-state models.

2.3.2 Transient Flows at a T-junction

The problem of quantifying transient flows becomes even more acute once they are combined with T-junctions. Unlike the case of simple pipe flows, there are no commercial simulation codes for branching networks. This problem is addressed in part by Azzopardi (1993), who attempted to illustrate what may occur if there was a sudden change in the inlet liquid flowrate by considering the T-junction steady-state conditions before and after that change. The data was presented in terms of the actual liquid phase mass flowrates in both the side-arm and the run plotted against the fraction of gas taken off in the side-arm. Azzopardi (1993) considered annular flow, in both vertical and horizontal junctions, as well as horizontal stratified flows and vertical bubbly flows.

In the case of horizontal annular flow, shown in Figure 2.20, when 40% of the gas is removed the variation of the liquid flowrates in the side-arm is relatively small but the flow continuing in the run increases considerably. Azzopardi (1993) notes that an increase in the liquid flowrate, particular in the run, will increase the resistance in that part of the pipework and force more gas out of the side-arm. The change in liquid split would be expected to be small since the observed trends with gas fraction are also small. A change in the gas flowrate, with a constant liquid flowrate, would not affect the split of the liquid unless the gas flow reduced sufficiently to produce a transition to stratified flow, when the majority of the liquid would be expected to carry on into the run exit.

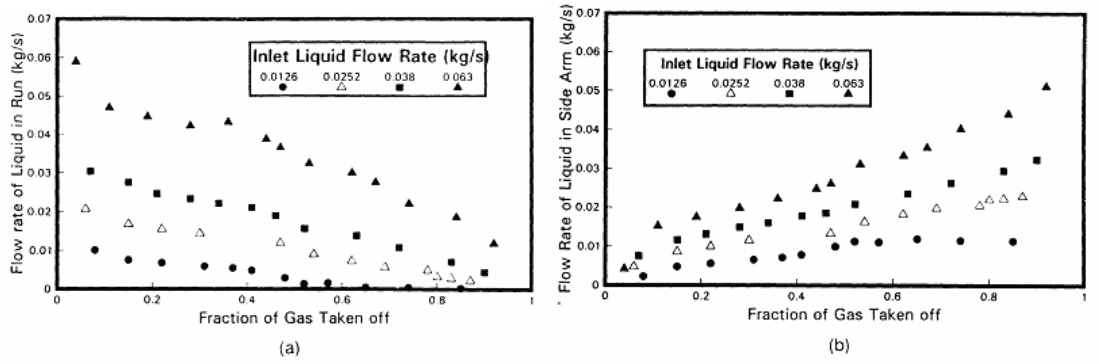

Figure 2.20: Flow rates of liquid emerging from (a) run and (b) side-arm for horizontal annular flow; gas flowrate at inlet = 0.101 kg/s

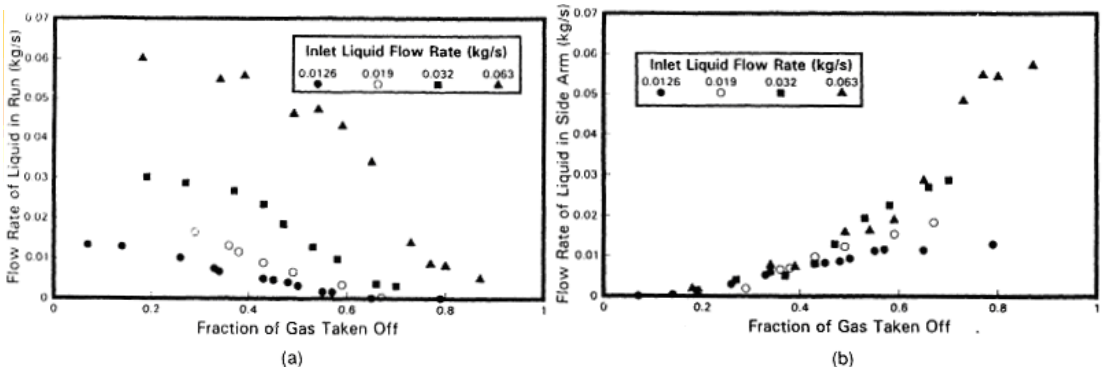

Figure 2.21: Flow rates of liquid emerging from (a) run and (b) side-arm for horizontal stratified flow; gas flow rate = 0.024 kg/s

For stratified flow approaching the T-junction, Figure 2.21, a reasonable separation can be seen with a gas take off of 30%, with the majority of the liquid flow emerging in the run. As for the annular flow case, increasing the inlet liquid flowrate results in the most of the excess liquid leaving in the run. However, this increase in liquid flow will cause an increase in the pressure drop at the run diverting more gas into the side-arm. This would then increase the liquid take off in the side-arm. Azzopardi (1993) concludes that with the extra downstream equipment required to cope with this extra liquid there may not be any real benefit for this particular split.

More recently, Ottens *et al.* (2001) have undertook a study on transient flows at a fully horizontal T-junction, following on from previous work by Ottens (1998). Both studies used a 0.051 m diameter regular T-junction, with an inlet-to-junction length of 8 m (160*D*), a run length of 12 m (240*D*) and a side-arm length of 6 m (120*D*). By continuously measuring the phase flowrates in the inlet, side-arm and run, the effect of introducing a transient could be monitored. Since these studies were mainly concerned with the problem of route selectivity of liquid condensate in natural gas transportation, the two liquid flowrates employed, 0.0009 m/s and 0.004 m/s, are significantly less than those used in this study.

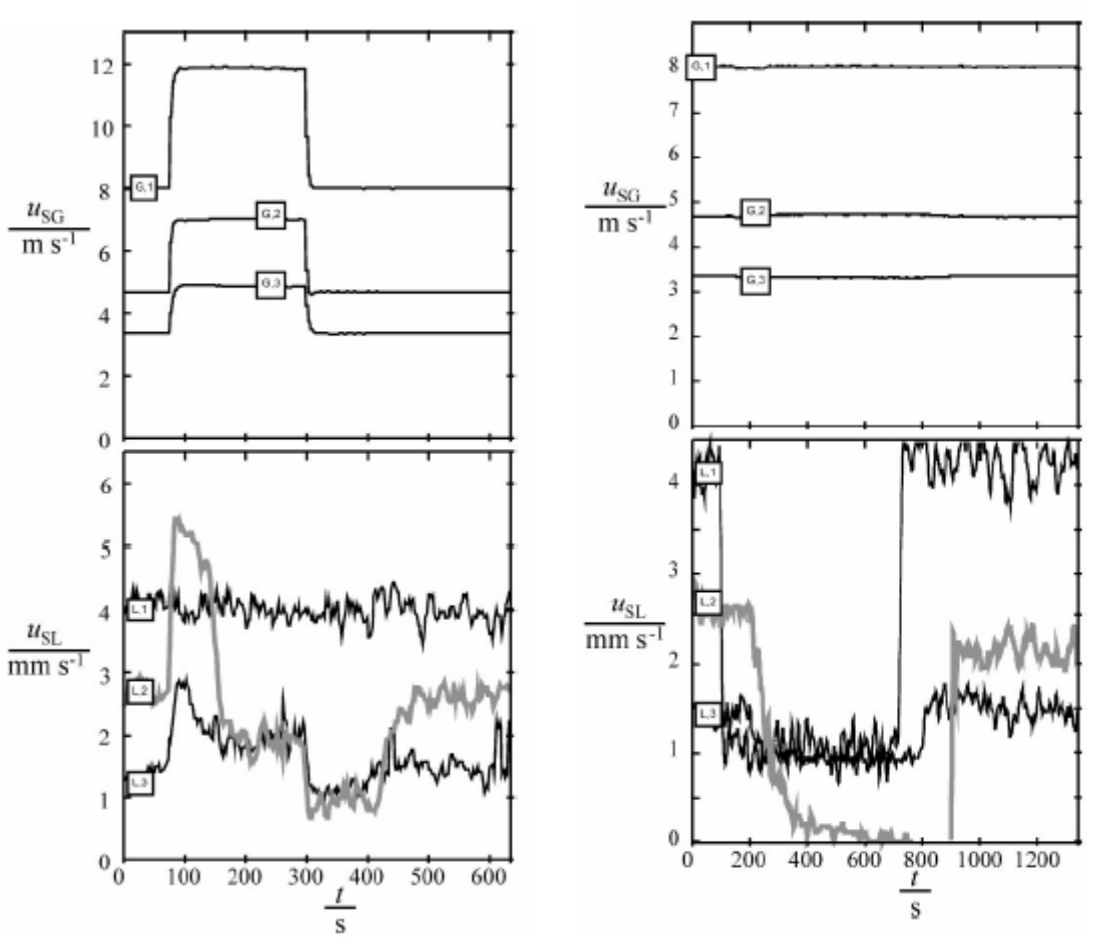

Figure 2.22: Transient gas-liquid flows at a regular T-junction. *Left*: U_{gs} transient 8 m/s to 12 m/s to 8 m/s with U_{ls} = 0.004 m/s. *Right*: U_{ls} transient 0.004 m/s to 0.0009 m/s to 0.004m/s with U_{gs} = 8 m/s

Due to the high gas quality it is unsurprising that the fraction of gas taken off is unaffected by the liquid transient, Figure 2.22 *right*, or that the take-off ratio remains constant during a gas transient, Figure 2.22 *left*. However, the situation is much more interesting for the liquid. For a sudden increase in the gas flowrate, Figure 2.22 *left*, the liquid outflows are initially higher, as liquid is swept out and the flow adjusts to the new higher void fraction associated with the increased gas flow. At this point, the liquid split ratio between the two exits remains unaltered by the surge. However, over time the phase split moves to a value corresponding to one expected for the high gas flowrate. When the gas flowrate is reduced back to the original value, the liquid goes

through a similar reverse sequence. The outlet liquid flowrates are temporarily lower, as the liquid builds up in the pipe, and eventually the liquid split reverts back to its initial value. For a decrease in the liquid flowrate, Figure 2.22 *right*, the effect on the liquid outlets is observed other a longer time period, eventually total phase separation is achieved but at a point in time after the feed has been increased again. Increasing the liquid flowrate back to the starting value produced a delayed but more dramatic change in the run outlet, while the side-arm response is more gradual. They also looked at decreasing the rate of change of the transient. This had no effect on the processes that took place but did reduce the liquid peaks at the onset of the transient.

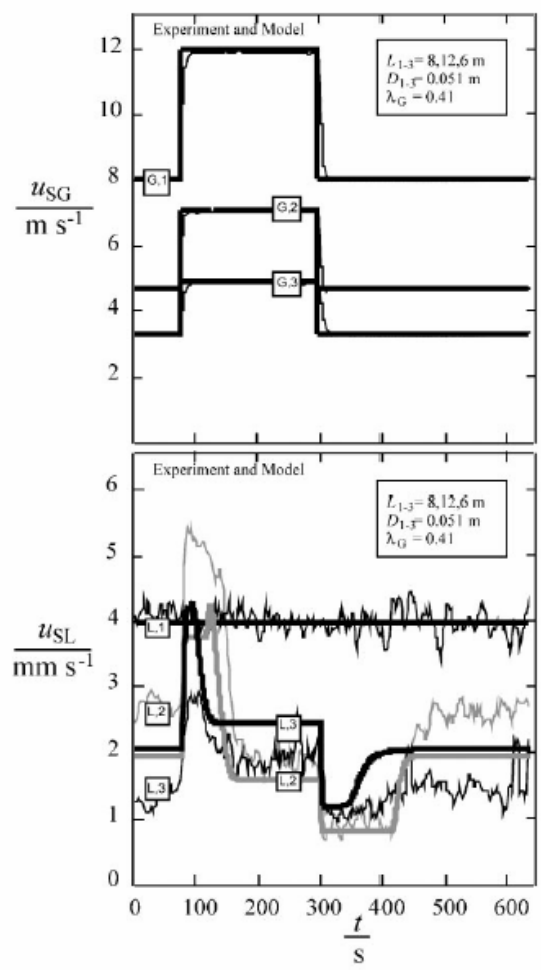

Figure 2.23: Comparison between the experimental results and transient model of Ottens *et al.* (2001). Thin line represents experimental data(as shown in Figure 2.15); thick line represents the model

Ottens *et al.* (2001) also provide a transient T-junction model based on their studies. This uses the T-junction route selectivity model for low liquid-loading flows developed by Ottens *et al.* (1994) based on the work of Hart *et al.* (1991) and the predictive model for transient flow in pipes as proposed by Taitel *et al.* (1978) and further modified by Grolman and Fortuin (1996). Figure 2.23 shows a comparison between their model and experimental data for a disturbance in the gas flowrate. The model follows the general trend of the experimental data well, although it tends to over predict the liquid flow in the run, while under predicting the liquid flowrate in the side-arm. It is unclear whether this is attributed to the model for the transient flow or the phase split.

2.3.3 Summary of Transient Flows

The prediction of transients within multiphase pipelines is a key issue for industry. This necessity has lead to the development of many commercial codes that are unavailable for research applications. Nevertheless, researchers have attempted to provide simplified approaches to the problem of transient flow simulation. The initial model suggested by Taitel *et al.* (1978) has provided the background for the majority of the models presented in the literature and has been subject to various moidifications, however, not all of them can be considered as improvements. It seems that within the expected accuracy of any two-phase flow calculations, the prediction of transient flows has reached an adequate level using basic assumptions providing relatively easy calculations.

However, whereas there are many commercial packages available for calculating transients in multiphase pipelines it is clear that there is a lack of information on the response of T-junctions to such flows. Since it is expected that transients are an unavoidable problem within the petroleum, and other, industries, this shortfall in knowledge has to be a concern and a probable reason why T-junctions are not used in situations where they could be advantageous. In order to justify the use of T-junctions as partial phase separators, it seems reasonable to be able to give some indication of the response of the system to fluctuations in the feed conditions. Hence,

this study will not only optimise the steady-state performance of the proposed T-junction separator but it will also examine the transient responses as an aid for future developments of transient T-junction models.

CHAPTER 3

Experimental Arrangement

Chapter 1 introduced the overall objectives of this study, with specific mention of the potential applications to the oil industry, whilst Chapter 2 reviewed the relevant literature on the concept of using T-junctions as partial phase separators. The objective of this chapter is to outline the experimental arrangements and equipment used here to investigate the phase separation characteristics of a T-piece separator. It describes, in detail, the methodology and procedures undertaken to acquire the necessary experimental data. Section 3.1 gives an overview of the entire experimental facility with Section 3.2 giving more detailed information on important facility components. Section 3.3 details the data acquisition hardware and software while the fluid physical properties are detailed in Section 3.4. Due to the choice of kerosene, as the liquid phase, in an attempt to better simulate gas-oil flows and to allow the use of electrical capacitance tomography, careful safety considerations had to be made. This produced a Safety Case, (Clark and Baker, 2000) for the experimental facility, detailing all aspects of design and operation. A summary of the key safety considerations along with the key operational procedures are then given in Section 3.5.

3.1 Overview of the Flow Facility

The experimental facility consists of two regular 0.0381 m internal diameter T-junctions placed in series. All the pipes have an internal diameter of 0.0381 m,

except for the air feed lines into the gas-liquid mixing section, which are 0.022 m internal diameter. Figure 3.1 presents a schematic diagram of the final revision of the experimental facility employed in this study.

In all the experiments the air is fed into the facility from the main laboratory 6 bar_a compressed air loop in 0.022 m internal diameter stainless steel pipes. A pressure regulating valve, RV1, sets the maximum air inlet pressure and a pressure relief valve, PV1, set at 110% of the required feed pressure, protects the facility against overpressure. A non-return valve on the air feed line, NV1, is situated just prior to the gas-liquid mixing section, thus preventing liquid entering the main air loop. Under steady-state conditions the air flow rate is adjusted by a gate valve V6, with gate valve V8 and actuated cock, AC2, both closed. For transient experiments both valves V6 and V8 are used in conjunction with the actuated cock, AC2. For high air flows AC2 is open while for low air flow rates it is closed. Both the air flow rate and gauge pressure are measured prior to entering the mixing section, using the differential pressure across a 0.016 m diameter orifice plate, with a digital manometer, and a standard pressure gauge, P1, respectively. All orifice plates used within these investigations were machined to the dimensions detailed in BS1042 and operated within the stated guidelines with the pressure tappings positioned a distance D upstream and $D/2$ downstream of the orifice.

The liquid feed is pumped into the facility from the main laboratory kerosene storage tank, TK2, situated outside of the laboratory, by a rotary gear pump, GP1. The liquid is isolated from the facility inside the building by globe valve V2. A recycle loop was installed to allow some, or all, of the kerosene to be returned to the main kerosene storage tank, TK2. This arrangement aided flow stability and allowed better control of the liquid feed flowrate then could be otherwise achieved by means of simple feed systems.

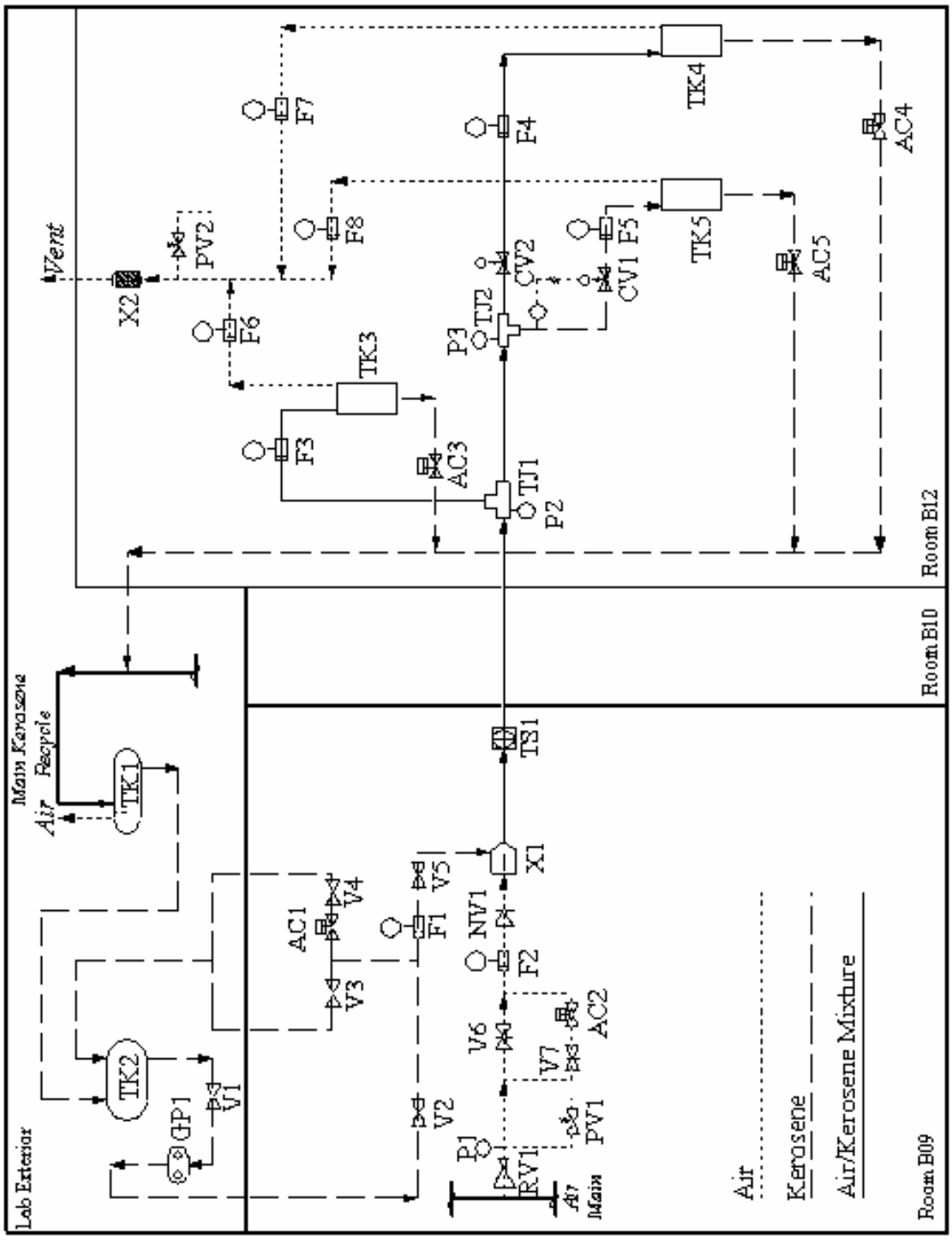

Figure 3.1: Schematic diagram of the final configuration the experimental flow facility

For normal steady-state operations the actuated cock, AC1, on the liquid recycle line was always open. Under steady state conditions the liquid feed flow rate is maintained by adjustment of globe valve, V5, with the actuated cock AC1 fully closed. During a transient experiment the actuated cock, AC1, is instantaneously closed thus reducing the recycle back to the main kerosene storage vessel and hence increasing the flow through the experimental facility. The liquid feed flowrate is thus set by adjustment of the three globe valves, two on the recycle, V3 and V4, and one just before the gas-liquid mixing section, V5. In either case the flowrate is metered prior to entering the mixing section by measuring the differential pressure across a 0.008 m diameter orifice, F1, using a calibrated digital output from a differential pressure transducer.

The two separate phases are then mixed at the gas-liquid mixing section, X1 (see Section 3.2.1). From the mixing section the two-phase mixture flows along 6 m of clear acrylic resin pipe sections before reaching the electrical capacitance tomography (ECT) device, TS1 (see Section 3.2.4). The transparent pipework allows important visual inspections of the two-phase flow. After the ECT unit, the two-phase flow travels a further 6.6 m to the T-junction arrangement. The middle 4 m section of this pipework consists of stainless steel pipe sections, for safety reasons as the flow facility traverses through an office space. The first T-junction, TJ1, with the side-arm orientated vertically upwards, is thus a total distance of 12.6 m from the gas-liquid mixing section. This gives a flow development length of approximately 150 pipe diameters to the ECT sensor and a total of approximately 330 pipe diameters to the first T-junction. Although these development lengths are shorter than the 600 pipe diameters suggested by Penmatcha *et al.* (1996) for steady state two-phase flow, the flow was still expected to be fully developed as it approached the ECT device. Both T-junctions are machined from acrylic resin, with sharp corners to eliminate the possible effects of the radius of curvature.

Beyond the first T-junction the facility is constructed in small modular pipe sections, of either transparent acrylic resin, where flow observations are desirable, or standard uPVC piping. The flowrate along any of the T-junction branches is affected by

closure of either a globe valve or a pneumatically activated control valve depending on the configuration of the facility. The pneumatic control valves themselves, *CV1* and *CV2* were linear valves supplied by Baumann Inc., Model 24688. The specific valve characteristic curves are presented in Appendix D. The modular design allows the layout of the facility to be easily changed, providing the flexibility to position the two control valves at practically any point around the system. All pressure measurements, both differential and gauge, are obtained using pressure transducers connected to the data acquisition system, as detailed in Section 3.3.

The gauge pressure, P2, is recorded 0.10 m upstream of the vertical side-arm of the first T-junction. The vertical outlet from the T-junction travels upwards for 0.99 m before turning through a 90° bend and travelling a further 2.06 m horizontally. For transient flow experiments orifice plates (see Section 3.2.3) can be installed 1.10 m along this horizontal section, F3. A series of horizontal 90° bends and small pipe sections then follow. Finally the two-phase flow is delivered into the separation tank, TK3, via another vertical 90° bend with a vertically downward 1.60 m pipe section.

The second T-junction, TJ2, orientated vertically downward, is positioned 1.89 m downstream of the horizontal exit of the first junction. The downward leg extends for 0.90 m before turning through a 90° bend and travelling 1.48 m horizontally. There is the facility to position an orifice plate 0.56 m along this horizontal pipe section for transient experiments, F5. The stream is then fed into the top of separation tank, TK5, via a small vertical pipe section. Again the gauge pressure, P3, is recorded 0.10 m upstream of the downward side-arm at the second junction. The final two-phase flow section, the horizontal outlet of the second T-junction, travels 1.01 m before turning horizontally through another 90° bend. The final section of pipe is 1.40 m long and again, there is a two-phase orifice plate positioned 0.44 m along this section for transient studies, F4. Another 90° vertical bend followed by a 0.43 m vertical pipe section feeds the flow into the final separation tank, TK4.

At these phase separation tanks (see Section 3.2.2) the air and kerosene are gravity separated. The liquid exit streams are at the bottom of each of the separation tanks

with a vortex breaker fitted above each exit to prevent gas pull through. Actuated cocks, AC3, AC4 and AC5, are positioned on each of the liquid exit streams and are closed during an experimental run thus allowing the tanks to fill with kerosene. Sight glasses on the side on the tanks allow a visual observation of the liquid level, while differential pressure transducers are used to collect experimental readings of the change in level of all three tanks. The three liquid exit streams combine before being gravity fed out of the building and into the separation tank, TK1. This vessel allows any entrained air bubbles to disengage before returning the kerosene, again using gravity, to the storage tank, TK2. The fraction of the inlet liquid that flowed into each separation tank is then determined from the integration of the change in liquid height in each tank over a known time period.

An air stream exits the top of each of the tanks through a knitted mesh pad installed to prevent liquid droplets emerging. The air flowrate for each individual stream is obtained by measuring the differential pressure drop across two orifice plates in series, one for high flowrates (0.031 m diameter) and the other for low flows (0.025 m diameter). These individual streams then combine in a larger 0.10 m diameter uPVC pipe. A water lute, branched off the combined air stream and with a one metre water depth acts as a pressure relief system, PV2, for the separation tanks.

For environmental and safety reasons it was necessary to ensure that the air vented to atmosphere was free from kerosene vapour. In order to achieve this requirement a packed bed absorber, X2, was installed in the combined air exit line. This consisted of a horizontal packed section with a constant square cross-section of area 0.0256 m^2 and a 0.30 m depth of activated carbon granules. A 0.15 m space was installed before and after the packing to encourage an even air distribution through the packing. The packing needed to be checked periodically to make sure that the bed had not been saturated.

3.2 Flow Facility Components

3.2.1 Gas-Liquid Mixing Section

The mixing of the gas and liquid phases must be done in such a way as to try and minimise the flow instability, thus providing maximum time for the two-phase flow to develop. This was achieved by using a purpose built mixing unit. The feed arrangements for the air and kerosene streams have already been described, in Section 3.1 above, both for steady state and transient experiments.

The mixing unit itself is made from a machined acrylic resin block (0.025 m (L) by 0.0235 m (W) by 0.0195 m (H)). The liquid feed is split after the flow control valve at a T-piece and the two streams are fed into the mixing section at opposite sides of the mixing block. Air is fed from the rear of the block directly into the 0.0381 m diameter machined section. The liquid is introduced into the two-phase stream through a porous wall section, thus creating a more even circumferential mixing effect.

3.2.2 Gas-Liquid Separation Tanks

The separation tanks serve two purposes, to separate the two-phase mixture, so that the kerosene can be returned to the storage tank and to measure the liquid mass split through the T-junctions. A schematic diagram of a tank is shown in Figure 3.2. Each tank was built in two separate pieces, to allow for ease of maintenance, and braced to maintain shape during operation.

At these phase separation tanks the air and kerosene are gravity separated. The two-phase mixture is fed into the top of each tank through a flow distributor system, to prevent jetting. A vortex breaker is fitted at the bottom of the tank to prevent gas entrainment when the tank is emptied. Actuated cocks are shut during a measurement period to allow the tank to fill with the liquid. This increasing liquid level can be monitored both visually using the sight glass and electronically using a differential

pressure transducer. The air stream exits the top of each of tank through a knitted demister mesh pad installed to prevent liquid droplets being entrained.

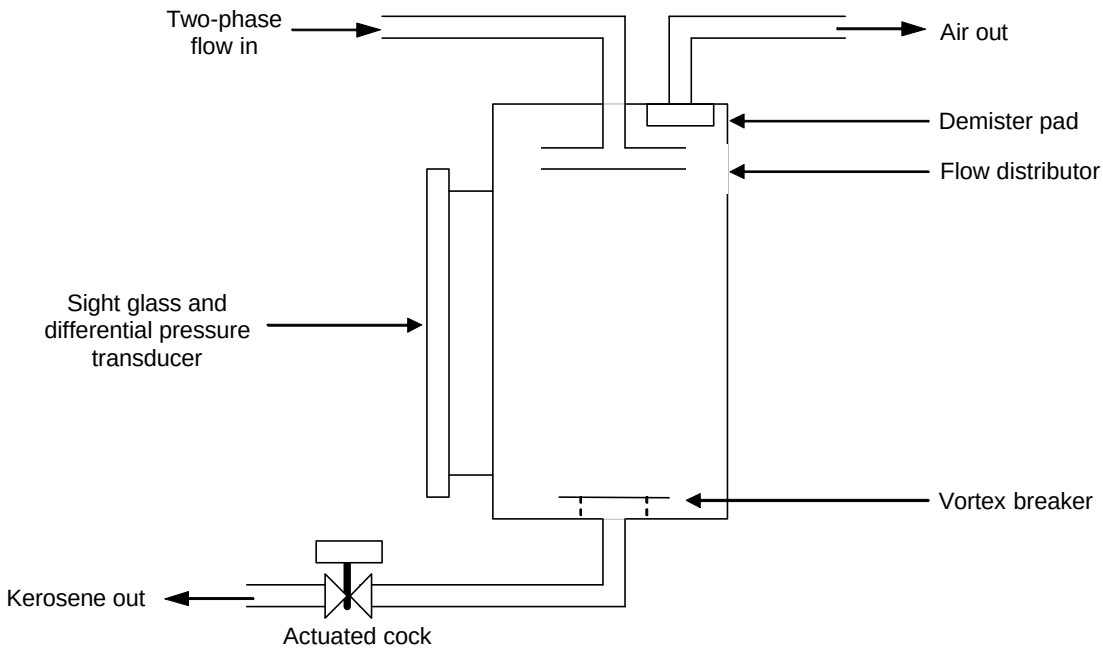

Figure 3.2: Schematic diagram of a separation measurement tank

3.2.3 Orifice Plate Meters for Two-Phase Flows

For studies on transient flows there was a requirement to be able to have a measure of the variation of the liquid phase mass flowrate from each of the exit streams with time. In order to be able to determine this information orifice plate meters were installed in these exit streams, prior to the separation tanks. In the case of the downwards side-arm of the second T-junction, which will be shown later to be a liquid-only exit stream, a conventional orifice plate meter, F5, with an orifice diameter of 0.013 m could be installed. However, the remaining two outlets had a requirement to deal with simultaneous gas-liquid flows.

The measurement of a two-phase pressure drop is not as straightforward as for single phase situations. A review by Lin (1986) discusses the use of orifice plates as a means of measuring two-phase flow and includes many published correlations for the prediction of the pressure drop. However since all these correlations are essentially semi-empirical relationships, Lin notes that they should not be used for applications outside of their corresponding experimental ranges and concludes that further research must be carried out within this area. A quick review of the various correlations indicated that they were nearly exclusively derived from high pressure data, where the density ratio of liquid to gas is in the order of 5:1. This is well in excess of the liquid/gas density ratio of approximately 500:1 in this work. It was thus necessary to do a manual calibration for the two-phase orifice plates employed within this study. Since the mass flowrate of the air travelling in any of the possible outlets is already measured, by the orifice plate meters F6, F7 or F8, there is a simple requirement to obtain a one-parametric measurement based on determining the liquid flowrate from the known gas flowrate and corresponding two-phase pressure drop.

The initial sizing of the orifice was based on expected flow splits determined from preliminary experimental results and the two-phase orifice correlation of Lorenzi and Muzzio (1977). They based their work on experiments with air-water mixtures at pressures in the range of 1.41 to 1.49 bar and temperatures of 14 to 18 °C. This gave an orifice size of 0.022 m for the first vertically upwards T-junction side-arm, F3, and 0.016 m for the second vertically downwards T-junction run arm, F4. A series of calibration runs were then performed where both the kerosene and air flowrates were set and the whole of the combined two-phase flow diverted along either the vertical T-junction path or the horizontal run arm path. The resultant differential pressure drop across the orifice was then recorded, using a differential pressure transducer. All the measurements were obtained over a 60 second time period, with a reading taken every 0.25 seconds. The final pressure drop and flowrates were then taken as the average of these 60 second data sets. This was repeated for a wide range of gas and liquid flowrates, spanning the extremes of the flowrates to be investigated within this study.

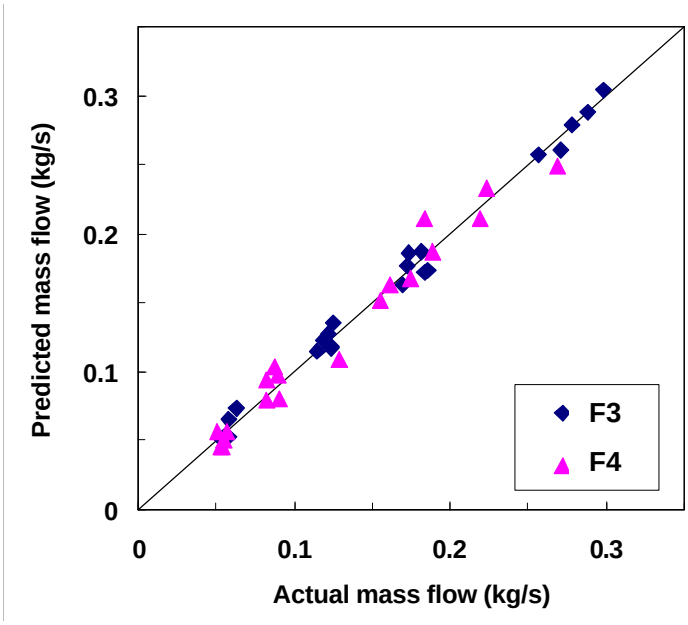

Figure 3.3: Predicted liquid mass flowrates using orifice plate meters for two-phase flow measurements

The resultant data were then implemented into a multiple regression calculation to obtain a function relating the liquid mass flowrate with the two-phase pressure drop across the orifice and the known air mass flowrate. Figure 3.3 shows the final predicted liquid mass flowrates, obtained by regression, against the actual liquid mass flowrates for the up arm, F3, and the run, F4. It is clear that the final predictive equations were in very good agreement with the actual experiment values. The final equations, which were implemented into the data acquisition software, had correlation factors of 0.994 and 0.970 for F3 and F4, respectively.

3.2.4 Electrical Capacitance Tomography Unit

As previously stated, it is known that the two-phase flow pattern approaching a T-junction will have a direct consequence on how those phases separate, Azzopardi (1993). It will also be shown later in this study that the knowledge of the flow pattern is an important factor for control purposes. The electrical capacitance tomography (ECT) unit, shown photographically in Figure 3.4, is a non-invasive and

online technique for the determination of the two-phase flow pattern inside a pipe. Since in this work interest lies only in the application of such a device, only a brief outline of the theory will be given here. For more detailed information the reader should refer to the edited work of Williams and Beck (1995).

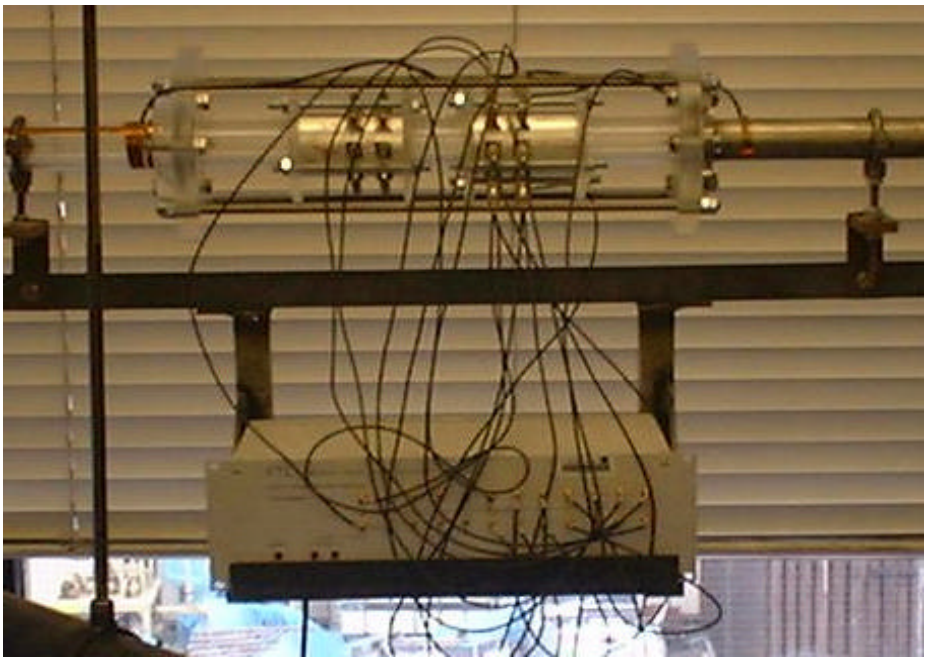

Figure 3.4: Photograph of the installed ECT device

The ECT sensor can be positioned anywhere upstream of the T-junction to provide information on the phase distribution across the pipe cross-section. The sensor, built by PTL Tomography Ltd, has eight circumferentially evenly distributed electrodes 0.035 m in length. It operates at a maximum rate of 100 frames per second, taking 23 ms to complete a cycle of measurements around the pipe.

The application of electrical capacitance tomography is truly non-invasive since the sensing electrodes are not in contact with the medium under observation. The imaging parameter, the permittivity, is the dielectric property of each of the phases in

the two-phase system. Figure 3.5 shows a cross-sectional view of the measurement principle of an eight electrode ECT sensor.

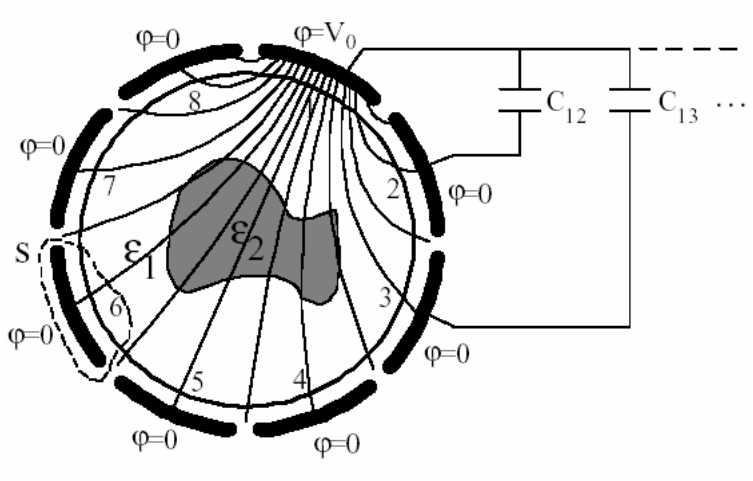

Figure 3.5: Measurement principle for an ECT sensor

In one measurement cycle, the electrodes are excited one by one, while maintaining the others at a reference potential ($j_i = V_0$, $j_j = 0$ *for* $i \neq j$) and the capacitance values are collected between the resulting electrode pairs, C_{ij} (where i is the firing electrode, $i,j = 1\ldots8$, $i \neq j$). Since the self-capacitances, C_{ii}, are ignored and the symmetry of the system is taken into account, so that $C_{ij} = C_{ji}$, it can be shown that there will be $n(n\text{-}1)/2$ available measurements, where n is the number of electrodes. In almost every ECT system, the frequency of the electrical signal used for the sensing field will be in the order of 1000 Hz. Therefore, it can be shown by Equation 3.1 that the wavelength of the electromagnetic field will be typically in the order of a few hundred metres.

$$l = c/f = 3\times10^8/10^6 = 3\times10^2[m] \qquad [3.1]$$

where c is the characteristic speed of electromagnetic propagation a vacuum and f is the frequency. Thus since the wavelength far exceeds the dimensions of the sensor the potential distribution inside the sensor abide by the electrostatic field theory and Poisson's equation can be applied.

$$\nabla.\left[e\left(r\right)\nabla j\left(r\right)\right]=0 \qquad [3.2]$$

The capacitance values obtained for a given electrical field distribution are expressed according to the ratio of the charge on the electrode, Q, to the potential difference, V_c, between the considered electrode pair. Equation 3.3 defines the capacitance, in terms of the Gauss surface, S (shown in Figure 3.5), encompassing the measuring electrode.

$$C=\frac{Q}{V_c}=\frac{\oint_S e\left(x,y\right)\nabla j\left(x,y\right)dS}{V_c} \qquad [3.3]$$

The final step is then to normalise the obtained capacitance values, so assigning them a value between 0 and 1. This involves a manual calibration of the system where for a given electrode pair, ij, the minimum and maximum C_{ij} values are obtained. This is achieved by taking the electrode pair measurements with the pipe full of the low permittivity fluid, C_{ij}^{min}, and again with the pipe filled with the high permittivity phase, C_{ij}^{max}. The normalised capacitance value is then obtained from Equation 3.4.

$$C_{ij}=\frac{C_{ij}^{effective}-C_{ij}^{min}}{C_{ij}^{max}-C_{ij}^{min}} \qquad [3.4]$$

The equipment, comprising the sensor and image reconstruction software, will be capable of detecting the flow pattern by comparison of various electrode pairs, as discussed in Chapter 2. As well as this flow pattern recognition approach the online reconstructed images are still available. This provides a virtual real time cross-sectional view of the flow in the pipe. Figure 3.6 shows a set of typical reconstructed

images obtained form the ECT system and the flow pattern determined using the electrode comparison approach.

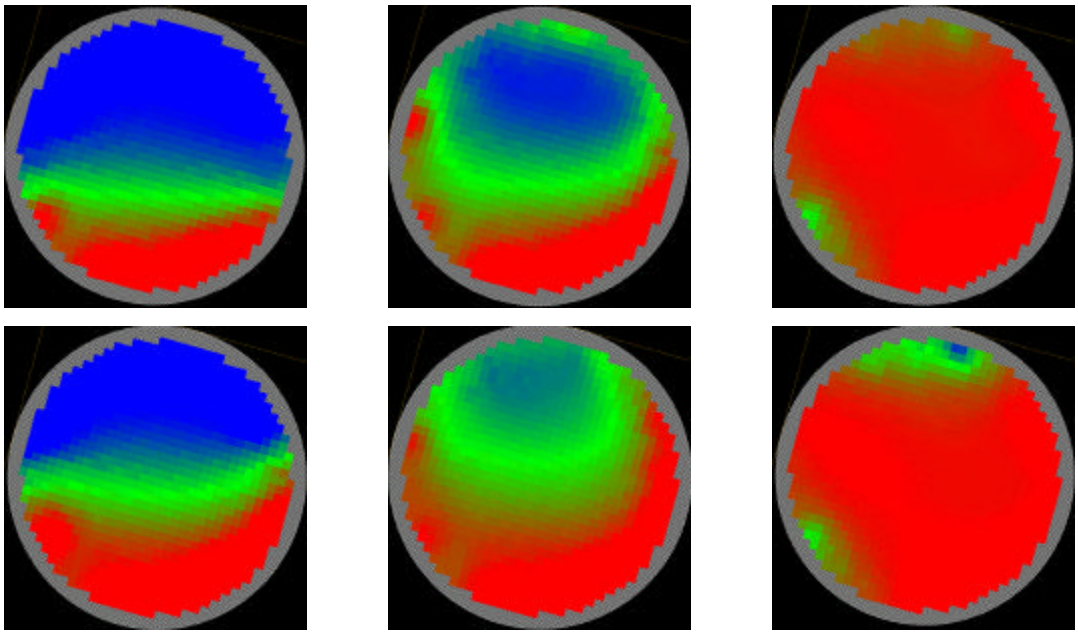

Figure 3.6: Typical online reconstructed electrical capacitance images

Here the blue areas represent the low permittivity component, in this case air, and red corresponds to the high permittivity phase, kerosene. The green areas indicate the transition boundary between the two-phases, produced as a result of the measured capacitance values being averaged along the length of the electrode.

3.3 Data Acquisition

Central to the experimental facility is the data acquisition system. This Section outlines the data acquisition system, both in terms of the hardware and software.

There are two main elements, the sensors to take the measurements, and the data acquisition system to process, display and record these measurement signals.

3.3.1 Data Acquisition System

Figure 3.7 shows the general configuration for the data acquisition system employed on this facility.

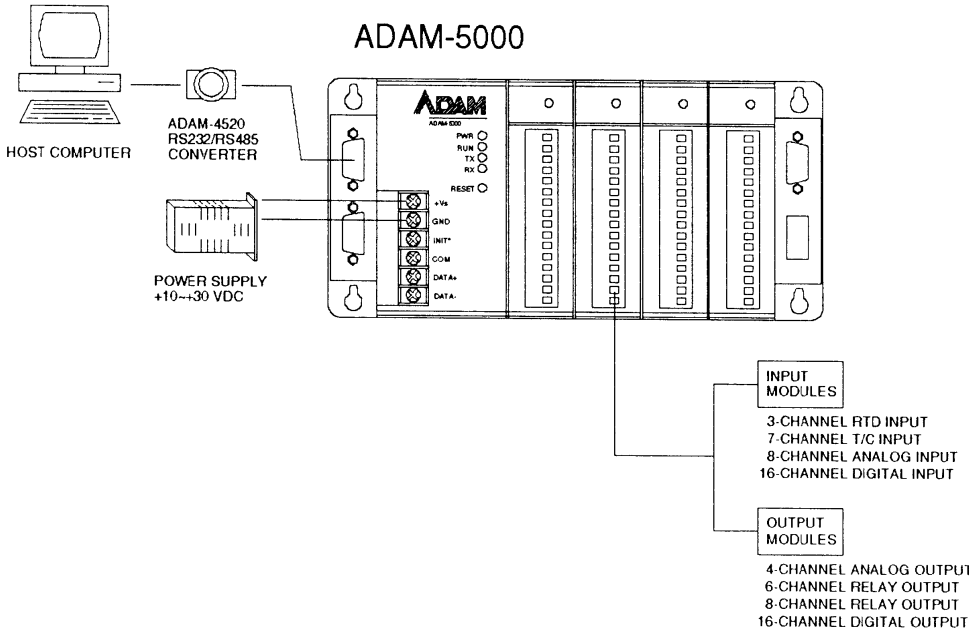

Figure 3.7: General configuration for an ADAM-5000 data acquisition system

The data acquisition system was based around the ADAM®-5000, supplied by Advantech Co. Ltd. This was connected to the control PC via a RS-485 data cable using a PCL-745S interface card, again supplied from Advantech. The data acquisition and visualisation software used was Advantech's VisiDAQ®. Relevant screen shots of the control software are given in Appendix D.

The major problem encountered with the system was a very poor signal to noise ratio associated with the differential pressure transducers whose output signal is in the range of 0 to 15 mV. In order to overcome this issue it was necessary to install an amplification circuit for the sensor output signals. This arrangement, shown in Figure 3.8, increased the signal approximately 100 times. However, since each amplification circuit produced a slightly different input/output ratio it was important that each sensor was assigned to an individual amplifier and each of these pairings were then manually calibrated.

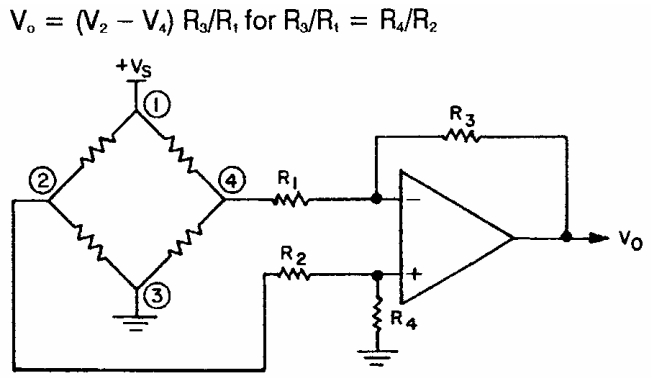

Figure 3.8: Amplification circuit used for the pressure transducers

3.3.2 Pressure Sensors

There are types of pressure transducers associated with the facility, one for measuring the gauge pressure and the other set for differential pressures. All were supplied by Micro Switch, a division of Honeywell Ltd.

3.3.2.1 Gauge Pressure Sensors

There was a desire to electronically record the gauge pressure at both T-junctions. For these measurements Type 24PC pressure transducers were selected. They

operated with a maximum pressure range of 6.8 bar_g (100 psi_g), a maximum response time of 1 ms, and a quoted linearity of ±0.25% of the span.

Each sensor was subject to an online calibration. This involved simply closing the exit valves on all three outlets from the T-junctions and incrementally increasing the feed pressure at regular intervals using a standard pre-calibrated pressure gauge. A typical calibration curve is shown in Figure 3.9, along with the correlation coefficient (R^2 value). The associated equations were then programmed into the data acquisition software.

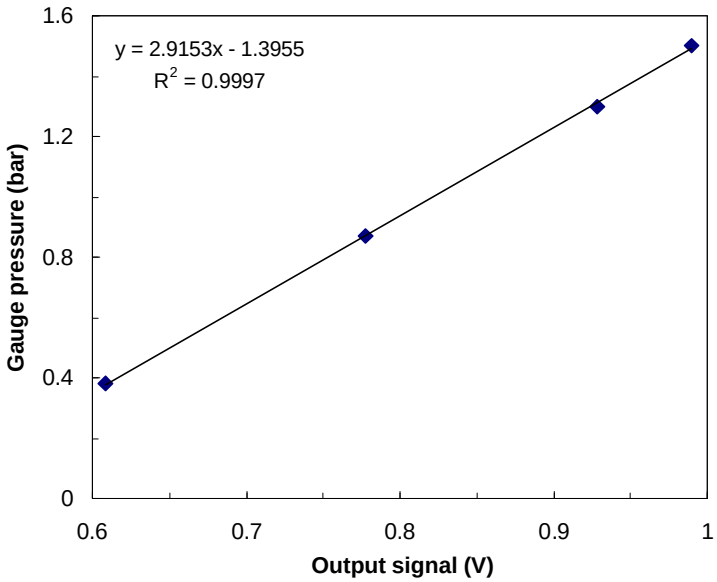

Figure 3.9: Typical calibration curve for a gauge pressure transducer

3.3.2.2 Differential Pressure Sensors

The differential pressure sensors were employed in the measurement of three different parameters, the air mass flow after the separation tanks, transient liquid flowrates at the orifice plates installed within the two-phase pipe sections and the liquid level in the separation tanks. Two different types of differential pressure transducers were used on the facility. The first sensor, Type 26PC, measured a differential pressure in

the range of 0-0.068 bar (0-1 psi), while the second one, Type 170PC, measured very low differentials, 0-0.017 bar (0-7 inches of water). These sensitive low differential pressure sensors were installed on the three air exit lines in series with the other sensors, thus allowing the entire range of air mass flows to be measured.

For the differential pressure transducers a simple manual calibration method was performed. This consisted of a large measuring cylinder, capable of holding a depth of water equivalent to 0.035 bar_g. The low pressure port of the sensor was left open to the atmosphere and a tube, attached to the high pressure port, was then carefully lowered into a known depth of water. The sensor output was noted and the procedure repeated for several different depths.

A typical calibration curve is presented in Figure 3.10 along with the equation and the correlation coefficient. As for the gauge pressure sensors the transducers all exhibited similar linear trends. It was unnecessary to span the entire range of the 26PC sensors because of the linear response of the transducers. As for the pressure gauge sensors the relevant calibration equations were then directly programmed into the visualisation software.

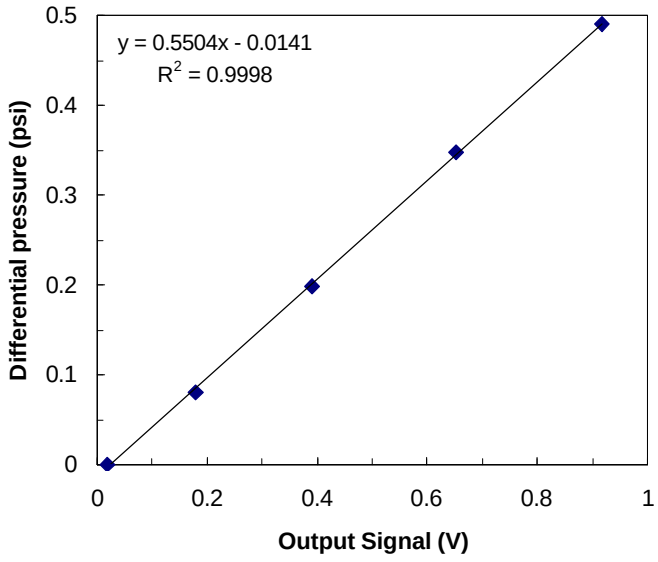

Figure 3.10: Typical calibration curve for a differential pressure transducer

3.4 Experimental Fluids

The selection of the liquid phase was based primarily on one important physical property, namely the relative permittivity. Due to the requirements of the ECT device the relative permittivity value for the liquid phase needed to be relatively low. This requirement therefore meant that water, which has a relative permittivity value of approximately $78.3\varepsilon_0$, could not be considered as a practical option. Table 3.1 outlines the relevant physical properties of the fluids employed for this study at atmospheric pressure and room temperature.

Table 3.1: Physical properties of the experimental fluids at 20 °C and atmospheric pressure

	Density (kg/m^3)	**Viscosity (kg/m s)**	**Permittivity Constant[1] (F/m)**	**Surface Tension (N/m)**
Kerosene	797	0.0018	$2.7\varepsilon_0$	0.034
Air	1.207	0.000018	$1.00059\varepsilon_0$	

[1] $\varepsilon_0 = 8.8542\ e^{-12}$ F/m

3.5 Operating Procedures and Safety Considerations

This Section gives details on both the operating procedures for the experimental facility as shown in Figure 3.1 and outlines the extensive safety review that was carried out prior to commissioning the facility.

3.5.1 Operating Procedures

In all situations, before starting the facility it should be checked for integrity before being used for any further investigations.

3.5.1.1 Start-Up

The procedure for start-up was as follows:

(i) Switch on electronics and computers and check the control valves are operational.

(ii) **Establish air flow:** The air needs to be introduced before the kerosene to prevent the kerosene back-flowing into the main compressed air line. For steady state experiments only valve V6 is used to set the flowrate, with valve V7 remaining closed. In transient experiments the lowest flowrate is set first, using the same method as for steady-state measurements, then the high flowrate is set by opening valve V7 with actuated cock, AC2, open. Obviously closing the actuated cock, AC2, will then return the flow to the low setting.

(iii) **Establish liquid flow:** Once the air is flowing it is safe to introduce the kerosene into the facility. The pump is turned on with the recycle lines open but the inlet to the flow facility, V5, closed. Sufficient time is allowed for the flow to stabilise around the recycle loop before valve V5 is slowly opened. The desired flowrate will be obtained by adjusting the recycle loop valves and the main facility inlet valve in combination. For transient experiments again both flowrates need to set prior to the experimental run, again using the same method as for individual steady-state measurements combined with the actuated cock, AC1. Closing the actuated cock, AC1, will reduce the recycle flowrate and increase the flow into the facility. Careful considerations must be taken in order to achieve both the low and high flowrates of transient experiments.

(iv) **Establish steady-state:** Once the air and kerosene are travelling along the pipe, the separation tank liquid exit streams need to be closed to allow the tanks to fill. Any valves should then be set in the position

required for the experiment. Sufficient time must be given to allow steady state to be reached within the system. Fortunately, this time period, in the order of several minutes, is essentially equal to the time it takes to fill the tanks up to a significant datum level.

(v) **Perform measurements:** Once steady-state is achieved the measurement period can begin. For steady-state experiments this means logging the measurement data over a five minute period. This time is limited by the capacity of the tanks, especially TK4 at the higher liquid flowrates, but is still more then sufficient time for reliable results to be obtained. Mass balances on both the air and kerosene are performed at the end of each run. The result is then recorded only if the mass balances obtained are all within ±5% of the required flowrates. Appendix B outlines the error analysis performed. For transients flows the data is logged continuously while transients of step changes in the gas or liquid flowrates are performed every 60 seconds.

3.5.1.2 Shutdown

The shutdown procedure is dependent on whether it is a planned shutdown or an emergency situation.

(i) **Normal shutdown:** For a planned shutdown the kerosene inventory in the separation tanks should be removed first, by opening the actuated cocks on the liquid outlets. The valves around the T-junctions should then be opened fully. The main kerosene feed valve should then be closed forcing all the liquid around the recycle loop before switching off the kerosene pump. This procedure prevents air entering the liquid loop when the kerosene pump is turned off. The air should be left running for a sufficient period of time as to clear the facility pipework of remaining kerosene. After the system is free from kerosene the air feed can be then be closed.

(ii) **Emergency shutdown:** In an emergency situation the emphasis is placed on stopping the flow and removing the current inventory of kerosene as quickly as possible. Thus the emergency procedure involves switching off the kerosene pump and the control system, since all automated valves are designed to fail open. The air should be left running to help remove the kerosene as quickly as possible from the system.

3.5.2 Safety Considerations

Safety was considered paramount during the design, commissioning and experimental operation of the flow facility. A thorough review of all aspects of safety, including maintenance, safe-working practices was performed by Clark and Baker (2000). This included a HAZOP study of the possible hazards, performed under the guidelines of Sinnott (1993).

The study considered three potential areas of risk. These were explosions and fires, contamination and pollution. It was concluded that through normal safe practices and the inclusion of special precautions, for example the installation of a bund wall around the separation tanks, any risks could be significantly reduced.

The major area of concern was the potential to form mist flows of the air-kerosene mixture within the pipelines. A mist flow can be characterised as a two-phase mixture where the liquid travels as very small droplets, in the order of 50 microns in diameter. Such flows behave like vapours and would be more susceptible to explosives risks than other two-phase mixtures. Calculations were performed to assess the likelihood of such flows forming in the pipework. It was found that only a small fraction of the kerosene, less than 8% in the worst case and normally much less than 1%, would travel as very small droplets over a very wide range of gas and liquid superficial velocities.

Based on these calculations, a maximum gas superficial velocity was imposed on the facility well within the boundary where mist flows could start to form. Thus the maximum gas superficial velocity was set at a conservative 10 m/s. This still allowed a full study of the stratified and slug flow regimes. It was also noted that the problem of mist flow formation would be enhanced by the presence of obstructions to the flow, such as orifice plates and control valves. To reduce this possibility, coalescent mesh was placed immediately downstream (1-2*D*) of all such constrictions.

CHAPTER 4

Simulation of a T-junction

The integration of control valves and T-junctions to provide flexibility and control to a T-junction partial phase separator is an all together novel concept. Most T-junction work has been motivated by fundamental flow split studies, where fixed resistances on the two exit lines are used to generate the phase split characteristics of a junction. The work presented here steps beyond this and seeks to examine how these resistances can be manipulated to control and exploit the flow split. As a precursor to the main work a feasibility study has been carried out based around a simple T-junction separator with actively controlled valves positioned on each outlet. By means of computer simulation based on previous knowledge of two-phase flows and T-junctions the modelling became a preliminary exercise prior to the onset of the experimental work. The objectives for the simulation work were to gain insight into the principal features of the proposed component integration and to develop simple active control strategies that could then be used, at least in part, as a precursor to the to the experimental work.

4.1 T-Junction Separator Under Active Control

The primary goal of this work is to develop a T-piece separator, utilising a combination of T-junctions, control valves and a flow detection system. As discussed in Chapter 3 the flow pattern identification will be provided by the electrical capacitance tomography system. Such tomography sensors can provide information

on three key variables, the stream quality, the flowrate and the phase distribution, or flow pattern, within the pipe. A notional T-piece separator with active control, as shown in Figure 4.1, would be based on measurement data obtained via tomography units (labelled FXTs) mounted both upstream and downstream of the junction. The two automatic control valves could then operate under a non-linear and adaptive control strategy based around the application of known two-phase flow correlations as appropriate to the known flow regime approaching the separator.

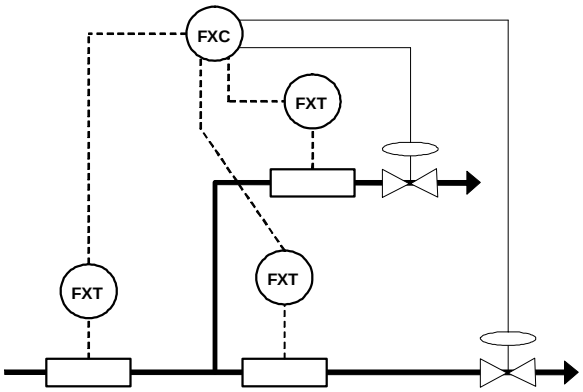

Figure 4.1: Notional T-piece separator with active control based around electrical capacitance tomography (FXT)

4.2 Process Description and Modelling

The formulation of the simulation model is based on consideration of the case of a fully horizontal regular T-junction with a control valve positioned on both exit streams. The assumption of a fixed pressure source, as opposed to a fixed flowrate, is made somewhat arbitrarily, as there is no clear consensus on the operation of an actual oil well riser. However, the choice does link more closely with the operation of the actual experimental facility.

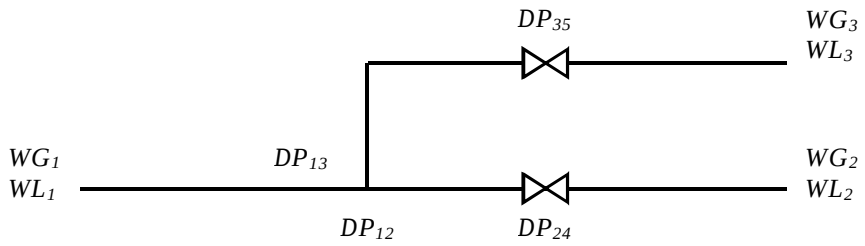

Figure 4.2: Schematic diagram of a horizontal T-junction with control valves on exit streams

Figure 4.2 shows a schematic of this junction configuration and highlights the key parameters that need to be considered within the simulation model. A complete description of the developed model is presented in Appendix C.

The mass flowrates of the gas and liquid are represented by WG_i and WL_i, respectively, where *i* indicates the stream under consideration, the inlet (1), run (2) or side-arm (3). There are two pressure drops associated with the T-junction; inlet-to-run, DP_{12}, and inlet-to-side-arm, DP_{13}. Finally there are two further pressure drops associated with the control valves, DP_{24}, for the run, and DP_{35}, for the side-arm.

The steady-state performance for such an arrangement has been investigated by a number of authors (including Shoham *et al.*, 1987, Azzopardi *et al.*, 1988 and Hwang *et al.*, 1988), for a wide range of flow conditions and various flow regimes. They have examined both the phase split characteristics of a gas-liquid feed and the pressure variations associated with the T-junction. Since the majority of the published material focuses on stratified and annular flows, the simulation will only consider these two flow regimes.

In order to completely represent the T-junction and control valve system there needs to be a numerical description of all pressure drops as well as the two-phase flow split. The inlet-to-run pressure drop, DP_{12}, is described by a momentum balance approach while the inlet-to-side-arm pressure drop is based on the homogeneous model. The pressure drops across the control valves, which are taken to be significantly higher

than those at the junction, are described by the equations of Morris (1985). For the initial description of the flow split the model of Shoham *et al.* (1987) was used. That model was based on the existence of dividing streamlines for both annular and stratified flows approaching the junction.

To overcome the high computational overhead time associated with the solution of the two-phase flow equations at each integration step, the flow split model of Shoham *et al.* (1987) was first solved across a wide range of regularly spaced flow conditions. The matrix of data points produced could then be directly interpolated within the simulation for the given flow conditions at each integration step.

All the appropriate equations that describe the pressure losses along with the phase split data set, were then implemented within a Matlab® code and solved using standard numerical integration methods as outlined in Appendix C.

4.3 Simulation Results

The purpose of the simulation is to provide some insight into how a T-junction might perform under active control. For the simulation runs a set of nominal operating conditions were chosen, for each flow regime, and the control valves were then moved at set increments across their range of operation. It was found that at extreme flow splits the phase split model became very sensitive and occasionally unstable, thus placing a lower limit on the valve fraction open of 0.2 for both valves. A sign of this instability is observable in the annular flow results as a sharp deviation occurring at the *x-y* intercept.

4.3.1 Effect of Flow Pattern on Simulation Model

Figures 4.3, for stratified flow, and 4.4, for annular flow, show the outputs of the simulation utilising the flow split model results of Shoham *et al.* (1987).

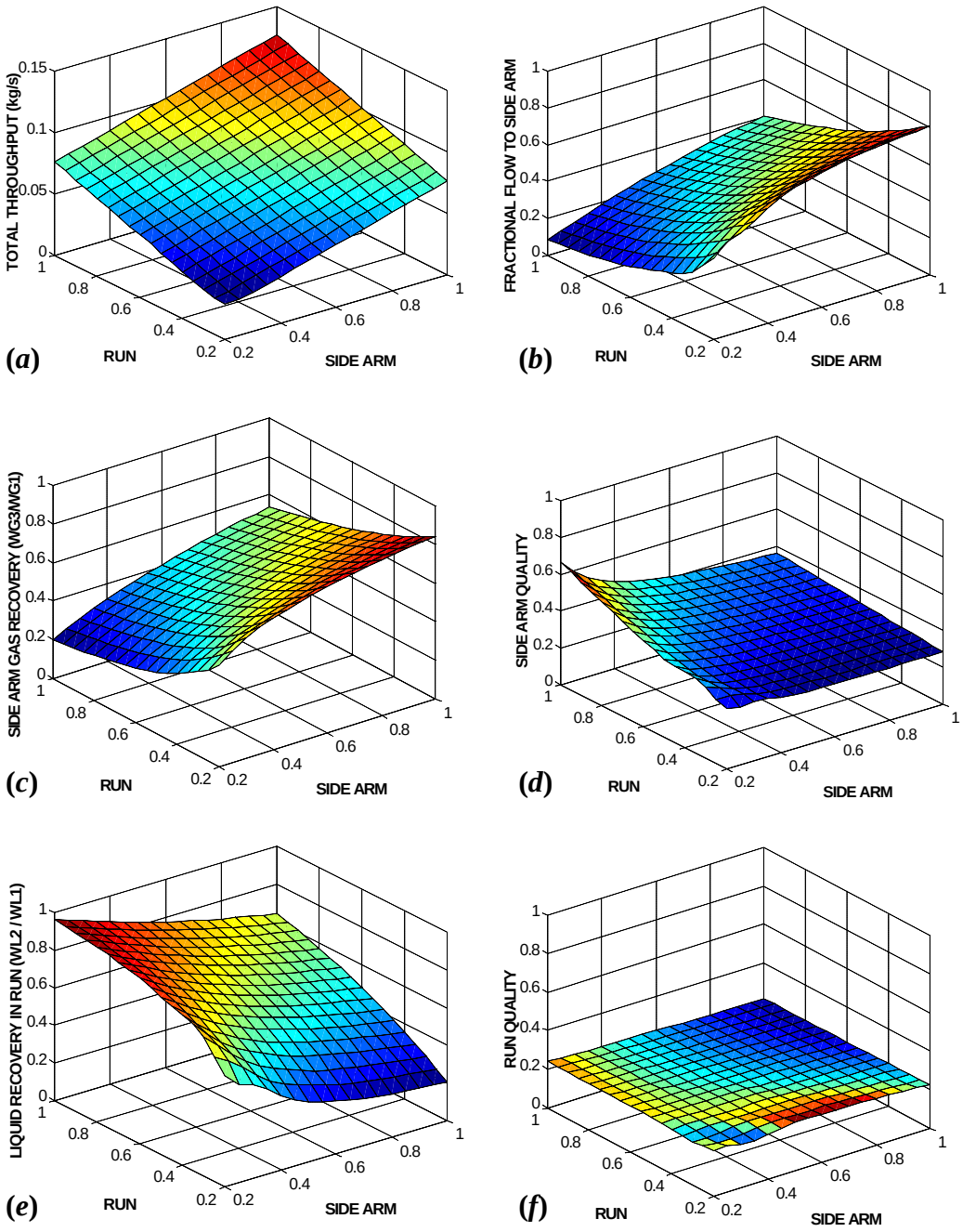

Figure 4.3: Simulation results based on stratified phase split model of Shoham *et al.* (1987) showing effect of run and side-arm valve fraction position (1 is fully open)

(a) Total mass flowrate **(b) Flow fraction in side-arm**
(c) Fraction of feed gas in side-arm **(d) Side-arm quality**
(e) Fraction of feed liquid in run **(f) Run quality**

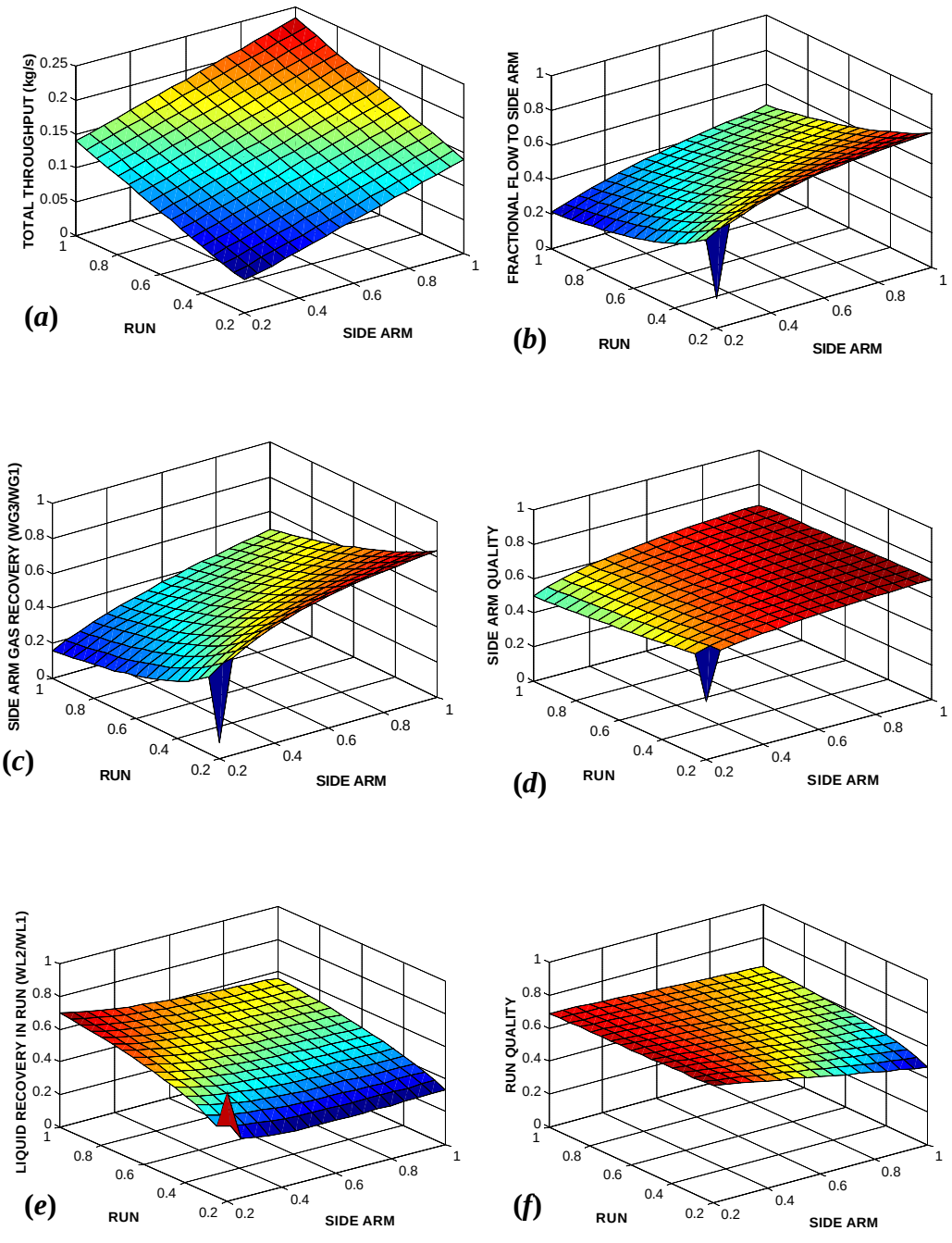

Figure 4.4: Simulation results based on annular phase split model of Shoham *et al.* (1987) showing effect of run and side-arm valve fraction position (1 is fully open)

(a) Total mass flowrate **(b) Flow fraction in side-arm**
(c) Fraction of feed gas in side-arm **(d) Side-arm quality**
(e) Fraction of feed liquid in run **(f) Run quality**

As expected the total throughput of the system becomes effectively a linear function of valve setting, see Figures 4.3*a* and 4.4*a*. Thus a fixed value of total fluid throughput can be maintained by equal counter-movement of the control valves. However, because of the nature of two-phase flow passing through a T-junction, there is a maldistribution of this total flow. This effect can be observed in both the stratified and annular flow cases, Figures 4.3*b* and 4.4*b* respectively, although it is more pronounced within the stratified regime.

Examination of the two outlets, which should correspond to gas-rich and liquid-rich streams, gives some indication of how the two phases are distributed at the junction. Considering the case of stratified flow, there are several key features that are highlighted by comparison of Figures 4.3*c*-*f*.

As the side-arm valve is gradually closed, the quality of the side-arm stream increases, Figure 4.3*d*. However, this increased quality is a combination of two factors, a low gas fraction in the side-arm, Figure 4.3*c*, coupled with a very high liquid recovery in the run, Figure 4.3*e*. Thus, while the side-arm quality is high, it only corresponds to a very small stream mass flowrate, with less than 10% of the inlet flow being diverted. This is due to the fact that gas will preferentially enter the side-arm, while the liquid, which travels with a much higher momentum, will tend to carry straight on into the run. As the run valve is closed the resistance to the flow down the run will increase and more of the flow will be diverted into the side-arm. Hence, while the gas recovery in the side-arm increases, the liquid recovered in the run decreases. At the point where the side-arm valve is fully open and the run valve is 20% open, the qualities in both outlets tend to the same value, but approximately 80% of the inlet flow is leaving through the side-arm. In all cases the run quality, Figure 4.3*f*, is essentially constant, with the value being unaffected by the position of either control valve.

For the annular flow case, the results show a similar, but less pronounced, trend to that observed for the stratified flow model. The only difference is that both the side-arm and run qualities are shown to be almost constant over the entire range of

flow conditions. This distinction can be attributed to the higher qualities associated with the annular flow regimes.

4.3.2 Separation Performance

In order to evaluate the separation performance of the junction a Separation Factor, S_F similar to that used for distillation calculations, was defined in terms of the gas-liquid ratios of the two outlets. Hence,

$$S_F = \frac{WG_3}{WG_2}\frac{WL_2}{WL_3} \qquad [4.1]$$

where, WL_i/WG_i is the liquid/gas mass flowrate (kg/s) in the run (2) or side-arm (3).

For gas dominated take-off through the side-arm, the Separation Factor becomes greater than one, for liquid dominated take-off it becomes less than one. When the factor is equal to unity there is no phase separation occurring. Figure 4.5 gives the variation of the separation factor in terms of the movement of the control valve.

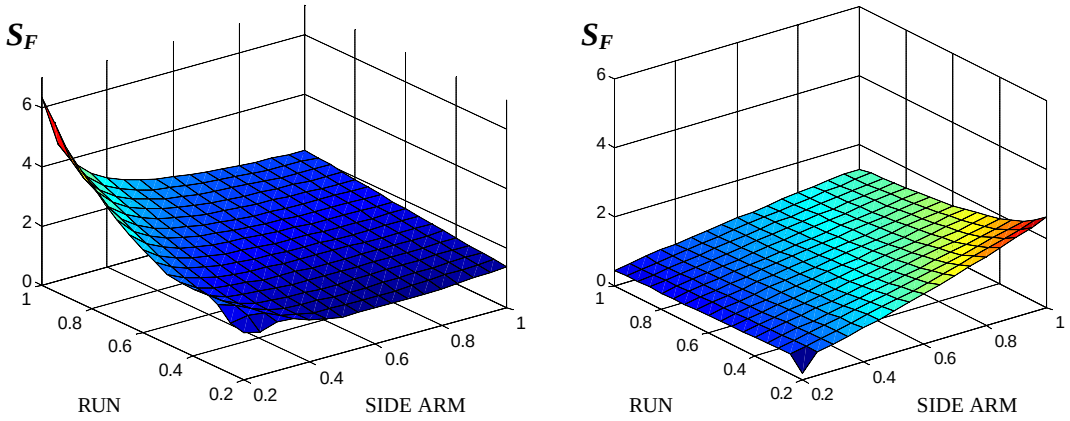

Stratified **Annular**

Figure 4.5: Effect of run and side-arm valve fractional positions on the Separation Factor, S_F

On a basic level it is clear that there is a performance difference between the two cases, with the stratified flow attaining a maximum separation factor approximately three times higher than the annular flow case. Generally the separation achieved is much better for the stratified case than for the annular flow case, indicated by the higher values of the separation factor. This can be attributed to the characteristic differences between the two flow patterns. The optimum separation for stratified flow occurs when the side-arm valve is nearly closed and the run valve is fully open, while for annular flows the situation is reversed, with the run valve slightly open and the side-arm valve fully open. This corresponds to the observations made in Section 4.3.1, relating to the diversion of the gas-liquid flow around the system.

4.3.3 Effect of Phase Split Model on Simulation Results

From the above it is clear that there is an effect of flow pattern on the separation performance of the T-junction model, a fact already highlighted within the reviewed literature. However, the complexity of two-phase flow, with the added complications of flow through a junction, makes accurate predictive modelling difficult. As previously mentioned many different authors have studied the flow split at T-junctions and they have all suggested different models to try and describe the phase split phenomenon. In order to try and assess the influence of the phase split model on the results of the simulation model it was repeated with a different model.

The annular flow regime was chosen for comparison and the new model chosen was that of Azzopardi (1988) with the modifications of Hurlbert and Newell (2000) to allow for circumferential film variations. The reason for the choice was that the annular flow model of Shoham *et al.* (1987) has been shown, by Azzopardi (1999b), to be rather simplistic in modelling the real situation. It basically assumes that there is no entrainment of liquid drops within the gas core and that the circumferential film is evenly distributed around the pipe wall, so neglecting gravity effects. Both of these assumptions have to be considered as poor approximations to the actual flow pattern. The model of Azzopardi (1988) takes into account both phenomena, giving a much better description of the actual flow pattern.

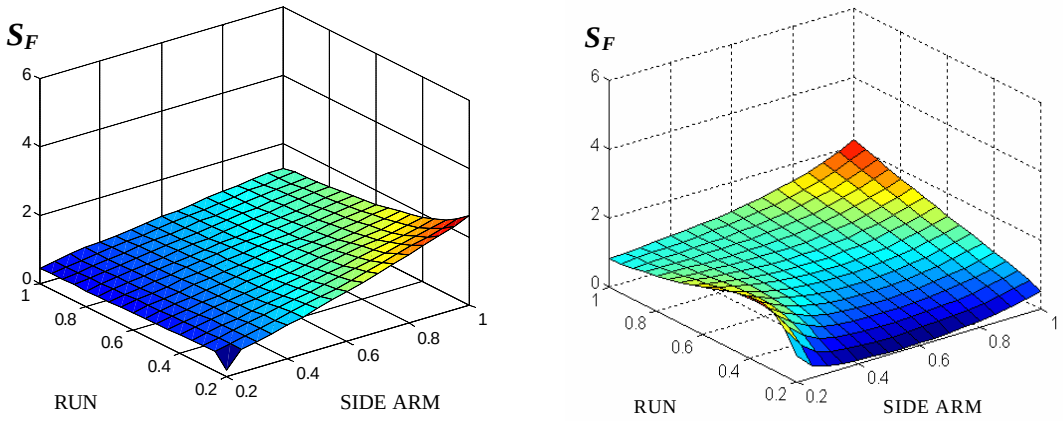

Shoham *et al.* (1987) **Azzopardi (1988)**

Figure 4.6: Comparison of the Separation Factor for the annular flow T-junction models of Shoham *et al.* (1987) and Azzopardi (1988)

A comparison for the two different flow split models is based on the Separation Factor, since it has been shown that this Factor conveys all relevant information about the performance of the junction. Figure 4.6 shows a comparison of the Separation Factor for the two annular flow cases.

It is clear that there is a distinct difference between the two different models in the prediction of operation of the junction, although the maximum values of the two separation factors are essentially equal. In the case of the model of Azzopardi (1988) the result indicates that there is no benefit to be obtained from using the control valves on either exit legs as the best separation is achieved with both valves fully open. Closing the run valve reduces the separation, as more of the total flow is diverted into the side-arm, this is in contrast to the prediction of Shoham *et al.* (1987) that indicate that the high momentum liquid by-passes the side-arm even when the run arm is 20% open. Closing the side-arm will reduce the total flow taken off through it but it also increases the quality, hence the slight increase in the phase separation.

The reasons for the discrepancies are found in the modelling of the annular flow regime. As was stated previously, the model of Shoham *et al.* (1987) presents a simplistic representation of annular flow, while Azzopardi (1988) attempts to introduce both liquid entrainment and variable circumferential film thickness. Obviously closing the run valve forces more gas and, hence, more entrained liquid into the side-arm, reducing the separation performance.

4.3.4 Control Strategy

The reason for considering the simulation model results is not to design the separation system, as it is already been known that the phase separation performance of a regular horizontal T-junction is not sufficient to fulfil the defined separation criteria. Nevertheless, the simulation was useful in validating the concept of developing an active T-piece separator.

Analysis of the combined T-junction and control valve problem indicates that for a system like that defined in Figure 4.1 there are two degrees of freedom for operation and control purposes. This implies that independent positioning of the two control valves will fully define the system performance. Remembering that the simulation has already been designed to operate with a fixed pressure, in accordance with the experimental facility, then one primary variable for control is the total fluid flow through the system. The remaining degree of freedom is then taken up by the control of the separation performance, which is akin to the side-arm quality. Under the conditions of fixing the side-arm quality, the prime objectives of the control scheme would be to maintain the total throughput while meeting the side-arm quality targets, in the face of varying feed conditions.

Considering the case of stratified flow, for the two chosen regulated variables, the simplest strategy to employ would be a conventional Single-Input-Single-Output control strategy. The question that then has to be answered is the choice of which measurement/control valve pairing is the most favourable. Work by Wilson *et al.* (2000) suggests that Relative Gain Array (RGA) analysis can be used to

gain insights into the possible combinations. Such analyses indicate that the best combinations are to control the total throughput by adjustment of the side-arm valve, with the side-arm quality then being controlled by the run valve.

Contour plots of the two process variables, total throughput and side-arm quality as functions of steady-state valve positions are shown in Figure 4.7. These plots give some indication of the degree of interaction. The straight diagonal lines represent values of constant flow through the system, while the curved lines represent values of constant side-arm qualities. In each case three contours are shown, with the central one representing the target set point.

For an idealised situation, where there is no interaction between the controlled variables, the contours would form a grid of perpendicular lines parallel to the axes. In that situation changing the position of one valve would only affect one variable. For example, opening the run valve to change the throughput would have no impact on the side-arm quality. Clearly, in real process operations such a situation can never feasibly be achieved.

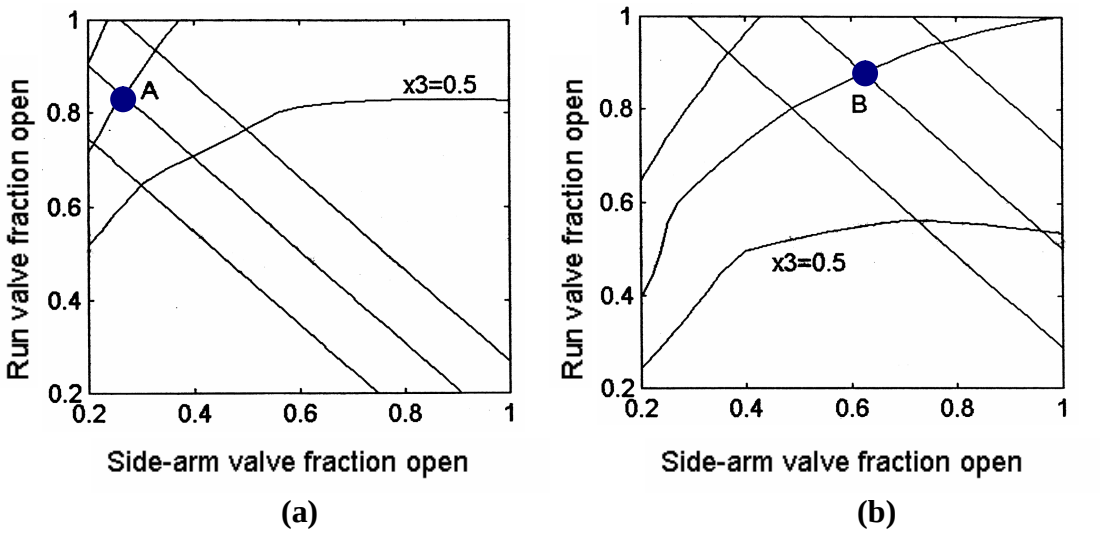

Figure 4.7: Contour plots for stratified flow for (a) normal inlet feed quality and (b) 50% higher feed quality

Figure 4.7*a* shows the situation under normal feed conditions. The target operation is positioned at point A. Here the run valve is nearly fully open while the side-arm valve is almost closed. The contour corresponding to a side-arm quality, x_3, of 0.5, representing gas qualities below the set point, shows that sensitivity to the side-arm valve movement is lost when it is greater than about 60% open. This confirms the merit of the measurement/control valve pairing selected by the RGA analysis.

A similar outcome appears in Figure 4.7*b*, where the inlet feed has a 50% higher quality. The same contours are shown with the target operating point now positioned at B. This change in feed condition results in a large movement of the side-arm valve setting but a relatively small shift in the run valve position. This makes practical sense as well as being in agreement with the RGA analysis. Since the feed now has increased gas content it seems reasonable to want to open the side-arm valve to divert it into the gas-rich exit. A closer inspection of Figure 4.7*b* highlights the fact that the 0.5 quality contour travels through a peak value as the side-arm valve moves to around 70% open. Hence, for a fixed run valve position the effect of side-arm valve movement reverses. Such a situation would need to be guarded against in operation as it corresponds to a loss of performance.

Based on the above analysis it is possible to deduce a conventional Single-Input-Single-Output control strategy. This is shown in Figure 4.8, with two tomographic units, one measuring the feed conditions and controlling the side-arm valve and the other measuring the side-arm quality and controlling the run valve.

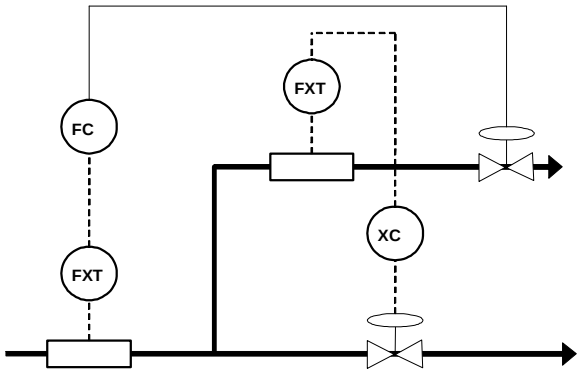

Figure 4.8: Conventional control of T-piece separator with tomographic sensors

The final area of interest is to examine the dynamic performance of the specified control system under PI control. This is demonstrated in Figure 4.9 for the case of the step change in feed quality as illustrated previously in Figure 4.7. Here there is a 50% increase in the quality after 3 seconds, returning to the initial value after 50 seconds.

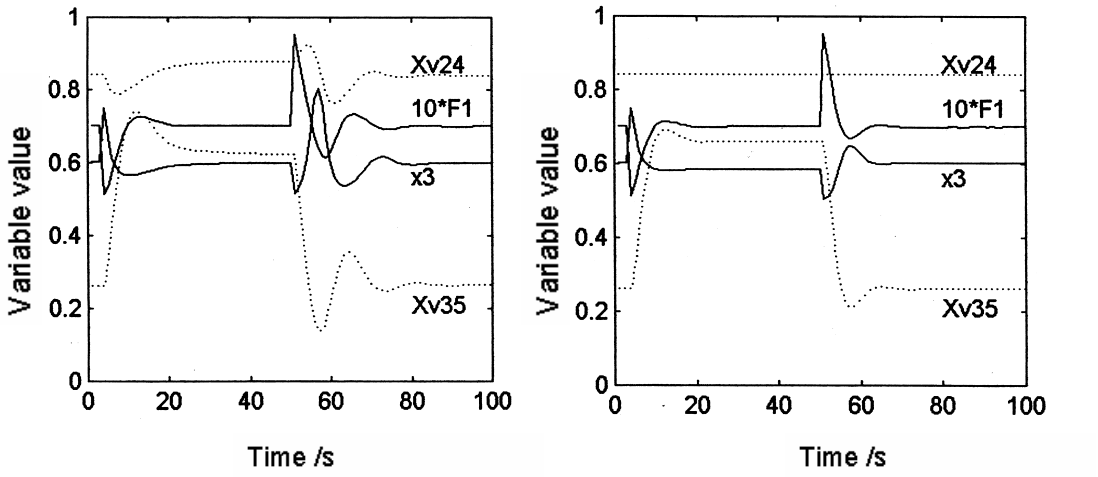

(*a*) Both valves operating (Xv24, Xv35) (*b*) Fixed run valve (Xv24)

Figure 4.9: Responses to 50% increase in side-arm quality using conventional control as shown in Figure 4.8

Considering the case where both valves are under active control, Figure 4.9*a*, the problem of process non-linearity is evident in that when the reverse disturbance occurs a significantly different transient response shape appears between the positive and negative perturbations. As predicted, there are significant interactions between the flow and quality controls. These can be easily observed if Figure 4.9*a* is compared to the situation shown in Figure 4.9*b*. In this case only the flow loop is active and the run valve, *Xv24*, operates at a fixed position, removing the effect of the loop interaction. In fact, operating with a fixed run valve position could potentially be a control option because of the strong influence of run valve position on the side-arm quality. Having achieved an acceptable quality by fixing the run valve, the operator could leave the quality running in an open loop mode and control only the total flow through the system, avoiding the strong interaction effects. The quality need only be checked periodically and the run valve adjusted as required.

4.4 Conclusions

The feasibility of using a pipework T-junction combined with an active control system as a partial phase separator for a two-phase stream has been examined. This was achieved by incorporating existing well-known T-junction phase split models with two-phase pressure drop correlations to simulate a horizontal T-junction with control valves on both outlet streams.

The results validate the concept that the phase separation performance of a T-junction is affected by the flow pattern of the approaching two-phase flow. From the predictive T-junction models used, there is a definite difference between the separation of stratified and annular flows, with stratified flows having the better separation performance. This is attributed to the difference characteristics of the two flow regimes. With such a strong observable influence of the flow pattern on the T-junction performance, there could be a definite advantage in switching between different control strategies depending on the flow regime within the pipeline.

By use of this model it has been shown that both separation performance and system throughput can both be regulated in the face of varying feed conditions. Analysis has shown that control using two control valves on the exit streams of the junction will be non-linear and interactive. For stratified flow a simple control strategy based on conventional Single-Input-Single-Output control loops has been shown to be adequate to regulate both throughput and side-arm quality. Under certain conditions the side-arm quality can become insensitive to the run valve position, providing the opportunity to reduce the inherent interaction by allowing the quality to run independently.

This simulation work has also highlighted potential problems of relying solely on available phase split models in predicting the operation of a T-junction. It is apparent that it is not feasible to simply rely on predictive models as different models indicate different phase split characteristics. This can be related to the fact that different authors focus on specific issues that they consider to be important, based on their own experimental investigations. In view of this, there may is a potential need to obtain actual experimental data for a specific T-junction in order to assess the system characteristics properly. This is even more important in situations where the side-arm is orientated vertically as there are no general predictive models available for these geometries.

CHAPTER 5

Preliminary Investigations

The work on the development of the computer simulation reported in Chapter 4 highlighted the importance of having a good description of the flow split for a particular T-junction system. As the flows are complex and general phase split models are not available, such information must initially be obtained experimentally. This chapter presents results of experiments performed to assess the potential of the T-junction system in attaining the required separation performance as set out in Chapter 1. The series of experiments performed include looking individually at two T-junctions, with upwards and downwards side-arms, in isolation and comparing the gas-liquid separation with published data to check the validity of the results. Finally, the two junctions were linked in series and the final separator configuration was studied.

5.1 Phase Split at a Vertically Upwards T-Junction

Since it has been shown that the flow pattern can have a major impact on the phase split at a T-junction the experiments will examine two regimes relevant for this work, stratified and slug flows. As stated in Chapter 2 the main influences on phase separation at a horizontal T-junction with a vertical side-arm are gravity and phase momentum. Thus for a gas-liquid flow, the denser liquid phase will preferentially flow along the bottom of the pipe, with the less dense gas flowing above it. So for a vertically upwards branch, there is a greater tendency for the gas to be extracted since

the liquid will not only have to undergo a large vertical movement to reach the side-arm entrance but also travel upwards with enough momentum to overcome gravity pulling it back down. The liquid phase will also have a much higher momentum in the horizontal direction than the gas and this will further reduce the side-arm influence, both in terms of force and actual passage of time.

5.1.1 Experimental Configuration for the Upward T-Junction

The configuration of the facility operating with only the vertical upward T-junction is shown in Figure 5.1.

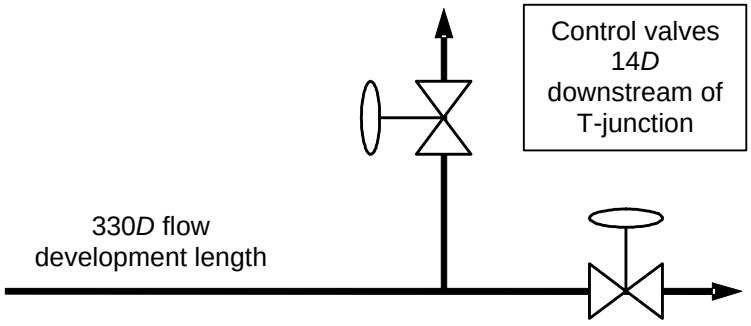

Figure 5.1: Schematic diagram for vertically upward T-junction

The T-junction is positioned 12.6 m downstream of the gas-liquid mixing section, giving a flow development length of 330 pipe diameters. A control valve is positioned on each exit stream at a distance of 0.53 m from the centre lines of the junction. Beyond this there are a series of straight pipes and bends to feed the two-phase flow into the separation tanks for measurement and metering purposes, as previously described in Chapter 3. The two control valves could be manually and independently set within the full range of their operation (i.e. 0-100 % open). For the experiments performed a systematic approach was adopted so that one valve was left in a fixed position while the other was then set at regular intervals across the full

range, starting at 20% open and increasing in steps of 20%. This was repeated for both valves across the entire operating range giving a final potential for obtaining a grid of 27 phase split data points, including the extreme cases of having either valve fully closed. In reality, because of the increased pressure drops associated with only opening both valves by a small amount some of the extreme cases, like both valves 20% open, were not studied.

5.1.2 Observations on the Phase Split for an Upwards Side-arm

For these preliminary investigations one set of flow conditions were chosen within each of the significant flow regimes under study, stratified and slug. Figure 5.2 shows the phase split at a vertically upwards side-arm for stratified flow, with low gas and low liquid inlet flowrates. The partial phase separation potential of the T-junction is clearly observable for these flow conditions, with the branch arm forming a pure gas stream consisting of approximately 90% of the inlet gas. There needs to be a significant gas-take off into the side-arm before any liquid is diverted with it. However, once the liquid starts to enter the side-arm there is a dramatic increase in the take-off associated with a very small increase in the gas take-off. This is the same trend that has been described by several authors and is evidence of the hydraulic jump effect described by Azzopardi and Smith (1992).

Figure 5.2 also shows a comparison with the data of Smith and Azzopardi (1990), obtained in a T-junction with the same diameter inlet as the one considered here using air and water at a pressure of 3 bar_a. The main difference between the studies was that Smith and Azzopardi used a reduced diameter side-arm (D_3/D_1 = 0.6), however locating the control valve so close to the junction exits within this study may result in the side-arm stream acting in a similar fashion as a reduced pipe since it is close enough to have a physical influence on the flow. The comparison, based on the flows having similar phase momenta, definitely indicates that the same phenomena are occurring at both junctions. One noticeable difference in the current study is that total gas extraction is never achieved. This can be accounted for by the systematic valve movement procedure used to obtain the phase split data, where the aim is to

accurately assess the affect the valve settings have on the flow split rather than just to determine the phase split characteristics of the junction.

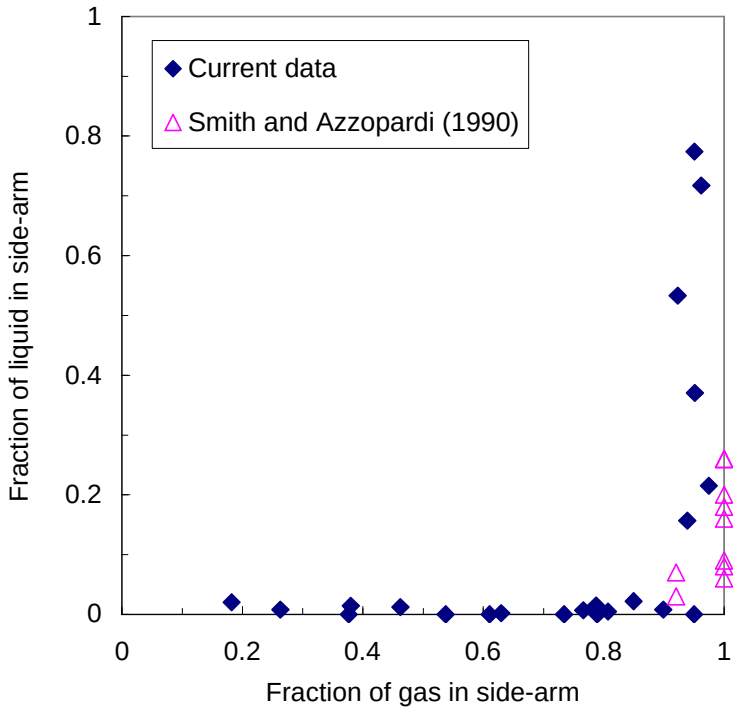

Figure 5.2: Phase split of stratified flow at a T-junction with vertically upwards side-arm. Current data: U_{gs} = 5.1 m/s, U_{ls} = 0.07 m/s

The results of a slug flow, with low gas and high liquid flowrates, splitting at the same T-junction is shown in Figure 5.3. The data here is significantly more scattered, an effect attributed to the method of obtaining the phase split data. Unlike stratified flows, there have been far fewer studies undertaken on the split of slug flows at T-junctions, and even less with a vertically orientated side-arm.

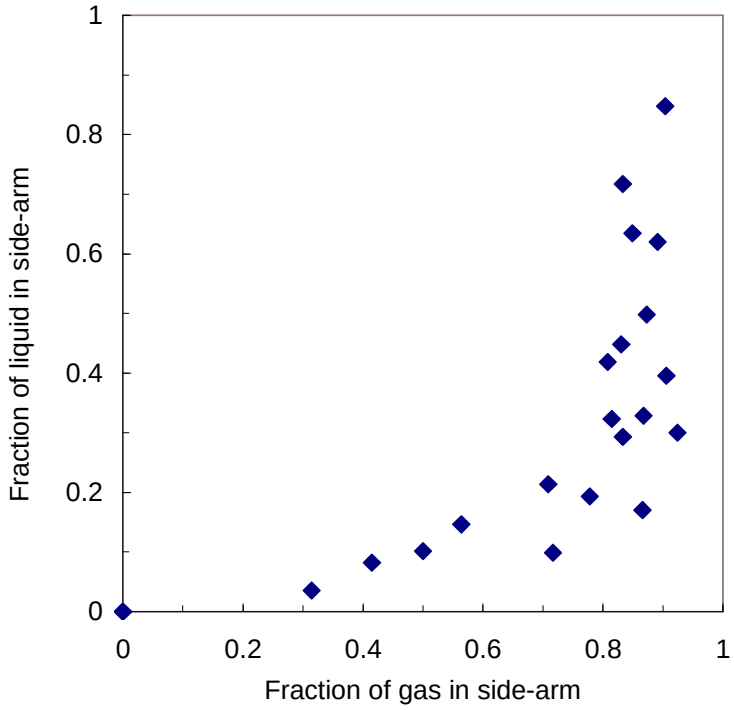

Figure 5.3: Phase split of slug flow at a T-junction with vertically upwards side-arm, U_{gs} = 3.3 m/s, U_{ls} = 0.18 m/s

This lack of published material prevents comparisons of the flow split data but the expected trends are still evident within the results. Again, like the case of stratified flow total gas extraction is not achieved. For gas extractions of less than 60%, the phase split data appears to lie on a straight line. Extrapolation of this linear trend indicates that the onset of liquid extraction begins at a gas take-off of approximately 25%. This is significantly less than the 90% observed for the stratified case. This comparison highlights the significant impact that the flow pattern can have on the flow split at a T-junction. Similar to the stratified flow split at the high gas take-off region the fraction of the liquid that is diverted into the side-arm increases rapidly over a narrow range of gas extraction, here 55% more liquid is diverted for a 10% increase in the gas take-off.

5.2 Phase Split at a Vertically Downwards T-Junction

By orientating the side-arm vertically downwards it is expected that the phase split will become liquid dominated. In this situation gravity is used to enhance the phase separation by pulling the denser liquid down into the branch, while the gas phase continues to travel above the liquid into the run.

5.2.1 Experimental Configuration for the Downward T-Junction

The configuration of the facility operating with only the downwards T-junction is shown in Figure 5.4.

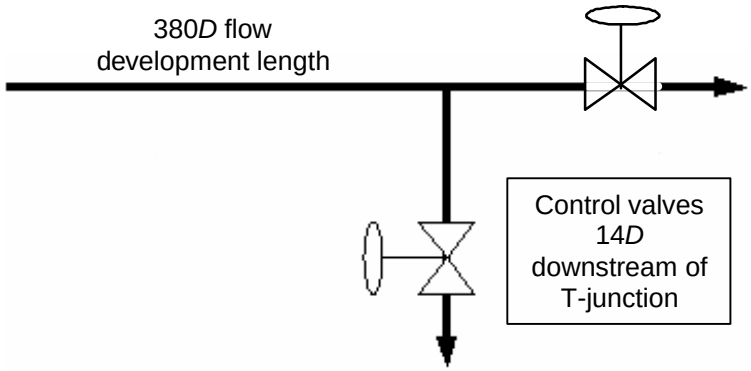

Figure 5.4: Schematic diagram for vertically downward T-junction

In this case the T-junction is positioned 14.5 m downstream of the gas-liquid mixing section, equivalent to 380 pipe diameters. As for the upward T-junction, one control valve is positioned on each exit stream a distance 0.53 m from the centre of the junction. Again these two valves are independently but systematically set to obtain the phase split data.

5.2.2 Observations on the Phase Split for a Downwards Side-arm

For these preliminary investigations the flow split of two different slug flow conditions were examined. The results, presented in Figure 5.5, confirm the liquid dominated nature of the separation. In a reverse situation to the upward case, there is a period where only liquid is extracted into the side-arm, then at some critical liquid take-off gas starts to be diverted. Once gas break-through has been achieved, there is a linear relationship between the fractions of gas and liquid extracted. This is, in part, in agreement with the findings of Wren (2001). In that study however, which used a larger 0.127 m diameter junction, the gradient of the phase split line was much steeper and total liquid extraction was achieved before total gas extraction, which is not the case for the data presented here. One probable explanation for this is the difference in the scale of the two investigations.

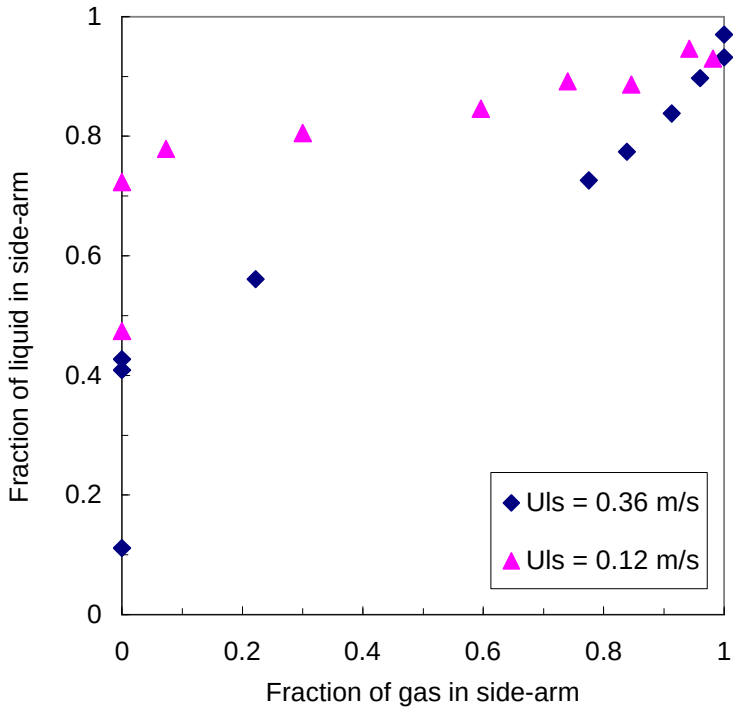

Figure 5.5: Phase split of slug flow at a T-junction with vertically downwards side-arm, U_{gs} = 3.3 m/s

The onset of gas entrainment clearly depends on the liquid flowrate, the higher the flowrate the lower the onset of gas entrainment occurs. This is in agreement with the findings of both Wren (2001) and Reimann *et al.* (1988), who suggest that the critical liquid take-off increases as the flow becomes more stratified. The results presented here agree with that idea, as the higher liquid flowrate case is well within the slug flow regime while the lower flowrate is close to the slug/stratified transition boundary.

5.3 Phase Split Obtained Using Two Junctions in Series

The combination of placing two oppositely orientated T-junctions in series was first considered by Wren (2001). The preliminary investigations presented here examine the influence of the downward leg on the phase split at the upstream vertically upward T-junction, while subsequent experiments develop the notion of a T-junction separator. The results of Wren (2001) clearly indicate that the introduction of the downward T-junction improved the phase separation at the upward one. This was confirmed by the ability to combine the final run with the upward side-arm to produce a gas-rich stream which contained a greater mass fraction of the inlet gas with less liquid when compared to the corresponding single vertical upwards side-arm case with the same flow conditions.

5.3.1 Experimental Configuration for two T-junction Placed in Series

The configuration of the experimental facility operating with both junctions in series is fully detailed in Chapter 3 and is a combination of the two layouts described above. Figure 5.6 shows a schematic of the facility, detailing the relevant distances of the key components.

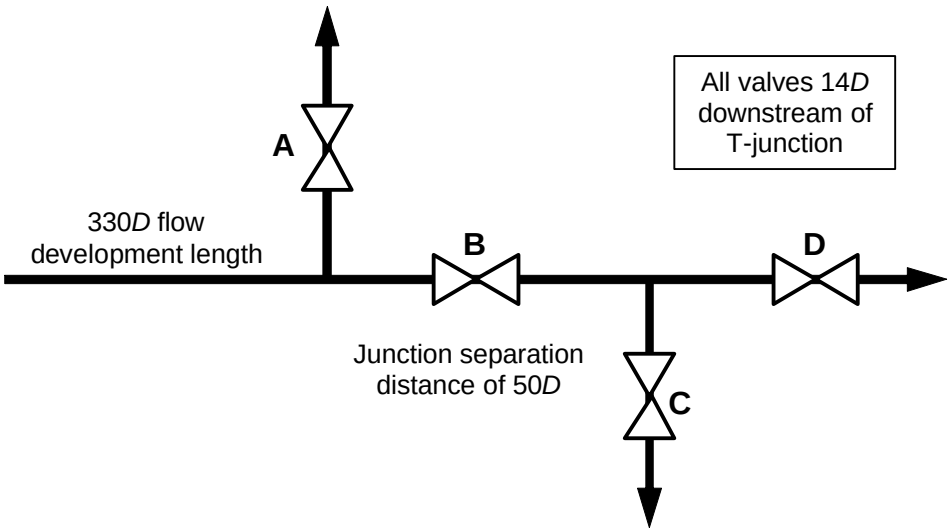

Figure 5.6: Schematic diagram for two T-junctions in series

The first T-junction, orientated vertically upwards, is positioned 12.6 m (330*D*) downstream of the gas-liquid mixing section. The second junction, vertically downwards, then has a separation distance of 1.9 m (50*D*) from the first. A valve, either manual or automatic, is placed on the exit stream of each junction, highlighted as points *A*, *B*, *C* and *D* on Figure 5.6.

5.3.2 Effect of Downward Branch on the Phase Split at the Upward Side-Arm

In the first series of experiments the downward leg valve was left fully open and the phase split at the vertical upward branch was obtained using the same method as described in Section 5.2.1. The same two flow conditions were chosen as for the previous work on the upward junction only, to allow easy comparisons to be drawn.

Figure 5.7 shows the influence the down leg has on the phase split of a stratified flow at the vertical upward junction. Although the effect is not striking there is a definite impact on the phase separation by the introduction of the downward junction. Essentially it is observed that less liquid is extracted into the upward branch for the same gas take-off. It is also evident that the sharp increase in the liquid take-off as

observed for the upward junction only case does not occur until a point beyond total gas extraction. Thus the increased separation performance is emphasised by the appearance of a total gas extraction point with only 8% of the inlet liquid being diverted into the branch with it. For the case of the upward junction alone total gas extraction was not observed at all, and this results supports the idea that the downward side-arm will reduce the impact of hydraulic jump effects. Examining the phase split data in terms of the relative volume of the two phases, the gas-rich stream produced by the upward branch has a liquid content of 1.6 % v/v. This is well below the predefined target of less than 10% v/v, which is considered indicative of a good initial partial phase separation.

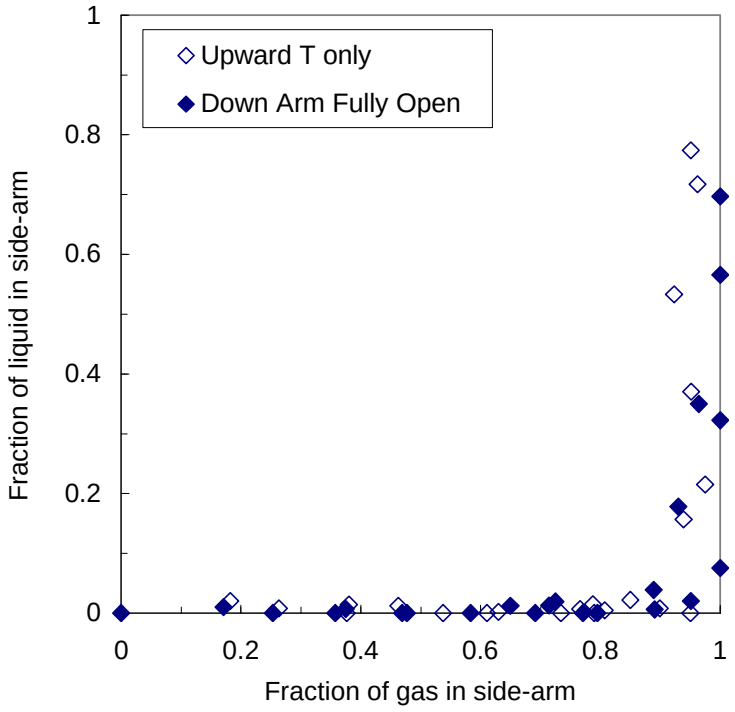

Figure 5.7: Effect of having a vertically downwards side-arm on the phase split of stratified flow at a vertically upwards side-arm, U_{gs} = 5.1 m/s, U_{ls} = 0.07 m/s

For the case of slug flow there appeared to be no immediate benefit from the introduction of the down leg on the phase split in the upward junction. This may be expected since the mechanisms affecting the flow split of slug flows are different to those of stratified flows. In stratified flow the liquid has to be lifted to the side-arm opening, this effect being emphasised by the formation of the hydraulic jump. Hence the existence of the downward leg reduces the liquid take-off by removing this jump effect. For slug flows hydraulic jumps are not considered to be an important factor affecting the phase split but rather it is the structure of the flow itself that determines the flow split.

In slug flow a large amount of liquid travels within intermittent slug pockets that span the pipe cross-section. The presence of the control valves so close to the T-junction provides a restriction to the flow of the two-phase mixture along the pipes. Within the slug flow regime, the liquid slugs will travel with a relative high velocity, and as the run valve is closed there is a greater tendency for the liquid to accumulate in front of these valves. This effect is evident in the pressure trace for the first T-junction. Figure 5.8 compares two such traces for the same slug flow conditions but different settings of the run valve position, 100% and 20% open.

Both traces show the expected trends for slug flow with the characteristic intermittent peaks of higher pressures. However, for the run valve only 20% open these pressure peaks are significantly higher than for the fully open case. This is indicative of the liquid being held-up at the junction by the valve, restricting the flow and so increasing the upstream pressure. Visual observations show that there is an almost continuous stationary liquid presence at the junction. This significantly reduces the vertical travel distance and the oncoming gas flow will tend to sweep a large fraction of this liquid up into the side-arm.

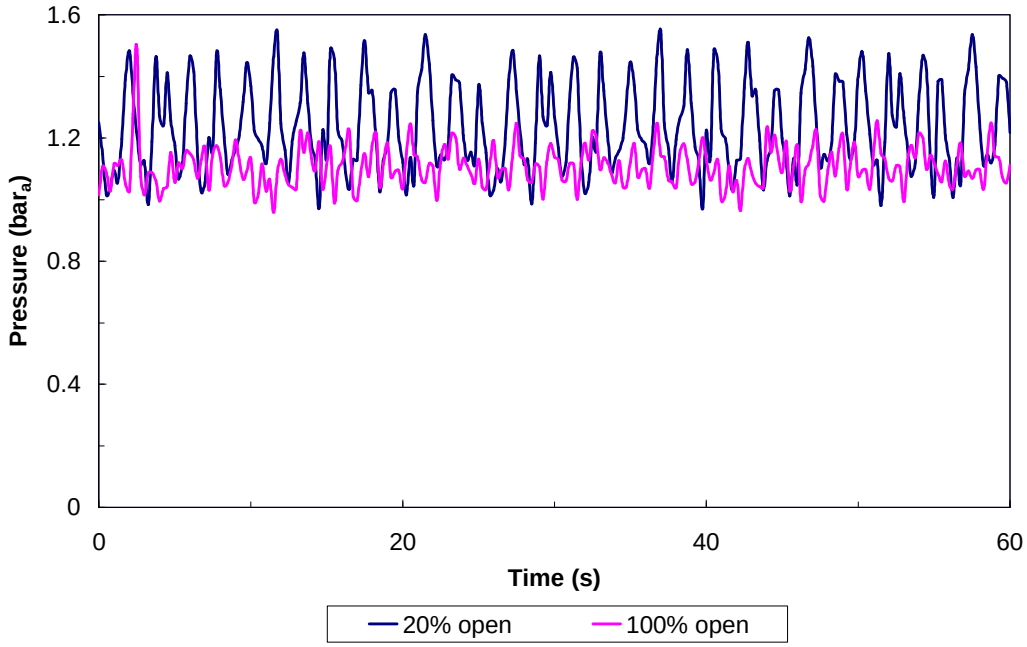

Figure 5.8: Effect of run valve position on the pressure traces for slug flow at the first T-junction, U_{gs} = 3.3 m/s, U_{ls} = 0.18 m/s

So, for the current configuration, the downward branch does not have sufficient influence on the phase split of slug flows at the upward T-junction. However, since the position of the control valve between the two T-junctions could have an adverse affect on the phase split at both junctions the next stage of the study is to remove the valve between the two T-junctions, referred to as *B* in Figure 5.6 and insert a new valve on to the final run, position *D*.

5.3.3 Effect of the Downward Branch Valve on Phase Separation

As stated above the next step in the developmental work is the introduction of valves around the downward T-junction to try and regulate the flow split down this leg. At this stage there are three valves still associated with the facility, again referring to Figure 5.6 these are located at points *A*, the up arm, *C*, the down arm, and *D*, the final run. Figure 5.9 shows the effect of closing the down arm valve on the phase split of a slug flow at both the upward and downward T-junctions. The two data sets relate to

two different settings of the control valve on the run exit stream, namely 100% open and 20% open.

The first observation to be made is that the opening position of the run arm valve has no effect on the phase separation at the upward side-arm. This is indicative of the results presented above, where for slug flows the downward leg had no influence on the phase split at the upward side-arm. Closing the valve on the downward leg does not alter the gas and liquid take-off proportions in the upward side-arm but it does tend to force more of the flow into the upward branch. This is in direct response to an increase in the downstream resistance to the two-phase flow caused by closure of the run valve.

In contrast to previous observations, movement of the run valve does have a pronounced effect on the phase split in the down arm. In general, the phase split results obtained at the downward T-junction show that the liquid take-off may be considered to be independent on the gas take-off. This is indicated by the almost horizontal nature of the data points in Figure 5.9. Thus there is a critical liquid take-off value that is maintained regardless of the amount of gas extracted down the side-arm. A similar result is presented by Penmatcha *et al.* (1996) for stratified flows splitting at a downward side-arm inclined at 60°. Like the current data, their phase split curves travel with an almost flat trajectory essentially parallel to the gas take-off axis.

Closing the down arm valve will increase the resistance in that branch; this will then tend to reduce the amount of gas extracted with the liquid. Since liquid preferentially enters the side-arm, under the effect of gravity, it will create a barrier against gas extraction, further increasing the resistance in the branch. Thus with the down arm valve fully open, 40% of the gas leaves with the liquid but with the same valve 50% open there is a liquid only stream produced containing 70% of the inlet liquid, created as a result of a continuous liquid presence above the valve. This effect is comparable to that discussed in Section 5.2 for the downward branch only case.

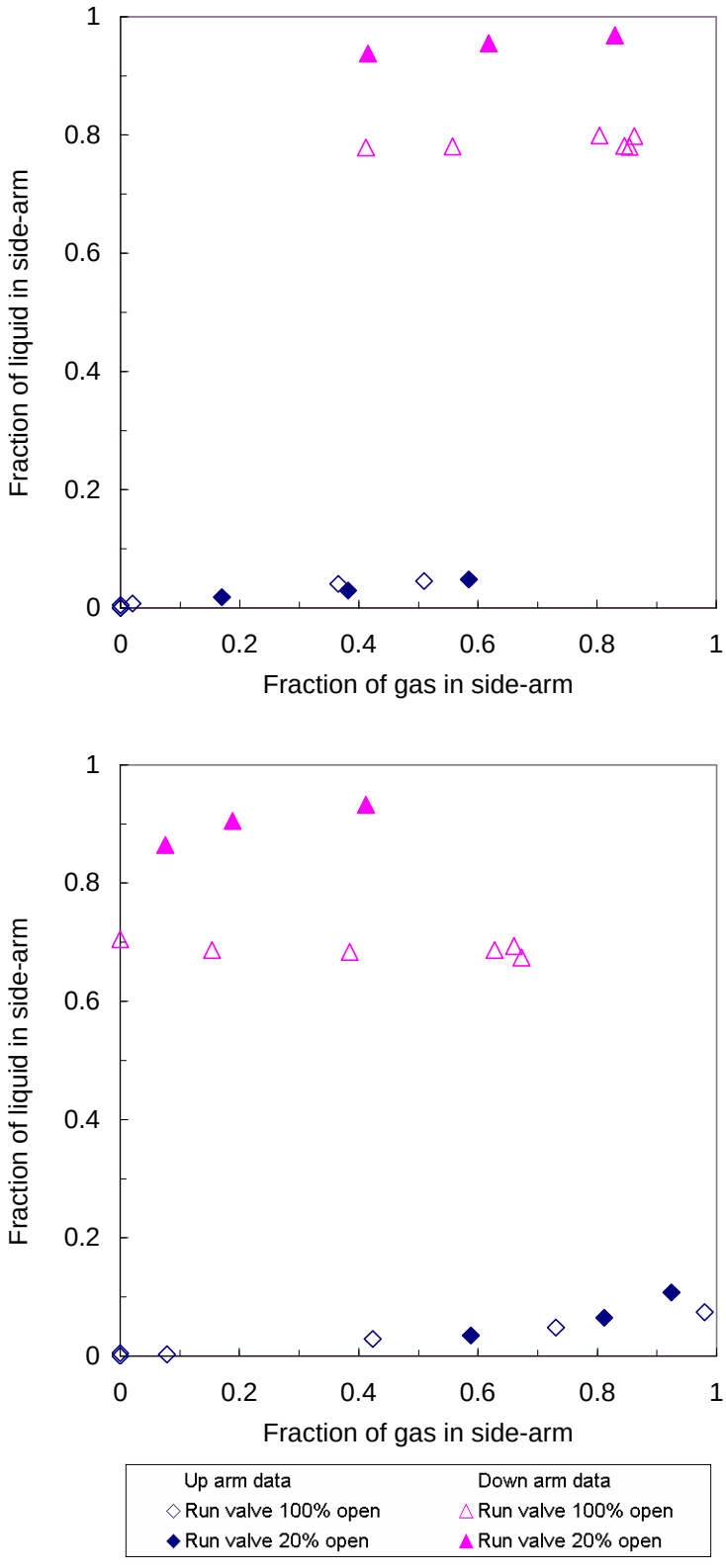

Figure 5.9: Effect of closing down arm on phase split of slug flow: U_{gs} = 3.3 m/s, U_{ls} = 0.35 m/s. Top: Down arm valve 100% open; Bottom: Down arm valve 50% open

Conversely, closing the run valve does not have much influence on the shape of the phase split data at the upward side-arm, it merely introduces an offset. Thus, more liquid is extracted for the same fraction of gas taken-off. This is attributed to an increased liquid hold-up at the junction when the resistance in the run exit is increased. The greater liquid presence at the junction gives more of the liquid a greater opportunity to fall into the downward branch opening, increasing the fractional take-off, without affecting the gas take-off.

Based on the above results the extreme case that ensures a liquid-rich stream is to maintain a constant liquid level within the downward leg, and so preventing any gas leaving in the down leg. Initially this was achieved by manual manipulation of the down arm valve in response to the variations in the liquid height. Figure 5.10 shows the results for the same slug conditions as presented previously in Figure 5.9, again showing both the upward and downward side-arms for two different settings of the run valve. Again, the upward take-off data exhibits a trend unaffected by the position of the run valve although there is a sharp increase in the liquid take-off beyond a gas-take-off of 85%. Similarly the liquid take-off increases as the run valve closes, reflecting the above results and associated with the increasing liquid hold-up.

One further advantage in removing the control valve from the horizontal exit of the first T-junction is a reduction in the pressure fluctuations within the system. Remembering that in Figure 5.8 it was observed that when the run valve was closed pressure surges were observed at the T-junction as the flow of the liquid slugs was restricted. Figure 5.11 shows that for this new configuration these pressure variations are significantly reduced. Although there are occasional spikes observed when the run valve, now positioned after the second junction, is 20% open, in general there is little difference between the two cases. In terms of industrial applications, maintaining a steady pressure within a system is a preferential operating condition than continuous cyclic fluctuations.

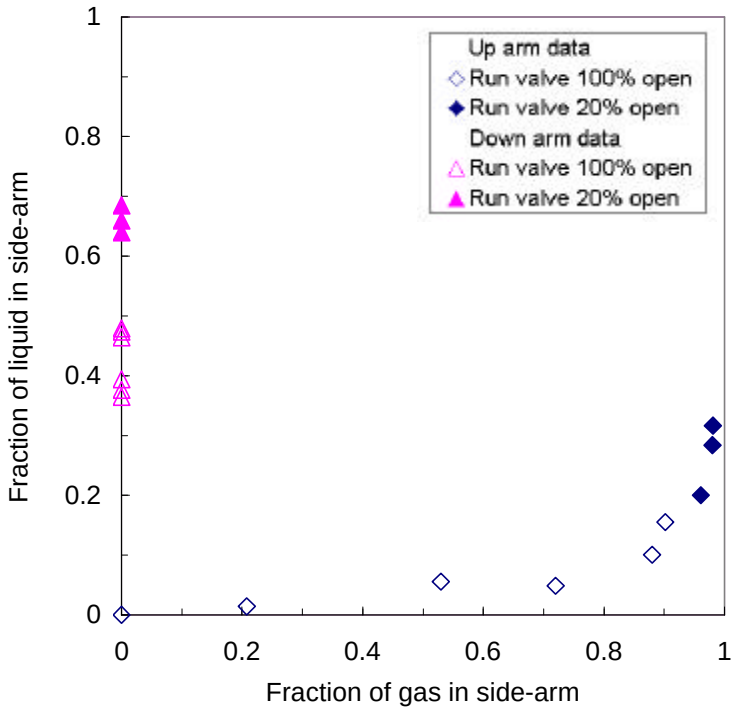

Figure 5.10: Effect of maintaining a constant liquid level in the down arm on phase split of slug flow: U_{gs} = 3.3 m/s, U_{ls} = 0.35 m/s.

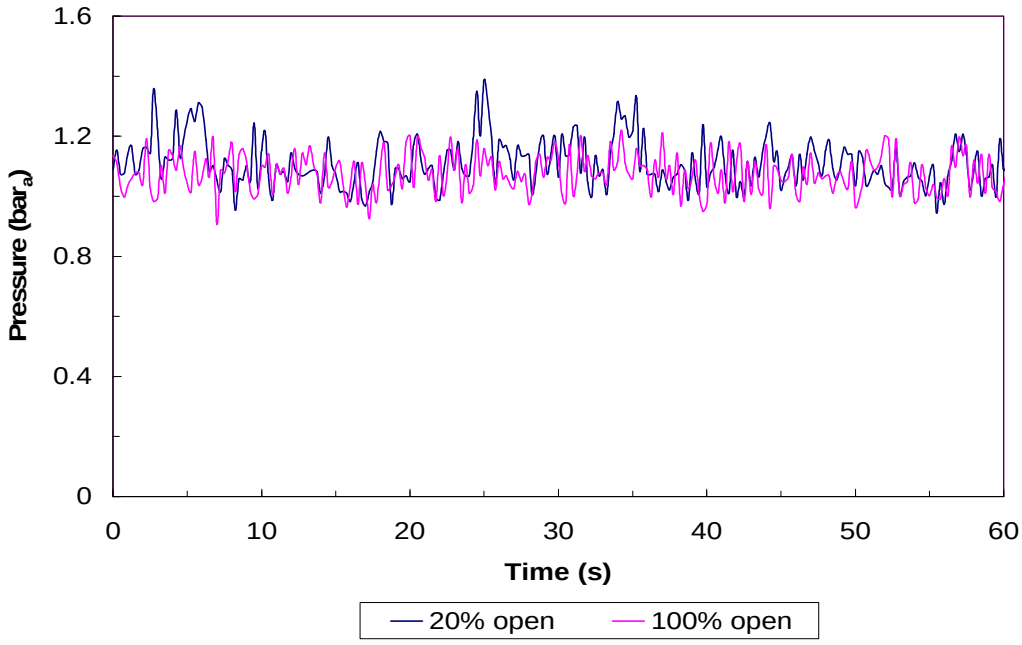

Figure 5.11: Effect of run valve position on the pressure traces for slug flow at the first T-junction, U_{gs} = 3.3 m/s, U_{ls} = 0.35 m/s

5.4 Target Separation Criteria

It has already been stated that a good partial separation can be defined in terms of the relative phase distribution within each of the two exit streams. The criterion chosen within this study was to produce a gas-rich stream with less than 10% v/v of liquid and a liquid-rich stream with less than 10% v/v of gas present. In the case of a single T-junction there are obviously only two exit streams that need to be considered, the side-arm and the run. However, the situation changes when two junctions are placed in series, when there will now be three exit streams. In order to fulfil requirements of a practical phase separation system two of these streams need to be combined. The choice of which streams to select will obviously be based on the relative phase volumes produced.

Table 5.1 presents a comparison of the stream volumetric compositions for the various configurations that have been considered. The data is presented in terms of the existence of gas-rich and liquid-rich streams, calculated at the optimum separation conditions observed.

It is evident that for a single T-junction with a vertically upwards side-arm the target separation can be achieved for the gas-rich stream but the amount of gas in the liquid stream is excessively high for both stratified and slug flows. Rotating the side-arm through 180° to produce a downward branch provides a means of obtaining a liquid only stream by maintaining a constant liquid level and barrier against gas entrainment. The remaining stream is then considered to be rich in gas and leaves through the run with less than 10% v/v of liquid. Thus the separation criterion is achieved in this instance.

The introduction of the down leg in series with the upwards branch greatly increases the phase separation potential of the system. For the two preliminary cases studied here the down leg enhances the vertically upward flow split such that total gas extraction is achieved for both the stratified and the intermediate slug flow. Closing the down arm valve and so restricting the flow gives two options for stream

combination. Considering the gas stream to be solely composed of the upward side-arm take-off produces a liquid in gas composition of less than 1 % v/v but also a liquid stream with a gas content of 16 % v/v. A better result is obtained if the run and up arm streams are combined to form a gas-rich stream with a liquid content of only 3.2% v/v and a liquid stream with no gas content at all formed from the down leg.

Table 5.1: Comparison of the relative volumetric compositions for the optimum separation achieved at the T-junction configurations considered

Junction Configuration	Inlet Superficial Velocity (m/s)		Flow Pattern	Gas-rich stream	Liquid-rich stream
	U_{gs}	U_{ls}		% Liquid in gas	% Gas in liquid
Upward side-arm - only	5.1	0.07	Stratified	0.0 (up arm)	75.6 (run arm)
	3.3	0.18	Slug	2.1 (up arm)	62.6 (run arm)
Downward side-arm - only	3.3	0.12	Slug	3.7 (run arm)	0.0 (down arm)
	3.3	0.36	Slug	7.3 (run arm)	0.0 (down arm)
Upward side-arm + down arm 100% open	5.1	0.07	Stratified	0.4 (up arm)	0.0 (run + down)
	3.3	0.18	Slug	2.2 (up arm)	0.0 (run + down)
	3.3	0.35	Slug	0.87 (up arm)	80.0 (run + down)
Upward side-arm + down arm 50% open	3.3	0.35	Slug	0.83 (up arm)	16.0 (run + down)
				3.2 (up + run)	0.0 (down arm)
Upward side-arm + Automatic level control on down arm	5.1	0.08	Stratified	0.1 (combined up + run)	0.0 (down arm)
	3.3	0.18	Slug	1.0 (combined up + run)	0.0 (down arm)
	9.6	0.17	Slug	0.2 (combined up + run)	0.0 (down arm)
	3.3	0.36	Slug	4.4 (combined up + run)	0.0 (down arm)

5.5 Automatic Level Control on Downward Branch

In Section 5.3.3 it was found that maintaining a constant liquid level in the downward leg by manual manipulation of a valve proved to be an effective method of attaining a good separation. Not only did it have the potential to produce two streams that met the target separation, by the combination of the up and run arms, but it also helped reduce pressure fluctuations in the system. Expanding this concept further it is evident that an automatic level control could be incorporated within the downward branch to maintain a constant liquid level thus preventing gas extraction through this stream.

A simple level control was implemented to operate under a proportional control method. Using this method, the controlled process input is regulated to a value proportional to the difference between the control set point and the measured value. The larger the value of the proportional constant, the harder the system will react to the difference between the set point and the actual measured value.

From the above studies it is also evident that the gas-rich stream will be formed by the combination of the upward side-arm and the final run arm, leaving a gas-free liquid stream produced by the level control. With the current configuration this means that there are two control valves associated with the gas-rich stream, one on the up arm and the other on the run. From a viewpoint of practical operation of a phase separation system it would be more sensible to remove one of theses control valves.

It was also shown in Section 5.3.3 that the run valve could beneficially influence the separation performance by increasing the liquid hold-up at the downward T-junction and so increasing the liquid take-off in the down leg. The degree of interaction between two valves operating on what is essentially the same pipe could be a considerable problem, leading to unfavourable operational conditions. Thus with the apparent importance of the run valve established it would be more prudent to remove the upward side-arm control valve allowing that branch to operate freely.

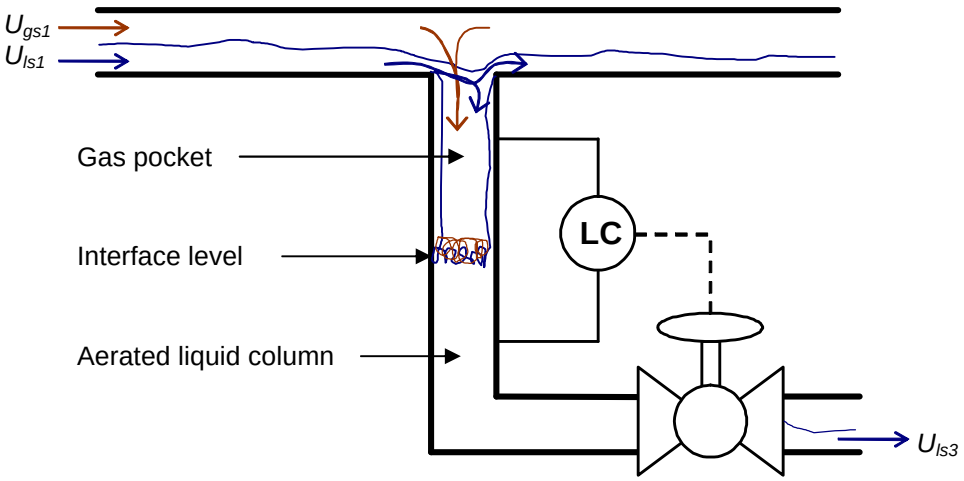

Figure 5.12: Schematic of the automatic liquid level control in down leg

Figure 5.12 shows a schematic of the automatic liquid level control positioned on the downward leg. A differential pressure transducer is used to measure the liquid level between two tappings. The total length of the downward leg is 0.90 m, the two pressure tappings are located a distance of 0.1 m below the centreline of the main horizontal pipe and 0.1 m above the bottom bend. This gives a maximum differential height of 0.70 m relating to a maximum differential pressure of 0.055 bar (0.8 psi); although because of aeration the actual differential pressure will be less. The control valve is then positioned on the horizontal section of the side-arm, 0.25 m downstream of the bend.

A liquid level set point was chosen to be 0.4 m and the automatic level control system was tuned to maintain the level as effectively as possible for a representative set of inlet flow conditions. More details about the automatic control system as well as the tuning experiments are reported in Appendix D.

The experiments reported in Section 5.3.3 were repeated with the automatic level control replacing the manual control previously used and with the run valve set at a number of incremental values. Figure 5.13 gives the corresponding phase split plot for the slug flow condition. Obviously, the down arm data all fall along the *y*-axis, as

there is no measurable amount of gas extracted in the down arm. The up arm data still shows the expected trend of a sudden increase in the liquid take-off at high values of gas take-off.

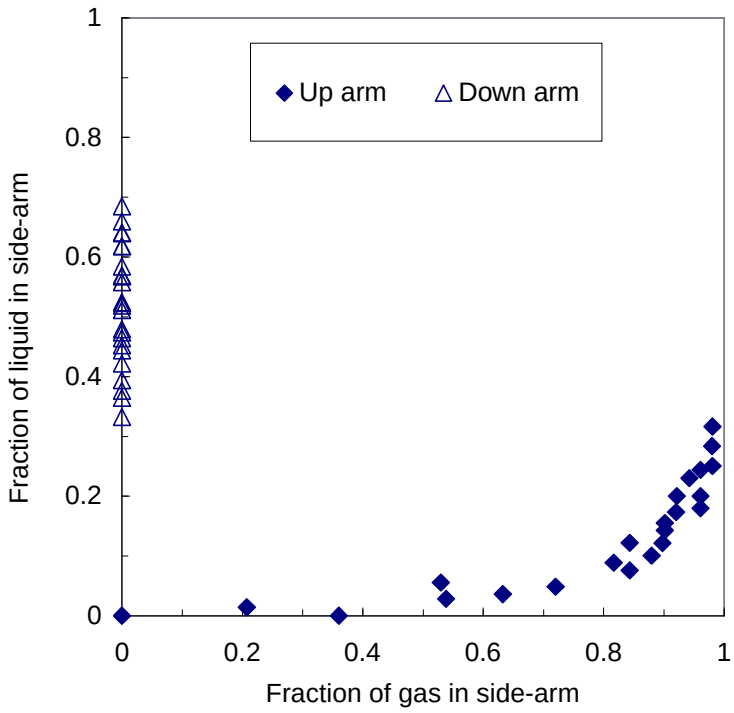

Figure 5.13: Effect of automatic level control maintaining a constant liquid level in down arm on phase split of slug flow: U_{gs} = 3.3 m/s, U_{ls} = 0.35 m/s

A typical response of the automatic level control systems is shown in Figure 5.14. The control valve is required to stroke across the entirety of its operational range in order to maintain the level around the set point (400 mm). The cyclic motion of the control valve is evident as it responds to surges of liquid produced by the arrival of intermittent slugs of liquid. This rapid increase in the height of liquid into the branch produces a rapid response from the valve as it moves from a fully closed position to fully open in a time period of less than 3 seconds. After the liquid slug passes, there

is a period of stratified flow, associated with a significantly reduced liquid loading. With the valve fully open the height of the liquid column is quickly reduced thus the valve needs to close in an attempt to try and maintain the liquid level in the down arm.

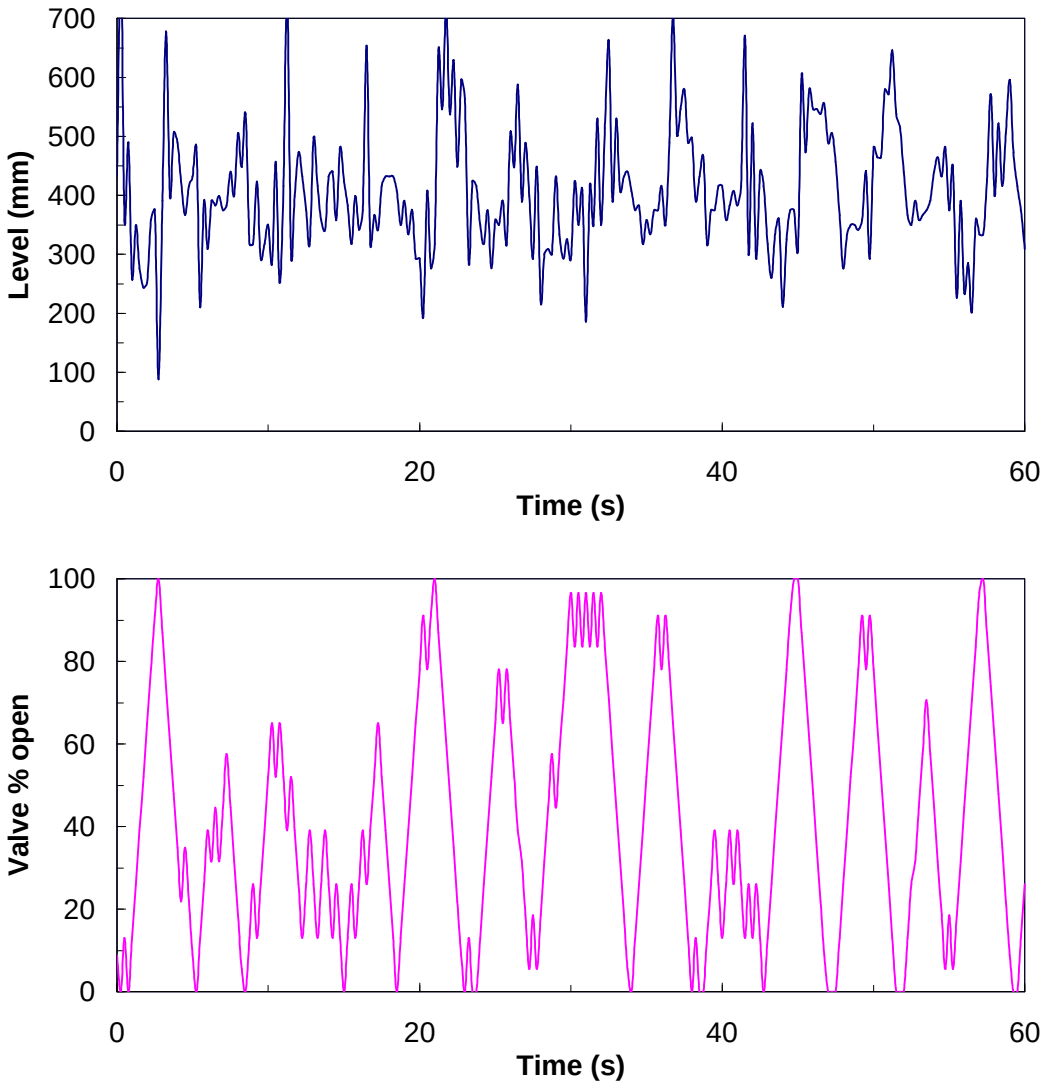

Figure 5.14: Response of automatic level control under slug flow conditions: U_{gs} = 3.3 m/s, U_{ls} = 0.35 m/s (Run valve 100 % open)

In the case of stratified flow where the liquid flow is not intermittent the flow split is dominated by the vertical distance between the stratified gas-liquid interface and the opening of the upward side-arm. This distance makes it much more difficult for the liquid to enter the up arm in comparison to the gas. The slower travelling liquid has a much lower velocity and, therefore, a reduced momentum than the liquid slugs present within the slug regime, and hence has a much longer travel time over the downward branch opening. Thus the vast majority of the liquid will fall into the down leg. Figure 5.15 shows the phase split plot for both up and down arms of the T-junction separator for the stratified flow case. Here over 95% of the inlet liquid leaves through the down leg, while over 98% of the gas feed is extracted in the up arm with no liquid carryover.

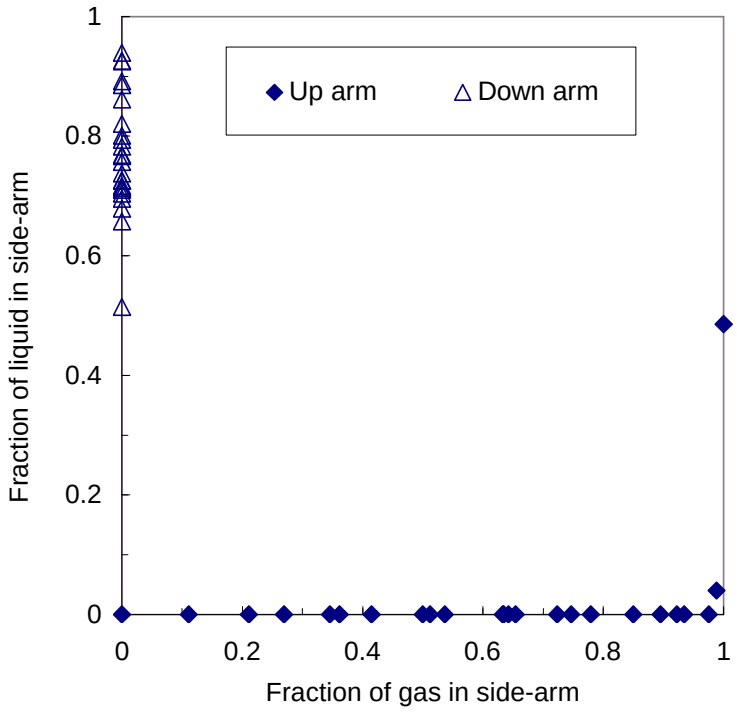

Figure 5.15: Effect of automatic level control maintaining a constant liquid level in down arm on phase split of stratified flow: U_{gs} = 5.1 m/s, U_{ls} = 0.08 m/s

In stratified flow the liquid is delivered into the down leg in a much more constant manner. This is clearly visible on examination of a typical response of the automatic level control, as shown in Figure 5.16. The variation in the liquid level within the down leg is far less severe when compared to slug flow, with maximum deviations from the set point of no more than ±150 mm.

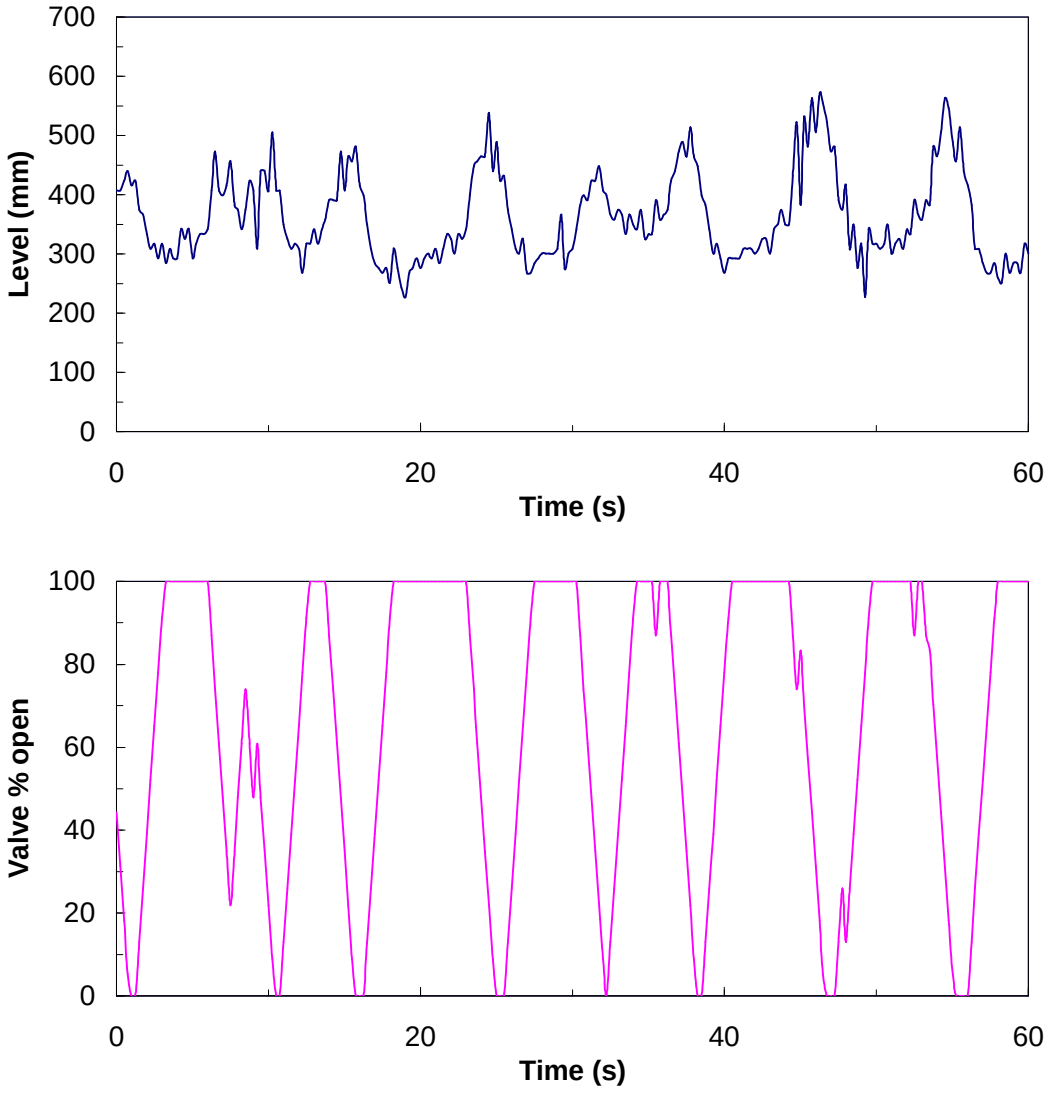

Figure 5.16: Response of automatic level control under stratified flow conditions: U_{gs} = 5.1 m/s, U_{ls} = 0.08 m/s (Run valve 100 % open)

Table 5.2: Comparison of the relative volumetric compositions for the optimum separation achieved at the T-junction separator with automatic level control on the down leg

Junction Configuration	Inlet Superficial Velocity (m/s)		Flow Pattern	Gas-rich stream	Liquid-rich stream
	U_{gs}	U_{ls}		% Liquid in gas	% Gas in liquid
Upward side-arm + Automatic level control on down arm	5.1	0.08	Stratified	0.1 (up + run)	0.0 (down arm)
	3.3	0.18	Slug	1.0 (up + run)	0.0 (down arm)
	9.6	0.17	Slug	0.2 (up+ run)	0.0 (down arm)
	3.3	0.36	Slug	4.4 (up + run)	0.0 (down arm)

Although the response times and cyclic nature of the control valve are similar to those observed for the slug flow case, the valve movement is noticeably smoother. This is indicative of the more stable flowrate associated with this flow regime. Overall it is unsurprisingly easier to maintain a constant liquid height for stratified flows, where the liquid flowrate is essentially constant, than for slug flows, where natural surges create large variations in the liquid level over a relatively short time period.

The final assessment of how good the achieved phase separation can once again be found from the examination of the volume ratios, as previously used in Section 5.4. Remembering that a target separation is set at 10% v/v of the unwanted phase within a particular phase-rich stream Table 5.2 compares the deliverable separation for the T-junction with the level control.

Even from the small number of preliminary studies there are observable and expected trends. Stratified flows achieve a better separation than slug flows. This can be attributed to three main factors, the lower liquid loading of the inlet flow, the vertical travel distance for the liquid to enter the up arm and the lower momentum of the liquid phase as it approaches the down leg. The lower momentum of the liquid within

the stratified flow regime means that it has more chance to fall into the downward branch. For slug flow, the high velocity slugs travel with enough momentum so that some fraction of the inlet liquid will always by-pass the branch opening altogether. Thus there is a requirement to restrict the flow out of the final run to increase the liquid residence time at the second junction. This is achieved by closure of the control valve positioned on that run arm.

Finally, there are strong effects of the gas and liquid volumetric ratio of the inlet stream. By increasing the inlet liquid loading increases the amount of liquid leaving through the combined gas-rich stream. Conversely, increasing the gas inlet loading increases the volumetric purity of the final gas-rich stream.

5.6 Conclusions

The phase split has been investigated for a number of T-junction configurations in order to evaluate the best arrangement of junctions and control valves to achieve optimum separation performance. From these initial experiments it is clear that flow pattern has a significant affect on the phase split and the operation of the T-junction separator. Regardless of the configuration, stratified flows were separated more easily than slug flows. This was considered to be the combined effect of lower liquid loading in the feed, a reduced liquid momentum and the greater vertical distance between the liquid and the top of the horizontal inlet pipe.

The phase split at the vertically upwards side-arm was gas dominated for both stratified and slug flows. However, only the gas-rich stream fell within the target criterion of less than 10% v/v liquid-in-gas that defines a good separation. The other stream contained a large volumetric proportion of gas. For the case of the downwards T-junction the flow split became liquid dominated and the presence of a continuous liquid level within the down leg, thus preventing gas extraction, provided a means of obtaining target separation on both exit streams.

When two T-junctions were combined in series, the phase split at the upward side-arm was improved by reducing the fraction of liquid extracted with the gas. By the installation of an automatic level control, operating under proportional control, on the down leg it was then possible to maintain a constant liquid level within that branch regardless of the phase flowrate variations in the feed. This constant liquid level provides a barrier against gas entrainment leaving through this down arm allowing for a gas-free liquid stream to be produced from that outlet. Manipulation of the control valve on the final run exit stream was seen to have an affect on the amount of liquid extracted through the down leg, in direct response to changes in the liquid hold-up at the second junction.

A gas-rich stream could be produced by combining the other two outlets, the up arm and the final run. From the preliminary results this gas-rich stream would fall within the separation criteria, containing less than 10% v/v of liquid.

In all cases, the simple T-junction, when combined with control valves and a proportional level control strategy, has been exploited as a viable option in obtaining a first stage partial phase separation.

CHAPTER 6

Steady-State Phase Separation Results

The previous chapter introduced the concept of controlling the down leg separation by the use of an automatic level control. Here a more rigorous set of experiments will examine the phase separation performance of the combined T-junction separator over a wide range of gas and liquid inlet superficial velocities, covering both the stratified and slug flow regimes. With the first level of the control strategy focused around the automatic level control the next stage is to develop a second control idea that will maximise the phase separation performance of the system. A strong relationship between the run arm control valve setting and the liquid take-off at the downward side-arm, associated with the liquid hold-up at the downward T-junction, was highlighted in the previous chapter. This chapter will try and exploit this result as fully as possible to establish any useful relationship between the phase separation performance and the run valve setting to aid in the development of a complete control strategy.

6.1 Experimental Configuration

A full description of the experimental configuration of the facility along with the operating procedures is given in Chapter 3. For simplicity Figure 6.1 shows a schematic representation of the system. The system now consists of two junctions, the first with a vertically upwards (+90°) side-arm, the second with a vertically downwards (-90°) side-arm, separated by a distance of 1.9 m.

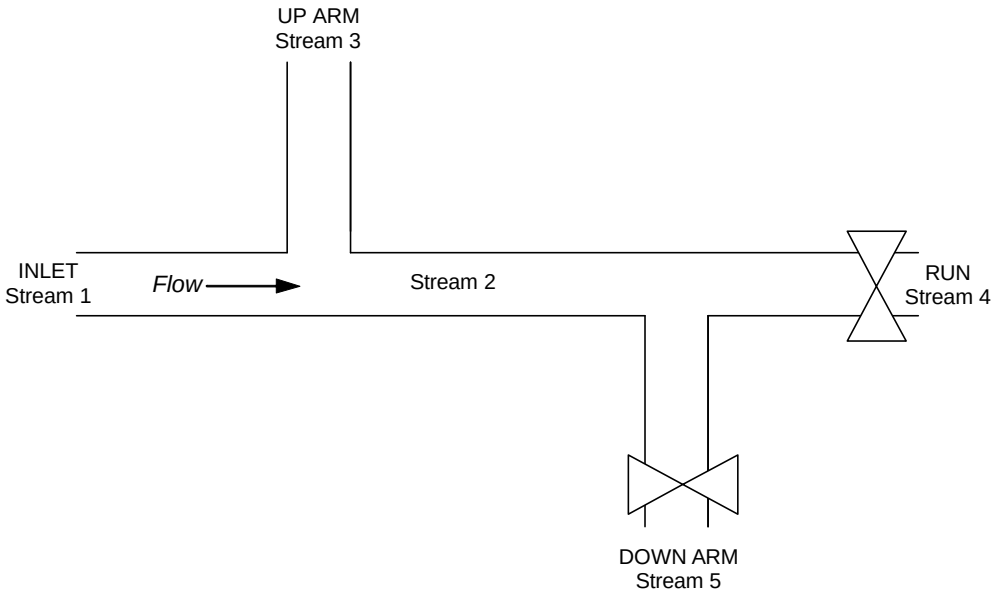

Figure 6.1: Systematic diagram of the T-junction configuration

The data in the remainder of this thesis will be presented in terms of the stream numbers as indicated above, where stream 1 is the two-phase inlet and streams 3, 4 and 5 are the three respective junction outlets. Stream 2 is the section of pipework between the two junctions and could be envisaged as the inlet to the second T-junction. Two control valves regulate the flow through the system, one associated with the automatic level control and the other located on stream 4, the horizontal run exit of the second T-junction.

During steady-state measurements the system was allowed to achieve equilibrium before any the data was collected. The gas flowrates through all three exits were obtained by the use of differential pressure gauges that measure the pressure drop across an orifice plate, while the liquid flow split was determined by measuring the change in volume of the separation tanks, again using differential pressure as previously described in Chapter 3. Only when the data fulfilled the mass balance criteria of ±5% were they accepted as part of the experimental results.

6.1.1 Experimental Conditions

In order to fully investigate the phase separation of the proposed system a wide range of gas and liquid flowrates were chosen, covering both stratified and slug flow regimes. A systematic matrix of flow conditions were selected based on a 5 by 5 grid system. This gave a data set with essentially five lines of constant gas flowrate and five lines of constant liquid flowrate.

A flow pattern map for the facility was produced using the methodology of Taitel and Dukler (1976). Figure 6.2 shows this map along with the grid of flow conditions, plotted in terms of their observed flow regimes used for the steady-state analysis. Visual observations of the actual flow patterns within the pipe illustrate the limitations of the method of Taitel and Dukler (1976) in predicting the annular flow boundary.

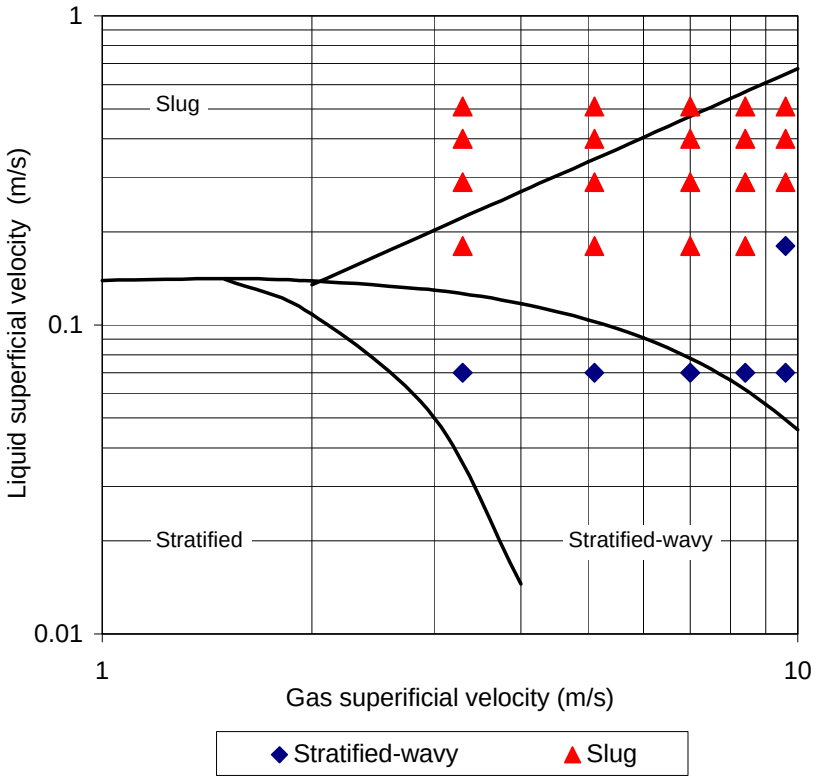

Figure 6.2: Flow map for experimental facility showing experiment conditions and observed flow regimes

6.1.2 Representing the Phase Split Data

The unique nature of the data produced by this two T-junction system makes presentation in the traditional manner, using standard phase split plots, difficult. Operating with only two exit streams, derived from the liquid down leg with the associated level control, and the combined gas-rich streams, the up and the run arms, standard flow split plots do not convey any useful information. For the situation of no gas take-off in the down leg, all data falls on the extremities of the plot. A typical set of results plotted using this method is shown in Figure 6.3. Here the down arm data is plotted as the fraction of inlet liquid in the downward branch (L') against the fraction of gas withdrawn in the same branch (G'). For this case of no gas take-off with the liquid the data lies on the $G' = 0$ line. The remaining streams are then combined to give the gas-rich stream, producing a pseudo side-arm composition. In this case all the data are located along the $G' = 1$ line.

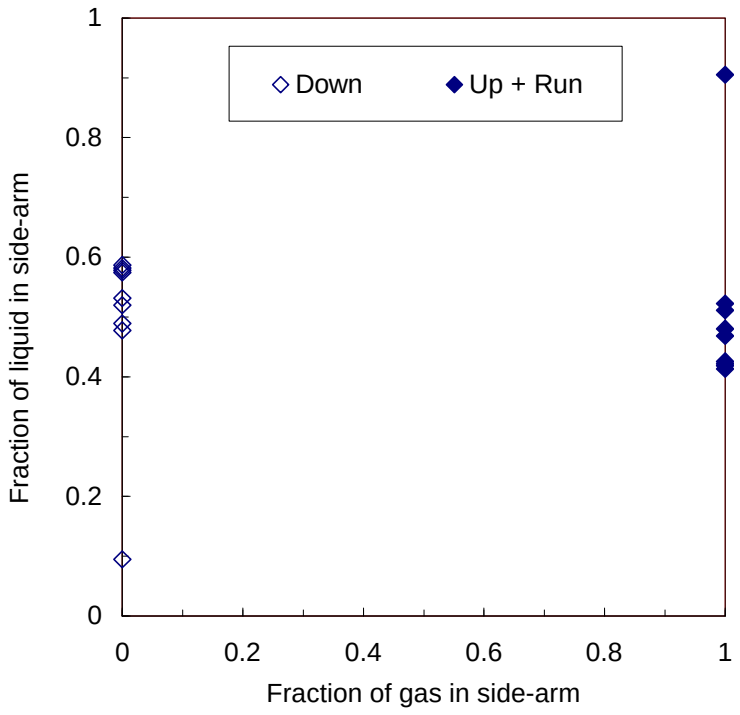

Figure 6.3: Standard phase split plot for T-junction separator

In Chapter 4, the dynamic simulation results were compared using a newly defined Separation Factor term. This was a measure of the disengagement of the two phases in a single fully horizontal T-junction, defined by Equation 6.1.

$$S_F = \frac{WG_3}{WG_2}\frac{WL_2}{WL_3} \qquad [6.1]$$

where, WL_i/WG_i was the liquid/gas mass flowrate (kg/s) in the run (2) or side-arm (3).

For the present situation, with two actual outlets produced from three exit streams, the Separation Factor can be written in an equivalent form, as shown in Equation 6.2.

$$S_F = \frac{WG_5}{(WG_1 - WG_5)}\frac{(WL_1 - WL_5)}{WL_5} \qquad [6.2]$$

where, WL_i/WG_i is the liquid/gas mass flowrate (kg/s) in the inlet (1) or down leg (5).

However, this method, which still attempts to describe the separation in terms of both phases, will always produce a separation factor of zero, since the mass flow of the gas in the down leg (WG_5) is always zero.

Since there is a requirement to determine the possible interactions between the run valve settings and the separation performance of the T-junction system, something that cannot be achieved using standard phase split plots or the Separation Factor, a better method of representing the data is needed. Since in all cases it is known that all measurable gas leaves in the combined gas stream (up plus run arm), the only variable of interest is the amount of liquid diverted into the down leg.

Since the liquid extraction is most likely to be controlled by the setting of the run arm valve a better way of presenting and analysing the phase split data is in relation to this valve setting. This approach produces a graph showing the dependency of the fraction of liquid diverted into the side-arm on the run valve setting. Figure 6.4 shows the same phase split data as previously plotted in Figure 6.3 using this new approach.

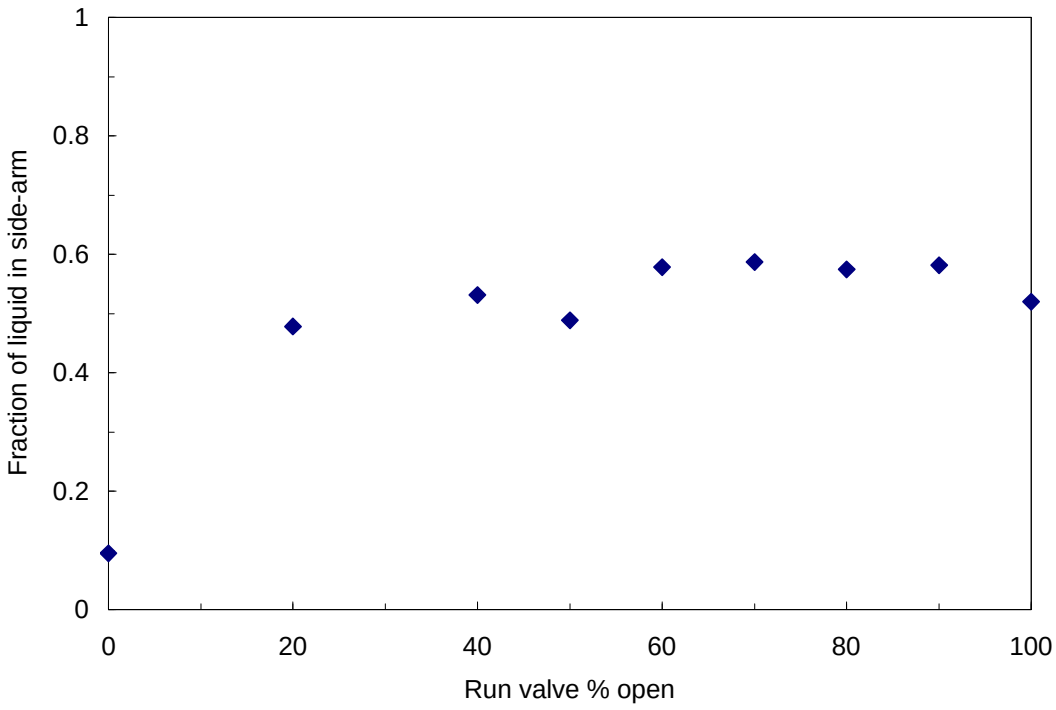

Figure 6.4: Alternative flow split plot for T-junction separator showing influence of run arm valve setting on the fraction of liquid diverted into downwards side-arm (same data as plotted in Figure 6.3)

Comparing the two different representations, Figure 6.3 and 6.4, it is clear that the second graph conveys a lot more useful information. From the first plot, the only relevant piece of information available is the maximum liquid take-off achieved, while the second plot indicates not only this maximum liquid extraction but also the open percentage of the run valve that achieves this optimum recovery. It is also easy to visualise the effect of closing the run valve on the liquid take-off down the side-arm. In this case the best recovery is not associated with the valve fully open but at a setting of around 70% open. Although the phase split does not seem to vary much with the different valve settings, closing the valve beyond 20% open causes a dramatic reduction in the separation.

Although the new plot does show the relationship between the two important variables it does tend to suggest that the dependency of the liquid recovery on the valve setting is relatively constant over quite a wide-range. In order to enhance the characteristics within the data set a further modification was made to the alternative phase split plot. A new Separation Effectiveness Factor, S_{eff}, is defined in terms of the ratio of the mass flowrate of the liquid diverted into the down leg to the mass flowrate of the liquid extracted with the gas. Hence,

$$S_{eff} = \frac{WL_5}{WL_3 + WL_4} = \frac{WL_5}{WL_1 - WL_5} \qquad [6.3]$$

where, WL_i is the liquid mass flowrate (kg/s) in the inlet (1) or down leg (5).

On inspection this Separation Effectiveness is actually the inverse of the liquid-part of the previously defined Separation Factor (Equation 6.2). Using this concept the Separation Effectiveness can take any positive value. A Separation Effectiveness of one implies half of the liquid enters the down leg, while a value of two would imply that twice as much liquid leaves in the down leg compared with the gas stream.

Figure 6.5 shows the Separation Effectiveness plot for the same data as previously plotted in Figures 6.3 and 6.4. The advantage of using this ratio approach can be clearly seen. Such a plot magnifies the effect of the run valve setting on the liquid recovery. This makes it easier to locate the value of the run valve setting at which the Effectiveness Factor takes its highest value, which is the optimum run valve setting. An addition of a curve of best-fit, in this case a second-order polynomial, also acts to highlight the key optimum point of operation.

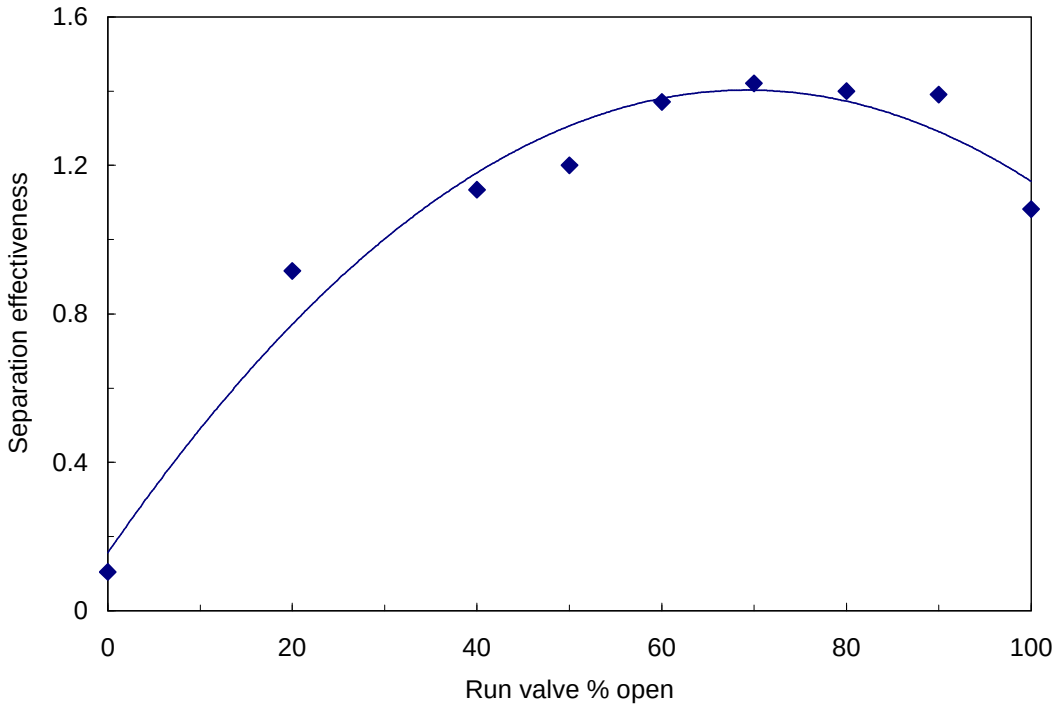

Figure 6.5: Separation effectiveness plot for downward branch of T-junction (same data as plotted in Figure 6.3)

6.2 Phase Separation Performance

The use of the run arm valve in enhancing the phase separation of the T-junction system was previously highlighted in Chapter 5. It was proposed that more liquid could be diverted into the liquid exit stream if the liquid hold-up at the downward junction could be increased. This is best achieved by closure of the run valve, thus reducing the flow out of the run arm and increasing the residence time of the liquid at the T-junction. By implementation of the previously described systematic grid of gas and liquid flowrates, traversing the stratified and slug flow regimes, it is possible to identify the trends associated with variations in both phase flowrates.

Since there are fundamental differences between the stratified and slug flow patterns, in terms of phase velocities and distributions across the pipe cross-section, it would be expected that the separation performance may also differ. Indeed Chapter 5 has

already highlighted the potential dependency of the flow split on the flow pattern, thus the results of the two cases will be considered separately.

6.2.1 Separation of Stratified Flow

The Separation Effectiveness results for stratified flows, corresponding to the lowest liquid flowrate, are shown in Figure 6.6. Across the entire range of superficial gas velocities studied there is a pronounced peak value of the Separation Effectiveness all corresponding to a valve setting of 20% open. It is observed that as the gas inlet superficial velocity increases, the peak Separation Effectiveness value decreases. There are several reasons why this may occur.

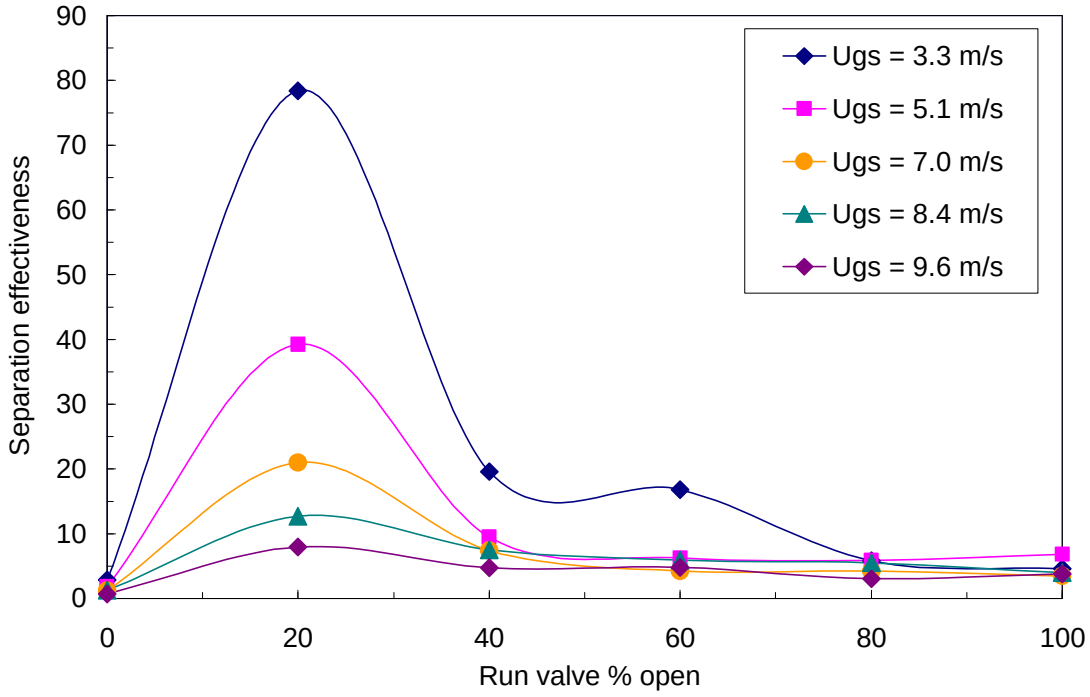

Figure 6.6: Separation Effectiveness plot for stratified flows with a constant liquid superficial velocity, U_{ls} = 0.07 m/s

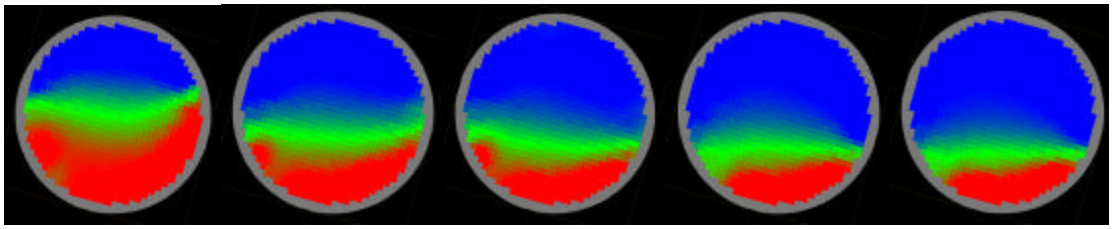

U_{gs} = 3.3 m/s 5.1 m/s 7.0 m/s 8.5m/s 9.6 m/s

Figure 6.7: Typical set of tomographic image showing effect of increasing gas superficial velocity, U_{ls} = 0.07 m/s

Examining the reconstructed electrical capacitance tomography images for each of the flow conditions can provide some insight into the obtained flow split results. Figure 6.7 shows a typical set of tomographic images for a constant liquid superficial velocity of 0.07 m/s and increasing gas flowrates. The blue area represents the gas phase, the red zone indicates the liquid phase and the green band shows the region of the gas-liquid interface. This green band, considered as an *area of uncertainty*, is a consequence of three factors. The first is that the capacitance measurements are obtained across 0.035 m long electrodes. This implies that they are more correctly interpreted has being only the average capacitance values representative of the flow in that pipe section. Figure 6.8 shows a simplified schematic representation of a stratified gas-liquid flow passing the electrode zone and the associated reconstructed image. The size of this area of uncertainty will depend on the frequency and height of any interfacial waves.

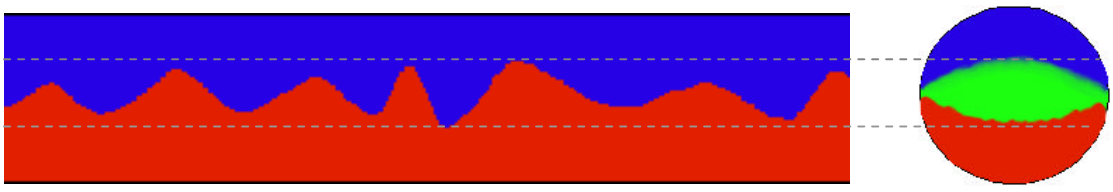

Figure 6.8: Schematic of gas (blue) and liquid (red) flow passing the electrodes showing an associated reconstructed tomographic image highlighting the problem of the wavy interface

The second factor leading to the green zone is the entrainment of gas bubbles within the liquid phase. This is especially apparent within the slug flow regime, where the liquid slugs can be highly aerated leading to lower pseudo-permittivity values. Finally, the reconstructed image itself is only a simple 32 by 32 pixel grid representing the much finer permittivity distribution grid. This will obviously imply some loss of information and a much poorer spatial resolution, in the order of 1.2 mm.

So, although the tomographic images are a good representation of the flow within the pipework they are do not have sufficient spatial resolution to accurately determine liquid heights. Nevertheless, they provide evidence of the expected trends that have been well documented within the literature, for example by Taitel and Dukler (1976), that as the gas superficial velocity increases the equilibrium liquid height decreases and, by the theory of continuity, the actual liquid velocity within the stratified layer must increase. This faster travelling liquid has more momentum to pass through the partially run opened valve and the hold-up the downward T-junction is reduced. As the actual liquid velocity decreases, the stratified layer in the pipe increases in depth and this extra depth and reduced momentum means increases the liquid hold-up at the junction. Thus more liquid is given the opportunity to fall into the down leg.

These same trends are observed within the results of other workers who have studied two-phase flow split using more conventional downwardly inclined side-arm junctions. For example, Wren (2001) observed that the onset of gas entrainment, the critical liquid take-off value before which no gas leaves with the liquid in the vertical down leg, decreases with increasing gas superficial velocity. This was explained by the fact that before the gas could enter the downward side-arm it had to pass through the liquid layer flowing along the bottom of the pipe. As this liquid layer reduces in depth, by increasing gas superficial velocity for a constant liquid velocity, it becomes easier for the gas to overcome the pressure difference between the inlet and the branch and breakthrough the liquid layer. As a result the gas can be pulled through the stratified layer sooner, and so the onset of gas entrainment occurs for lower values of liquid fraction take-off. These same trends are also observed within the data of Reimann *et al.* (1988), Peng (1994) and Penmatcha *et al.* (1996).

By examining the flow split at the first vertically upward T-junction it is also possible to identify another reason why the Separation Effectiveness reduces with increasing gas superficial velocity. Figure 6.9 shows the effect of gas superficial velocity on the flow split at the vertical T-junction for stratified flow, with a constant liquid superficial velocity of 0.07 m/s.

With a vertical side-arm the liquid cannot simply fall into the junction opening but it has to be physically transported upwards by the gas stream. When the actual gas velocity in the side-arm is low, it is not sufficient to overcome the inertia of the higher momentum liquid phase, even though the liquid is travelling relatively close to the top of the pipe. Thus when the gas superficial velocity is 3.3 m/s, for a liquid superficial velocity of 0.07 m/s, no liquid enters in the up arm. In this case, all the liquid reaches the down leg and, since it travels with the lowest momentum, this correctly corresponds to the best separation performance. Interestingly these conditions agree with the empirical equation of Reimann *et al.* (1988), for the maximum branch mass flux where only gas is extracted. In that study an empirical relationship was defined in terms of the diameter of the pipe and the physical properties of the fluids. For stratified flow the relevant equation becomes:

$$MG_{3,x=1} = 0.23\left(gD\left(\rho_l - \rho_g\right)\rho_g\right)^{0.5} \qquad [6.4]$$

Solving this for the current fluid properties and pipe geometry produces a maximum gas flux of 4.702 kg/m^{2}s. This corresponds to a gas mass flowrate of 0.0054 kg/s, which is equivalent to an inlet gas superficial velocity of 3.4 m/s. This result reflects the observations found from the current study.

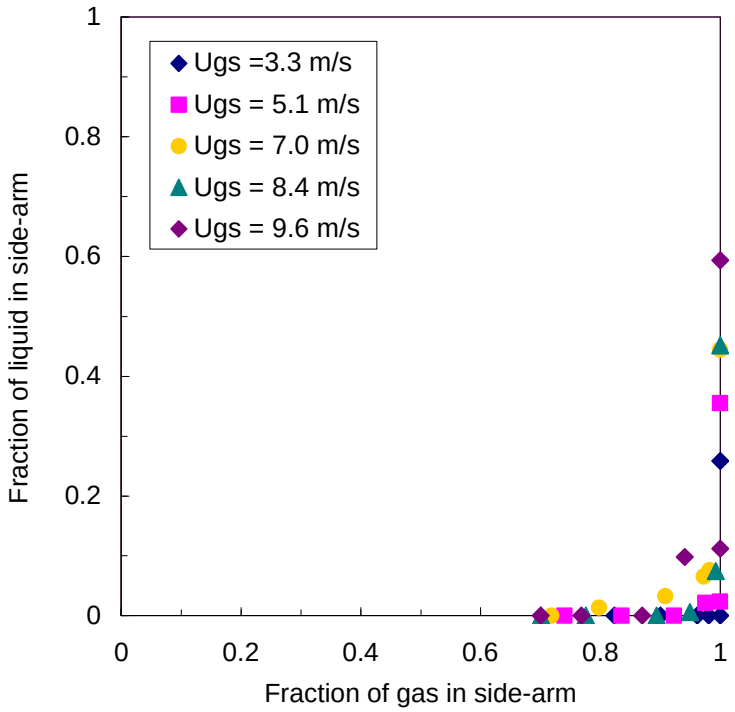

Figure 6.9: Effect of gas superficial velocity on the phase split at the upward side-arm for constant liquid superfcial velcoity = 0.07 m/s

As the gas velocity in the side-arm increases the fraction of liquid extracted also increases. This is in accordance with the Bernoulli Effect, where as the gas velocity in the side-arm increases it tends to reduce the pressure, pulling more liquid upwards. This effect is seen most clearly at the extreme situation of total gas extraction in the side-arm, when the run arm valve is fully closed. Here the liquid fraction entering the side-arm increases with the gas superficial velocity. Again, these findings are confirmed by the results of other workers, including Reimann *et al.* (1988), Smith and Azzopardi (1990) and Wren (2001). Obviously as more liquid is extracted with the gas in the up arm less becomes available for recovery in the down leg and the Separation Effectiveness values will decrease. The combination of these two effects, hold-up at the downward T-junction and increasing liquid take-off at the upward junction, leads to an inverse exponential-type relationship between the gas flowrate and the maximum Separation Effectiveness value achieved.

6.2.2 Separation of Slug Flow

The Separation Effectiveness curves for slug flows are quite different to those for stratified flows. Figure 6.10 shows a comparison between two such cases. Here the gas superficial velocity is 9.6 m/s and the liquid superficial velocity varies from 0.17 m/s, for stratified flows, to 0.29 m/s and 0.40 m/s, for slug flows.

There are three things that are immediately noticeable from the plots. The first is that the stratified flow case follows the same trend as discussed above for different liquid flowrates, with a distinct peak occurring at a valve setting of 20% open. This confirms that the optimum valve setting for stratified flows is independent of both the gas and liquid superficial velocities.

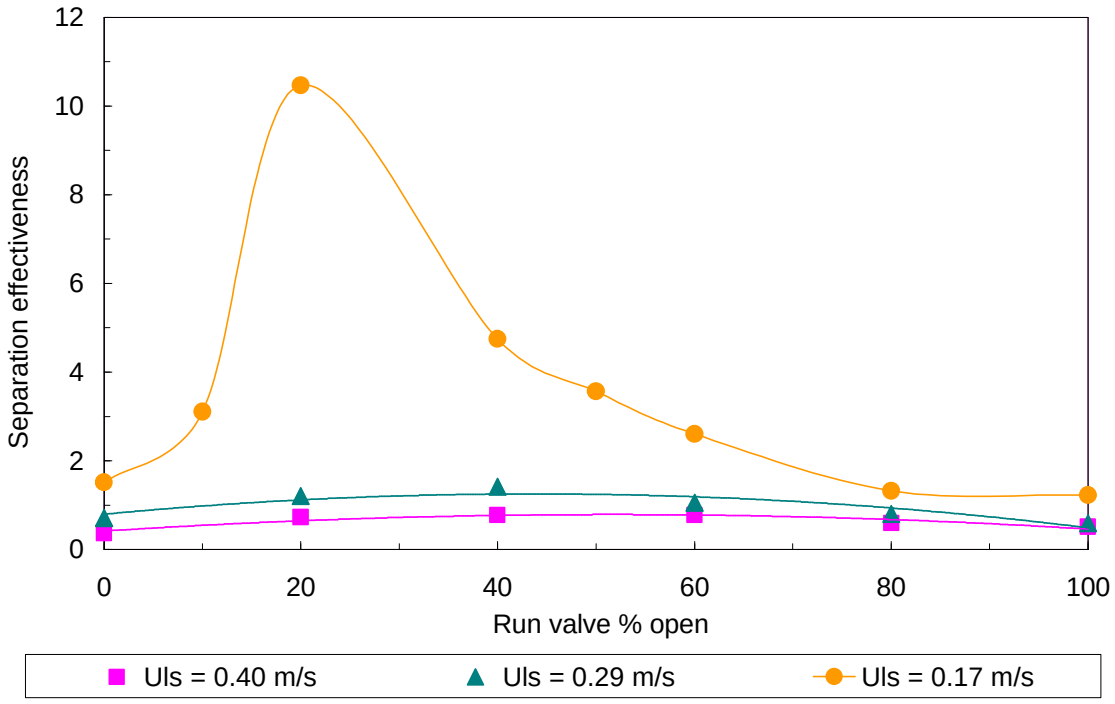

Figure 6.10: Separation Effectiveness plot for constant gas flow, U_{gs} = 9.6 m/s, highlighting difference between stratified (U_{ls} = 0.17 m/s) and slug flows (U_{ls} = 0.40 m/s and 0.29 m/s)

The second point to note is the contrast in the shapes of the Separation Effectiveness curves between stratified and slug flows. Finally, the value of the maximum Separation Effectiveness is considerably greater for stratified flow than for slug flow. This highlights how much easier it is to separate stratified flows due to the lower phase momenta associated with stratified flows coupled with the more uneven gravity-induced phase distribution.

Figures 6.11 to 6.14 show the Separation Effectiveness data for a range of liquid and gas superficial velocities. The lines are the second-order polynomial lines of best-fit to the experimental data. In all cases the data are well represented by these simple functions, with the coefficients of determination, the R^2 values, calculated to be in the range of 0.823 to 0.995.

An initial consistent observable trend is that as the liquid superficial velocity increases, under constant gas flowrate conditions, the Separation Effectiveness value decreases. This effect being most noticeable for the lowest gas superficial velocity, Figure 6.11. As the liquid flowrate is decreased the flow tends to be more stratified in nature and as observed by Reimann *et al.* (1988), the more stratified the flow, the greater tendency for the liquid to preferentially enter a downward side-arm. This can be attributed to the characteristics of the slug flow regime. In general, slug flow is described as an intermittent flow, with two distinct gas-liquid regions, a liquid slug body with entrained gas bubbles, and a gas-pocket region with the liquid flowing as a stratified layer. These two zones will have a different flow splitting nature.

The gas-pocket zone with the liquid flowing as a stratified layer below the gas, could be expected to behave in a similar way as to normal stratified flow. This will then have the same consequences as outlined in Section 6.2.1 above for actual stratified flows. With both phases travelling with more momentum, more liquid would be entrained upwards with the gas at the first junction and the liquid will tend to have enough momentum to by-pass the downward side-arm.

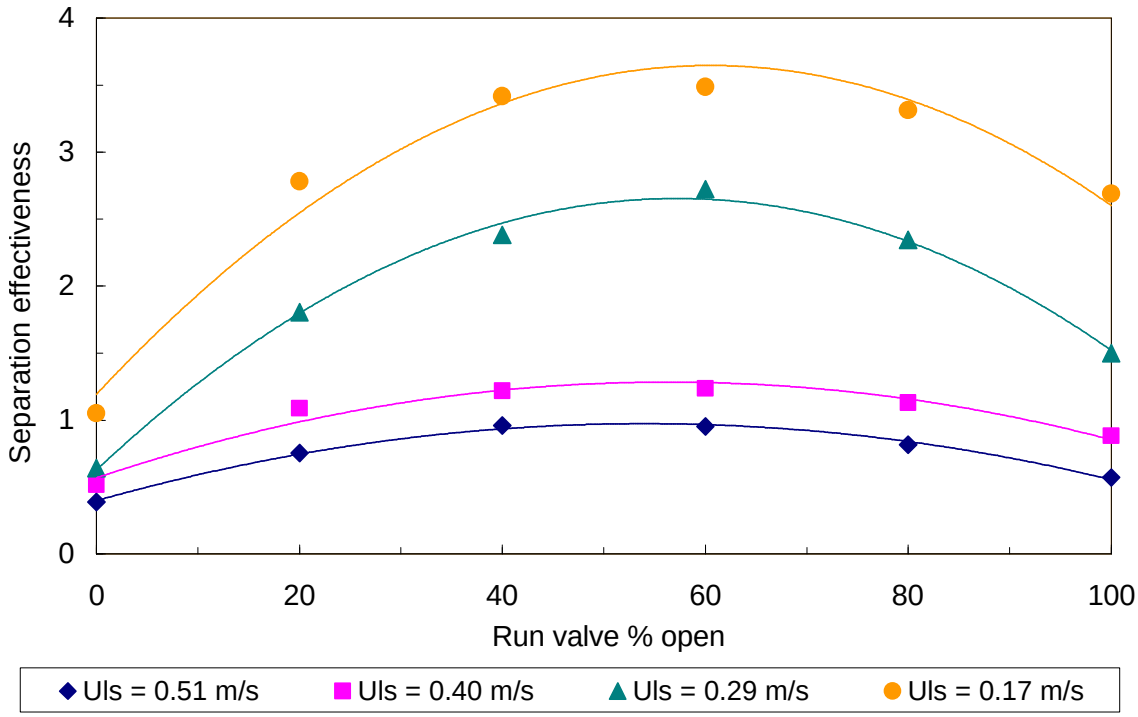

Figure 6.11: Separation Effectiveness plot for slug flow with a constant gas superficial velocity, U_{gs} = 3.3 m/s,

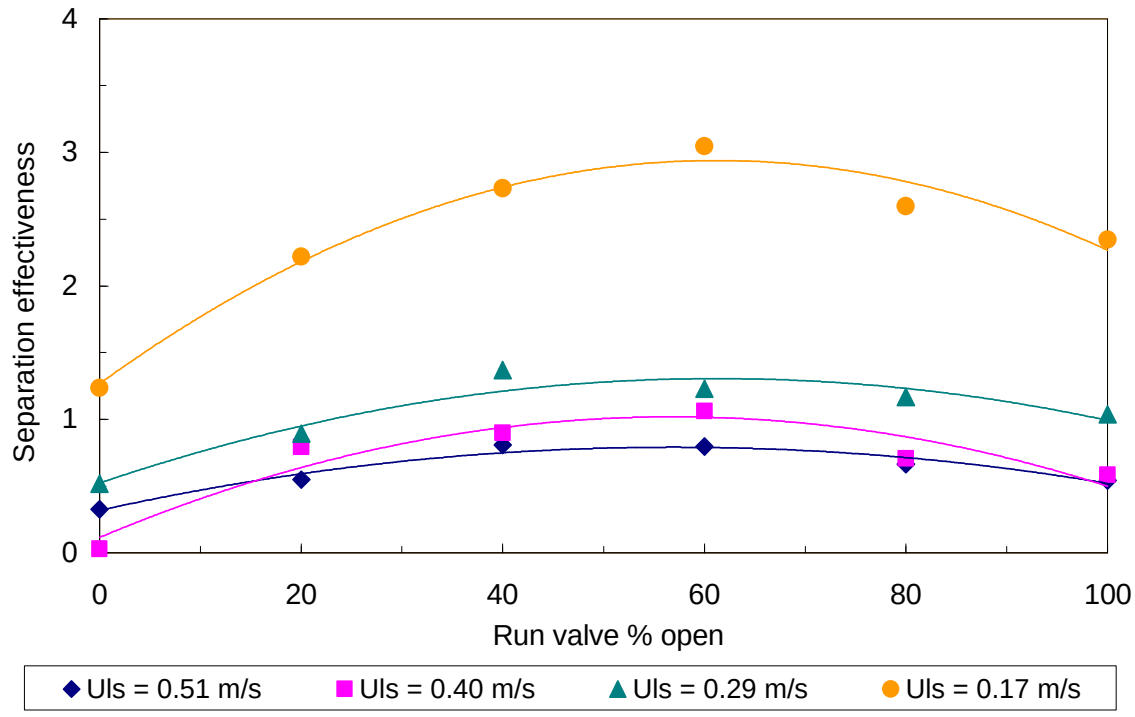

Figure 6.12: Separation Effectiveness plot for slug flow with a constant gas superficial velocity, U_{gs} = 5.1 m/s

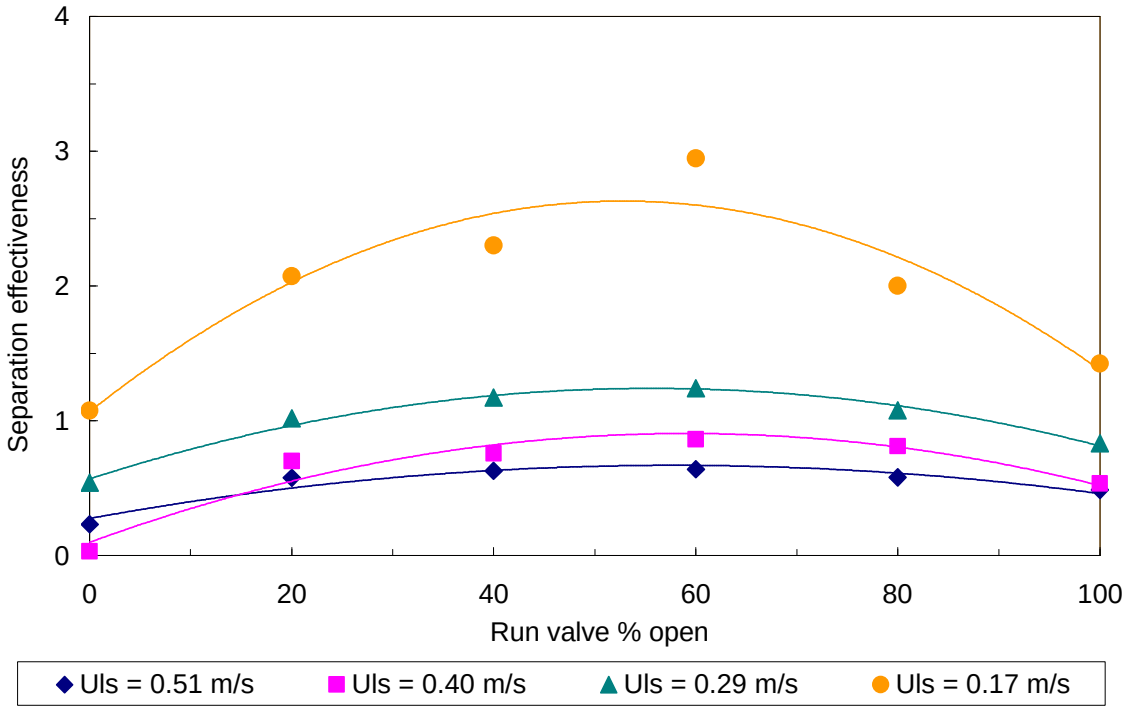

Figure 6.13: Separation Effectiveness plot for slug flow with a constant gas superficial velocity, U_{gs} = 7.0 m/s

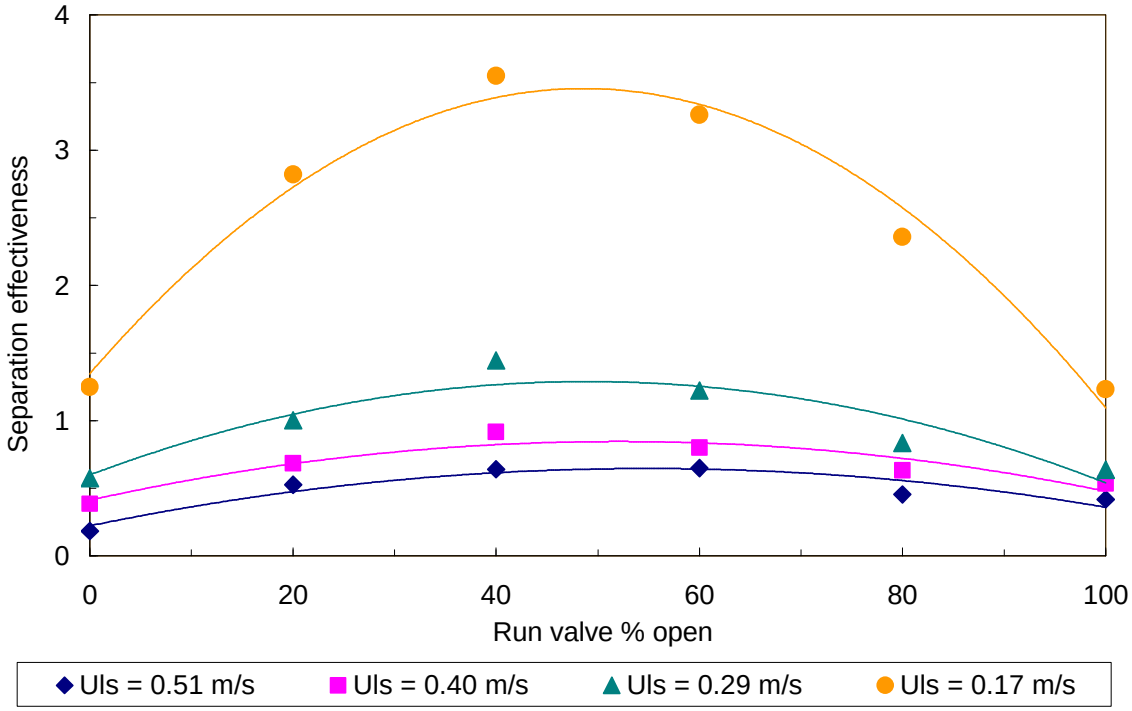

Figure 6.14: Separation Effectiveness plot for slug flow with a constant gas superficial velocity, U_{gs} = 8.4 m/s

The liquid slug zone itself will be comprised of a liquid body with entrained gas bubbles, travelling with approximately the mixture velocity; that is the sum of the gas and liquid inlet superficial velocities. In general, the majority of the liquid will travel within this slug body and it will have a significantly higher momentum than the stratified flow behind it.

From the shape of the Separation Effectiveness curves, it may be suggested that it is the liquid slug zone that has a greater influence on the flow splitting performance. If it were the stratified regions that had the larger impact then it could be expected that the separation curves would show the same peak values at a valve setting of 20% open. However, although different to the stratified flow cases, the slug flow data exhibit comparable trends in the shape of the Separation Effectiveness plots. The peak Separation Effectiveness, although not as pronounced as for the stratified regime, still exits for slug flows.

With the valve fully open the liquid especially that contained in the slug body will tend to by-pass the down leg, reducing the Separation Effectiveness. Conversely, with the run valve fully closed, the Separation Effectiveness value is even lower. Observations show that with the valve closed no fluids can leave through the run so the system then operates with only two exit streams. This is more like a standard single junction with a vertically upward side-arm. However, with the presence of the liquid level control on the downward exit stream, the pressure drop through the system is increased. The liquid velocity beyond the first T-junction was significantly reduced by the higher pressure drop at this downwards outlet. Visual observations show the liquid forming almost stationary slugs in the pipe section between the two junctions, and at certain times these slugs were seen to oscillate forwards and backwards in response to pressure fluctuations caused by the arrival of gas pockets at the first junction. These surges of gas into the side-arm could then easily sweep large fractions of the very slow moving liquid into the branch with it. This phenomenon was most prominent at the highest liquid flowrates.

Examination of the liquid level data for the two extreme operational cases, fully open and fully closed, illustrates this trend. Figure 6.15 compares the liquid level variation over a one minute time period for the same set of inlet conditions with the run valve set in the two positions. With the valve fully open, the liquid height shows the expected large deviations associated with slug flows. However, with the valve fully closed the liquid flow into the down leg was dramatically reduced and the automatic level control could not maintain the set point value of 400 mm as the liquid level showed a gradual reduction in height over time.

As the liquid superficial velocity increases the Separation Effectiveness shows a decrease. This can be explained in two ways. The first is that as the liquid velocity increases the slug frequency also increases and so the relative fraction of liquid travelling within the liquid slug body increases as well as the overall liquid hold-up in the system. As described above, slugs with a higher momentum, tend to by-pass the down leg more readily than the stratified liquid region.

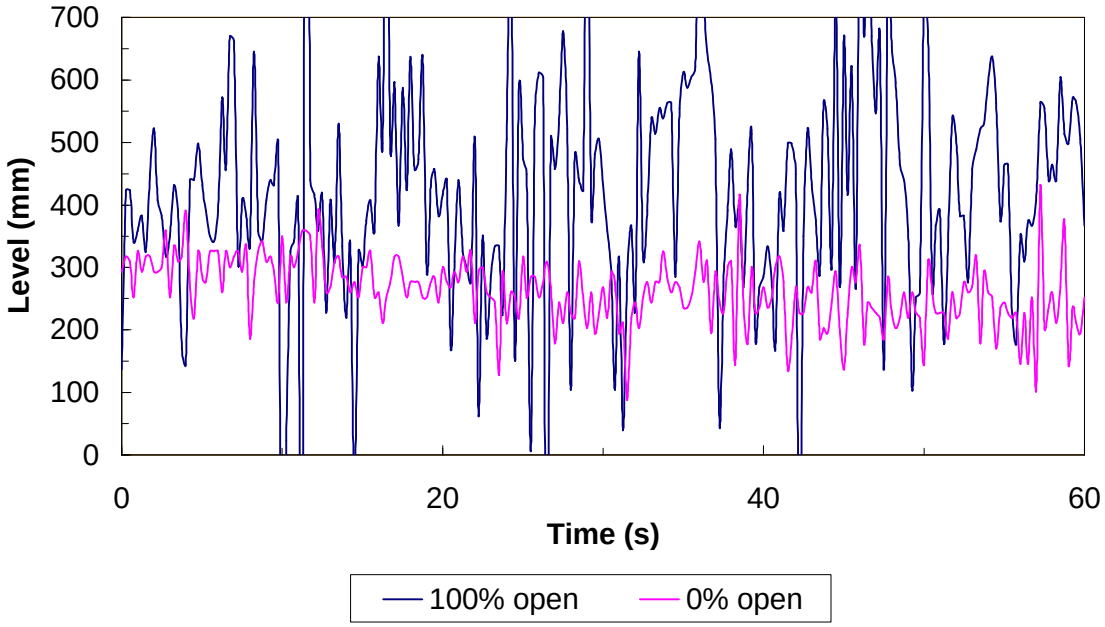

Figure 6.15: Variation of the liquid level in down leg for slug flow for different run control valve settings (U_{ls} = 0.40 m/s, U_{gs} = 5.1 m/s)

The second, and more prominent, reason why the Separation Effectiveness decreases with increasing liquid flowrate can be observed within the flow split data at the first vertical upward T-junction. Figures 6.16 and 6.17 illustrate the effect of liquid superficial velocities on the flow split at the vertically upward T-junction for two different gas superficial velocities. The trend is clearly observable, increases in the liquid superficial velocity produce increases in the fraction of liquid leaving in the upward side-arm for a given gas take-off. These results are similar to those described by, among others, Reimann *et al.* (1988), who suggest that it is the flow in the upper part of the pipe that is most influenced by the upward T-junction. The lower the void fraction is in the upper part of the pipe cross-section, the lower the void fraction will be in the resultant branch stream.

Since the void fraction within the pipe will decrease with increasing liquid flowrates, there is a greater chance of liquid entering the side-arm. Comparing Figures 6.16 and 6.17, the gas superficial velocity appears to have relatively little effect on the liquid take-off, except at the lowest liquid velocities, where more liquid is extracted at lower gas take-off values. Again, this is attributed to the Bernoulli Effect, as described previously in Section 6.2.1, where as the gas velocity in the branch arm increases it is more capable of pulling liquid into the side-arm with it.

Thus, combining the two effects described above, there must be a balance in the operation of the run control valve. It needs to be sufficiently open to allow liquid to flow through it, thus reducing the pressure drop and preventing a stationary liquid presence at the first T-junction, but also sufficiently closed to provide a liquid hold-up at the second T-junction.

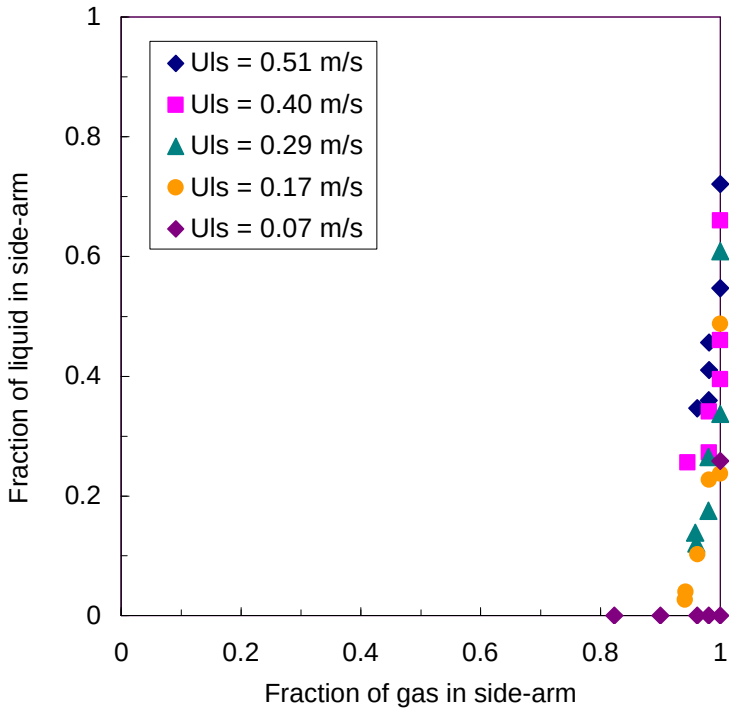

Figure 6.16: Effect of liquid superficial velocity on the phase split at the upward side-arm for constant gas superficial velocity = 3.3 m/s

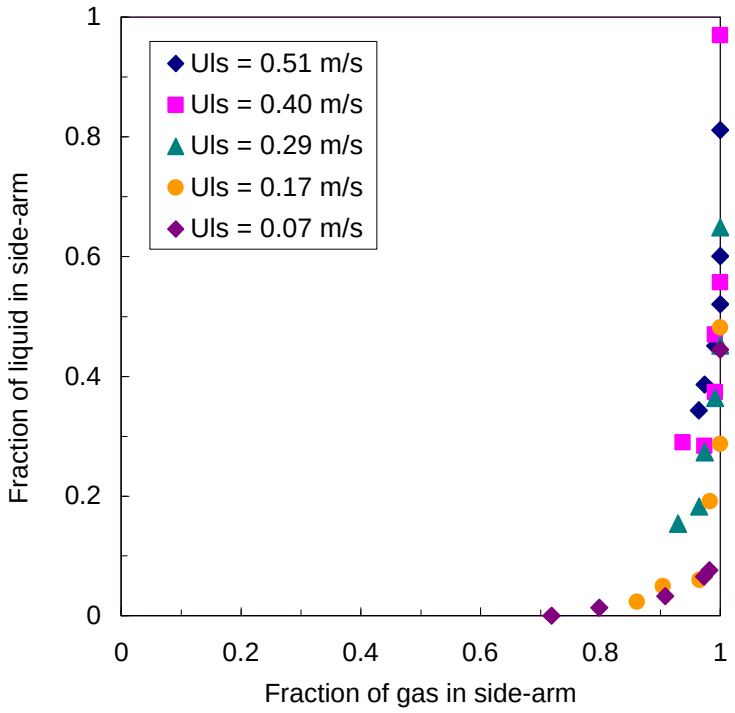

Figure 6.17: Effect of liquid superficial velocity on the phase split at the upward side-arm for constant gas superficial velocity = 7.0 m/s

6.2.3 Further Observations on the Flow Split at the Upward T-junction

Although the flow split at the first vertically upwards T-junction as already been discussed in reference to the Separation Effectiveness curves there are other interesting observations that can be made.

Figures 6.18 and 6.19 compare the flow split at the vertical T-junction with various gas superficial velocities for two different liquid superficial velocities. The extreme case, with the lowest liquid superficial velocity has previously been shown in Figure 6.9. At the highest liquid flowrate, where slug flow is always observed, the high gas take-off flow split is seen to be independent of the gas flowrate. Again this is agreement with the data of Reimann *et al.* (1988), who found that at values of high gas take-off the flow split tended towards the limit of total gas separation irrespective of the individual phase velocities.

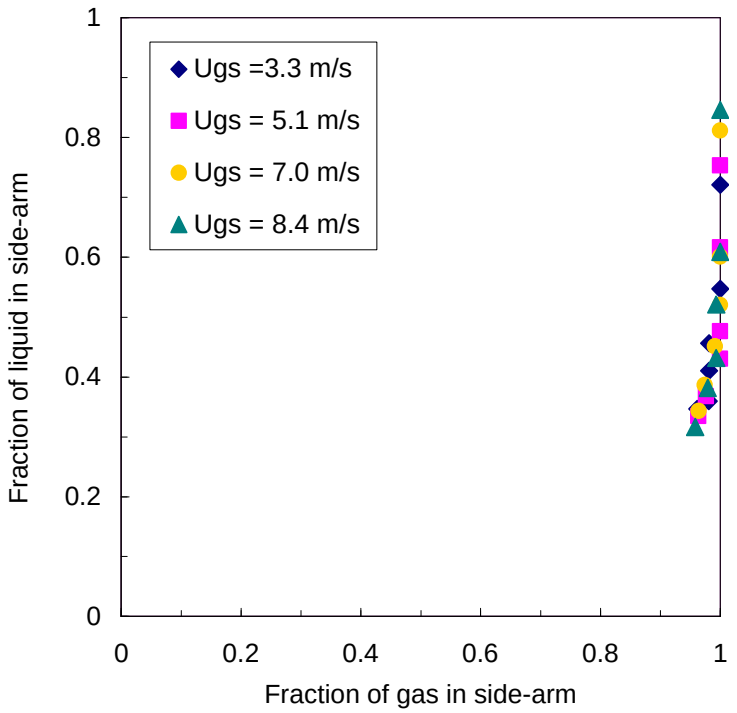

Figure 6.18: Effect of gas superficial velocity on the phase split at the upward side-arm for constant liquid superficial velocity = 0.51 m/s

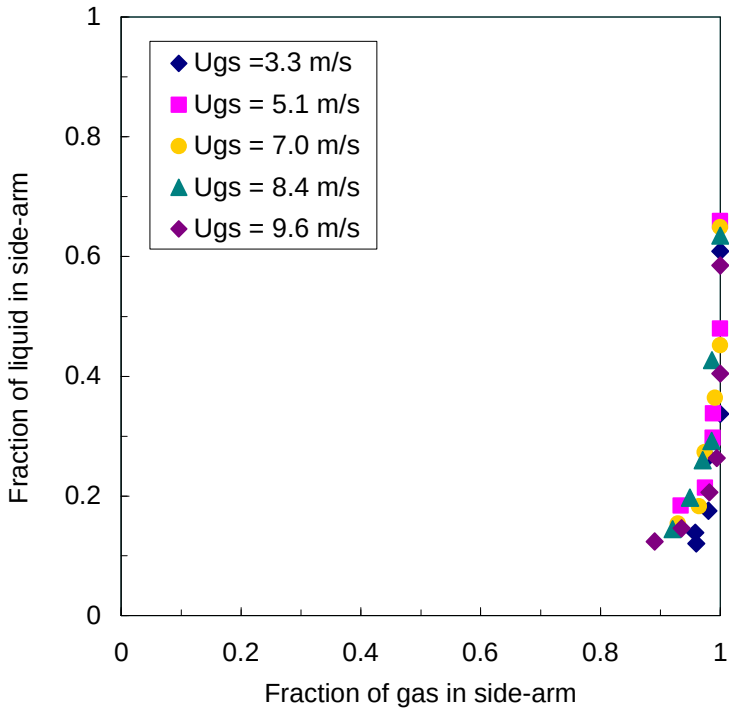

Figure 6.19: Effect of gas superficial velocity on the phase split at the upward side-arm for constant liquid superficial velocity = 0.29 m/s

As the liquid superficial velocity is reduced, there is a tendency of the flow split to diverge, with the lowest gas superficial velocity having the lowest liquid take-off. As the liquid flowrate is reduced less liquid is extracted for a given value of gas take-off. This is yet another occurrence of the Bernoulli Effect, where at the low gas flowrates the gas velocity in the side-arm is not sufficiently high to pull the liquid into the branch.

6.2.4 Optimum Run Valve Settings

The main reason for studying the dependency of the liquid recovery on the run valve setting is to try and establish a control strategy based on the principle of maximising the gas-liquid separation. Identification of the maximum Separation Effectiveness Factor, and hence the optimum run valve setting, can be obtained by analysis of the Separation Effectiveness plots. Since the separation data had very different shapes,

depending on the flow regime within the system, two different methods need to be employed. However, the basic notion in both situations remains that the optimum setting of the run arm valve must occur when the liquid recovery in the down leg is at a maximum. This maximum liquid take-off has a direct relationship to the maximum Separation Effectiveness.

For stratified flows there always exists a definite maximum Separation Effectiveness value at a run valve setting of 20% open. This can be visibly identified within Figure 6.10. In the case of the slug flow regime data, the same pronounced peak is not observed, but a maximum Effectiveness value does still exist. It has been confirmed previously, in Section 6.21, that the Separation Effectiveness within the slug flow regime is a function of the valve setting and the two inlet flowrates:

$$S_{eff} = f(V, U_{ls}, U_{gs}) \qquad [6.5]$$

Here S_{eff} is the Separation Effectiveness, V is the percentage valve setting and U_{ls} and U_{gs} are the liquid and gas superficial velocities, respectively. Furthermore, for a given set of inlet conditions the Separation Effectiveness plot can be adequately described by a simple second-order polynomial. Thus for known gas and liquid superficial velocities Equation 6.6 represents the Separation Effectiveness, S_{eff}, solely in terms of the valve setting, V, and experimental determined constants, a, b and c.

$$S_{eff} = aV^2 + bV + c \qquad [6.6]$$

The maximum (or minimum) value of any second-order function occurs when the gradient of the curve it represents equals zero. Mathematically this relates to the solution of the first derivative of the function equated to zero. By inspection of the Separation Effectiveness curves it is known that only a maximum value can be obtained within the limits of the run valve being fully closed and fully open (0 - 100% open).

Thus, solving Equation 6.4 for each set of gas and liquid flowrates will provide the optimum run valve setting, V_{opt}, as given in Equation 6.7.

$$\frac{\mathrm{d}S_{eff}}{\mathrm{d}V} = 2aV_{opt} + b = 0 \qquad [6.7]$$

Substituting the obtained optimum run valve setting into the corresponding second-order polynomial will then generate the corresponding maximum Separation Effectiveness, $S_{eff,\,MAX}$. Since the fraction of liquid diverted into the down arm can be directly related to the Separation Effectiveness the maximum liquid off-take can be obtained using Equation 6.8.

$$L'_{MAX} = \frac{S_{eff,MAX}}{S_{eff,MAX} + 1} \qquad [6.8]$$

The same optimum valve setting data can also be obtained graphically, as the maximum Separation Effectiveness values can be interpreted directly from the relevant plots. This process is illustrated in Figure 6.20. Here the red horizontal dashed-line is the tangent of the curve parallel to the *x*-axis, the point when the gradient equals zero. This line intercepts the *y*-axis at the maximum Separation Effectiveness value, $S_{eff,\,MAX}$. The vertical red dashed-line is then the normal to the polynomial curve at this tangential point and will intercept the *x*-axis at the corresponding optimum valve setting, V_{opt}.

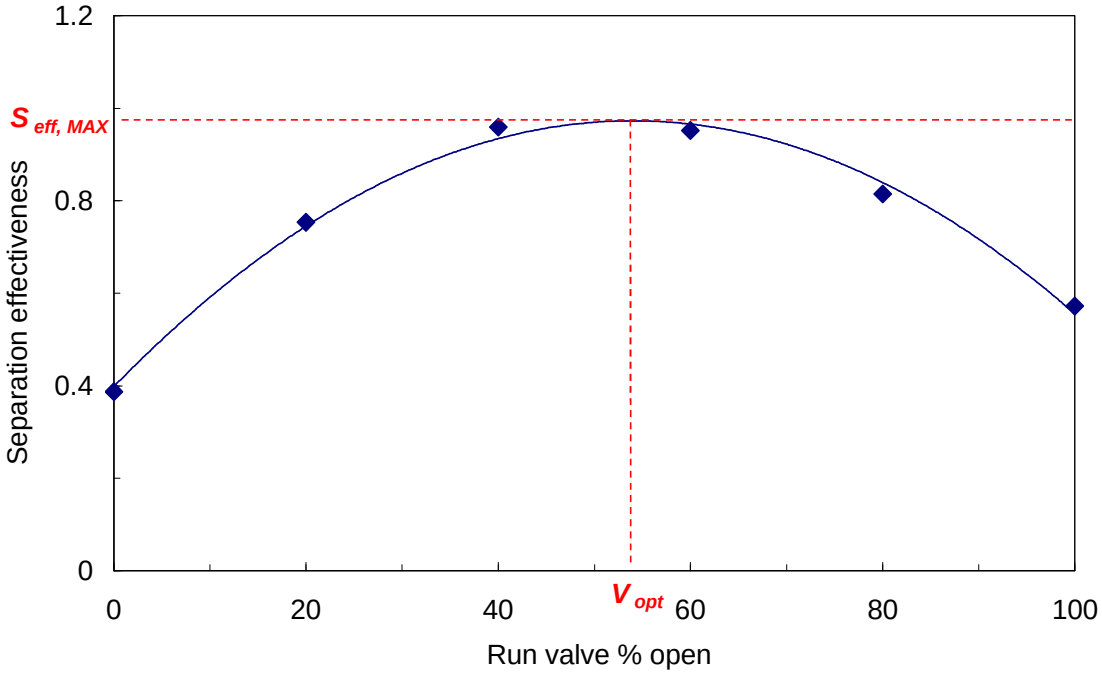

Figure 6.20: Determination of the optimum run valve setting, U_{gs} = 3.3 m/s, U_{ls} = 0.51 m/s

The above methodology was then applied to the entire slug flow data set to obtain the optimum valve settings for the full range of gas and liquid superficial velocities investigated. For the stratified flow cases remember that the optimum valve setting and maximum Separation Effectiveness values are obtained through direct inspection of the data. Figure 6.21 shows the results of this analysis in terms of the individual gas and liquid superficial velocities. The clear distinction already observed between stratified and slug flows is further highlighted here.

For stratified flows (U_{ls} = 0.07 m/s for all gas flowrates and U_{ls} = 0.17 m/s with a gas flowrate of U_{gs} = 9.6 m/s) the optimum run valve setting always takes the value of 20% open. This is, of course, only a confirmation of the expected results already directly observed from the Separation Effectiveness data.

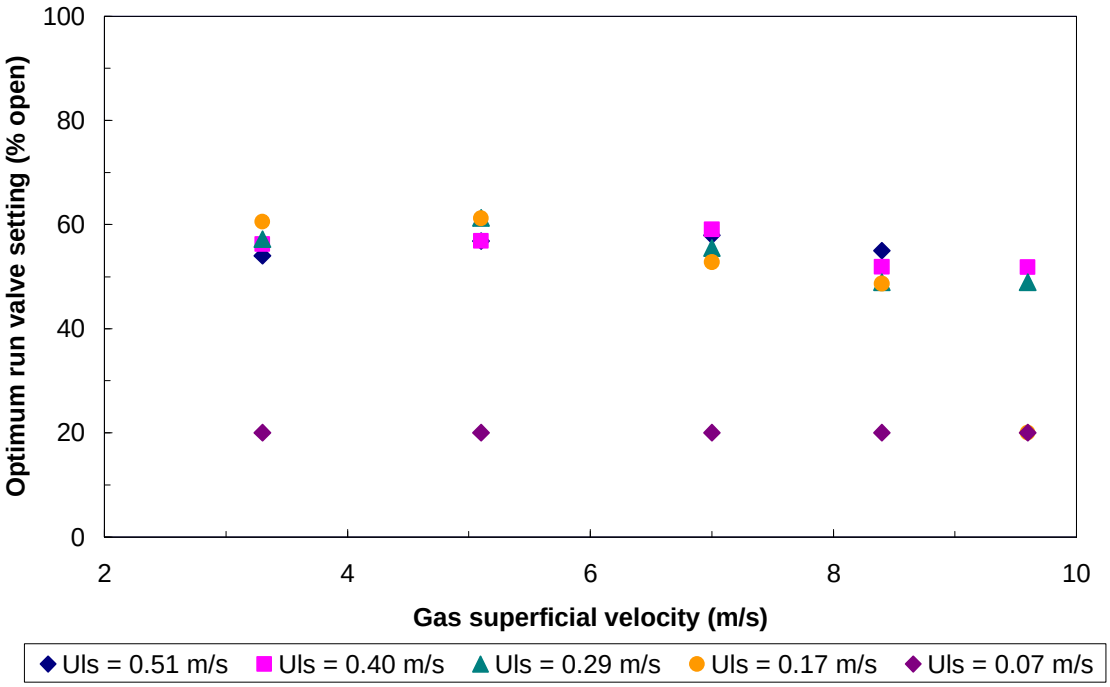

Figure 6.21: Dependency of the optimum run valve setting on the inlet phase superficial velocities

In the case of the slug flow regime the results also exhibit an interesting trend. Over the entire range of flow conditions investigated there is a negligible influence of either liquid or gas superficial velocity on the optimum valve setting. This result suggests that it is possible to assign a single value for the run valve setting within the slug flow regime, independent of the flow conditions. Assuming this single setting to be represented by the mean of the total data set, the optimum run valve setting for the slug flow regime can be calculated to be 55% open.

Solving the slug flow polynomial equations, in the form of Equation 6.6, for this valve setting of 55% open will then identify the maximum Separation Effectiveness value for each set of flow conditions. Substituting these maximum values into the equivalent form of Equation 6.8 for each data set it is then possible to calculate the associated maximum liquid mass fraction that can be expected to leave the T-junction separator through the liquid only down leg. For the stratified flow cases the

maximum Separation Effectiveness value can be directly interpreted from the data and then inputted into Equation 6.8 to calculate the maximum liquid fractions.

The results of these maximum liquid take-off calculations, for both flow regimes, are shown in Figure 6.22, again based on the individual phase superficial velocities. It is worth noting that the average absolute error between the liquid fractions taken for the average run valve settings (55% and 20% open for slug and stratified flows, respectively) and those obtained with the valve set at its fully optimised condition for each individual case is only 1.03%. These negligible differences emphasise the above proposal of assuming a constant run valve setting dependent only on the flow pattern within the pipe.

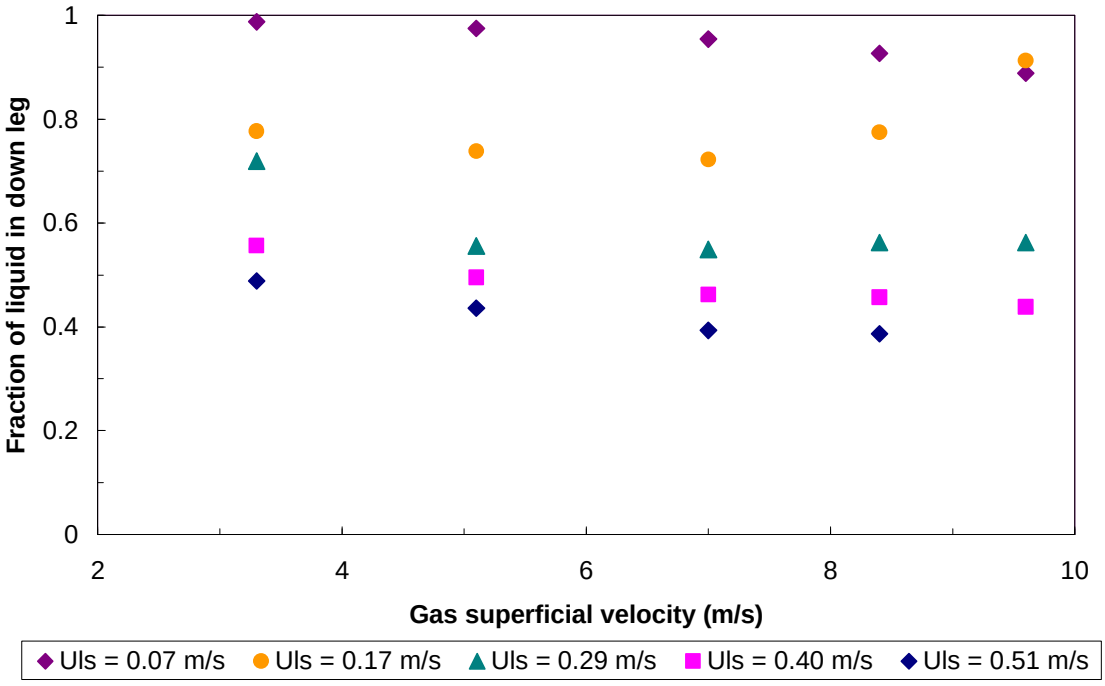

Figure 6.22: Effect of gas and liquid superficial velocities on the maximum liquid fraction diverted into down leg based on determined run valve settings (stratified flow: 20% open, slug flow: 55% open)

The fraction of liquid diverted into the down leg follows a similar trend to that observed for the run valve setting, in that it appears to be almost independent of the gas superficial velocity over the range of flowrates investigated.

The aim of the partial separation system proposed is to satisfy a set separation criterion as already defined in Chapter 1. Recalling these criteria the objectives are to obtain a gas-rich stream with less than 10% v/v of liquid and a liquid-rich stream with less than 10% v/v gas. The latter requirement is met by the implementation of the automatic level control preventing any measurable amount of gas leaving with this liquid stream. The other stream composition is then determined by the optimised setting of the run valve, which maximises the liquid recovery and so reduces the liquid content of the gas-rich stream.

Figure 6.23 shows the liquid percentage volumetric content in the gas-stream in relation to the gas and liquid superficial velocities. The important point to note is that in all cases there is always less than 10% v/v liquid within the gas exit stream, thus the separation criterion is always achieved. Further inspection shows that only one point has a liquid content significantly over 5% v/v and within the stratified regime the final gas stream always contains less than 0.20% v/v liquid. The general trends show that the liquid volumetric fraction increases both with decreasing gas superficial velocity and increasing liquid superficial velocity. This is in agreement with the previous discussions on the flow split at the junctions.

An alternative method to evaluate the separation performance is to examine the liquid content of the gas exit stream with respect to the feed stream composition. Figure 6.24 shows a plot of the ratio of the volumetric fraction of liquid in the gas-rich exit stream to the volumetric fraction of liquid in the feed stream. Here a value of one would represent no phase separation occurring, while a value greater than one would imply that less gas is present in the exit stream than in the two-phase inlet. The lower the value of this ratio, the better the achieved separation is. Here the value for this ratio is always less than 0.6, and so it is possible to conclude that in all cases the T-junctions have provided some degree of phase separation.

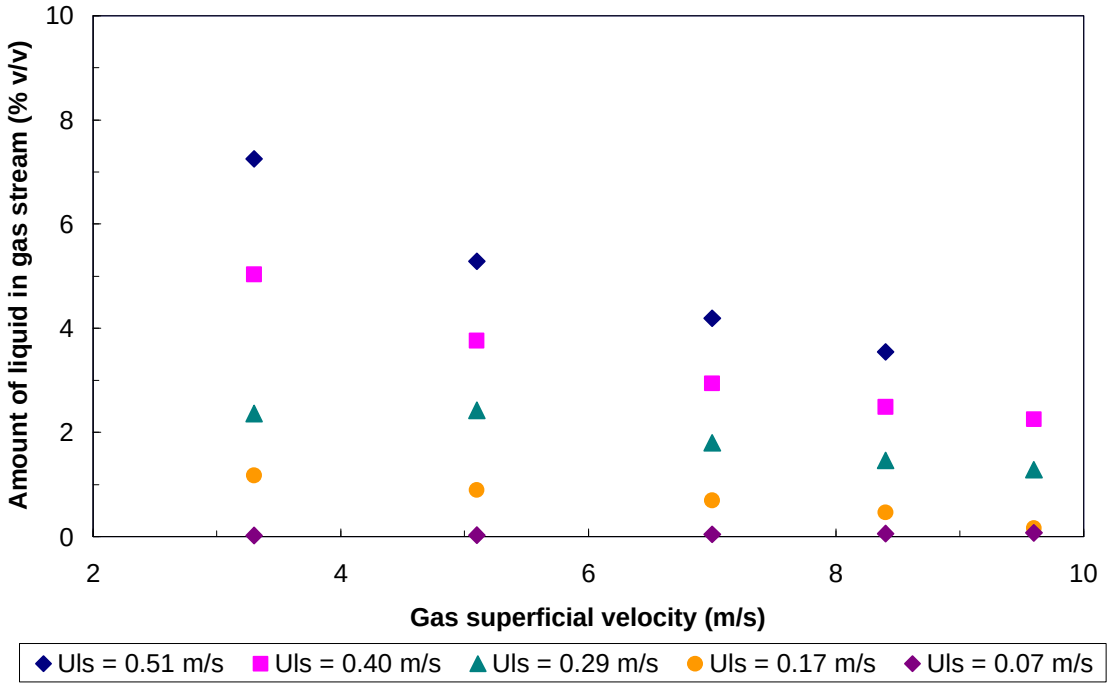

Figure 6.23: Amount of liquid in the gas stream based on determined run valve settings (stratified flow: 20% open, slug flow: 55% open)

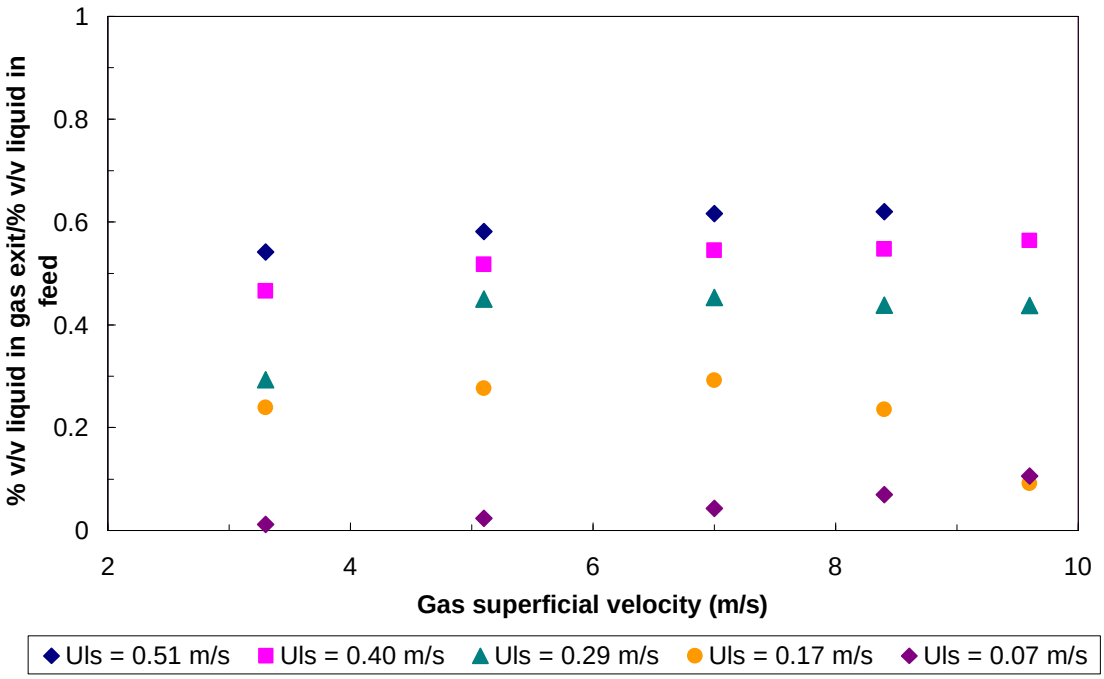

Figure 6.24: Ratio of volumetric fraction of liquid in the gas exit stream to the volumetric fraction of liquid in the feed stream (stratified flow: 20% open, slug flow: 55% open)

The flat shape of the ratio curves in Figure 6.24 shows that the ratio is constant over the range of gas and liquid flowrates investigated. This implies that the volumetric liquid content of the combined gas-rich stream does, as expected, depend on the volumetric flowrate of liquid in the feed stream and not on the actual phase flowrates.

6.3 Proposed Control Scheme

One of the objectives of this thesis is to devise an automatic control strategy for optimising the phase separation occurring at T-junctions. From the above work it is now possible to construct a simple control scheme to optimise the phase separation within the T-junction system. The final control strategy is based around two very distinct control loops. This removes one of the main problems identified with the simulation work presented in Chapter 4 that of interaction between the two control valves.

The first control loop is the automatic level control on the down leg, creating a permanent liquid barrier within the down pipe. As already discussed this successfully prevents any gas leaving with the liquid stream, producing a liquid only exit stream. The second loop is then based on the electrical capacitance tomography system identifying the flow pattern within the inlet stream. A simple feed-forward control system can be based on this knowledge of the flow pattern. From the above analysis it is clear that for stratified flows the optimum run valve setting is 20% open, while for slug flows the proposed optimum setting is 55% open. Both of these control systems are shown schematically in Figure 6.25.

The dependence of the setting of the final run control valve only on the approaching flow pattern within the pipe is essential to the operation of the system. The electrical capacitance tomography unit has the advantage of being able to be positioned anywhere upstream of the first T-junction. This flexibility means that there can be variable lead times between the flow pattern recognition and the associated movement of the run arm control valve. However, with modern control valves the expected response times should be sufficiently quick to negate the need to have the flow pattern

recognition unit a great distance upstream. Indeed the control should not be operating as a fast loop system, as the flow pattern should be relatively constant and this problem becomes relatively insignificant. Similarly, in industrial level control applications the response of the control valve is generally not an issue for concern because, unlike the experimental case presented here, it is normally lost within the time constant of the process.

The run valve setting would be controlled by a simple control program analysing the key electrode pairings measurements of the electrical capacitance tomographic unit, as discussed in Chapter 3, and setting the valve based on the determined flow pattern. While the automatic level control will operate independently as a simple proportional control loop. Based on this design, there are then two exit streams. The first is a liquid only stream, produced from the down leg and the second is a combination of the two other junction exits, producing a gas-rich stream, which has been shown to contain less than 10% v/v of liquid over a wide range of inlet conditions.

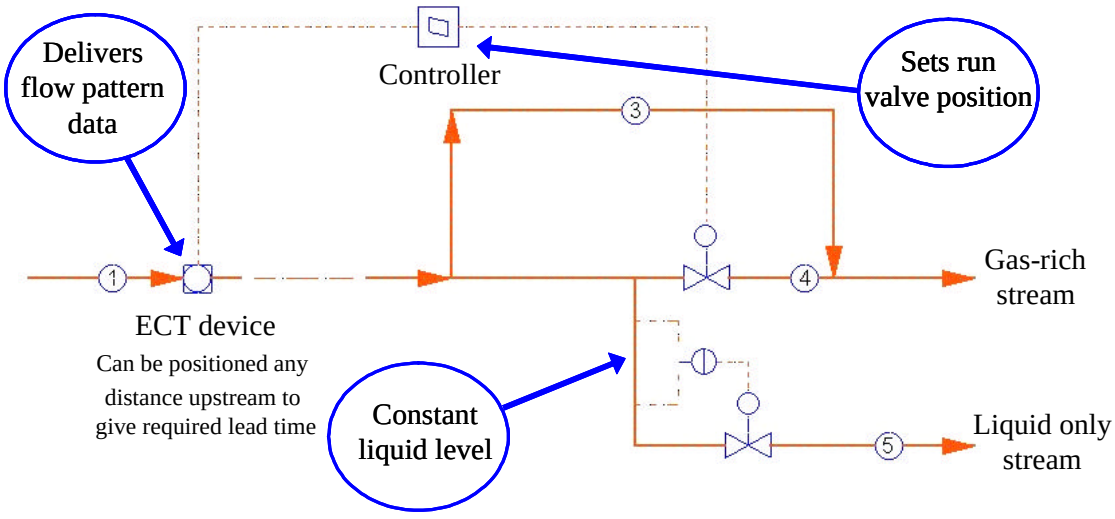

Figure 6.25: Proposed conceptual T-junction separator

6.4 Possible Design Method for a T-junction Separator

In order to make best use of T-junction separators, an attractive concept for industry would be a simple calculation method for design. In simple terms this can be achieved by providing knowledge of the expected flow split at a T-junction installed within a pipeline. However, the complexities of the flow and the numerous variables, both geometric and flow related, make predictions difficult. The benefit of the current T-junction separator system devised in this work is that the flow split can be represented by simple relationships based on inlet superficial velocities and liquid fractions recovered in the down leg.

From Figures 6.22 and 6.24 it is seen that the gas superficial velocity has a negligible effect on the liquid fraction recovered in the down leg and, hence, the phase separation achieved. Converting the liquid fractions in the gas exit stream to values of liquid superficial velocity, as shown in Figure 6.26, suggests that the superficial liquid velocity in the side-arm is independent of the inlet gas superficial velocity. The only major deviations are seen to occur within the stratified flow regime, where the achieved separation is much better than for slug flow because of reasons already discussed, namely, lower liquid momentum and all the liquid travelling at the bottom of the pipe, combining to make it easier for liquid to fall into the down leg.

The curve in Figure 6.26 then represents all the current experimental data obtained for the T-junction system and can be considered to be the system Equilibrium Separation Curve. In Chapter 4, the assessment of the separation performance for a single fully horizontal regular T-junction, the Separation Factor, was based on a concept similar to that used in distillation column design. The presence of an Equilibrium Separation Curve, dependent only on the inlet liquid superficial velocity, also has similarities to distillation column design. In the design of distillation columns for two component mixtures, the McCabe-Thiele method can be used to determine the number of theoretical stages required to perform a given separation. This method essentially relies on a prior knowledge of the equilibrium curve for the two component mixture to be distilled, the feed composition and the final product composition required.

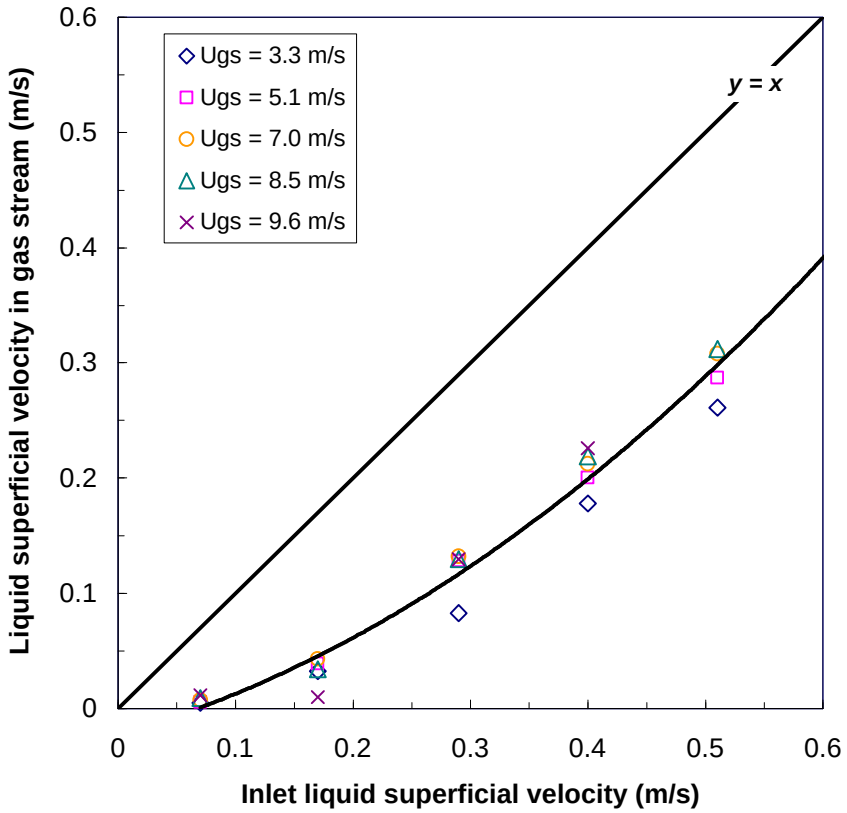

Figure 6.26: Equilibrium separation performance for the combined gas exit stream

A similar method can then be applied to the design of a T-junction separator system. In this case the equilibrium data is taken to be the Equilibrium Separation Curve, as obtained in Figure 6.26, the feed conditions are taken to be the liquid inlet superficial velocity and the final product is defined in terms of the volumetric percentage of liquid with in the gas exit stream.

Figure 6.27 shows an example of a required calculation approach. Here the inlet liquid superficial velocity is 0.50 m/s and the final gas-rich exit stream must contain no more than 1% v/v liquid over a range of inlet gas superficial velocities of 2 m/s to 10 m/s, represented by the shaded band.

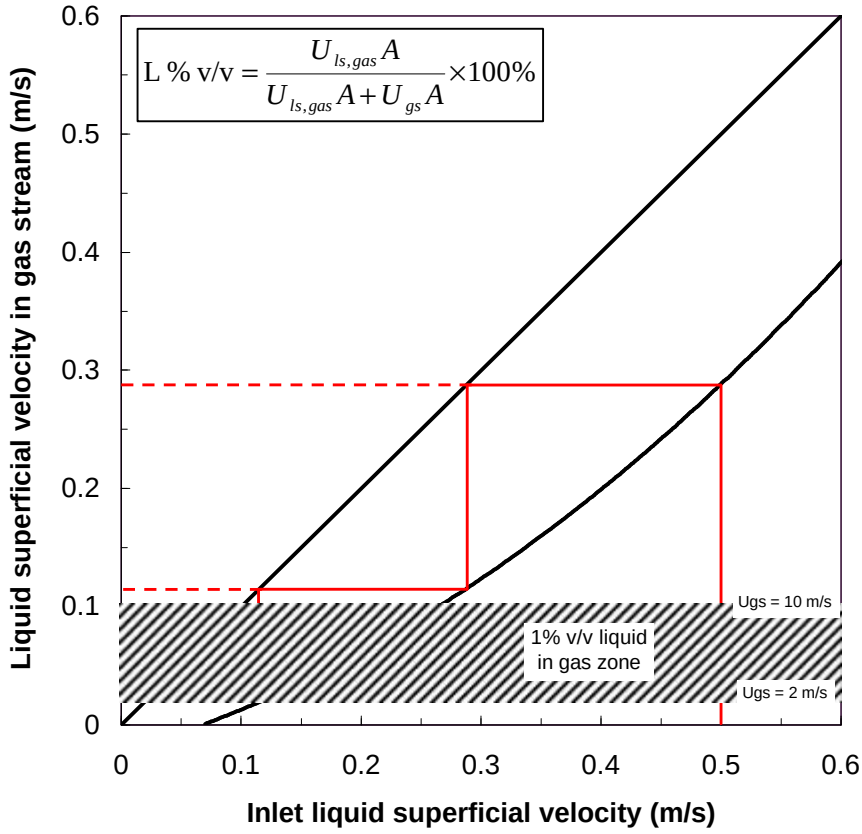

Figure 6.27: T-junction separator design curve, showing three stages achieving a 1% v/v liquid in gas for an envelope of superficial gas velocities in the range 2 to 10 m/s

A vertical line is drawn from the starting inlet liquid superficial velocity to the equilibrium separation curve and the corresponding liquid superficial velocity in the gas-rich side-arm is read from the *y*-axis. This new velocity is then used as a feed into the next T-junction separator, giving a new gas exit liquid velocity. This sequence is repeated until the final liquid velocity is such that the gas stream contains less than the specified liquid content, in this case 1% v/v liquid. The final number of steps represents the number of separation stages required to satisfy the separation criteria, in this case three. Although this design method still relies on experimentally obtained data, with better models developed for vertically orientated T-junctions the method has the potential to become much more widely applicable.

6.5 Conclusions

The phase separation performance of two T-junctions placed in series coupled with two control valves has been investigated for a wide range of gas and liquid superficial velocities covering stratified and slug flow regimes. The two controlled valves were placed after the second T-junction, one acting as a continuous automatic liquid level control on the down leg and the other positioned on the run arm to affect the liquid hold-up at the downward junction.

In order to assess the separation performance of the two T-junctions system, operating with a liquid level control on the down leg, a new Separation Effectiveness term was devised. This method was based on maximising the liquid recovery in the down leg with respect to the run control valve setting.

In all cases the T-junction separator successfully provided partial phase separation for the entire range of inlet flow conditions investigated. It was found that stratified flows achieved a better separation than slug flows. The primary reasons for the difference was a combination of the lower liquid momentum associated with stratified flows coupled with the higher void fraction, especially in the upper part of the pipe.

Based on this maximum liquid recovery concept, optimum run valve settings were determined for the entire range of flowrates investigated. These settings were found to be independent of the inlet superficial velocities but were only dependent only on the flow regime approaching the first T-junction. Thus, a set of control parameters were devised based on the experimental results such that for stratified flow the optimal valve setting was found to be 20% open while for slug flow the valve setting required was 55% open. Using these optimised valve settings it was found that the phase separation criterion of less than 10% v/v liquid in gas was always achievable.

The degree of phase separation was found to depend on both the liquid and gas inlet superficial velocities. For a constant liquid superficial velocity the volumetric content of the combined gas-rich stream decreased as the gas superficial velocity increases.

Similarly, for a constant gas superficial velocity, the volumetric content of the liquid in the gas stream decreases as the inlet liquid superficial velocity decreases. Further analysis of the liquid flow split results at the downward junction showed that the liquid take-off can be regarded as independent of the gas superficial velocity.

A novel compact gas-liquid separator has been proposed capable of producing a liquid only stream and a gas-rich stream. This system is based on the concept of the run valve setting being adjusted on the flow pattern which can be determined by using the electrical capacitance tomography system, positioned upstream of the first junction and the automatic level control.

Further to this a method for designing a T-junction separator system has been developed. This is based on the McCabe-Thiele Method for two-component distillation design. In this case the calculation method is based on superficial velocities, with distillation equilibrium curve replaced by an equilibrium separation curve. By assuming equilibrium separation is reached, the number of stages can be "stepped-off" the design plot to provide a defined liquid content in the final gas-rich stream. By using three T-junction separator systems in series, a high liquid-loaded feed could be separated to contain less than 1% v/v of liquid in the gas stream in three stages, over a wide range of feed gas superficial velocities.

CHAPTER 7

Transient Flow Results

In Chapter 6 the steady-state performance of a T-junction separator was investigated for a wide range of gas and liquid superficial velocities. Such studies provide important knowledge of the mechanisms associated with gas-liquid flows at T-junctions as well as providing key design information. However, within industrial applications it is rare to operate under steady-state conditions and there will always be at least one time-dependent parameter, for example flowrate or pressure.

Such transients may occur over a short time period, in the order of seconds or minutes, or may evolve over a more substantial time period of hours, or even days. Obviously the longer the time frame involved the less severe impact the transient will have on the operation of equipment. However, if the flowrate is subjected to a sudden change, the equipment must be either capable of responding quickly enough to adapt to the variation or be able to absorb the change without adversely affecting the overall system performance. Examples of general transient situations, involve plant shutdown and start-up, changes in flowrates in response to planned operating conditions and emergency situations. Even more relevant to the petroleum industry however, is bringing an additional oil well on line.

Within the petroleum industry the problem of multiphase transient flows has lead to the development of many commercially available prediction packages. Such

packages deal exclusively with pipes and hitherto there are no models applicable for branched networks, as would be encountered at a T-junction separator.

This chapter aims to assess the very different dynamics that occur when two-phase transient flows occur. By comparing the same transients through both a simple pipe and the T-junction system it is hoped that further insight may be gained into the complex mechanisms taking place.

7.1 Transient Flow in a Pipe

To aid understanding of transient flows through the T-junction system, it is useful to appreciate how transients behave in a single pipe. Transient two-phase flows can be considered in many different ways. In general they can be thought of as a change from one steady-state to another over a period of time. If the transients occur over an indefinite period of time, a number of quasi-steady states would be observed as the flowrates changed. When the flowrates undergo a rapid change all of these quasi steady-state effects can be expected to occur but there will also be additional features which are not directly associated with the new steady-state conditions.

7.1.1 Experimental Arrangement

To study transient flows in a straight pipe the experimental facility was arranged with the electrical capacitance tomography (ECT) unit positioned 330 pipe diameters downstream of the entrance to maximise the flow development length prior to measurement. This position also corresponds to the first T-junction in the separator configuration. Therefore, it gave flow data equivalent to that which would be expected at the first T-junction. Figure 7.1 shows a schematic for the pipe configuration, indicating the relative position of the measurement sensors. The transient flowrates were delivered by manipulation of two actuated cocks positioned on the gas and liquid inlet loops, as outlined previously in Chapter 3.

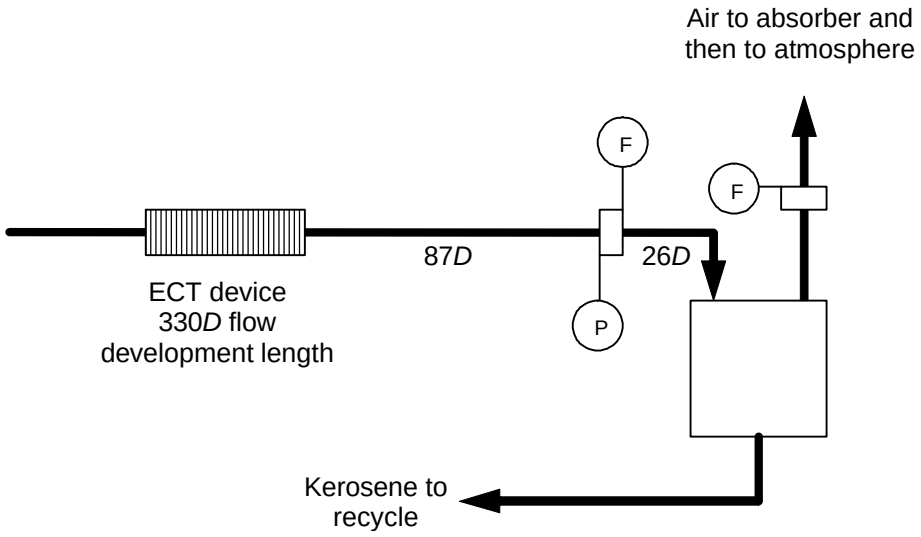

Figure 7.1: Schematic diagram for ECT measurements of transient flows in a straight pipe

This configuration provides a flow development length, from the mixing section to the ECT device, of 12.6 m. Beyond the ECT unit, there is a further 4.3 m (113*D*) of straight pipe feeding the two-phase flow into the separation tank. In order to measure the liquid transients an orifice plate was installed 3.3 m (87*D*) downstream of the ECT unit. A significant distance was placed between the ECT and the orifice plate to prevent the ECT measurements from being disturbed by the orifice constriction. The pressure was also recorded just prior to the orifice plate. Chapter 3 has already highlighted the design and relevant calibration of the orifice plates used within the two-phase environment. Essentially, these orifice plates measure the pressure drop, using a differential pressure sensor, associated with the gas-liquid flow flowing through it. Since the air flowrate leaving the system is already measured, using the two orifice plates in series, the time resolved liquid flowrate can be determined.

The complete system then delivers simultaneous time-resolved measurements of the four key parameters; the outlet liquid flowrate, the outlet gas flowrate, the pressure and the liquid hold-up. The ECT unit was used to obtain void fraction measurements

of the flow operated at a frequency of 25 Hz, while the other measurements were recorded using the VisiDAQ data acquisition system at a frequency of 4 Hz.

7.1.2 Flow Conditions

As previously mentioned, a transient can be considered to be a change from one set of steady-state conditions to another set over a set period of time. In terms of gas-liquid flows in a pipe it is possible to identify three potential transient parameters. These are the gas or liquid inlet flowrates and the system pressure, which can all undergo increases and decreases, either independently or simultaneously. For a fixed pressure system, as previously defined in the simulation work reported in Chapter 4, four distinct transients remain, namely increases or decreases in the gas or liquid flowrates. Although such transients could also occur simultaneously, this study will be restricted to examining each transient in isolation thus allowing the individual effect of each phase transient to be compared and assessed.

The time period over which transient changes occur will also affect the responses of the outlet flows and pressure. An increase in a phase flowrate occurring over several hours will not have the same severe consequences as the same increase occurring over a few seconds. By making the timescale of the transient as small as possible, the step changes can be assumed to occur instantaneously. The use of fast-acting actuating cocks on both the gas and liquid inlet loops implies that this transition time becomes negligible and in this study all the transients are assumed to occur instantaneously.

Early studies by Sakaguchi *et al.* (1973) and Taitel *et al.* (1978) highlighted the existence of intermediate, and potentially harmful and unexpected flow regimes that can occur even for transients between two stratified flow steady-state conditions. These transitory effects were generally associated with increasing gas flowrate transients. Studies carried out by King *et al.* (1998) on flowrate transients purely within the slug flow regime concluded that liquid transients had very little effect on the frequency of the slugs or liquid hold-up. In contrast, gas flowrate transients produced temporary periods of increased, or decreased, slugging and corresponding

pressure fluctuations. Observations on the current facility confirm the existence of these transitory periods.

Based on the existing knowledge, the aim of these new investigations is to determine the effects of both increases and decreases in gas and liquid flowrates within and across the stratified and slug regimes. To achieve this, a series of runs or cycles were chosen to give the widest range of parameters. However, they were also selected to have common elements so as to facilitate comparisons. Given the wide range of flowrates available the selection of possible transients is almost an arbitrary decision. To help reduce the number of choices there is a requirement to span the operational range of the facility. As noted in Chapter 3, there is an upper limit on the gas superficial velocity of 10 m/s due to safety considerations. Examination of the flow data conditions already used for steady-state evaluation of the T-junction separator in Chapter 6 provides a basis for the selection of the phase flowrates selection. Figure 6.2 shows that moving horizontally across the flow pattern map, by varying the gas flowrate will provide transients within one flow regime, either stratified or slug flow. Moving vertically across the flow map, by varying the liquid flowrate will provide transients across the transition boundaries, from stratified to slug and vice versa.

This provides four distinct cases, as already mentioned above, but does not take into account the possible influence of the non-transitory flowrate on the step change responses. Considering that there could be a distinction between an increase in the gas flowrate within the stratified regime and the same increase within the slug flow regime it is apparent that there will be twice the number of transients. These are best considered in terms of a forward and backward loop around four steady-state conditions. Figure 7.2 illustrates one such complete transient cycle.

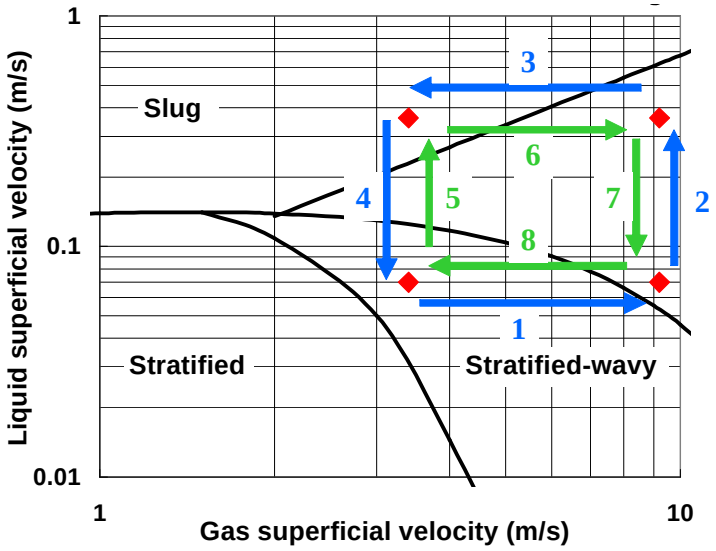

Figure 7.2: Taitel and Dukler (1976) flow pattern map for experimental facility showing forward (blue) and backward (green) transient loops

Given that there is a requirement to undertake eight transient steps, the limiting factor in the choice of the time for each transient becomes the maximum safe capacity of the separation and measurement tanks. Calculations based on the maximum expected liquid flowrates identified a suitable time period of 60 seconds for each transitional state to be maintained. Observations also show that this time period is sufficient to allow the flow to reach steady-state. Thus, one transient cycle will take 540 seconds to complete. Table 7.1, with reference to Figure 7.2, classifies the eight transients that exist around one complete cycle in terms of the relative gas and liquid flowrates for a given cycle.

By inspection of the steady-state data already obtained it is possible identify six transient cycles that provide a wide range of flow conditions. Table 7.2 lists the full set of transients investigated, showing the four steady-state gas and liquid flowrates and the associated flow regimes.

Table 7.1: Classification of the eight transients that occur around one complete cycle

Time (s)	Loop step	Relative gas flow	Relative liquid flow	Final steady-state flow regime
0-60	0	Low	Low	Stratified
60-120	1	High	Low	Stratified
120-180	2	High	High	Slug
180-240	3	Low	High	Slug
240-300	4	Low	Low	Stratified
300-360	5	Low	High	Slug
360-420	6	High	High	Slug
420-480	7	High	Low	Stratified
480-540	8	Low	Low	Stratified

These choices are based on comparing the same gas transients with different changes in liquid flowrates, hence different slug flow characteristics, and also maintaining set liquid transients while forcing less severe gas transitions. Thus Cycles 2, 3 and 6 have a constant step change in the gas flowrates but varying step changes in the liquid flowrate. Similarly, Cycles 3, 4 and 5 can be compared to examine the effect on the transients of applying different relative magnitude step changes in the gas flowrate.

Table 7.2: Steady-state gas and liquid superficial velocities and associated flow regimes used in transient studies

Cycle	U_{gs} (m/s)	U_{ls} (m/s)	U_{gs} (m/s)	U_{ls} (m/s)	U_{gs} (m/s)	U_{ls} (m/s)	U_{gs} (m/s)	U_{ls} (m/s)
1	2.4	0.06	8.0	0.06	8.0	0.35	2.4	0.35
2	3.4	0.06	9.0	0.06	9.0	0.22	3.4	0.22
3	3.4	0.06	9.0	0.06	9.0	0.35	3.4	0.35
4	3.4	0.06	5.5	0.06	5.5	0.35	3.4	0.35
5	5.5	0.06	9.0	0.06	9.0	0.35	5.5	0.35
6	3.4	0.06	9.0	0.06	9.0	0.14	3.4	0.14
Regime	**Stratified**		**Stratified**		**Slug**		**Slug**	

7.1.3 Data Analysis

For each transient cycle a set of three nominally identical experiments were performed. These three separate data sets could then be compared to check for reproducibility and reliability and also combined to provide a mean data set for each cycle. This proved to be especially useful within the slug flow regime, where the natural disturbances of the intermittent flow could obscure the transient responses of interest. By averaging the parameters some of the inherent randomness of two-phase flows can be removed.

Figure 7.3 gives an example of the consistency of the results obtained, in this case showing a comparison of the pressure fluctuations for the three individual runs with the average trace.

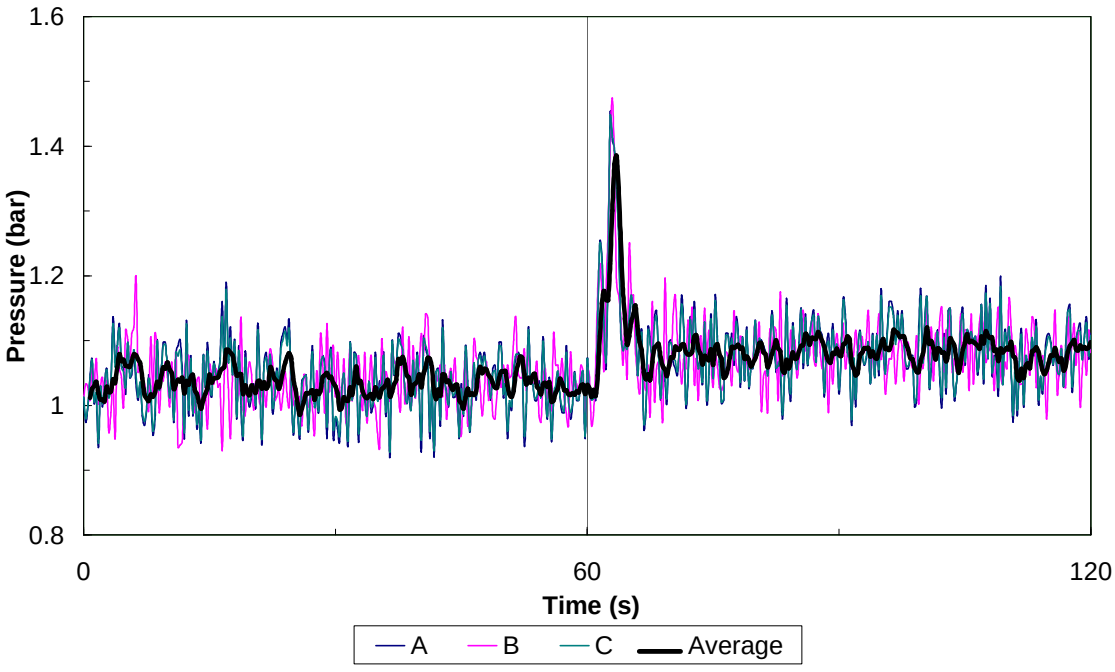

Figure 7.3: Typical pressure traces showing consistency of the three individual runs and the resultant average trace

Although the individual runs show local variation in the pressure fluctuations within the steady-state periods the important pressure surge caused by the instantaneous increase in the gas flowrate, shown in Figure 7.4, is consistent in all three cases. The average trace removes the majority of what can be essentially considered as noise and so highlights the pressure surge. The same result is observed in the corresponding gas mass flowrate transient. Figure 7.4 also highlights the reproducibility of the system and gives confidence in the experimental data obtained. These results plainly show the benefits of using the average trace values in interpretation of the transient data.

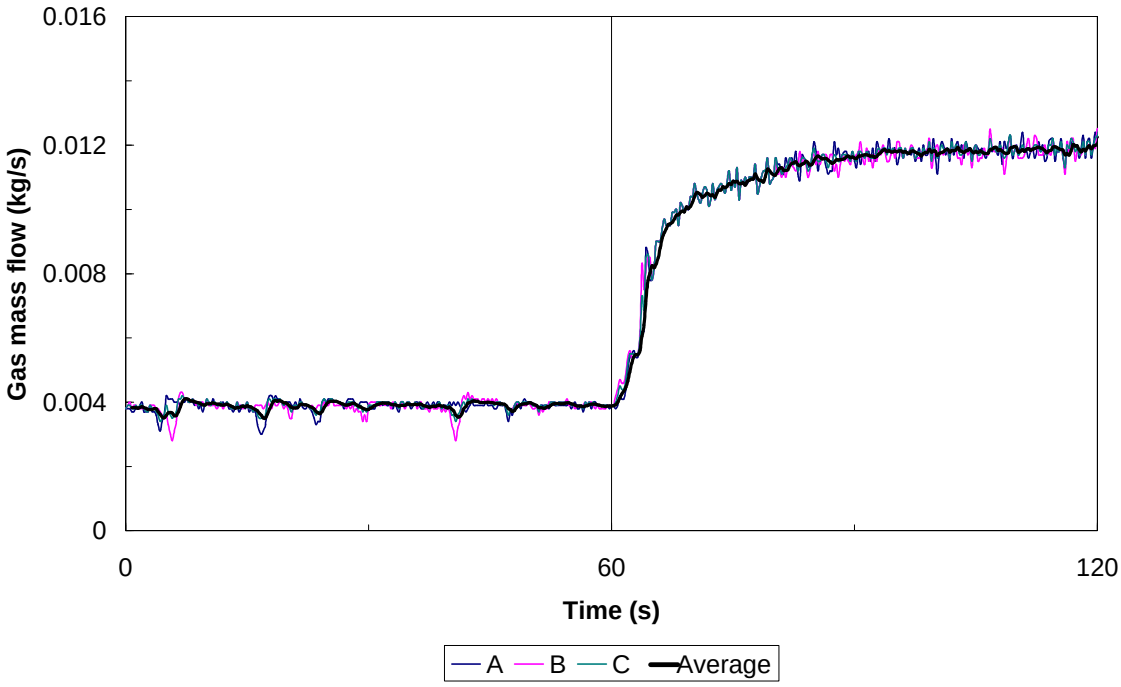

Figure 7.4: Outlet gas mass flow transient corresponding to the pressure trace above, showing the three individual runs and the average

When considering transients it is difficult to isolate one specific parameter and examine it without reference to the others because of the inevitable interactions and interdependencies that exist. To aid the visualisation of these relationships easily it is helpful to produce combined traces of the relevant parameters. Such a combined trace

plot is shown in Figure 7.5. Here the axis for the outlet gas mass flowrate is scaled by a factor of 100 for ease of interpretation on the same graph as the pressure and outlet liquid mass flowrates.

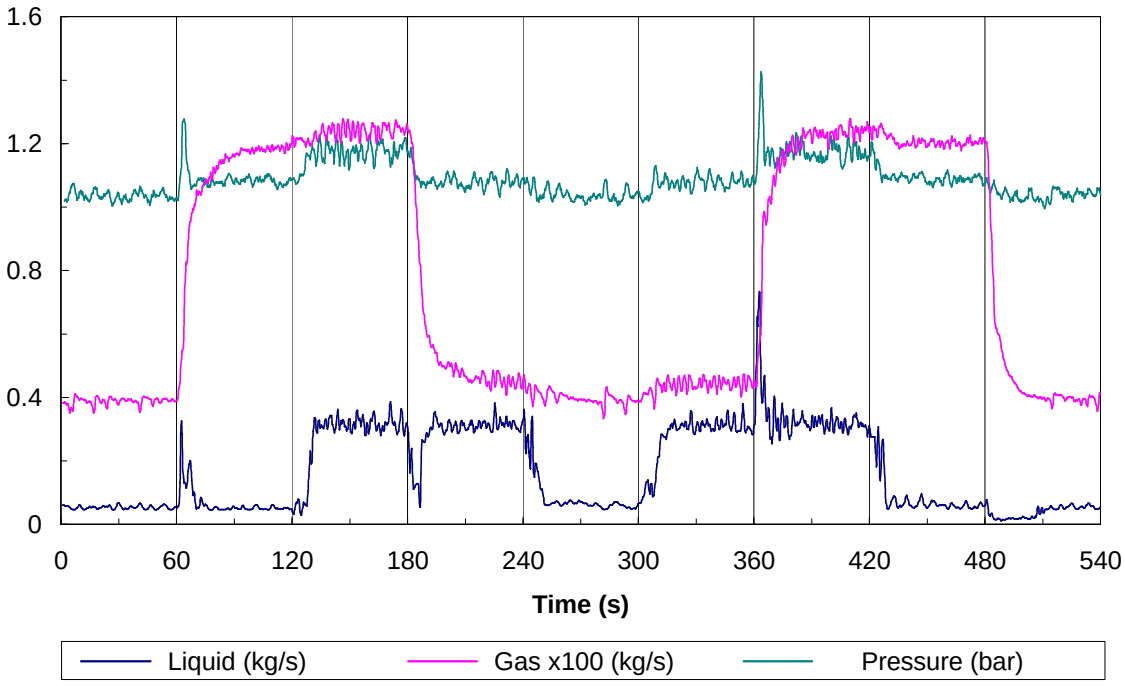

Figure 7.5: Combined trace plot for full transient Cycle 1, showing outlet liquid mass flow, the outlet gas mass flow (scaled upwards by a factor of 100) and the pressure fluctuations

7.1.4 General Transient Observations

Before undertaking an in-depth discussion on the many aspects of the transient flow data it is important to understand the general patterns observed. Such trends are present within each individual cycle, to a greater or lesser extent dependent on the relative phase flowrates, however to illustrate these trends Cycle 2 will be discussed. Figure 7.6 shows the combined trace plot for Cycle 2 and when compared with

Cycle 1, which has been presented previously in Figure 7.5, it is clear that the same qualitative trends are present throughout the all the cycles.

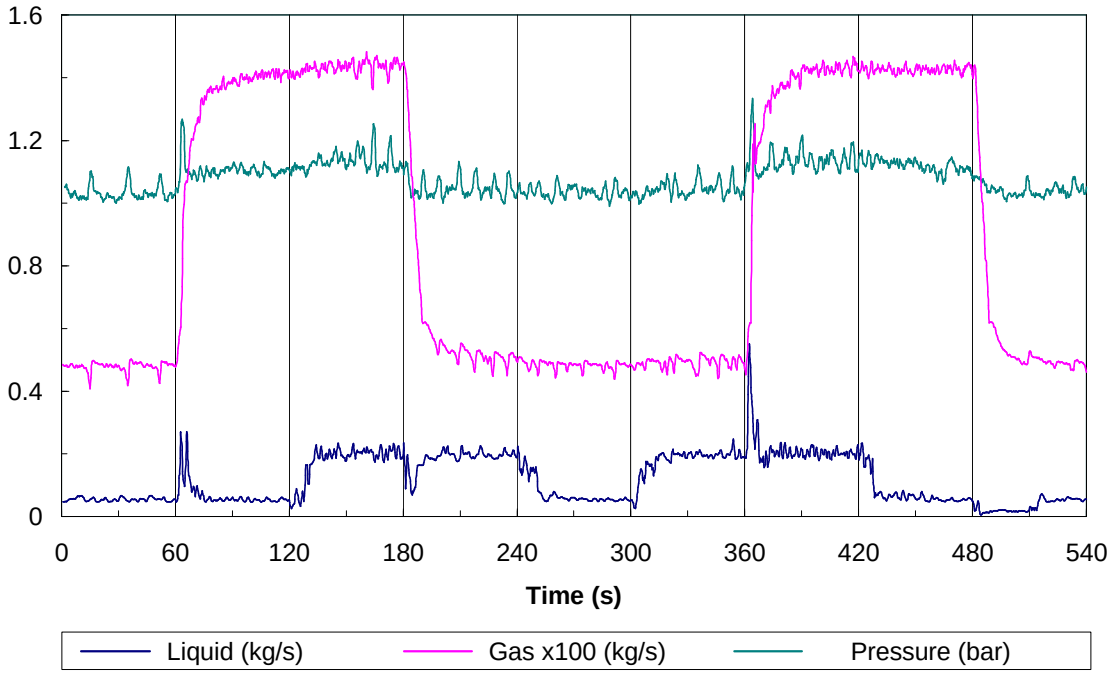

Figure 7.6: Combined trace plot for full transient Cycle 2, showing outlet liquid mass flow, the outlet gas mass flow (scaled upwards by a factor of 100) and the pressure fluctuations

From the combined plots it is then possible to identify key phenomena that are only associated with transient two-phase flows. For convenience the transients will be discussed in temporal sequence.

The first transient step is an increase in the gas flowrate after 60 seconds, while maintaining the liquid flowrate constant. This represents a horizontal movement across the flow pattern map, implying that the initial and final steady-state flow patterns will be the same, in this case stratified. At this point the outlet liquid mass flow shows a rapid increase sustained over only a short time period before returning

to its steady-state value. Visual observations show that this exists as a temporary period of slugging; this same phenomenon was also described by Sakaguchi *et al.* (1973). At the same time the pressure also shows a temporarily increased value, typical of the overshoot observed by *King et al.* (1998), existing over the same timescale as the liquid transient. After this the pressure returns to its new steady-state value, which will be higher than the pressure before the gas flowrate increased.

It is generally agreed that a gas flowrate transient will be an instantaneous change along the entire pipe axial length and certainly much faster acting than a liquid flowrate transient. However, Figure 7.6 shows that such responses are not instant but occur over a similar timescale as the transient responses of the other outlet parameters.

The increase in the gas flowrate produces the extra liquid at the outlet. This is essentially because of a change in the liquid hold-up along the pipe. It is well known that within the stratified flow regime the liquid will achieve an equilibrium liquid height within the pipe (Taitel and Dukler, 1976). This height will be dependent on both the liquid and gas superficial velocities within the pipe. Thus, for a constant liquid flowrate an increase in the gas flowrate will reduce this stratified liquid height within the pipe. As the gas flowrate is suddenly increased it creates several large wave fronts that travel along the pipe. Liquid that would exist above the final new equilibrium level is swept away and forms slugs. The greater the gas step change the greater the amount of liquid that needs to be stripped from the system and the larger the liquid surge will be.

Analysis of the corresponding ECT liquid hold-up trace, shown in Figure 7.7, also highlights the liquid transient response. The liquid hold-up trace clearly shows the period of transitory slugging immediately after the increase in the inlet gas flowrate. Furthermore, the ECT data also highlights that after the gas is increased the liquid hold-up exhibits an undershoot response. This shows that the amount of extra liquid present within the slug surges is not simply the difference in hold-up of the two-final

steady-state conditions but that as the liquid slugs travel along the pipe more liquid is swept along, creating a temporary thinning of the stratified layer behind them.

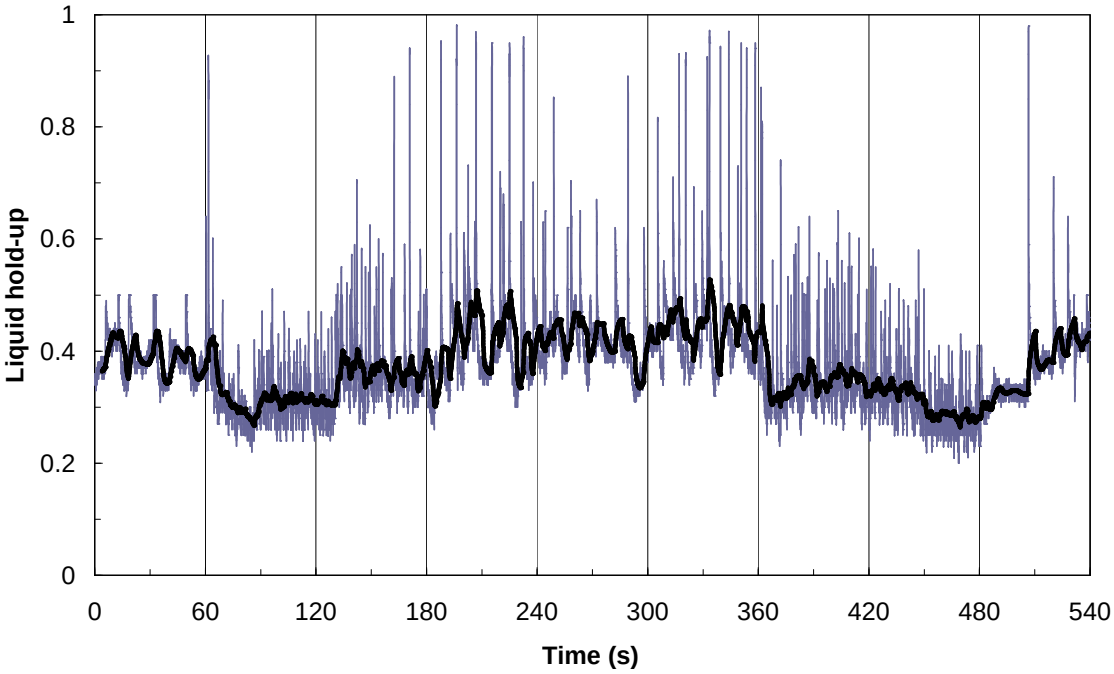

Figure 7.7: ECT liquid hold-up data in the pipe for Cycle 2, showing instantaneous value (thin blue line) and the 4 second moving average (thick black line)

The second transient, after 120 seconds, is an increase in the liquid superficial velocity, moving vertically up the flow pattern and crossing the flow transition boundary moving into steady-state slug flow. This transition is far less dramatic than for the gas increase situation. As for the previous case there is a delay before the transient phase flowrate reaches the final steady-state value. The increase in the liquid flowrate is accompanied by an increase in the system pressure but there are no signs of a pressure overshoot as observed for the gas transient. This is a consequence of the slower response of the liquid to changes in its flowrate. There is an initial period where the liquid level builds up in the pipe close to the mixing section. At a

certain time the liquid height reaches a point where it starts to form slugs. Within this slug region all the average traces still show the intermittent nature of the flow, with significant fluctuations in all three parameters corresponding to periods of liquid slugs and gas pockets. Again the associated ECT liquid hold-up data shows the expected increase and also indicates that it a takes a nominal period of time for stable slugs to form.

The third transient is a reduction in the gas flowrate back to the initial value, again horizontally traversing the flow pattern map and so remaining within the same flow regime. Again there is definite timescale within which all the associated transients occur. The gas flowrate trace shows the near opposite trend as for the increasing gas transient with a very quick decay. A quiescent period is seen in the liquid outlet flow where the flowrate drops significantly. This is again related to the liquid hold-up adjusting to compensate the reduced gas content and is clearly seen in the average hold-up data in Figure 7.7.

The forward loop is completed with a reduction in the liquid flowrate so the system returns to its original starting conditions. The liquid outlet flow slowly decays to its final steady-state value and the slug frequency subsides over a period of time. Neither the pressure nor gas flowrate are affected by this transient, except that they become relatively more stable as the flow enters the stratified regime.

Once the forward loop is completed the same flowrate step changes are repeated but in the reverse direction. This systematic approach than allows the comparison of the same transients in different flow regimes. For example, the increase in gas flowrate at time equals 60 seconds occurs in the stratified flow but in the backward loop the same increase, at time equals 360 seconds, takes place in the slug flow regime. Nevertheless the reverse loop data shows similar trends as those already discussed for the forward loop. The obvious difference in this case is in the size of both the pressure and liquid surge peaks. A sudden increase in the gas phase flowrate within the slug flow regime will again sweep out extra liquid as the system achieves it new steady-state. Since there is more liquid within the system in the slug flow regime it is

sensible to expect more liquid to be expelled, explaining why this surge is greater than the corresponding one within the stratified flow regime.

The final transient that is worthy of mention on the backward loop is the final one, when the gas flowrate is reduced, within the stratified flow regime after 480 seconds. Here the liquid out flow reduces significantly to almost a negligible output for a considerable time period, in the order of 30 seconds. This is again a consequence of the liquid equilibrium height adjusting to the new flow conditions. Since this liquid height will be higher for a lower gas velocity, the output from the exit is retarded as the level builds up in the pipe. After this period of adjustment a surge of liquid is observed, which is clearly visible on both the ECT liquid hold-up data and the liquid transient trace, as a slug.

7.1.5 Effects of Varying the Magnitude of the Transient on the Responses

As mentioned above, all the transient effects are observable in every transient cycle. The only expected differences will be in the magnitude of the measured values and the timescale over which the transient effects are observed. However, this work is not designed to gain quantifiable information on transients but to provide qualitative background work prior to studying transient flow through the T-junction system. The selection of the steady-state flow conditions allow simple comparisons to be made based on varying liquid flow transient step changes, with constant gas flow changes, or conversely, constant liquid flow changes with different step changes in the gas flow rates.

7.1.5.1 Transients with Varying Liquid Flowrates

To compare the effect of different step changes in the liquid phase three transient cycles were considered, Cycles 2, 3 and 6, see Table 7.1 for the flowrates involved. For each cycle the gas phase flowrate had a minimum value of 3.4 m/s and a maximum one of 9.0 m/s. All three cases had the same minimum liquid flowrate values of 0.06 m/s but different maximum values of 0.22 m/s, 0.35 m/s and 0.14 m/s,

respectively. The traces for the three measured parameters obtained for the cycles are compared in Figure 7.8.

The gas outlet mass flow transient traces for all three cycles are nominally identical. One appreciable difference is seen in Cycle 3, with the highest liquid flowrate, where the flow lies significantly further within the slug regime. Here the gas flow trace shows a more pronounced erratic nature as a result of the more intermittent nature of the flow. Observing that the traces all exhibit similar shaped responses, regardless of the liquid flowrates, it is evident that the gas transients are unaffected by the liquid flowrates.

Comparisons of the liquid outlet flowrates shows that there are different transient effects that can be distinguished. The first is that within the stratified flow regime with the lowest liquid flowrates (U_{ls} = 0.06 m/s for all three cycles) the increases in gas flowrate after 60 seconds and the decreases in the gas flowrate after 480 seconds, all exhibit very similar responses in terms of the time and magnitude of the deviation from steady-state.

In contrast there are appreciable differences in the response of the liquid outlet flowrates for variations in the liquid inlet flow conditions and inlet gas flowrate transients within the slug flow regime. Considering first the responses to changes in the liquid inlet flowrate, for both increases and decreases the transients occur in approximately the same time period. Thus, the greater the difference between the initial and final steady-state values, the greater the rate of change in the liquid flowrate must be over the transient time period. This transient response is also affected by the relative gas superficial velocity at the time of transient. With a high gas flowrate the transient response is quicker than for the case with a low gas flowrate. This can be attributed to the influence that the gas has on distributing the liquid along the pipe. Thus, the transient step after 120 seconds, when the gas flowrate is at a maximum, shows a rapid sharp change, while the same change with a lower gas flowrate, after 300 seconds, shows a more S-shaped response, with the increase occurring over the entire transient period.

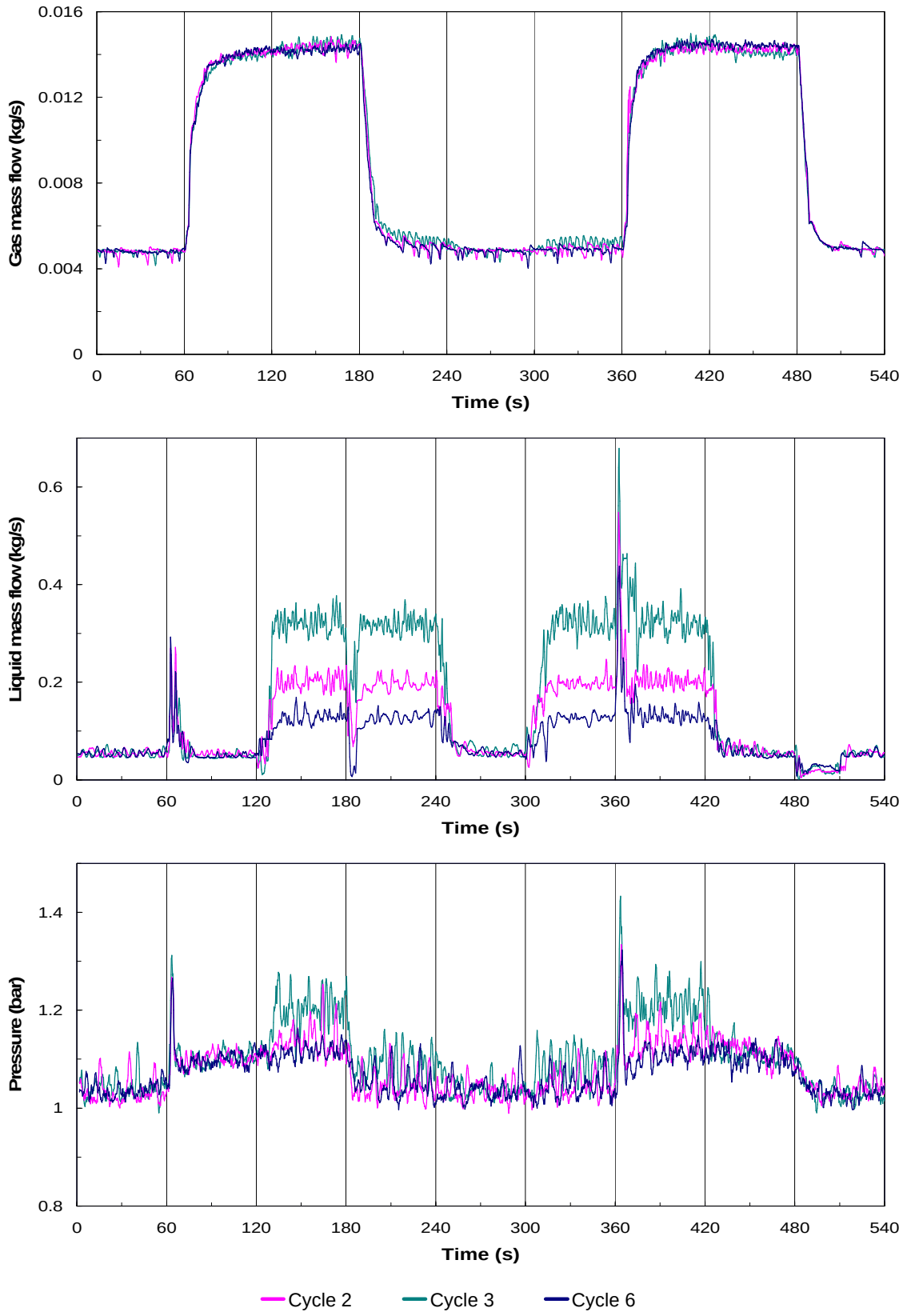

Figure 7.8: Comparisons of liquid outlet flow, gas outlet flow and pressure for Cycles 2, 3 and 6

Such trends are enhanced further as the magnitude of the liquid step change increases. A similar, but smaller, trend is observed when the liquid flowrate decreases, again due to the fact that a higher gas flowrate implies a faster liquid velocity and will tend to sweep out the extra liquid more quickly.

The final transients are in response to gas flowrate changes within the high liquid flowrate regions under slug flow conditions. When the gas flowrate is increased there is a period of intense slugging, again as the new steady-state conditions are approached. The amount of liquid ejected from the system as a result of these transients will increase as the liquid flowrate increases. This is a direct consequence of the higher liquid hold-up associated with the highest liquid flowrates. The timescale of this intensified slugging also increases with increasing liquid flowrates; again this is accounted for in the extra time required for the system to adjust to the new liquid hold-up along the entire pipe.

For decreases in the gas flowrate under slug flow conditions it is more difficult to distinguish the end of the transient response because of the inherent randomness of the slug flow regime. When the gas flowrate is decreased there is a period of a more stratified-like flow, as the liquid hold-up is allowed to increase and the liquid outlet flow shows a marked reduction. This is in accordance with the findings of King *et al.* (1996). From the current data it appears that this quiet period of reduced liquid outlet flow occurs over a very similar timescale regardless of the steady-state liquid flowrate.

The final measured parameter is the pressure within the pipe. These pressure traces follow the expected trends, mimicking the variations in the liquid outlet flowrates. As the liquid flow increases, the system pressure also increases, with the differences becoming much more apparent at the highest liquid flowrates.

7.1.5.2 Transients with Varying Gas Flowrates

A similar comparison to that presented above can be made to examine the effect of different step changes in the gas phase flowrates. Again three transient cycles are considered, referring to Table .7.1 these are Cycles 3, 4 and 5.

For each cycle the liquid phase flowrate had a minimum value of 0.06 m/s and a maximum one of 0.35 m/s. Cycles 3 and 4 had the same minimum gas flowrate values of 3.4 m/s but different maximum values of 9.0 m/s and 5.5 m/s, respectively, while Cycle 5 had a minimum gas flowrate of 5.5 m/s and a maximum value of 9.0 m/s. The average traces for the three measured parameters obtained for these cycles are compared in Figure 7.8.

Considering first the gas traces, it is noticeable that the gradients of the response curves for both increasing and decreasing gas flowrate are significantly different. However, the actual response times required to achieve steady-state after a transient are similar in all cases regardless of the magnitude of the step change involved or the relative values of the two steady-state flow conditions. Thus, as the step change increases in size, so does the driving force, in this case the pressure along the pipe, such that the final response time is independent of the gas flowrates.

The liquid responses show that all the final steady-state flowrates for each transition zone are nominally identical. Responses to liquid transients, for example after 120 and 240 seconds, all occur over the similar timescales even though the equivalent gas flowrates are different. Thus just as the gas transients were unaffected by variations in the liquid flowrates, the liquid transients are also unaffected by variations in the gas flowrates. The only noticeable difference is the magnitude of the peaks and troughs in response to the changes in the gas flowrate. This is in direct response to the different liquid hold-up values in the pipe associated with the relative gas-liquid fractions. Remember that for a constant liquid mass flowrate, the higher the gas flowrate the lower the liquid hold-up will be, so the largest gas flowrate step change will provide the largest change in the liquid hold-up and thus the largest change in the liquid outlet mass flow.

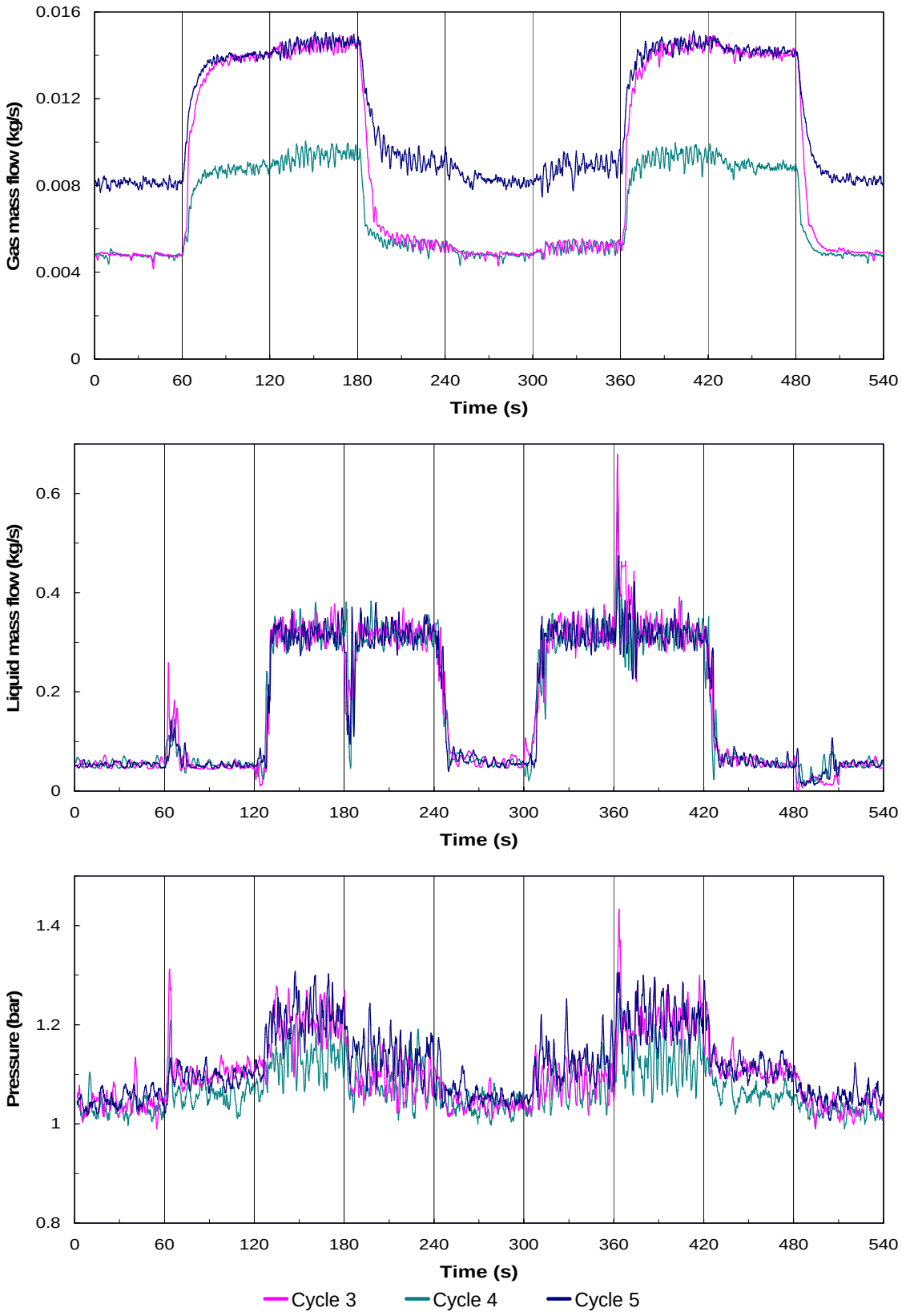

Figure 7.9: Comparisons of liquid outlet flow, gas outlet flow and pressure for Cycles 3, 4 and 5

Thus, for similar step change increases in the gas flowrate, Cycles 4 and 5, the liquid outlet flow surges show similar behaviour, both in terms of the timescales involved and the magnitude of liquid surge.

The pressure traces again show the expected close relationship corresponding to that of the liquid outlet flow responses. Larger peaks correspond to the highest liquid surges, related to maximum gas flowrate transients. Thus, Cycle 6, with the lowest maximum gas flowrate, has a pressure profile consistency lower than the other two.

7.1.6 Examination of the ECT data

Although the ECT system is primarily used for flow pattern identification it also has the ability to provide other important parametric data, such as liquid hold-up. Figure 7.7 shows the instantaneous liquid hold-up for Cycle 2, obtained using the ECT system. Further examination of this trace highlights the possibility of obtaining another important flow parameter, the slug frequency, for the two regions of slug flow studied for each cycle.

7.1.6.1 Liquid Hold-up

An accurate prediction of the liquid hold-up within a transport line is an important factor within many two-phase flow calculations and is often the starting point for many T-junction flow split models. Whereas there have been many experiments performed to validate predictive correlations for liquid hold-up in air-water systems the same cannot be said for non-aqueous systems, like the one presented here.

The electrical capacitance tomography unit delivers the instantaneous liquid hold-up within the pipe at a sampling frequency of 25 Hz. By measuring the capacitance between facing electrodes pairs the liquid hold-up can be determined based on a known calibration. Since it is accepted that the flow pattern could influence the measured capacitance even for a constant void fraction, the results presented here are based on measuring the normalised capacitance for known heights of stratified liquid, as shown in Figure 7.10. The calibration curve clearly reflects the non-linear

relationship but it is still represented relatively accurately, especially within the significant region of liquid hold-up greater than 0.4, by a third-order polynomial, which had a correlation coefficient of 0.9906.

Assuming that the flow in the pipe has achieved steady-state after 30 seconds of the transient being applied, which on analysis of the transient traces is a valid assumption, the average liquid hold-up for each set of flow conditions can be calculated from the mean of this 30 second period. Since each set of flow conditions are repeated as the cycle comprises of both a forward and backward loop, there will be potentially two liquid hold-up values for each set of flowrates, which should be, of course, essentially equal. Figure 7.11 shows the average void fraction measurements obtained for the range of flow conditions studied.

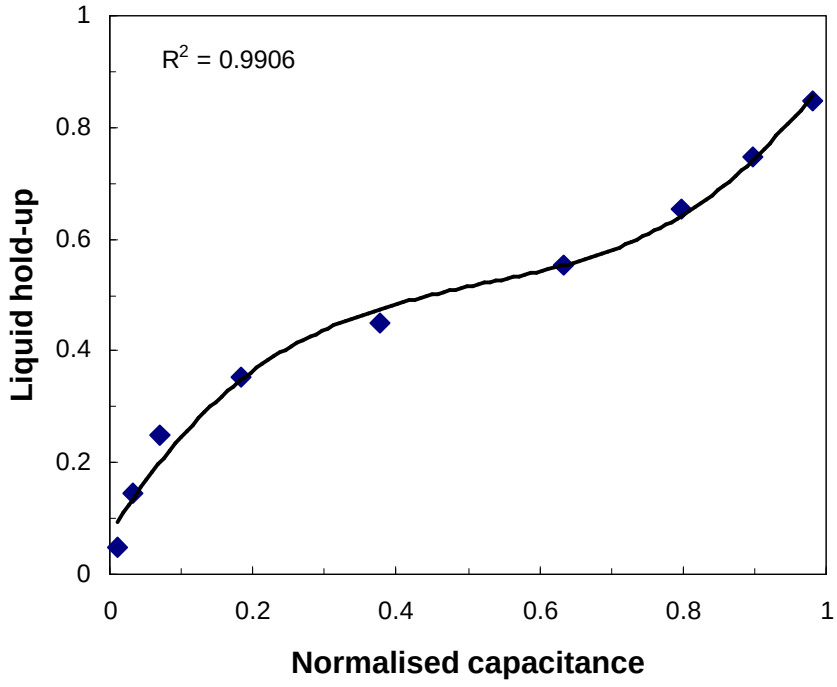

Figure 7.10: ECT calibration curve for the liquid hold-up based on capacitance measurements between facing electrode pairs

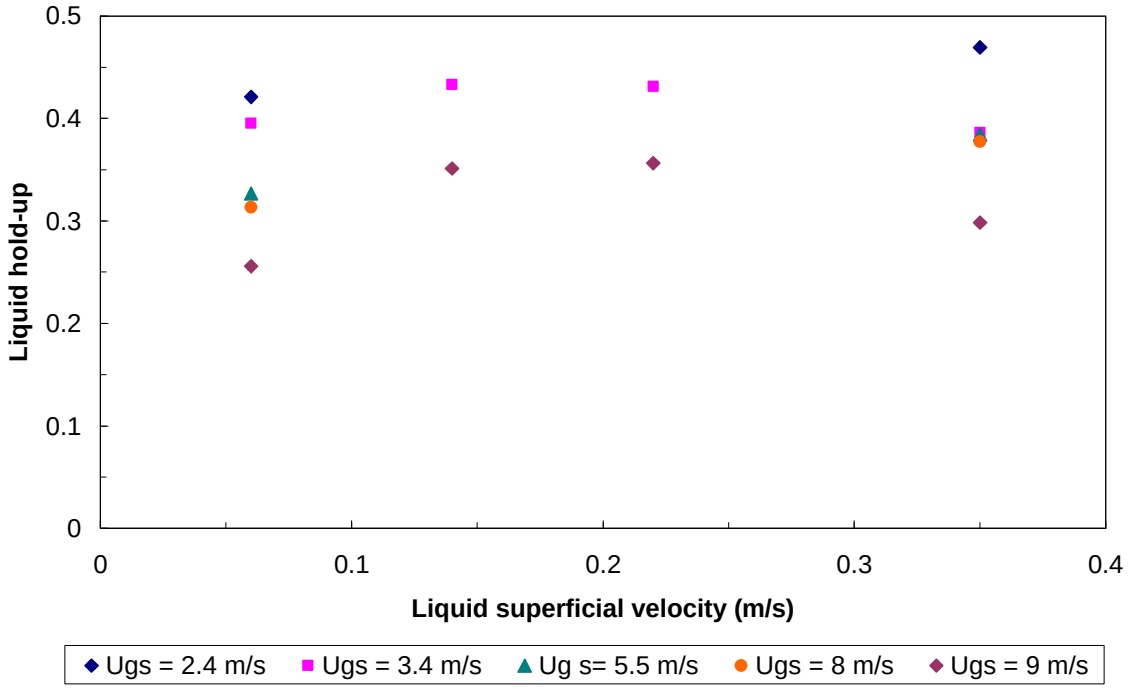

Figure 7.11: ECT measured liquid hold-up values for steady-state flow conditions

The results follow the expected trends, for constant values of liquid superficial velocity the liquid hold-up reduces as the gas superficial velocity increases. As the liquid flowrate increases there is an initial period of increasing liquid hold-up this corresponds to the flow regime passing from stratified into slug. Within this slug regime there appears to be a period of constant liquid hold-up, independent of the liquid flowrate but still affected by the gas velocity. Further increases in the liquid superficial velocity produce further reductions in the liquid hold-up. This can be explained by remembering that slug flow is an intermittent flow regime consisting of an aerated liquid slug and a stratified gas-pocket region. The determined liquid hold-up will then be an average of these two regions.

It has been shown (Dukler and Hubbard, 1975) that the length of stable liquid slugs is only a function of the diameter of the pipe and is generally in the range of 12 to 30 pipe diameters. Therefore the addition of extra liquid, by increasing the liquid superficial velocity, cannot be transferred into the liquid slug body because of this

known finite length. Thus, in order to accommodate this new material the gas-pocket region and the associated stratified liquid layer must have an increased liquid hold-up. This has the effect of increasing the overall length of the slug unit and so decreasing the average hold-up along its length. Figure 7.12 compares the liquid hold-ups for a low and high liquid superficial velocity slug flow with a constant gas superficial velocity. The traces show that although the slug frequency increases for the higher liquid flowrate case, the stratified region has a much lower liquid hold-up because the gas, and therefore the slugs, will be travelling faster and by the theory of Taitel and Dukler (1976) the equilibrium liquid height in the stratified region will be lower. Thus, the time-averaged void fraction value for the total slug flow will be less for the higher liquid velocity than for the lower velocity case.

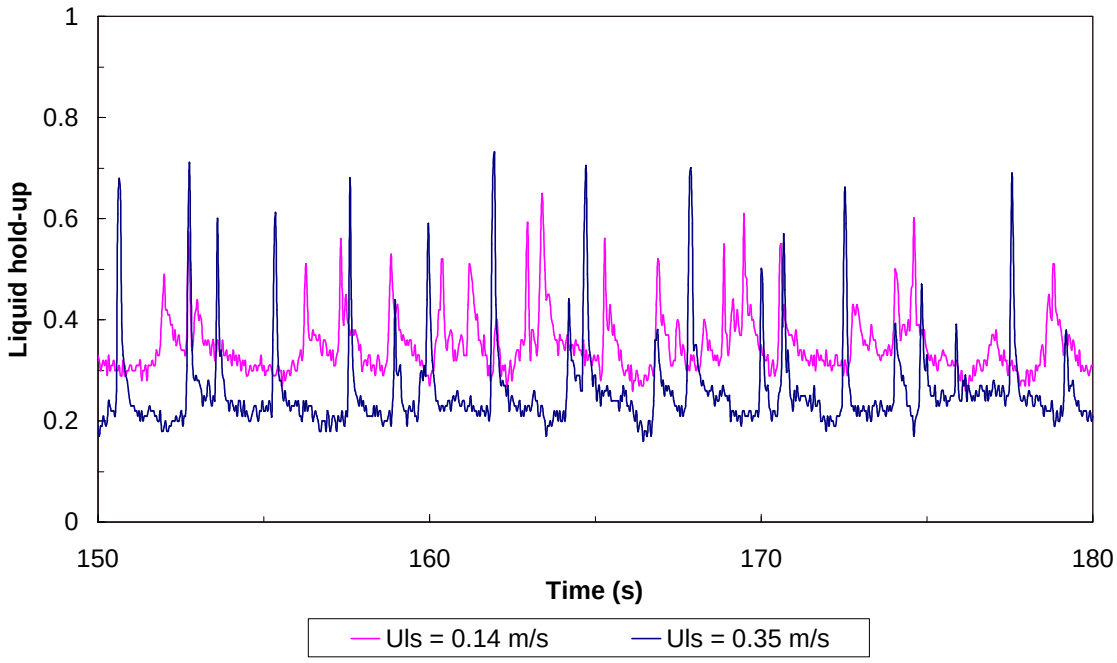

Figure 7.12: ECT measured liquid hold-up for slug flows with constant gas superficial velocity, U_{gs} = 9.0 m/s

For each set of flow conditions the well-known CISE correlation (Premoli *et al.*, 1970) was used to predict the liquid hold-up within the pipe. Figure 7.13 compares the values of the measured liquid hold-up obtained using the ECT unit with those predicted by this CISE correlation.

As can be seen in all cases the CISE correlation under predicts the liquid hold-up. There are two reasons why such a large discrepancy between the predicted and actual values could exist. The first reason is that the CISE correlation may simply not apply to the particular combination of fluids, pipe geometry and flow conditions. A second reason would be that the ECT is not reporting the correct liquid hold-up, although the calibration chart presented in Figure 7.10 shows a strong relationship. By comparing the current experimental data with available published data the validity of the ECT measurements can be further checked.

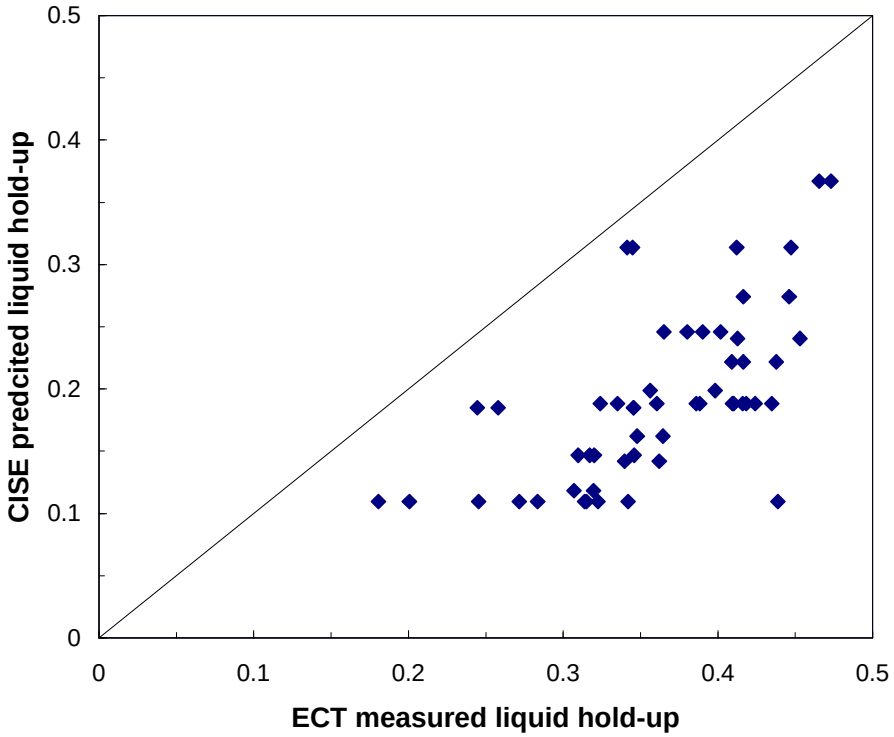

Figure 7.13: Comparisons of the ECT measured void fractions with the predictions of the CISE correlation

There is a limited amount of experimental data available where liquid hold-up has been measured using fluids of similar physical properties in a comparable geometry and at similar flow conditions. The only comparable data found is provided by Hoogendoorn (1959). In that study, which used a 0.0266 m diameter pipe, the liquid hold-up was measured by using a capacitance method, but unlike the ECT system used here, three circular electrodes were placed within the pipe in direct contact with the fluids. Dry air was used as the gas phase, while the liquid phase was a type of gas-oil. Table 7.3 gives a comparison of both the relative fluid physical properties and a summary of the geometries involved.

Having found a comparable set of physical properties the next step is to select similar flow conditions from the two studies based on the gas and liquid superficial velocities. This generated six suitable cases which are shown in Table 7.4. The current data contains sets of hold-up values for both the forward and backward loops, as well as the mean of these values. In all cases there is good agreement between the two current sets. By inspection of the current data and that provided by Hoogendoorn (1959) it is clear that there is good agreement between the comparable results. This provides confidence in the reliability of the hold-up values obtained from the ECT device.

Table 7.3: Comparison of the fluid properties used in the current work with those used by Hoogendoorn (1959)

	Current work		**Hoogendoorn (1959)**	
	Kerosene	Air	Oil	Air
Density (kg/m3)	797	1.4	838	2.2
Viscosity (kg/m s)	0.0018	0.000018	0.0076	0.000018
Surface tension (N/m)	0.034		0.031	
Pressure (bar)	1.2		1.8	
Pipe diameter (m)	0.0381		0.0266	
Pipe length (m)	17		25	

Table 7.4: Comparison of the current liquid hold-up data obtained with the ECT device with that of Hoogendoorn (1959)

Current Data					Hoogendoorn (1959)		
U_{gs} (m/s)	U_{ls} (m/s)	Liquid hold-up			U_{gs} (m/s)	U_{ls} (m/s)	**Liquid hold-up**
		Forward	Backward	**Average**			
2.4	0.35	0.470	0.469	**0.470**	2.5	0.34	**0.464**
3.4	0.22	0.365	0.348	**0.356**	3.1	0.23	**0.330**
3.4	0.35	0.402	0.447	**0.424**	3.7	0.34	**0.416**
5.5	0.06	0.310	0.320	**0.315**	5.8	0.06	**0.306**
5.5	0.35	0.345	0.364	**0.355**	6.1	0.34	**0.359**
9.0	0.35	0.315	0.341	**0.328**	9.8	0.34	**0.305**

These simple comparisons highlight the problem of applying two-phase flow correlations to a particular situation without proper consideration. Since, the vast majority of such two-phase correlations are based on air-water systems, caution needs to be applied when extending their use to other fluids with different physical properties.

7.1.6.1 Slug Frequency

On further analysis of the liquid hold-up trace it is possible to obtain another important flow parameter that of slug frequency, see Figure 7.11. As above, the flow is assumed to reach steady-state 30 seconds after the transient has been applied. Combining the three individual runs that comprise a Cycle and noting that within one Cycle each set of flow conditions are repeated, the total number of regions available for slug frequency calculations is six.

For a single data set, this approach then implies two extreme slug frequencies, f_{min} and f_{max}, which are calculated using Equations 7.1 and 7.2, respectively.

$$f_{\min} = \frac{N}{t + \Delta t} \qquad [7.1]$$

$$f_{\max} = \frac{N+1}{t+\Delta t} \qquad [7.2]$$

where, N is the number of slugs, t is the time when the first slug is counted and Dt is the time period over which the slugs frequency is calculated.

The error, err_f, in a single measurement of the slug frequency then becomes:

$$err_f = \frac{f_{\max} - f_{\min}}{f_{\min}} = \frac{(N+1)-N}{N} = \frac{1}{N} \qquad [7.3]$$

For the six individual runs combined the minimum and maximum frequencies are then calculated by Equations 7.4 and 7.5, respectively.

$$f_{\min} = \frac{N_1 + N_2 + ... + N_6}{6(t+\Delta t)} = \frac{\sum_{i=1}^{6} N_i}{6(t+\Delta t)} = \frac{\overline{N}}{t+\Delta t} \qquad [7.4]$$

$$f_{\max} = \frac{(N_1+1)+...+(N_6+1)}{6(t+\Delta t)} = \frac{\sum_{i=1}^{6}(N+1)_i}{6(t+\Delta t)} = \frac{\overline{N}+1}{t+\Delta t} \qquad [7.5]$$

where, N_i is the number of slugs counted in each individual run, i, and $\overline{N}$ is the mean number of slugs.

The error in the calculated frequency then becomes:

$$err_f = \frac{f_{\max} - f_{\min}}{f_{\min}} = \frac{(\overline{N}+1)-\overline{N}}{\overline{N}} = \frac{1}{\overline{N}} \qquad [7.6]$$

Table 7.5 shows slug frequencies obtained from the ECT liquid hold-up measurements in the slug regime flow conditions for the three individual runs of Cycle 1. The results all show a high level of consistency.

Table 7.5: Slug frequencies obtained from the ECT liquid hold-up measurements for the slug regime flowrates of Cycle 1

Run	U_{gs} (m/s)	U_{ls} (m/s)	Number of Slugs, N	f_{min} (Hz)	f_{max} (Hz)	f_{mean} (Hz)	Error
A	2.4	0.35	14	0.467	0.500	0.483	0.0714
			14	0.467	0.500	0.417	0.0714
B			12	0.400	0.433	0.483	0.0833
			14	0.467	0.500	0.483	0.0714
C			14	0.467	0.500	0.483	0.0714
			14	0.467	0.500	0.483	0.0714
Mean	**2.4**	**0.35**	**13.7**	**0.456**	**0.489**	**0.472**	**0.0732**
A	8.0	0.35	17	0.567	0.600	0.583	0.0588
			16	0.533	0.567	0.550	0.0625
B			16	0.533	0.567	0.517	0.0625
			16	0.533	0.567	0.550	0.0625
C			15	0.500	0.533	0.550	0.0667
			15	0.500	0.533	0.517	0.0667
Mean	**8.0**	**0.35**	**15.8**	**0.528**	**0.561**	**0.544**	**0.0632**

Based on this excellent agreement Table 7.6 shows the combined results for all the slug flow conditions present within each Cycle. As predicted by Equation 7.6 the maximum error in the calculated slug frequency increases as the number of counted slugs present decreases.

Table 7.6: Combined slug frequencies obtained from the ECT liquid hold-up measurements for all the slug regime flowrates in all the Cycles

U_{gs} (m/s)	U_{ls} (m/s)	f_{min} (Hz)	f_{max} (Hz)	f_{mean} (Hz)	Error
2.4	0.35	0.456	0.489	0.472	0.0732
3.4	0.14	0.100	0.133	0.117	0.3333
3.4	0.22	0.250	0.283	0.267	0.1333
3.4	0.35	0.408	0.442	0.425	0.082
5.5	0.35	0.367	0.400	0.383	0.0909
8.0	0.35	0.528	0.561	0.544	0.0632
9.0	0.22	0.317	0.350	0.333	0.1053
9.0	0.35	0.467	0.500	0.483	0.0714

From the data presented in Table 7.6 there are clear identifiable trends. The simplest relationship that exists is that as the liquid superficial velocity increases the slug frequency also increases. For a constant liquid superficial velocity the slug frequency passes through a minimum value as the gas superficial velocity is increased. This is in agreement with other published slug frequency data. Traditionally, slug frequency data is plotted in terms of the mixture velocity, the sum of the gas and liquid superficial velocities, for constant liquid superficial velocities. Figure 7.14 shows a comparison between slug frequency data from three sources using three different fluid sets. In all cases the pipe diameter and liquid superficial velocities are approximately equal. A summary of the key physical properties of the individual fluids involved is a given in Table 7.7.

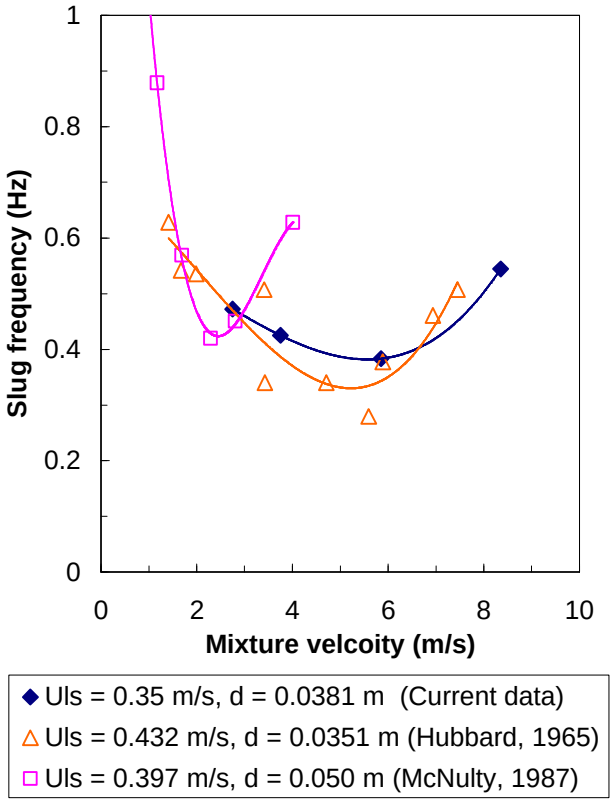

Figure 7.14: Variation of slug frequency with the mixture velocity for different fluid systems

Table 7.7: Physical properties of the three data sets used in the slug frequency comparison

Source	Fluids	r_L (kg/m^3)	r_G (kg/m^3)	r_L/r_G	m_L (kg/ms)	m_G (kg/ms)	m_L/m_G
Current	Air-kerosene	797	1.4	569	0.0018	0.000018	100.0
Hubbard (1965)	Air-water	1000	1.284	769	0.001	0.000018	55.5
McNulty (1987)	R-11	1358	22.6	60	0.00029	0.000012	24.2

Figure 7.14 confirms the existence of a minimum slug frequency as previously described. It has been shown by Jones *et al.* (2001) that pipe diameter can have a significant effect on the slug frequency. In that work the slug frequency of air-water mixtures were compared for three different pipe diameters (0.0351 m, 0.01905 m and 0.005 m) for similar inlet flow conditions. It was found that as the pipe diameter decreased the slug frequency was seen to increase. Another interesting finding was that the characteristic minimum slug frequency occurred at decreasing slug mixture velocities as the pipe diameter decreased. From the present comparison it is clear that fluid physical properties also influence the mixture velocity at which the minimum slug frequency occurs. With the refrigerant data of McNulty (1987) exhibiting a very sharp frequency minima at a much smaller mixture velocity than for the other two data sets.

Since slug flow is such an industrial important flow regime much effort has been directed in trying to predict various key parameters, for example liquid hold-up and slug frequency. Many predictive methods have been suggested in an attempt to calculate the frequency of slugging within pipes. Figure 7.15 shows a comparison of the present data with three predictive methods. It is clear that the early method of Gregory and Scott (1969) always under predicts the slug frequency for the set of flow conditions and fluid properties used here. This consistent discrepancy is most likely due to their prediction being based on the minimum slug frequency occurring at a slug mixture velocity of 6 m/s. Within the current data set the minimum actually occurs at a slightly larger value of 6.8 m/s. Although this may appear to be a minor difference it would be sufficient to produce the sort of constant offset observed.

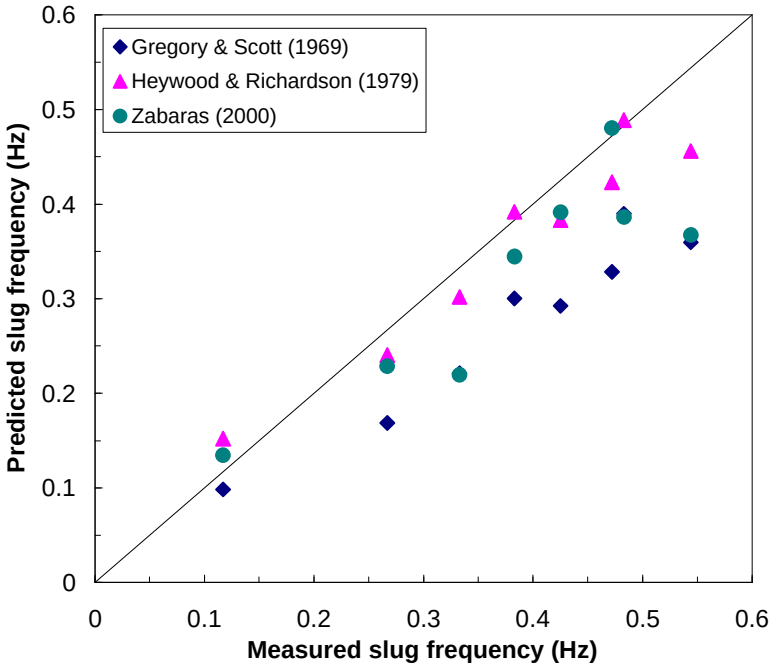

Figure 7.15: Comparisons between the current data and slug frequency predictions

The predictions of Heywood and Richardson (1979) show much closer agreement but nevertheless there is still a tendency to under predict the frequency. Finally Zabaras (2000) produced a modification of the Gregory and Scott (1969) method, based on a new slug frequency data base. However, the resultant correlation does not provide a significant improvement on the frequency predictions in this case. It is clear that more effort needs to be applied on the prediction of slug frequencies within non-aqueous systems.

7.2 Transient Flows at T-junctions

The study of transient flows through a straight pipe forms a basis for a complimentary study of transients through the T-junction system. Obviously the main difference between the two cases is the added complexity of having three possible exit streams. Within industrial situations there are strong possibilities that transient flows will regularly occur and the aim here is to try and gain an understanding of where the gas

and liquid flows will tend to distribute themselves in response to increases and decreases in the phase flowrates within the T-junction separator.

Considering the possible implications of transient gas-liquid flows within T-junctions it is surprising to find only one other study (Ottens *et al.*, 2001) that has been carried out on the subject. Unlike the present work, however, their experiments were designed with an emphasis on liquid condensate within natural gas transport lines. Thus, the liquid hold-up values are chosen to be less than 0.1, compared to the larger values (= 0.25) used in this study. Nevertheless the transient results reported show behaviour already observed within the straight pipe studies above and they could be expected to also occur within the current T-junction arrangement.

Figure 7.16 shows the traces obtained by Ottens *et al.* (2001) for two different transient runs, one with a step change in the gas flowrate, the other with a step change in the liquid flowrate. In all cases the liquid flowrates show much larger deviations around the mean than the gas flowrates, which essentially exhibit no deviations. For an increase in the inlet gas superficial velocity from 8 m/s to 12 m/s, Figure 7.16*left*, the liquid superficial velocities in both exit streams show a sharp increase. This large surge is associated with the rapid change in the liquid hold-up of the system, with the higher gas flowrate sweeping out the excess liquid. After this excess is removed the liquid flowrates return to their new steady-state positions, with a different flow split ratio then before. The gas exit streams show a quick but not instantaneous response to the step change in the inlet flow. When the gas goes through the reverse transient, the liquid exits both show a temporary period of reduced superficial velocities. This is again in response to the associated increase in the liquid hold-up along the pipe. Once the new equilibrium liquid level has been attained the exit flowrates return to the initial steady-state values. Again, the gas responses are quick but not instantaneous. Any differences in the response times of the two exit streams were determined to be due to the differences in the pipe lengths and fluid velocities within each branch.

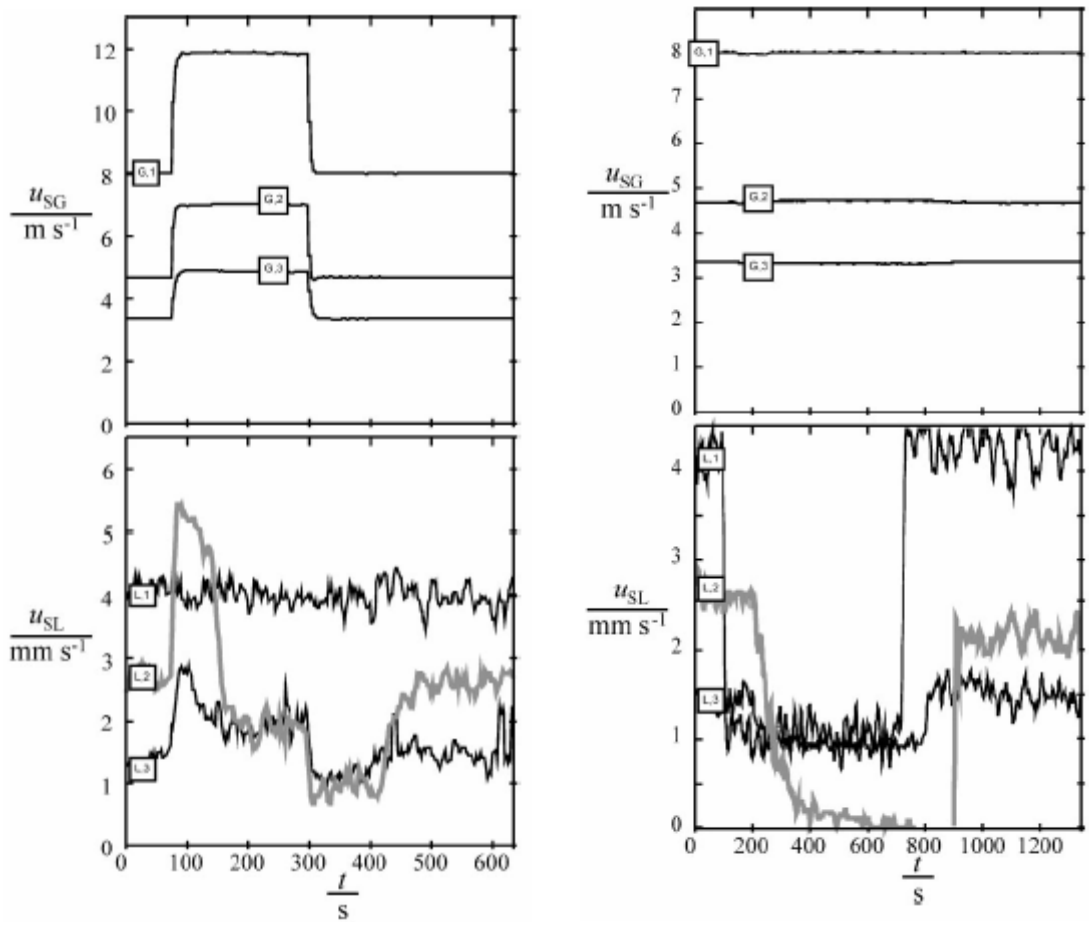

Figure 7.16: Transient gas-liquid flows results of Ottens *et al.* (2001)
***Left*: U_{gs} transient 8 m/s to 12 m/s to 8 m/s with U_{ls} = 0.004 m/s**
***Right*: U_{ls} transient 0.004 m/s to 0.0009 m/s to 0.004m/s with U_{gs} = 8 m/s**

The second case, Figure 7.16*right*, examines a reduction in the inlet liquid superficial velocity from 0.004 m/s to 0.0009 m/s. Although these flowrates are very small in comparison to the current studies this transient represents a step change in the superficial velocity of 77.5%. Such a large reduction goes some way to explain the complete phase separation reported during the transient period as well as the very sharp increase in the run when the liquid flowrate is retuned to its initial value. The gas outlets show a constant velocity being unaffected by the liquid transients. In contrast, the outlet liquid flowrates show a gradual reduction in the superficial velocity, with a significantly long time constant. This means that even after the inlet

flowrate has been increased back to its original value, the outlet liquid flowrate is still reacting to the initial decrease. Thus, the liquid has a longer reaction time than the gas phase obviously due to the orders of magnitude difference in the relative superficial velocities.

7.2.1 Experimental Arrangement and Flow Conditions

The experimental arrangement for studying transients through the T-junction is the same as that already used in Chapters 5 and 6, as detailed in Chapter 3. Figure 7.17 gives a schematic of the general layout indicating points where the pressure, *P*, and the two-phase pressure drops used to imply the liquid flowrates, *F*, are measured. Remember the gas flowrate is measured, using orifice plate meters, beyond the separation tanks (not shown).

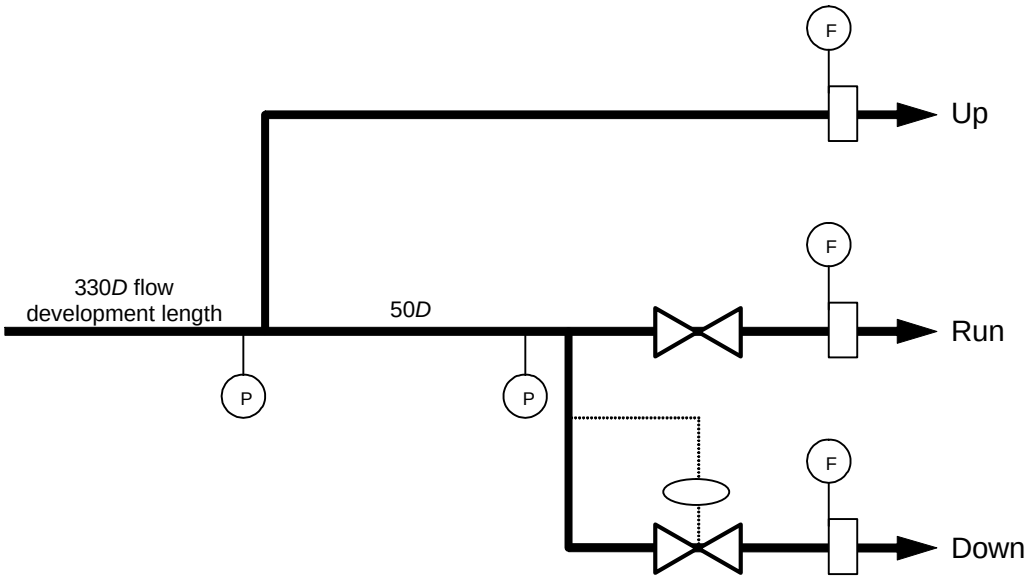

Figure 7.17: Schematic diagram of T-junction separator during transient experiments

In order to make comparison easier the flow conditions replicate those already used in the study of straight pipe transient flows (see Table 7.2). The exact same methodology of looping through a cycle in both directions is applied to again ensure that all the transient possibilities are investigated.

To reduce the level of complexity, the run valve, which is used to maximise the separation based on flow patterns, was left in the fully open position for all the transient experiments. However, the automatic level control still operated on the down leg to provide the gas-free liquid exit stream.

7.2.2 Data Analysis and Consistency

As for the straight pipe transients a set of three nominally identical experiments were performed for each cycle. This was used as a check for consistency and by taking the average of the three runs the inherent variations within the slug flow regime could be reduced. Figure 7.18 shows both the individual run traces and the resultant average of these runs of the outlet mass flowrates over the same period of time. As seen for the straight pipe case all the gas mass flow traces tightly fluctuate around the calculated average value, confirming the reproducibility and reliability of the results. However, in the case of the liquid mass flow traces the situation is a little different. Form the traces it is possible to identify the same general flow deviations exhibited throughout all the individual cases. Just as observed in the results from the pipe the average trace does remove the most severe random fluctuations and provides an easier method of assessing the transient trends.

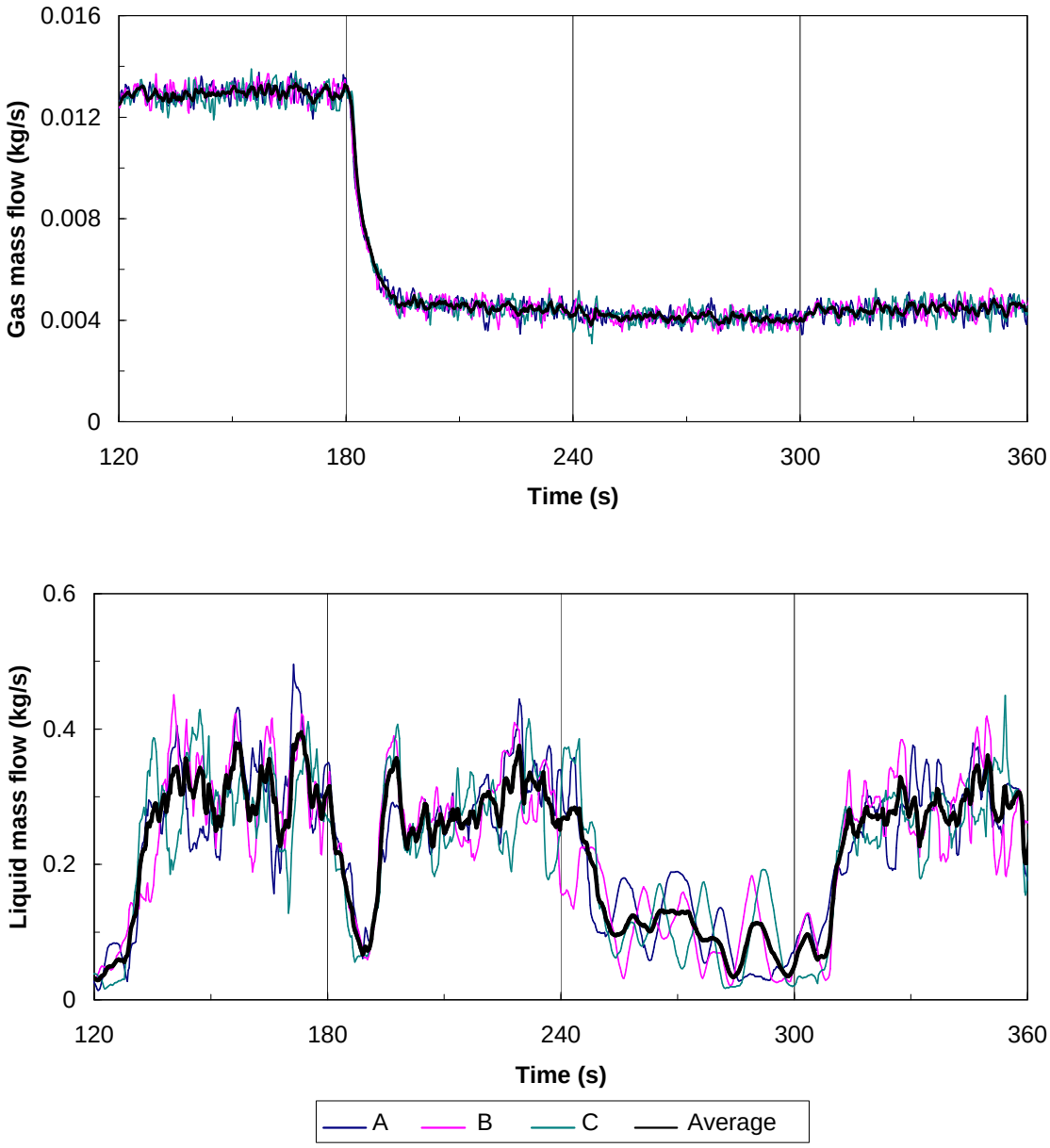

Figure 7.18: Comparison of three experimental runs (A, B, C) and the ensemble average for the combined gas and liquid mass flowrates out of the T-junction system

When the flow through the T-junctions is considered, there is a further complication associated with the existence of more than one exit stream and the definition of a total mass flowrate. Unlike the straight pipe case, here there are three probable exit streams for the liquid phase and, because of the automatic level control on the down

leg, two for the gas. The total phase mass flowrate through the system is assumed to be the total of the relevant exit streams at any point in time. Figure 7.19 shows this approach for both phases. In the case of the gas mass flow out of the system, Figure 7.19 illustrates that even though the air may distribute itself around the two exit streams differently over the period of one complete cycle the sum of the two streams, both for the high and low gas flows, shows a very consistent value. This emphasises the consistency of the calibration method and reliability of the orifice plates in determining gas flowrates. The traces also exhibit strong symmetrical-like characteristics, has the flow is diverted around the system.

The situation for the liquid mass flows is quite different. As for the gas flowrates the total flow through the system at any point in time is taken as the sum of the three individual liquid flowrates at that instant. Since the different exit streams have different distances to the orifice plates, used in the determination of the liquid mass flowrates, the transient effects do not necessarily arrive at each measurement point simultaneously. For the flow through the straight pipe the fluctuations during steady-state flows were relatively small when compared with those shown in Figure 7.19 for the T-junction. This is thought to be a combination of the nature of the flow splitting at the T-junctions as well as the action of the automatic control valve on the mass flow through the down leg. Steady-state phase split results provide, by definition, an average of the separation performance at T-junctions, ignoring the natural flow fluctuations. For continuous measurements it is expected that there will be periods where, especially for slug flows, the liquid would be more readily diverted into one of the three exits streams.

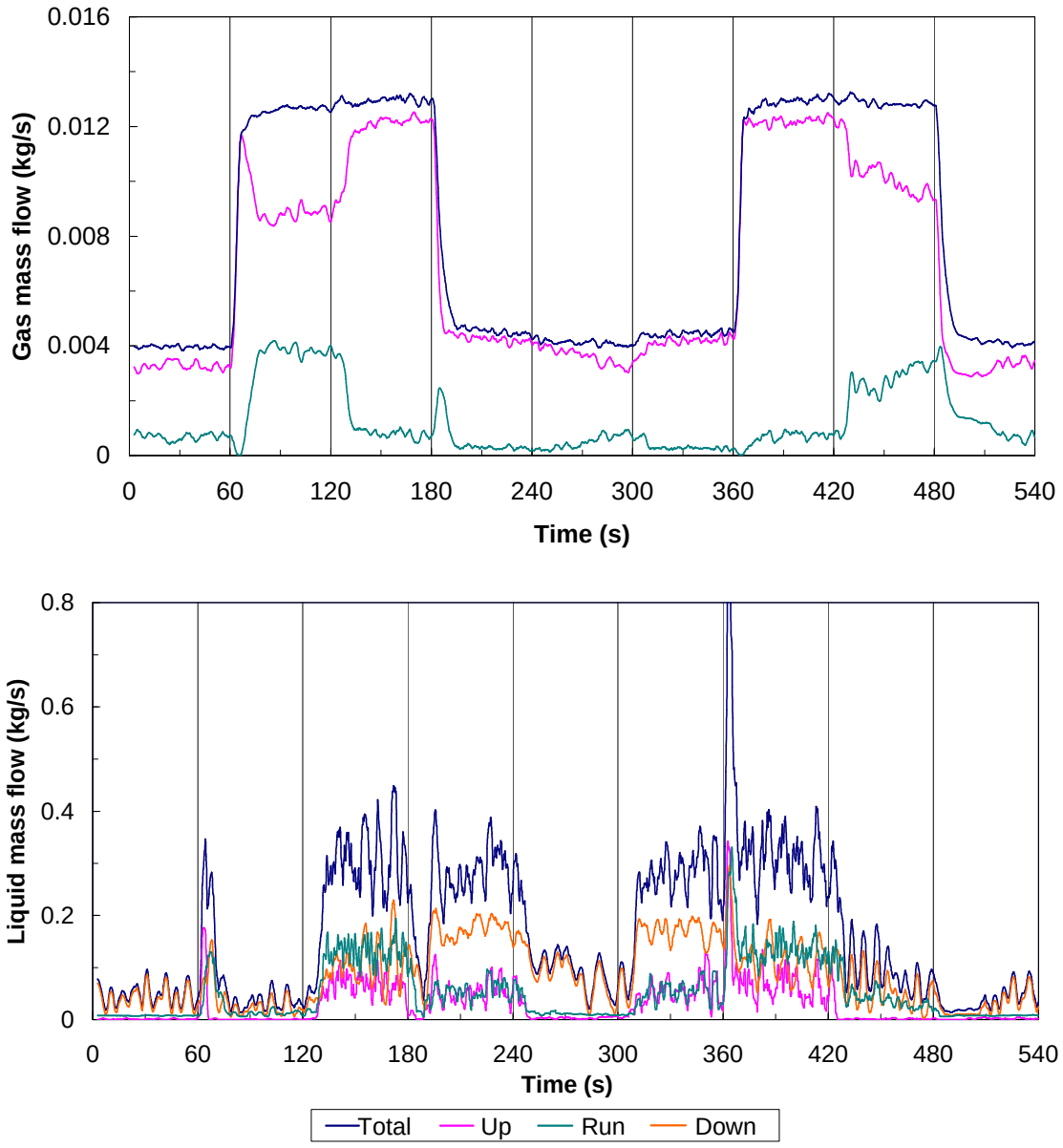

Figure 7.19: Liquid and gas outlet mass flowrates showing the individual exit streams and their sum totals for Cycle 1

The effect of non-continuous flow, presenting fluctuating liquid mass flows, is enhanced further by the existence of a very close relationship between the total mass flowrate and the down leg flowrate. This is especially emphasised during the periods of stratified flow, where from the steady-state flow splits data it is known that the liquid recovery in the down leg will be very high, as the slower moving liquid will

tend to fall down into the branch opening. Whereas for slug flows the split is more evenly distributed around the system, especially with the run arm fully open. Again, one detail that is not attainable from steady-state flow split data is the variation in the liquid flowrate through the level control system. It is expected that these two values will be closely related, since the more open the control valve the higher the flow through it will be. Previous work in Chapter 5 already highlighted a simple relationship between the liquid height in the down leg and the percent open setting of the valve. Using the specially calibrated orifice plate installed downstream of the control valve the local mass flowrate can be measured and compared with both the liquid height and the control valve setting. Figure 7.20 gives a comparison of typical traces for the liquid height in the down leg, the liquid mass flowrate exiting through the down leg and the control valve setting.

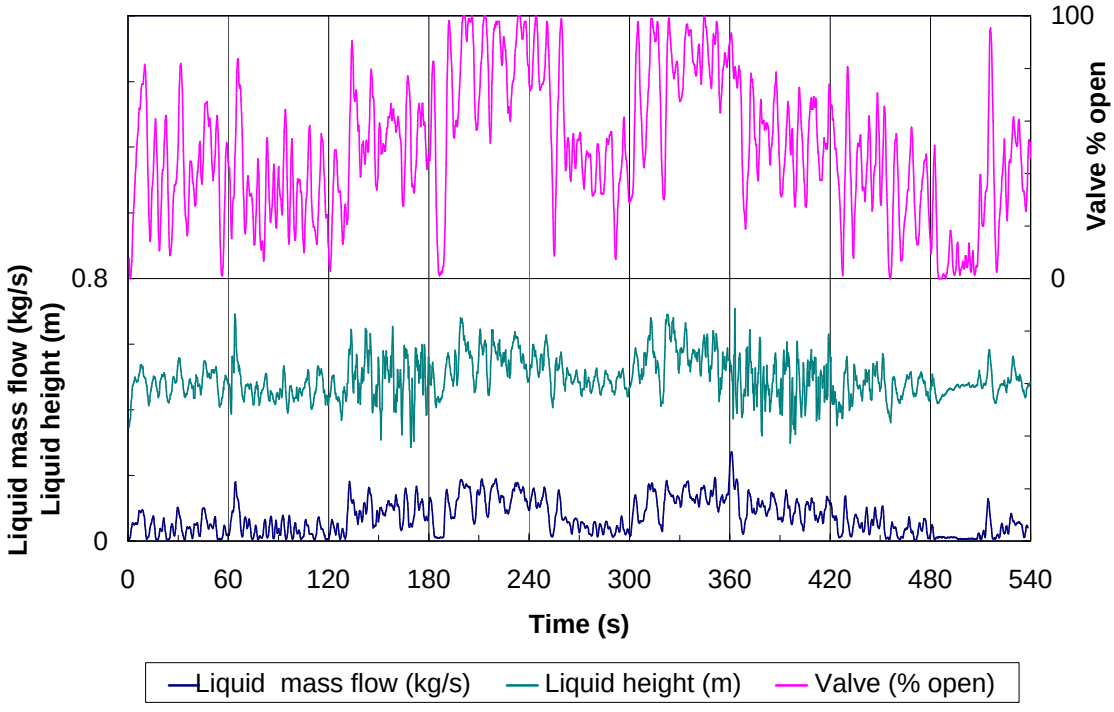

Figure 7.20: Comparisons of the liquid mass flowrate through the down exit stream with the height of the liquid level maintained in the down leg by the automatic control valve and the control valve setting for Cycle 2

As expected there is a strong inter-dependency on these three parameters. The automatic control valve is trying to maintain a constant liquid level within the down leg, thus, as more liquid enters the down leg, increasing the liquid level, the control valve opens further allowing more liquid to flow through it. This extra outflow of liquid will reduce the height above the valve, bringing the level below the set point, forcing the valve to try and adjust the level by closing, thus restricting the flowrate leaving the down leg.

As with all of the traces there are clear identifiable regions of transient behaviour visible. For example, the sudden increase in the gas inlet superficial velocity after 60 and 360 seconds is characterised by a sudden increase in the height as the excess liquid is swept out of the system. The control valve responds by opening and the liquid mass flow leaving in the down leg shows a temporary increase. After a short period the system returns to the previous steady-state conditions. Similarly, when the inlet gas flowrate is reduced, after 180 and 480 seconds, the liquid mass flowrates also reduce. This is most clearly seen when the transient occurs within the stratified region, after 480 seconds. Here the control valve closes in response to the reduction of the liquid level, and the liquid level shows a gradual rise back to its set point value.

Regardless of both these factors, the total liquid mass flowrate through the T-junctions achieved by the simple summing of the three exits does provide values that consistently fluctuate around the correct nominal liquid mass flowrates and are used as a good representation of the transient responses.

7.2.3 Observations of Transient Flows at T-junctions

It is difficult to discuss the effects of transient flows through the T-junctions without reference to the full data set. Composite plots similar to those used for the comparative studies of transients in the simple straight pipe (for example Figure 7.8) are not practical for the T-junction system because of the added complexity of each Cycle having potentially three exit streams. Hence the trace plots of the gas and liquid mass flows through the relevant exit streams for each individual Cycle are

given in Appendix E. As with the straight pipe both the gas and liquid phases need to be considered in parallel. Figure 7.21 shows representative traces (in this case for Cycle 1) that exhibit the typical trends observed throughout all the transient T-junction experimental data.

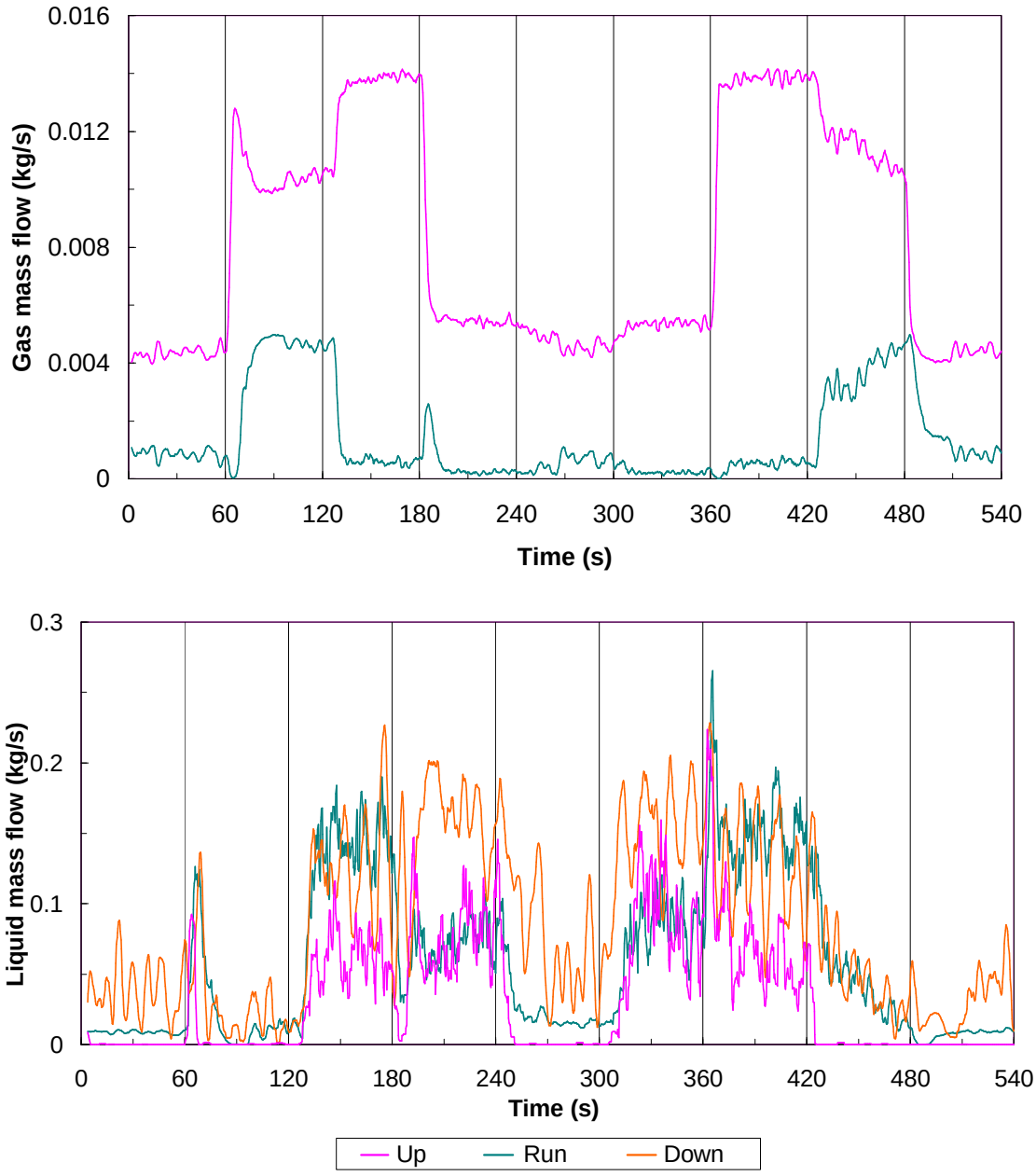

Figure 7.21: Typical transient responses of the outlet phase mass flowrates through the T-junction system (Cycle 1)

As discovered for the case of transient flows in a pipe, the greater the magnitude of the phase inlet flowrate step change, the more pronounced the outlet transient responses of the phases will be. For example, the larger the step increase in the gas inlet superficial velocity within the stratified flow regime, the more excess liquid is pushed out of the system in the form of slugs, appearing as a peak in the outlet liquid mass flows.

Using the same systematic approach as applied in Section 7.1.4 for the analysis of transient flows through the straight pipe, each step change will be discussed in sequence. The first transient is an increase in the inlet gas superficial after 60 seconds. As for the straight pipe this results in a surge of liquid formed by near-instantaneous slugs within the pipe. This confirms the results of Ottens *et al.* (2001) as previously discussed at the start of Section 7.2 and shown in Figure 7.16. Up to this point there tends to be no, or very little, liquid travelling in the up arm of the first T-junction and a stable flow leaving in the final run arm with the majority of the flow leaving in the down leg. This is in accordance with the steady-state phase split data for stratified flows. After the increase in the gas flowrate all three exit streams show a rapid surge in liquid outflow. Interesting the maximum liquid flow peak for all three streams appears at different times. This is clearly related to the relative distance the liquid needs to travel in each exit to reach the measurement orifice plate and the hold-up associated with the control valve on the down leg. In order to fully understand the mechanisms at work it is essential to examine the distribution of both phases through the system simultaneously. The associated gas outlet mass flows show there is a definite physical interaction between the phases so that the gas flow split can both affect and be affected by the liquid distribution within the pipework. At the onset of the transient the gas mass flow increases very rapidly in the up arm of the first junction. This corresponds to the sharp surge of liquid also leaving in that stream and also a reduction in the gas mass flow in the run arm. However, the liquid mass flow out of the run arm shows a large surge and so it is evident that this liquid surge will tend to completely fill the pipe and so forcing the gas to leave through the only available exit, the up arm. This explains the large spike in the up gas flow and the dip in the run arm flow. As this liquid gradually drains through the run arm it allows

more and more gas to flow with it. Thus the gas flow leaving through the up arm diminishes as the flow through the run gradually increases.

The next transient is an increase in the inlet liquid flowrate after 120 seconds, which moves the regime into slug flow. In this case there is a delayed increase in all three liquid outlets, in line with the steady-state phase split of slug flow. The extra liquid within the system tends to force more gas into the up arm, assumingly in response to the larger pressure drop in the run arm.

After 180 seconds the inlet gas superficial velocity is reduced back to its initial value. This has the effect of reducing the liquid mass flowrates out of all three outlets in response to the standard readjustment of the upstream liquid hold-up. As the liquid mass flowrate leaving in the run is reduced it is becomes momentarily easier for the gas to travel through the same branch rather than in the up arm. This is observed as a small surge in the gas mass trace. Nevertheless, because the flow is still in the slug regime, the final steady-state gas split still favours the gas exiting in the up arm. The fraction of liquid take-off in the up arm remains constant, in line with the steady-state results presented in Section 6.2.3, where for high liquid flowrates the take-off at the vertically upwards side-arm was seen to be independent of the superficial gas velocity. The reduced gas superficial velocity will reduce the velocity of the slugs and the slower moving slugs with a lower momentum will not be so able to by-pass the down leg opening and so the liquid mass flow in the run decreases as the down leg flowrate increases.

The final transient of the forward loop is to reduce the inlet liquid superficial velocity back to the initial steady-state value. Again the responses at the outlets are all associated with the changes of the upstream liquid hold-up. As the liquid hold-up gradually decreases the liquid mass flowrates in all three exit streams also gradually decrease. All the phase outlet mass flowrates then return to their respective initial steady-state values.

For the backward loop the increase in the inlet liquid superficial velocity, after 300 seconds, behaves as expected. The outlet streams all show a clear gradual increase in the liquid mass flowrates and the increase in the liquid leaving in the run forces more gas into the up arm.

After 360 seconds the inlet gas is again increased causing a period of intensive slugging within the pipe. As for the case of the same increase within the stratified regime, these faster travelling slugs tend to travel with a high enough momentum to by-pass the down leg so the excess liquid appear as surges within the up and run outlet streams. Unlike the case of stratified flow however the gas flowrate trace does not increase with a peak but rises very quickly to its final steady-state flowrate. This can be explained by the presence of the slug flow regime after the transient, as opposed to the same increase at 60 seconds when the steady-state flow regime was stratified. As seen for the region of high liquid and high gas flowrates the gas exits through the route of least resistance, which for this case is the liquid-lean up arm.

The decrease in the liquid inlet flowrate with a high gas velocity, after 420 seconds, has an effect on all the phase outlet streams. With less liquid leaving in the run, the gas flow through that stream once again increases significantly, obviously reducing the up arm flow. This reduced flow in the up arm coupled with the tendency of the flow to become stratified, almost immediately reduces the liquid take-off in that branch. As the flow gradually becomes more and more stratified in nature, as the hold-up slowly reduces, both the run and down leg exit streams shows a gradual linear decline in the liquid mass flowrates. Interestingly, in all cases the flowrate gradients for both the gas and liquid outlet responses have gradients of very similar magnitude, requiring the full 60 seconds period to achieve their steady-state values.

The final transient is the lowering of the gas superficial velocity, after 480 seconds, returning the system to its initial set of flow conditions. In this case the gas flow leaving through the up arm reduces significantly faster than that out of the run. With a reduction in the gas flowrate there is also an increase in the upstream liquid hold-up. The liquid phase velocity reduces to a much lower value, and so the liquid tends to

fall directly into the down leg opening, so the liquid mass flowrate in the run falls and in the case of Figure 7.21 temporarily stops altogether. However, once the system has achieved the steady-state and the new liquid equilibrium height has been established the liquid outlet flows recover to their nominal steady-state values.

At this point it is useful to return to the concept of evaluating the separation performance of the system for a transient Cycle. This can be represented by using the Separation Effectiveness Factor, as previously defined in Chapter 6, and also by considering the liquid volumetric content of the combined gas outlet. It must be remembered that the run valve was maintained at the fully open position throughout so that the presented results are not obtained at the optimum valve settings as previously determined in Chapter 6. Nevertheless, they can still be considered as indicative of the expected transient performance and both approaches are plotted for Cycle 1 in Figures 7.22 and 7.23, respectively.

Considering first the Separation Effectiveness plot, Figure 7.22, it is clear that both the individual phase flowrates as well as the actual flow pattern influence the system performance, has previously highlighted in Chapter 6. This is best illustrated by examining the first 240 seconds of data. Initially, the flow is stratified, with low gas and liquid superficial velocities, hence, as shown in Figure 7.22, it would be expected that a large fraction of the inlet liquid would be able to fall into the down leg even with the run valve fully open. The Separation Effectiveness shows very large deviations within known steady-state regions, which is characteristic of the level control valve influencing the liquid hold-up in the down. When the gas flowrate is increased after 60 seconds the Separation Effectiveness shows a characteristic dip corresponding to the period of high velocity liquid slugs that are formed and swept with the gas into the up arm and the run, by-passing the down leg. Once this period of instability has passed the steady-state flow regime is still stratified but because of the increased gas flowrate the liquid layer will be thinner and will thus travel with a higher momentum. This implies that the liquid will have less time to be influenced by the down leg opening and a greater fraction will leave the system through the run, reducing the average Separation Effectiveness.

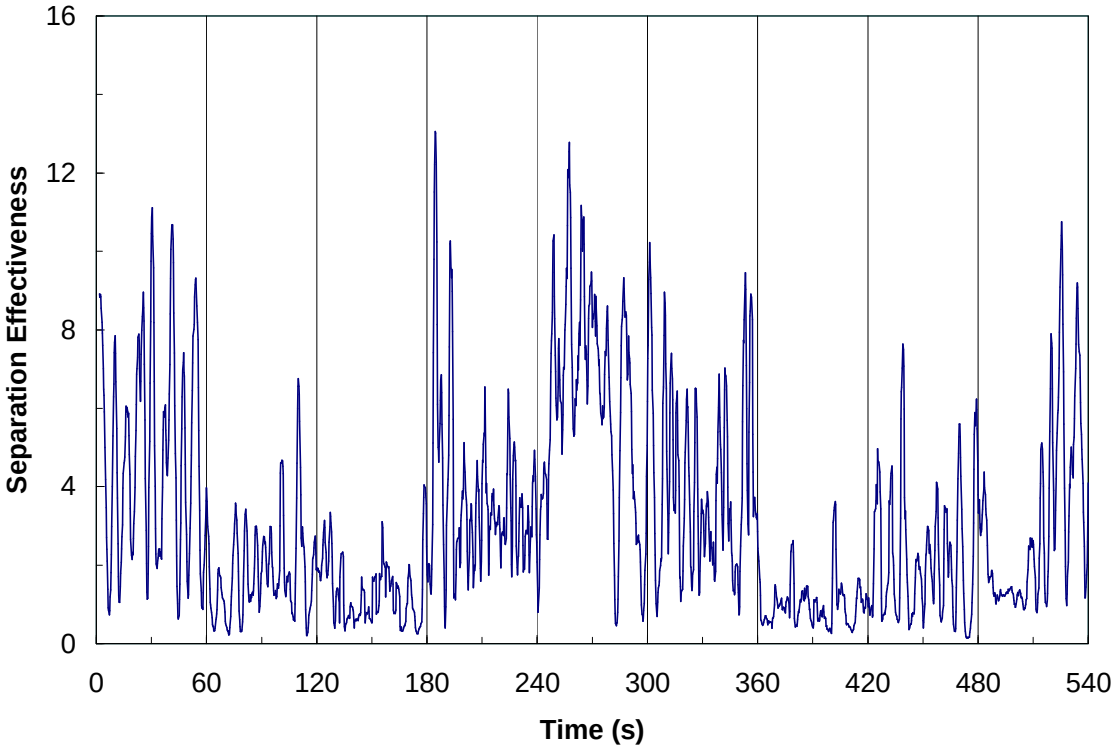

Figure 7.22: Separation Effectiveness Factor variation for Cycle 1 (with the run valve fully open)

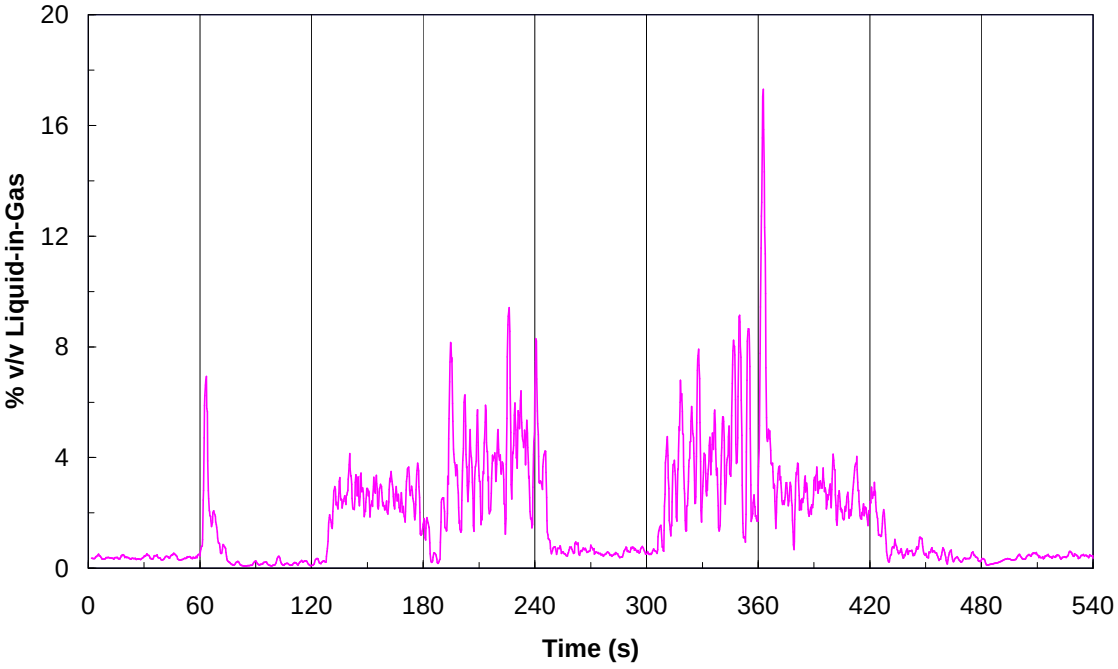

Figure 7.23: Volumetric liquid content of combined gas exit stream for Cycle 1 (with the run valve fully open)

The next step change is an increase in the liquid flowrate after 120 seconds, where slug flow becomes the new steady-state flow regime. Initially the Separation Effectiveness increases as the liquid hold-up increases within the pipe, until it has reached the point where stable slugs start to form. At this point the Effectiveness Factor then decreases because the slugs will now travel with a higher momentum compared to the previous stratified layer. Thus, the liquid has a much greater chance of leaving the system through the gas-rich streams. Finally, after 180 seconds, the gas flowrate is reduced and again there are immediate and long term responses. The initial response is a sharp increase in the Separation Effectiveness as the system reacts to the change in liquid hold-up along the pipe, corresponding to a period of less intensive slugging as previously discussed. Beyond this short term response the Separation Effectiveness then increases as the liquid slugs travel slower and more liquid will enter the down leg. This can be seen more clearly on the transient trace plot, Figure 7.21, where the fraction of liquid entering the run decreases by approximately a factor of two across the 180 seconds boundary, while the down leg mass flow increases.

A final consideration of the separation performance of the T-junction system can be obtained from reviewing the volumetric composition of the combined gas-rich stream, Figure 7.23. Remember that one of the declared criteria was to ensure that the final gas-rich stream contained less than 10% v/v liquid. Figure 7.23 clearly shows that even when there are significant transient flows through the non-optimised system, the gas-rich stream still operates within the constraints. The volumetric trace particularly highlights the points where the gas flowrate is increased, after 60 and 360 seconds. These are identified as sharp peaks corresponding to an increase in the liquid content produced as a result of the new equilibrium conditions with the gas sweeping away excess liquid out of the system. Indeed, it is one of these surges occurring after 360 seconds that produces a temporary period where the liquid content of the gas stream falls outside the set limits. Overall, the trace displays the expected trends, closely following the variations in the relative phase distribution within each steady-state region and the associated flow pattern, in line with all of the previous discussions.

7.3 Comparisons between Transients in pipes and T-junctions

A further useful step is to compare the transient flows through both the straight pipe and the T-junctions. Three comparisons are presented in Figures 7.24 and 7.25, from the pressure traces and both phase mass flowrates at the outlet, for the flow conditions of Cycle 1.

Figure 7.24 compares the temporal pressure profile for the two configurations. For the T-junction separator the gauge pressure is measured at two different points just prior to both T-junctions. In all cases the pressure traces show exactly the same transient behaviour and even numerically equivalent peaks consistent with the sudden increase in the gas inlet superficial velocity. Thus the presence of the multiple exits streams does not appear to influence the overall pressure distribution within the pipework.

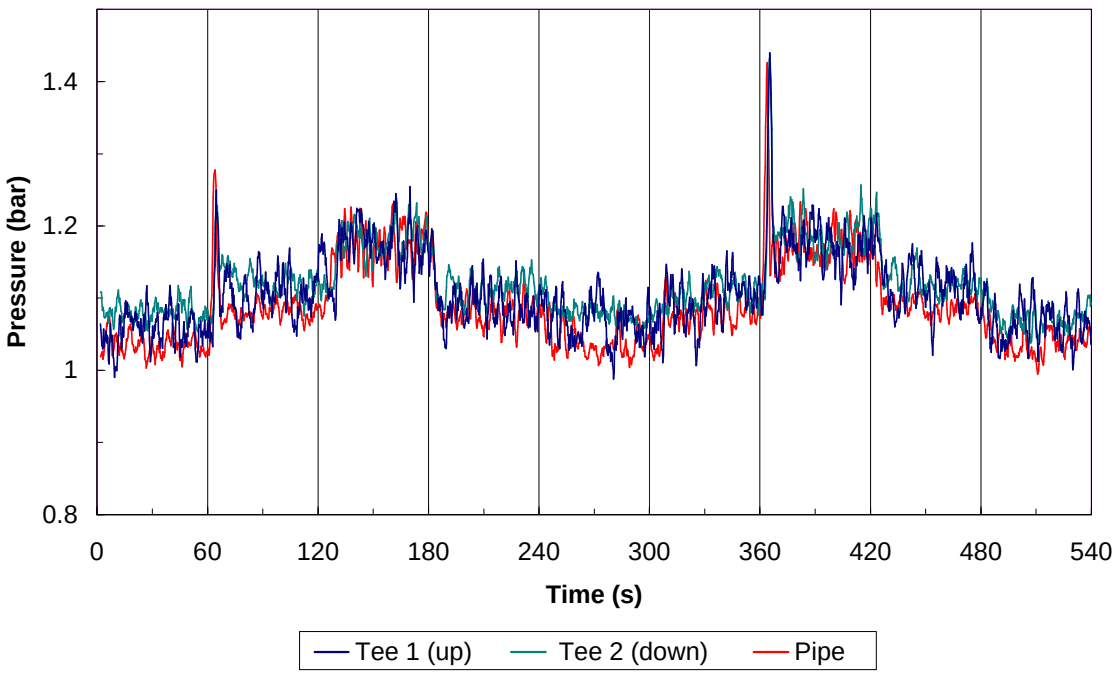

Figure 7.24: Comparisons of the pressure traces for the T-junction separator (at both tees) and the straight pipe

A more interesting comparison can be found in the results of the total flowrates of the gas and liquid phases, Figure 7.25. Remember for the T-junctions the total flowrates are obtained by the sum of the individual outlet streams at that point in time. In the case of the gas flowrate transients the final steady-state values in both cases are essentially equal. The only difference is in the response times of the two cases, where the T-junction gas mass flow is seen to respond faster to the inlet step changes than the straight pipe case. This is particularly highlighted for increases in the gas flow after 60 and 360 seconds. One possible explanation for this quicker response must be that for the T-junction the gas has two potential exit streams, with the first path from the upward T-junction having a shorter travel distance. Since the gas will tend to travel along the path of least resistance it is likely that is will tend to flow along the shortest path, in this case through the up arm. Although it is generally considered that gas transients can be assumed to occur instantaneously the clear difference in these cases identifies that there are some associated delays, related to the flow path length.

The equivalent comparison for the liquid outlet mass flowrates also shows that the two cases follow very similar traces. Comparing the T-junction data with the straight pipe again highlights the large deviations caused by the combined action of the uneven flow split, liquid hold-up in the down leg due of the automatic level control and the different equivalent length of pipe. The increasing transients, in both phases, show very similar outlet responses for both the pipe and the T-junctions, although the sizes of the liquid surges caused by increasing gas flows are smaller for the straight pipe but they do occur and last within same time frame. A more significant deviation is observed for the cases of reductions in the inlet flowrates. For example as the gas superficial velocity is reduced after 180 seconds, both liquid outlet flow traces show the same characteristic reduction has the liquid hold-up in the pipe increases in response. However, the response of the T-junction system occurs over a longer timescale and immediately after the trough the trace shows a definite spike. A response characteristic of the action of the automatic level control system.

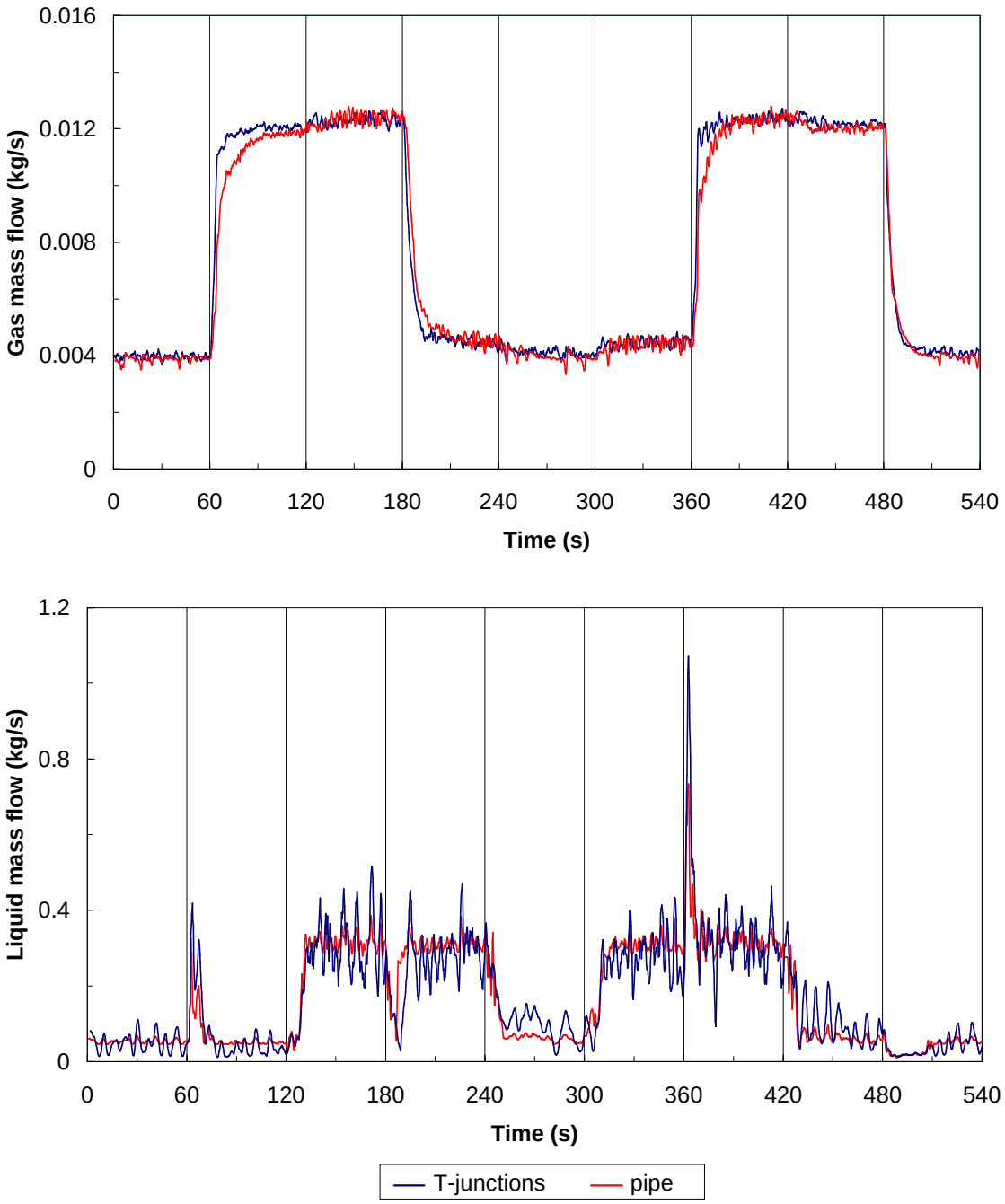

Figure 7.25: Comparisons of the outlet phase mass flowrate traces for the T-junctions and the straight pipe

During the transient period the liquid flowrate at all three outlets will be reduced as the liquid hold-up changes upstream. Thus the liquid flow into the down leg will be

reduced and the control valve will tend to close to try and maintain the level in the down leg, so reducing the out flow. Once the liquid flow increases back to its steady-state value, the flow into the down leg will increase sharply and the valve, again trying to maintain the set point level, will move to a near fully open position. Thus allowing the liquid within the down pipe to be released very quickly, creating the observed sharp peak at that time. This whole process is seen, for Cycle 1, in Figure 7.21, especially the rapid response of the control valve, as it first closes from approximately 80% open to less than 10% open and back to over 90% open within the timescale of the transient. Very much similar mechanisms can be used to describe the other responses for decreasing flowrate transients.

7.3.1 Numerical Comparisons of Transient Flows

It has been shown that the same general transient trends can be observed within every Cycle and that these trends are common to both T-junctions and the pipe flows. The only differences will be in the relative size and timescale of the transient responses, as already observed from the straight pipe analyses of Sections 7.1.5. For example, at the T-junctions a reduction in the maximum steady-state liquid mass flowrate will tend to make the flow regime more stratified in nature. Thus less liquid will tend to exit through the up arm because of the greater vertical distance the liquid needs to be moved to enter the upward branch opening. Likewise as the gas transients are reduced in magnitude there will be reduced changes in the liquid hold-up and smaller mass surges.

A useful way of justifying this concept is to examine the deviation from steady-state of the outlet liquid mass flowrates. Assuming constant inlet mass flowrates and that all the transient changes occur instantaneously, for any time, *t*, the liquid mass flowrate perturbation, $WL^*(t)$, can be calculated using Equation 7.7.

$$WL^*(t) = WL_{exit}(t) - \overline{WL}_1 \qquad [7.7]$$

where, $WL_{exit}(t)$ is the liquid mass flowrate at any time, t, leaving the system (either through the straight pipe or the sum of the three exit streams of the T-junctions) and $\overline{WL_1}$ is the steady-state inlet liquid mass flowrate for each 60 seconds transient period.

This notion is illustrated, for the simple pipe of Cycle 3, in Figure 7.26 with the relevant peaks and troughs associated with the step changes in the inlet gas superficial velocity highlighted. The area under this curve within each step change boundary then gives an indication of the amount of extra liquid swept out of the system as the gas flow increased or the amount of liquid retained in the system as the gas flow is decreased.

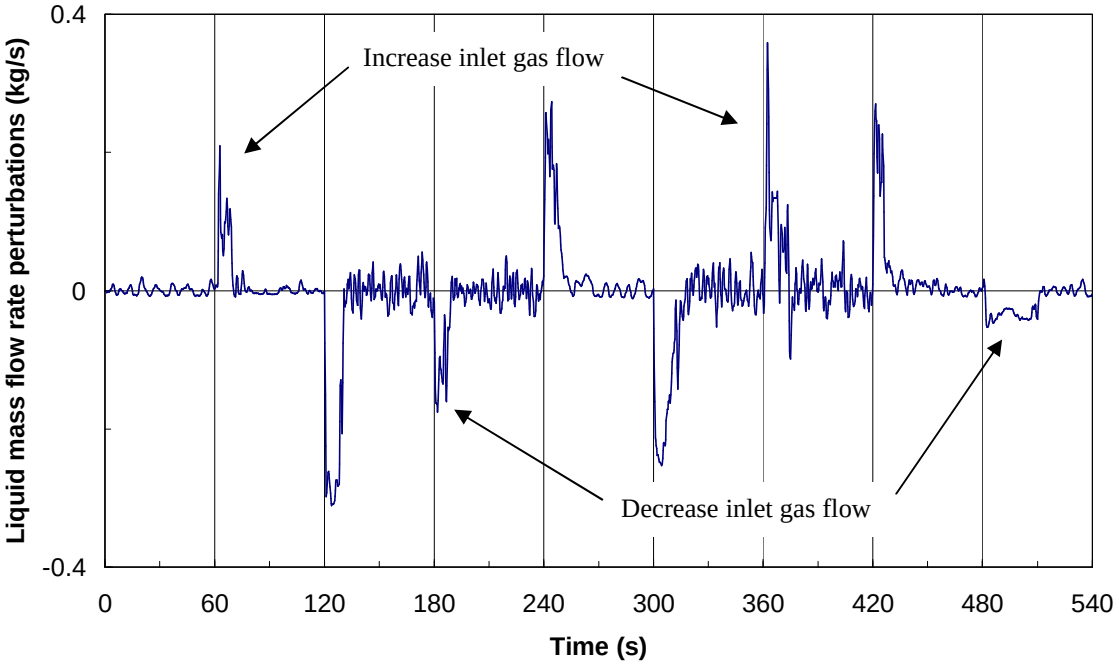

Figure 7.26: Perturbations from the steady-state inlet flowrates of the liquid mass flowrates through the simple pipe for Cycle 3

Applying the same method to all the transient data it is then possible to compare the variations in the liquid mass flowrates through both systems. The mass changes

assumed to be the total area under the curve within a specific time region were calculated using the simple Trapezium rule. The comparisons are shown graphically in Figure 7.27, where the mass changes that occur in the pipe are plotted against the mass changes through the T-junction for corresponding transients in each Cycle.

The general agreement between the two systems is very good. The major difference between the two sets of results is that for the T-junctions the data shows a tendency to have larger mass surges when compared to the straight pipe. This consistent difference can be explained by the action of the level control on the flow through the down leg of the T-junction, since this valve reacts to changes in the liquid height.

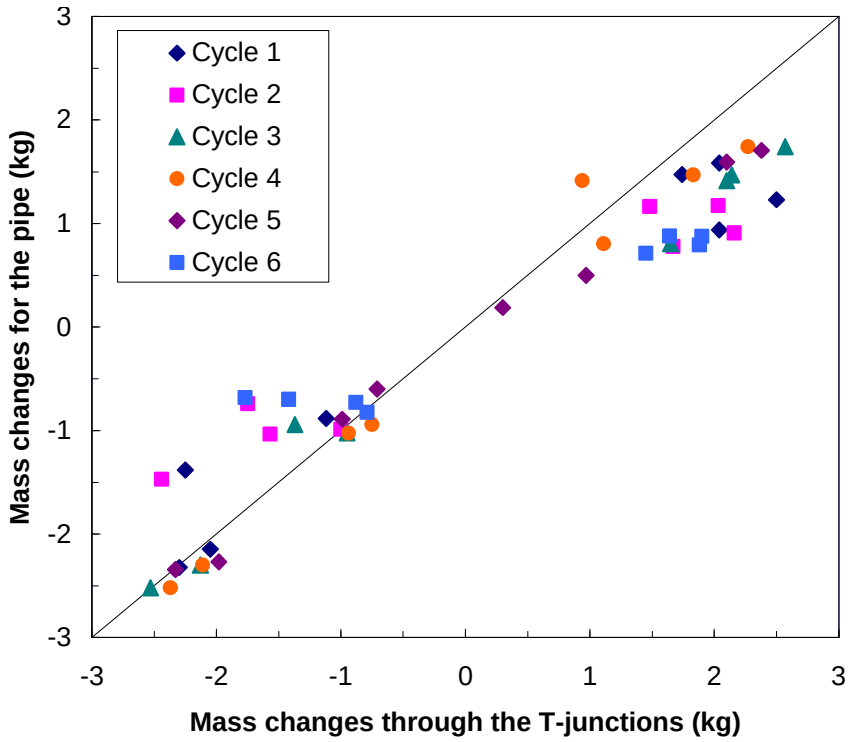

Figure 7.27: Comparison of the changes in the liquid mass for the T-junction and the straight pipe transient data

When the liquid flowrate approaching the junction increases, whether as a result of a step change in the gas or liquid, the level in the down leg will tend to increase rapidly and the valve will act to correct this by opening further, thus allowing extra liquid to flow. On the graph this is represented by more liquid mass leaving the system in the case of the T-junctions when compare to the simple pipe. Conversely, when the liquid flowrate into the down leg is reduced, the liquid level will start to fall more quickly and the control valve will have to close in response, decreasing the liquid mass flow through the exit stream. However, the mass of the liquid hold-up within the down leg becomes significant, especially for stratified flows, and this extra flow of liquid not present within the a straight pipe tends to increase the magnitude of the transient responses when compared to the straight pipe.

7.4 Conclusions

The study of transients flow both through a straight pipe and through the T-junction separator system has been undertaken. It was found that transient flows produce temporary periods of unexpected flow regimes within the pipe. Such occurrences could have a significant impact on downstream equipment and processes.

The transitory responses were most prevalent for changes in the gas inlet superficial velocity, where the system undergoes a rapid, but not instantaneous, global change in the liquid hold-up. During increases in the inlet gas superficial velocity, unexpected periods of intensive slugging were observed, even when the two steady-state flow regimes were both within the stratified region. Conversely, when the gas superficial velocity was decreased the flow experienced quiescent periods, where the outlet liquid flowrate decreased significantly especially when the change occurred within the stratified flow regime. In the simplest sense, a transient is considered to be a change from one steady-state inlet flow conditions to another set of steady-state flow conditions and the existence of transition flow regimes is associated with changes in the liquid hold-up of the system. As the gas flowrate is increased, the liquid hold-up decreases, so the excess liquid is swept out of the system, for the opposite condition

of decreasing gas flowrates, the liquid hold-up increases and the liquid outlet flowrates show a temporary reduction.

For changes in the inlet liquid superficial velocity, no unexpected transition flow regimes were observed. The outlet flowrate responses to changes in the liquid inlet flowrate were seen to exist over a much longer time period than for responses due to changes in the gas inlet flowrates. This is a direct consequence of the extra time required for the relatively slower moving liquid front to propagate along the entire pipe length.

It was seen that neither the magnitude of the liquid transients nor the actual liquid mass flowrate affected the gas outlet mass flowrate responses. Similarly, the relative magnitude of the gas inlet transients did not have an effect on the shape of the liquid outlet responses but only affected the amount of liquid removed or retained in the system. Thus, the relative magnitude of the peaks and troughs observed in the liquid outlet flow were in direct relationship with the relative magnitude of the inlet gas and liquid mass flowrates.

The T-junction system showed composite transient effects very similar to those observed for the straight pipe. With three outlets the flow split of a transient two-phase mixture was observed to be a very non-linear process. The phase split of the transient flow had no relationship to either the steady-state flow split before or after the transient period.

An increase in the gas flowrate is associated with a surge of excess liquid at the outlet and for the T-junction separator this excess liquid swept out by the faster moving gas tends to leave the system through the gas-rich exit stream. Similarly, for a decrease in the inlet gas flowrate, the outlet liquid flowrates diminishes significantly as the liquid hold-up in the upstream pipe increases. Thus, the amount of liquid leaving in the combined gas-rich stream decreases.

The presence of the control valve on the down leg provided an extra transient response effect not present for the straight pipe. Thus, the action of the automatic level control system tended to exaggerate the transient response, leading to larger transient surges than suggested by the simple straight pipe data.

Analysis of the instantaneous liquid hold-up obtained using the electrical capacitance tomography system identified two other useful parameters associated with gas-liquid flows. The first was mean liquid hold-up for the various flow conditions investigated, gained by simple averaging of the collected hold-up data. Such a parameter is very important and is used as an input for many two-phase flow models and calculations. Comparison with the widely applied CISE correlation showed that the predicted liquid hold-up values were always underestimated. A comparison with other experimental, based on similar fluid physical properties and flow conditions, confirmed the validity of the current data and establishes the ECT device as non-invasive method of determining liquid hold-up. This emphasises the danger in simply applying two-phase correlations to specific fluids and flow conditions without confirming its applicability and checking the validity of the predictions.

Further to this, the second parameter that could be implied from the hold-up data was that of slug frequency. Again, comparisons with present slug frequency prediction calculations highlighted the need for further studies to be undertaken. It was observed that the fluid physical properties had a large influence on the minimum mixture velocity at which the minimum slug frequency occurred. Since this quantity is an important starting point for may prediction methods identification of this value must be regarded as a key area for future research.

CHAPTER 8

Conclusions and Further Work

Within the present work the separation and control of gas-liquid flows at T-junctions has been considered within several key areas. The work has extended fundamental studies on the phase split of gas-liquid flows at T-junctions by integrating control valves and flow pattern identification systems to produce a robust partial phase separator. Special consideration was given to the development of active control strategies with the aim of enhancing the phase separation qualities of T-junctions over a range of gas and liquid inlet superficial velocities. Such control schemes were based on achieving predefined separation criteria of less than 10% v/v gas-in-liquid and less than 10% v/v liquid-in-gas.

By attaining such targets, the potential application of T-junctions as partial phase separators has been improved significantly. With the inherently low inventory and compact design, such T-junction separators could be implemented in situations where it is desirable to reduce the presence of highly flammable or toxic material, such as on off-shore oil platforms. This would be the first step within a more intensive phase separation scheme, aimed at reducing the inventory at any one point within the complete separation process.

Pertinent to such possible applications, is knowledge of the responses of the outlet flowrates to step changes in the inlet flow conditions. Thus, by advancing this under

researched area of transient two-phase flow through T-junctions a better understanding of even more complex flow dynamics has been gained.

8.1 Conclusions

The following conclusions can be drawn from the current investigations of the separation and control of gas-liquid flows at horizontal T-junctions:

1. Simulation models can be used to gain insight into the control and operation of a fully horizontal T-junction.

2. The orientation of a single T-junction has a large influence on the phase split. For a vertically upwards side-arm the flow split is seen to be gas dominated, while for a vertically downward T-junction the flow split becomes liquid dominated.

3. Two oppositely orientated vertical side-arm T-junctions placed in series have a better phase separation potential than a single T-junction. This produced the final two T-junction separator system consisted of a vertically upward side-arm T-junction placed upstream of a vertically downward side-arm T-junction. Two phase rich exit streams were formed one rich in gas, by the combination of the final run and up arm, the other rich in liquid, produced by the level control on the down leg.

4. An automatic liquid level control positioned on the down leg of the combined T-junction system, provided a means of preventing gas entrainment within the liquid only exit stream produced by maintaining a constant liquid presence independent of the flow conditions approaching the junction.

5. By manipulation of a control valve placed on the exit run of the combined T-junction system the fraction of liquid recovered in the down leg could be influenced, by varying the liquid hold-up at this second junction.

6. A new Separation Effectiveness Factor was devised to assess the separation performance of the combined T-junction system operated with the automatic level control on the down leg and the run hold-up valve.

7. Based on the Separation Effectiveness data, optimum control valve settings were determined. These were found to be independent of the inlet gas and liquid superficial velocities but depended on only the flow regime. It was found that stratified flows had different phase splitting characterises to slug flows. Thus, for stratified flows the run valve was set at 20% open and for slug flows the run valve was required to be 55% open.

8. Operating the combined T-junction separator at these two optimum settings provided a means of meeting the defined separation performance criteria. The gas stream always contained less than 10% v/v liquid and the liquid rich-stream was gas free.

9. The transient responses of the gas and liquid outlet flowrates were compared for a straight pipe and the T-junction separator. Numerically the agreement was very good. The differences were considered to be the action of the level control system and the related variation in the liquid hold-up within the down leg of the T-junction separator.

10. Increases in the gas inlet superficial velocities were accompanied by periods of excessive slugging for both stratified and slug flows. Decreases in the gas inlet superficial velocities were accompanied by periods of reduced liquid outputs. Both phenomena were fast-acting and associated with changes in the liquid hold-up of the system, either sweeping the excess liquid out or building it up in the pipe. No similar effects were observed for changes in the inlet liquid superficial velocity, as the transients occurred over a much longer timescale and were associated with just traversing steady-state flow pattern transition boundaries.

11. The phase split of transient flows through the T-junction separator was observed to be highly non-linear. Increases in the gas inlet superficial velocities tended to dramatically increase the liquid flow leaving through the up arm. When the liquid inlet superficial velocities were increased the liquid recovery in the down leg increased.

12. The electrical capacitance tomography system successfully measured the instantaneous liquid hold-up in the pipe. The well-known CISE correlation was shown to under predict the liquid hold-up for all cases. Further analysis of this hold-up data allowed the slug frequency to be obtained for a new combination of fluid physical properties, which compared well with data taken for different fluids within similar pipe diameter systems.

8.2 Future Work

From this study of gas-liquid flow separation at horizontal T-junctions significant progress has been made in highlighting the potential application of such systems as partial phase separators. Nevertheless, several further recommendations for future work can be made.

1. In the current study the T-junctions were arranged in series with the vertically downwards side-arm placed downstream of the vertically upwards one. In theory there are a further five simple configurations available for combining two T-junctions in series, dependent on the orientation of the junctions and the sequence in which they are placed. The configuration developed in the present was found to be the optimum choice based on the required separation targets and flow conditions. However, there is a possibility that for different applications with different separation targets and a different range of inlet flowrates that another geometrical configuration may prove more effective. Therefore, it would be interesting to test different configurations to determine a set of selection criteria for a much wider range of flow conditions.

2. A simple control strategy was developed based purely on flow pattern identification and a constant liquid level. One improvement on this would be to use neural networks connected to flow detection sensors as a means to allow the control strategy to learn how to operate valves to maintain effective separation targets. It would be expected that such systems would be better suited to handle inlet transient flows.

3. Although the knowledgebase has been expanded by consideration of more industrial relevant fluids (with different density, viscosity and surface tension properties than the standard air-water systems) further effort could be directed in investigating the effect of temperature and system pressure on the phase split. Furthermore, if there is the desire to implement such T-junction separators within industrial settings then it would be advantageous to gain experimental data on more industrially relevant pipe diameters.

4. Accurately predicting the flow split at T-junctions with vertical side-arms is still an area of weakness. The work on the development of the T-junction simulation model in this study has highlighted the disagreement between more established fully horizontal systems. If the flow split at T-junctions is going to be exploited successfully then much improved modelling and predictive methods need to be developed for the full range of geometries. This would allow more confident and accurate calculations and simulations to be undertaken at the design stage of a process plant.

5. The importance of understanding how transient flows behave through a T-junction has already been highlighted. However, even though the current investigations have made significant contributions to this under researched area it is evident that more rigorous investigations are required to fully assess the complex behaviour. This work examined separately the impact of step changes in the gas and liquid superficial velocities but there are clearly further potential variations, including variations in the inlet pressure or simultaneous step changes in both the inlet phase flowrates, to be considered.

References

Azzopardi, B. J. (1984), "The effect of the side arm diameter on the two-phase flow split at a T-junction", *International Journal of Multiphase Flow*, Vol. 10, No. 4, pp. 509-512.

Azzopardi, B. J. (1988), "Measurements and observations of the split of annular flow at a vertical T-junction", *International Journal of Multiphase Flow*, Vol. 14, No. 6, pp. 701-710.

Azzopardi, B. J. (1993), "T-junctions as phase separators for gas/liquid flows: possibilities and problems", *Transactions of the Institute of Chemical Engineers*, Vol. 71, Part A, pp. 273-281.

Azzopardi, B. J. (1999a), "The effect of side arm diameter on phase split at T-junctions", *SPE Annual Technical Conference and Exhibition*, Houston, Texas.

Azzopardi, B. J. (1999b), "Phase separation at T-junctions", *Multiphase Science and Technology*, Vol. 11, pp. 223-329.

Azzopardi, B. J., Colman, D. A., and Nicholson, D. (2002), "Plant application of a T-junction as a partial phase separator", *Transactions of the Institute of Chemical Engineers*, Vol. 80A, pp. 87-96.

Azzopardi, B. J. and Hervieu, E. (1994), "Phase separation at T-junctions", *Multiphase Science and Technology*, Vol. 8, pp. 645-714.

Azzopardi, B. J. and Memory, S. B. (1989), "The split of two-phase flow at a horizontal T: Annular and stratified flow", *4th International Conference on Multiphase Flow*, Nice, France.

Azzopardi, B. J. and Smith, P. A. (1992), "Two-phase flow split at T-junctions: Effect of side arm orientation and downstream geometry", *International Journal of Multiphase Flow*, Vol. 18, No. 6, pp. 861-875.

Azzopardi, B. J., Wagstaff, D., Patrick, L., Memory, S. B., and Dowling, J. (1988), "The split of two-phase flow at a horizontal T - Annular and stratified flow", UKAEA, Report AERE R 13059.

Baker, O. (1954), "Simultaneous flow of oil and gas", *Oil and Gas Journal*, Vol. 53, pp. 385-389.

Ballyk, J. D., Shoukri, M., and Peng, F. (1991), "The effect of branch size and orientation on two-phase annular flow in T-junctions with horizontal inlet", *International Conference on Multiphase Flows*, Tsukuba, Japan.

Barnea, D., Shoham, O., and Taitel, Y. E. (1980), "Flow pattern characterization for two-phase flow by electrical conductance probe", *International Journal of Multiphase Flow*, Vol. 6, pp. 387-397.

Barnea, D. and Taitel, Y. (1985), "Flow pattern transition in two-phase gas-liquid flows", in the Encyclopaedia of Fluid Mechanics, Gulf Publishing, Houston, Texas, Chapter 16, pp. 403-474.

Bevilacqua, M., Giacchetta, G. and Nielsen, K.L. (2000), "Two-phase liquid-gas separation with a new conception comb separator", *7th International Conference on Multiphase flow in Industrial Plants*, Bologna, 13-15 Sept.

Buell, J. R., Soliman, H. M., and Sims, G. E. (1994), "Two-phase pressure drop and phase distribution at a horizontal T-junction", *International Journal of Multiphase Flow*, Vol. 20, No. 5, pp. 819-836.

Butterworth, D. (1980), "Unresolved problems in heat exchanger design", *Interflow '80 - The Fluid Handling Conference*, Harrogate, England.

Cai, Y., Wambsganss, M. W. and Jendrzejczyk, J. A. (1996), "Application of chaos theory in identification of two-phase flow patterns and transitions in a small, horizontal, rectangular channel", *Journal of Fluids Engineering*, Vol. 118, pp. 383-389.

Clark, W. W. and Baker, G. (2000), "Safety Case: Operation of the multiphase flow controlled phase separation facility with air and kerosene", SChEME Report, University of Nottingham.

Collier, J. G. (1976), "Single-phase and two-phase flow behaviour in primary circuit components", NATO Advanced Study Institute on Two-Phase Flow & Heat Transfer, Report

Dukler, A. and Hubbard, M. (1975), "A model for gas-liquid slug flow in horizontal and near horizontal tubes", *Industrial Chemical Engineering Fundamentals*, Vol. 14, pp. 337-347.

Fouda, A. E. and Rhodes, E. (1974), "Two-phase annular flow stream division in a simple Tee", *Transactions of the Institute of Chemical Engineers*, Vol. 52, pp. 354-360.

Gregory, G. A. and Scott, D. S. (1969), "Correlation of liquid slug velocity and frequency on horizontal cocurrent gas-liquid slug flow", *AIChE Journal*, Vol. 15, No. 6, pp. 933-935.

Grolman, E. and Fortuin, J. M. H. (1996), "Transient gas-liquid flow in upward sloping pipes, approaching the wavy-to-slug flow transition", *Journal of Fluids Engineering: Transactions of the ASME*, Vol. 118, pp. 729-735.

Hart, J., Hamersma, P. J., and Fortuin, J. M. H. (1991), "A model for predicting liquid route preference during gas-liquid flow through horizontal branched pipelines", *Chemical Engineering Science*, Vol. 46, No. 7, pp. 1609-1622.

Hewitt, G. F., Gill, L. E., Roberts, D. N., and Azzopardi, B. J. (1990), "The split of low inlet quality gas/liquid flow at a vertical T-junction", UKAEA, Report AERE M-3801.

Hewitt, G. F. and Roberts, D. N. (1969), "Studies of two-phase flow patterns by simultaneous X-rays and flash photography", UKAEA, Report AERE M-2159.

Heywood, N. I. and Richardson, J. F. (1979), "Slug flow of air-water mixtures in a horizontal pipe: determination of liquid hold-up by gamma-ray absorption", *Chemical Engineering Science*, Vol. 34, pp. 17-30.

Honan, T. J. and Lahey, R. T. (1981), "The measurement of phase separation in wyes and tees", *Nuclear Engineering and Design*, Vol. 64, pp. 93-102.

Hong, K. C. (1978), "Two-phase flow splitting at a pipe tee", *Journal of Petroleum Technology*, Vol. 2, pp. 290-296.

Hoogendoorn, C. J. (1959), "Gas-liquid flow in horizontal pipes", *Chemical Engineering, Science*, Vol. 9, pp. 205-217.

Hubbard, M. G. (1965), "An analysis of horizontal gas-liquid slug flow", *Ph. D. thesis*, University of Houston, Texas, USA.

Hubbard, M. G. and Dukler, A. E. (1966), "The characterisation of flow regimes for horizontal two-phase flow", *Proceedings Heat Transfer and Fluid Mechanics Institute*, Stanford University Press, California.

Hurlburt, E.T. and Newell T.A. (2000), "Prediction of the circumferential film thickness distribution in horizontal annular gas-liquid flow", *ASME Journal of Fluids Engineering*, Vol. 122, pp. 1-7.

Hwang, S. T., Soliman, H. M., and Lahey, R. T. (1988), "Phase separation in dividing two-phase flows", *International Journal of Multiphase Flow*, Vol. 14, No. 4, pp. 439-458.

Isaksen, O. (1996), "A review of reconstruction techniques for capacitance tomography", *Measurement Science and Technology*, Vol. 7, pp. 325-337.

Jeanmeure, L. F. C. (2001), "Electrical capacitance tomography for flow control", *Ph. D.* thesis, University of Manchester Institute of Science and Technology, Manchester, England.

Jeanmeure, L. F. C., Dyakowski, T., Zimmerman, W. B. J. and Baker, G. (2001a), "Use of raw capacitance tomography data for flow pattern control", *2nd World Conference on Process Tomography*, Hanover, Germany.

Jeanmeure, L. F. C., Dyakowski, T., Zimmerman, W. B. J. and Clark, W. (2001b), "Direct flow-pattern identification using electrical capacitance tomography", *4th International Conference on Multiphase Flow*, New Orleans, USA.

Jingbo, X., Xiatie, Y. and Shi, W. (2000), "Flow pattern identification based on fuzzy neural network using multi-electrode capacitance sensor", *15th World Conference on Non-destructive Testing*, Roma, Italy.

Jones, R., Wren, E., Baker, G. and Azzopardi, B. J. (2001), "The split of slug flow at a small diameter horizontal T-junction", *Proceedings of the 5th World Conference on Experimental Heat Transfer, Fluid Mechanics and Thermodynamics*, Thessaloniki, Greece.

Jones, Jr, O. C., and Zuber, N. (1975), "The interrelation between void fraction fluctuations and flow pattern in two-phase flow", *International Journal of Multiphase Flow*, Vol. 2, pp. 273-306.

Katsaounis, A. (1987), "Flow pattern and pressure drop in tees", *Chemical Engineer Communication*, Vol. 54, pp. 119-138.

Katsaounis, A. and Schultheiss, G. F. (1985), "Diverging two-phase flow patterns in a T-junction and their influence on the form-resistance pressure drop", *23rd National Heat Transfer Conference*, Denver, Colorado.

Katsaounis, A., Papanikas, D. G., Fertis, D. K., and Margaris, D. P. (1997), "Dynamic T-junction separator for multiphase transport pipelines", *4th World Conference on Experimental Heat Transfer, Fluid Mechanics and Thermodynamics*, Brussels.

Keska, J. K. and Williams, B. E. (1999), "Experimental comparison of flow pattern detection techniques for air-water flow", *Experimental Thermal and Fluid Science*, Vol. 19, pp. 1-12.

King, M. J. S., Hale, C. P., Lawrence, C. J., and Hewitt, G. F. (1998), "Characteristics of flowrate transients in slug flow", *International Journal of Multiphase Flow*, Vol. 24, pp. 825-854.

Lahey, R. T. (1986), "Current understanding of phase separation mechanisms in branching conduits", *Nuclear Engineering and Design*, Vol. 95, pp. 145-161.

Lin, Z. H. (1986), "Two-phase flow measurements with orifices", in the Encyclopaedia of Fluid Mechanics, Gulf Publishing, Houston, Texas, Vol. 3, Chapter 28, pp 841-862.

Lorenzi, A. and Muzzio, A. (1977), "Two-phase flow rate measurements with sharp-edged orifices", *Journal of Termotechics*, No. 3.

Maciaszek, T. and Memponteil, A. (1986), "Experimental study on phase separation in a T-junction for steam-water stratified inlet flow", *European Two-Phase Flow Group Meeting*, Munich, Germany.

Mandhane., J. M., Gregory, G. A. and Aziz, K. (1974), "A flow pattern map for gas-liquid flow in horizontal pipes", *International Journal of Multiphase Flow*, Vol. 1, pp. 537-553.

Marti, S. and Shoham, O. (1997), "A unified model for stratified-wavy two-phase flow splitting at a reduced T-junction with an inclined branch arm", *International Journal of Multiphase Flow*, Vol. 23, No. 4, pp. 725-748.

McNulty, J. G. (1987), "Fluid property effects of Freon two-phase flow in a horizontal pipeline", *3rd International Conference on Multiphase Flow*, The Hague, Netherlands.

Minami, K. and Shoham, O. (1994), "Transient two-phase flow behaviour in pipelines - experiment and modelling", *International Journal of Multiphase Flow*, Vol. 20, No. 4, pp. 739-752.

Morris, S. (1985), "Two-phase pressure drop across valves and orifice plates", *European Two-phase Flow Group Meeting*, Marchwood Engineering Laboratory, Southampton, UK.

Mudde, R. F., Groen, J. S., and van den Akker, H. E. A. (1993), "Two-phase flow redistribution phenomena in a large diameter T-junction", *International Journal of Multiphase Flow*, Vol. 19, No. 4, pp. 563-573.

Muller, U. and Reimann, J. (1991), "Redistribution of two-phase flow in branching conduits: A survey", *International Conference Multiphase Flows*, Tsukuba, Japan.

Ostrowski, K. L., Luke, S. P., Bennett, M. A., and Williams, R. A. (2000), "Application of capacitance electrical tomography for on-line and off-line analysis of flow pattern on horizontal pipeline of pneumatic conveyor", *Chemical Engineering Journal*, Vol. 77, pp. 43-50.

Ottens, M. (1998), "Gas-liquid flow through pipes and T-junctions", *Ph.D. thesis*, Delft University of Technology, Netherlands.

Ottens, M., de Swart, A., Hoefsloot, H. C. J., and Hamersma, P. J. (1994), "Gas-liquid flow splitting in regular, reduced and impacting T-junctions", *Proceedings of Fluidodinamica Multifase Nell'Impiantistica, Industriale*, Ancona, Italy, pp. 26-37.

Ottens, M., Hoefsloot, H. C. J., and Hamersma, P. J. (1999), "Effect of small branch inclination on gas-liquid flow separation in T-junctions", *AIChE Journal*, Vol. 45, No. 3, pp. 465-474.

Ottens, M., Hoefsloot, H. C. J., and Hamersma, P. J. (2001), "Transient gas-liquid flow in horizontal T-junctions", *Chemical Engineering Science*, Vol. 56, pp. 43-55.

Peng, F. (1994), "A study of dividing steam-water flow in T-junctions: Experiments and analysis", *Ph. D. Thesis*, McMaster University, Ontario, Canada.

Peng, F. and Shoukri, M. (1997), "Modelling of phase redistribution of horizontal annular flow divided in T-junctions", *Canadian Journal of Chemical Engineering*, Vol. 75, pp. 264-270.

Peng, F., Shoukri, M., and Ballyk, J. D. (1998), "An experimental investigation of stratified steam-water flow in T-junctions", *3rd International Conference on Multiphase Flow*, Lyon, France.

Peng, F., Shoukri, M., and Chan, A. M. (1993), "Annular flow in T-junctions with horizontal inlet and downwardly inclined branches", *ASME, Gas Liquid Flows*, Vol. 165, pp. 13-24.

Peng, F., Shoukri, M., and Chan, A. M. C. (1996), "Effect of branch orientation on annular two-phase flow in T-junctions", *Trans ASME: Journal of Fluids Engineering*, Vol. 118, pp. 166-171.

Penmatcha, V. R., Ashton, P. J., and Shoham, O. (1996), "Two-phase stratified flow splitting at a T-junction with an inclined branch arm", *International Journal of Multiphase Flow*, Vol. 22, No. 6, pp. 1105-1122.

Persen, L. N. (1984), "Application of an optical scatterer to the study of two-phase flow in vertical pipes", in *Measuring Techniques in Gas-Liquid Two-Phase Flows*, International Union of Theoretical and Applied Mechanics, Springer, Berlin, pp. 165-173.

Prasser, H. M., Bottger, A., and Zschau, J. (1998), "A new electrode-mesh tomograph for gas-liquid flows", *Flow Measurement and Instrumentation*, Vol. 9, pp. 111-119.

Prasser, H. M., Krepper, E., and Lucas, D. (2001), "Fast wire-mesh sensors for gas-liquid flows and decomposition of gas fraction profiles according to bubble size classes", *5th World Conference on Experimental Heat Transfer, Fluid Mechanics and Thermodynamics*, Thessaloniki, Greece.

Premoli, A., Francesco, D. and Prina, A. (1970), "An empirical correlation for evaluating two-phase mixture density under adiabatic conditions", *European Two-phase Flow Group Meeting*, Milan, Italy.

Priestman, G. H. and Tippetts, J. R. (2000), "Fluidic level control in gas-liquid separators", *Transactions of the Institute of Chemical Engineers*, Vol. 78A, pp. 690-697.

Priestman, G. H. and Tippetts, J. R. (2002), "A compact gas-liquid separator with fluidic control", *3rd North American Conference on Multiphase Technology*, Banff, Canada.

Rea, S. (1998), "Stratified flow at T-junctions", *Ph. D. thesis*, University of Nottingham, Nottingham, England.

Reimann, J., Brinkmann, H. J., and Domanski, R. (1988), "Gas-Liquid flow in dividing T-junctions with a horizontal inlet and different branch orientations and diameters", Kernforschungszentrum Karlsruhe, Institut fur Reaktorbauelemente, Report KfK 4399.

Reinecke, N., Petritsch, G., Boddem, M., and Mewes, D. (1998), "Tomographic imaging of the phase distribution in two-phase slug flow", *International Journal of Multiphase Flow*, Vol. 24, No. 4, pp. 617-634.

Saba, N. and Lahey, R. T. (1984), "The analysis of phase separation phenomena in branching conduits", *International Journal of Multiphase Flow*, Vol. 10, No. 1, pp. 1-20.

Sakaguchi, T., Akagawa, K., Hamaguchi, H., and Ashiwake, N. (1973), "Transient behaviour of air-water two-phase flow in a horizontal tube", *ASME Annual Winter Meeting*, Detroit, Michigan.

Seeger, W., Reimann, J., and Muller, U. (1986), "Two-phase flow in a T-junction with a horizontal inlet. Part I: Phase separation", *International Journal of Multiphase Flow*, Vol. 12, No. 4, pp. 575-585.

Shoham, O., Arirachakaran, S., and Brill, J. P. (1989), "Two-phase flow splitting in a horizontal reduced pipe tee", *Chemical Engineering Science*, Vol. 44, No. 10, pp. 2388-2391.

Shoham, O., Brill, J. P., and Taitel, Y. (1987), "Two-phase flow splitting in a T-junction - experimental and modelling", *Chemical Engineering Science*, Vol. 42, No. 11, pp. 2667-2676.

Sinnott, R. K. (1993), *Chemical Engineering*, Vol.6, Second Edition, Pergamon Press, Oxford.

Smith, A. V. (1975), "Fast response multi-beam x-ray absorption technique for identifying phase distribution during steam water blowdowns", *Journal of British Nuclear Engineering Society*, Vol. 14, No. 3, pp. 227-235.

Smith, P. A. and Azzopardi, B. J. (1990), "The split of two-phase flow at a T-junction with a horizontal main tube and a vertically upward side arm", UKAEA, Report AERE R 13721.

Spedding, P. L. and Nguyen, V. T. (1980), "Regime maps for air-water two-phase flow", *Chemical Engineering Science*, Vol. 35, pp. 779-793.

Taitel, Y. and Barnea, D. (1997), "Simplified transient simulation of two phase flow using quasi-equilibrium momentum balances", *International Journal of Multiphase Flow*, Vol. 23, No. 3, pp. 493-501.

Taitel, Y. and Dukler, A. E. (1976), "A model for predicting flow regime transitions in horizontal and near horizontal gas-liquid flow", *AIChE Journal*, Vol. 22, No. 1, pp. 47-55.

Taitel, Y., Lee, N., and Dukler, A. E. (1978), "Transient gas-liquid flow in horizontal pipes: Modelling the flow pattern transitions", *AIChE Journal*, Vol. 24, No. 5, pp. 920-933.

Taitel, Y., Shoham, O., and Brill, J. P. (1989), "Simplified transient solution and simulation of two phase flow in pipelines", *Chemical Engineering Science*, Vol. 44, pp. 1353-1359.

Van Gorp, C. A., Soliman, H. M., and Sims, G. E. (2001), "The effect of pressure on two-phase flow dividing at a reduced tee junction", *International Journal of Multiphase Flow*, Vol. 27, pp. 571-576.

Walters, L. C., Soliman, H. M., and Sims, G. E. (1998), "Two-phase pressure drop and phase distribution at reduced T-junctions", *International Journal of Multiphase Flow*, Vol. 24, pp. 775-792.

Weisman, J., Duncan, D., Gibson, J. and Crawford, T. (1979), "Effect of fluid properties and pipe diameter on two-phase flow pattern in horizontal lines", *International Journal of Multiphase Flow*, Vol. 5, pp. 437.

Williams, R. A. and Beck, M. S. (Eds) (1995), *Process tomography - principles, techniques and applications*, Butterworth-Heinemann, Oxford.

Wilson, J. A., Azzopardi, B. J. and Baker, G. (2000), "Feasibility study on the control of a T-piece separator", *Conference on Advanced Process Control*, York, England, September.

Wren, E. (2001), "Geometric effects on phase split at a large diameter T-junction", *Ph. D. thesis*, University of Nottingham, Nottingham, England.

Xu, L., Han, Y., Xu, L., and Yang, J. (1997), "Application of ultrasonic tomography to monitoring gas/liquid flow", *Chemical Engineering Science*, Vol. 52, No. 13, pp. 2171-2183.

Zabaras, G. J. (2000), "Prediction of slug frequency for gas/liquid flows", *Society of Petroleum Engineers Journal*, Vol. 5, No. 3, pp. 252-258.

APPENDIX A

Determination of Fluid Physical Properties

This Appendix details the methodology of the determination of the relevant physical properties of kerosene. The physical properties of air were taken directly from literature sources along with the dielectric constant for kerosene. Table A1 details the final physical properties used throughout this study. The physical properties of the fluids will of course be influenced by temperature and, especially for the air, the operating pressure.

Table A1: Physical properties of fluids at 20 °C and atmospheric pressure

	Density (kg/m^3)	**Viscosity (kg/m s)**	**Permittivity Constant[1] (F/m)**	**Surface Tension (N/m)**
Kerosene	797	0.0018	$2.7\varepsilon_0$	0.034
Air	1.207	0.000018	$1.00059\varepsilon_0$	

[1] $\varepsilon_0 = 8.8542\ e^{-12}$ F/m

A.1: Density

The density of the kerosene was obtained by accurately weighing a known volume of liquid, in this case 25 cm^3. A number of measurements were obtained, all at a temperature of 20 °C.

A.2: Viscosity

The viscosity of the kerosene was obtained through the use of a dial viscometer (Brookfield, Model-LVT). Again a number of measurements were obtained at a constant temperature of 20 °C and the final value was taken to be the mean.

A.3: Surface Tension

The surface tension of the kerosene was acquired with the use of the torsion balance (White Electrical Instrument Co. Ltd, Model-OS). A number of readings were obtained and the mean value taken at a constant temperature of 20 °C.

APPENDIX B

Error Analysis

This Appendix summarises the Error Analysis performed on the experimental data. Measurements for the phase split data were only noted when the errors in the mass balances were less than ±5%. Errors in all cases were kept to a minimum by the data acquisition system used. For a typical experimental run, the minimum time for a measurement period was 120 seconds. Since the data acquisition software records at a frequency of 4 Hz, this gave a minimum of 480 individual data samples. The final steady-state values were thus obtained from the mean of this entire data set.

Given below is an example of an error analysis calculation performed on a randomly selected phase split result, using the principals outlined by Taylor (1997). For this case, the inlet gas superficial velocity, U_{gs}, was 5.1 m/s and the inlet liquid superficial velocity, U_{ls}, was 0.40 m/s.

Error Analysis on the Air Mass Balance

The air mass flowrates were obtained from measuring the differential pressure across an orifice plate. All these orifice plates were machined to the dimension detailed in BS1042 and operated within the stated guidelines.

Inlet air flowrate:

A digital manometer was used to measure the inlet air flowrate differential pressure across the orifice plate. The uncertainty in the reading was known to be ±0.5 mmH_20.

For the inlet flow, the average manometer reading was 96±0.5 mmH_2O, this corresponds to an inlet mass flowrate of 0.00825±0.0001 kg/s.

Outlet air flowrate:

The data acquisition system was used to record the differential pressure across an orifice plate for all three outlet air mass flowrates continuously taking 4 readings per second. The data acquisition system has a known accuracy of, at worst, ±0.01% of the maximum measurable voltage span.

For the Up arm:

The maximum measurable voltage span is set at 2 V (recording ±1 V). Thus, the measured voltage uncertainty equals ±0.002 V.

Therefore, the average mass flow reading was 0.00791±0.00002 kg/s

For the Run:

The maximum measurable voltage span was set at 66 mV (recording ±33 mV). Thus, the uncertainty in the measured voltage equals -0.0504±0.0066mV.

Therefore, the average mass flow reading was 0.00035±0.00001 kg/s

Overall mass balance:

The combined uncertainty in the measured air outlet = $\pm\sqrt{e_1^2 + e_2^2}$ = ±0.000022 kg/s

Thus, the overall measured outlet air balance is 0.00826±0.000022 kg/s compared to the inlet air mass flowrate of 0.00825±0.0001 kg/s.

The maximum error in the mass balance then becomes:

$$Err_{MAX} = \frac{WG_1}{WG_5} - 1 = \frac{0.00825 - 0.0001}{0.00826 + 0.000022} - 1 = -1.59\% \qquad [B.1]$$

This is within the acceptable mass balance limit of ±5%.

Any errors are significantly reduced by the averaging of the larger (480 individual readings per exit stream) data set. Figure B.1 shows the steady-state air outlet mass flowrates for the flow conditions under consideration. The traces show the consistent measurements obtained from the data acquisition system.

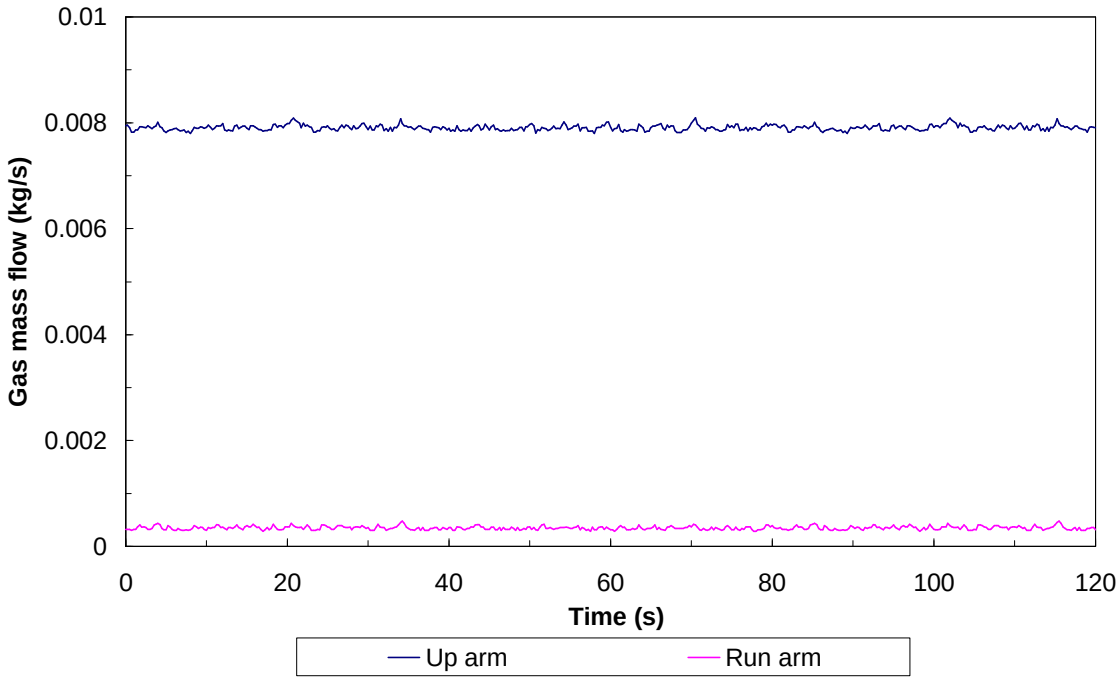

Figure B.1: Traces for steady-state measurement of gas exit streams

Error Analysis on the Kerosene Mass Balance

Inlet kerosene flowrate:

The kerosene inlet mass flowrate is metered using a differential pressure transducer with a calibrated digital scale (0-1500). The uncertainty in the reading was ±5% of the scale reading.

For the inlet kerosene flow the scale reading was 700±35, this corresponds to a liquid mass flowrate of 0.3549±0.008 kg/s.

Outlet kerosene flowrate:

As for the differential pressure transducers used for the air orifice plate pressure drop measurements the liquid level in each separation tank is recorded continuously at 4 readings per second. Since the time is digitally recorded by the software using the internal clock of the PC it is assumed to be exact, i.e. the error is zero.

Figure B.2 shows the variation of the liquid level for each separation tank over the measurement period. The gradients of the representative linear functions are equivalent to the change in liquid height over time. Since the cross-sectional area of each tank is constant along the full height, the mass flowrate through each exit dream is given by:

$$WL_i = A_{Ti}\, r_L \frac{\Delta H_{Ti}}{\Delta t} \qquad [B.2]$$

where, WL (kg/s) is the liquid mass flow, A_T (m^2) is he cross-sectional area of a tank, r_L (kg/m^3) is the liquid density, *DH/Dt* (m/s) is the gradient of the linear function and i indicates the stream number, up (3), run (4) or down (5).

The correlation coefficient (R^2) indicates the percentage certainty in the linear function for each exit.

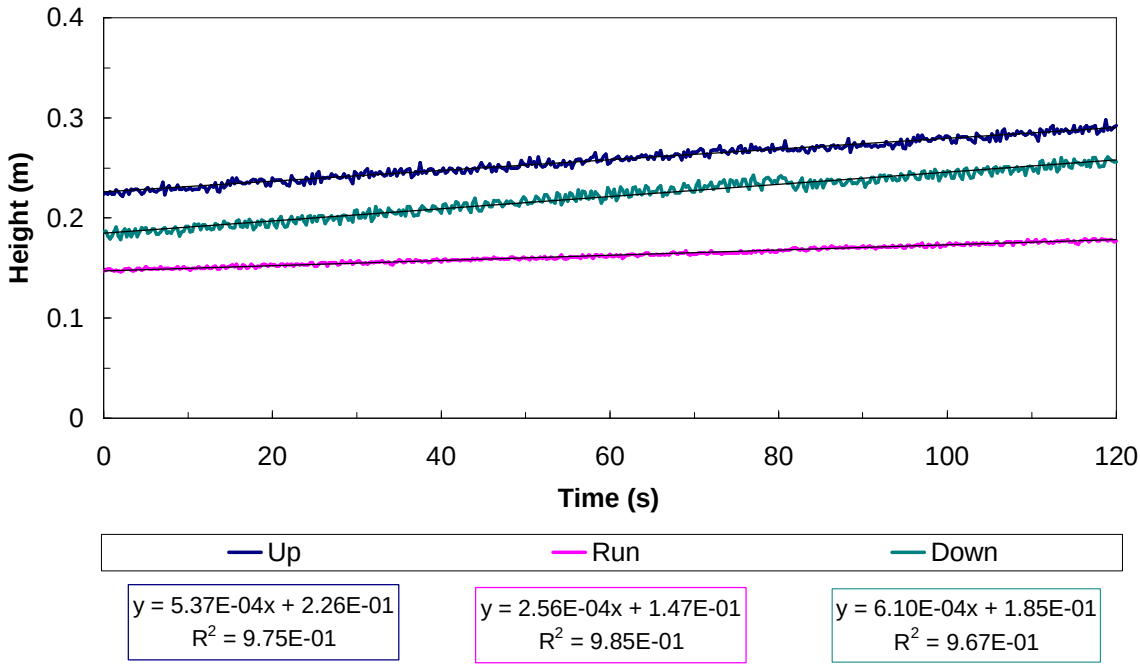

Figure B.2: Variation of the liquid level in each separation tank and the representative linear functions

For the Up arm:

Equation B.2 implies a liquid mass flowrate through the Up arm of 0.1053 kg/s. The uncertainty in this flowrate is ±2.5% of 0.1053 kg/s, or ±0.0026 kg/s.

For the Run:

Equation B.2 implies a liquid mass flowrate through the Run of 0.1278 kg/s. The uncertainty in this flowrate is ±1.5% of 0.1278 kg/s, or ±0.0019 kg/s.

For the Down arm:

Equation B.2 implies a liquid mass flowrate through the Up arm of 0.1196 kg/s. The uncertainty in this flowrate is ±3.3% of 0.1196 kg/s, or ±0.0039 kg/s.

Overall mass balance:

Thus, the overall measured liquid mass balance is 0.3527±0.0051 kg/s compared to the inlet liquid mass flowrate of 0.3549±0.008 kg/s.

The maximum error in the mass balance then becomes:

$$Err_{MAX} = \frac{WL_1}{WL_5} - 1 = \frac{0.3549 + 0.008}{0.3527 - 0.0051} - 1 = 4.40\% \qquad [B.3]$$

This is within the acceptable limit of ±5%.

References

Taylor, J. R. (1997), *An Introduction to Error Analysis. The Study of Uncertainties in Physical Measurements*, Second Edition, University Science Books, Sausalitio, California, USA.

APPENDIX C

Development of T-junction Simulation Model

This Appendix details the formulation of the T-junction simulation model as applied in Chapter 4.

Consider the case of a fully horizontal regular T-junction with a control valve positioned on both exit streams. Figure C.1 shows a schematic of the junction along with the key parameters to be considered.

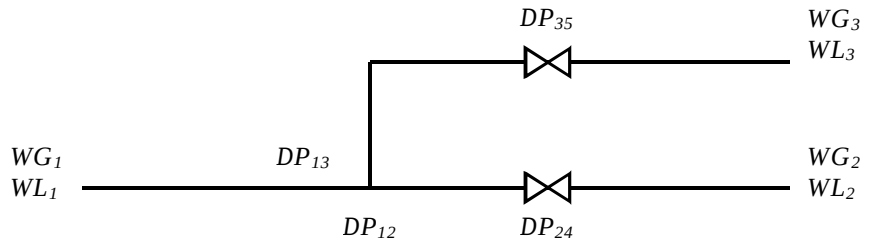

Figure C.1: Schematic diagram of a horizontal T-junction with control valves on exit streams

The mass flowrates (kg/s) of the gas, of density r_G (kg/m^3) and liquid, of density r_L (kg/m^3) are represented by WG_i and WL_i, respectively, where i indicates the stream

under consideration, the inlet (1), run (2) or side-arm (3). There are two pressure drops (N/m^2) associated with the T-junction; inlet-to-run, DP_{12}, and inlet-to-side-arm, DP_{13}. Finally there are two further pressure drops (N/m^2) associated with the control valves, DP_{24}, for the run, and DP_{35}, for the side-arm.

Assuming the pressure drops associated with the flow through the pipes and around the bends are negligible there are four distinct pressure drops that need to be described within this simple model. The first pair relate to the T-junction whilst the second pair are associated with the control valves.

Run pressure drop (DP_{12})

For the run pressure drop the use of a momentum balance approach has been suggested by several authors including, Saba and Lahey (1984), Hwang *et al.* (1988) and Reimann *et al.* (1988). So for separated flows, which is a good assumption for both stratified and annular flow regimes, the pressure drop can be described as:

$$\Delta P_{12} = k_{12}^{*}\left[\frac{\dot{m}_2^2}{r_{m2}} - \frac{\dot{m}_1^2}{r_{m1}}\right] \qquad [C.1]$$

where k_{12}^{*}, the momentum correction factor, determined from single-phase data, is assumed to be unity, $\dot{m}_i$ is the total mass flux (kg/m^2 s) and r_{mi} is the momentum density (kg/m^3) which are defined by Equations C.2 and C.3, respectively.

$$\dot{m}_i = \frac{WG_i + WL_i}{A_i} \qquad [C.2]$$

$$r_{mi} = \left[\frac{x_i^2}{e_{Gi}\, r_G} + \frac{(1-x_i)^2}{(1-e_{Gi})\, r_L}\right]^{-1} \qquad [C.3]$$

where x_i is the quality (the fraction of the total flow that is gas) and e_{Gi} is the void fraction (the fraction of space occupied by the gas) of the streams, defined by Equations C.4 and C.5, respectively.

$$x_i = \frac{WG_i}{WG_i + WL_i} \qquad [C.4]$$

$$e_{Gi} = \left[1 + U_R \frac{(1 - x_i)}{x_i} \frac{r_G}{r_L}\right]^{-1} \qquad [C.5]$$

Here U_R (m/s) is the slip ratio, which attempts to allow for the fact that the mean gas and liquid velocities are unequal. One simple equation for this ratio, proposed by Chisholm (1972), is given in Equation C.6.

$$U_R = \left[1 - x_i\left(1 - \frac{r_L}{r_G}\right)\right]^{1/2} \qquad [C.6]$$

Side arm pressure drop (DP_{13})

The simplest available equation for the side arm pressure drop uses the homogeneous model, based on the approach of Gardel (1957):

$$\Delta P_{13} = (\Delta P_{13})_{rev} + k_{13} \frac{\dot{m}_1}{2 r_L} f^2 \qquad [C.7]$$

where f^2 is the side arm two-phase loss multiplier, defined in Equation C.10. Assuming the flow into the side-arm can be considered to be homogeneous, based on the mixing that is induced as the fluids travel around the sharp bend, the reversible pressure difference is then given by Equation C.8.

$$\left(\Delta P_{13}\right)_{rev} = \frac{r_{h3}}{2}\left[\left(\frac{\dot{m}_3}{r_{h3}}\right)^2 - \left(\frac{\dot{m}_1}{r_{h1}}\right)^2\right] \qquad [C.8]$$

where the homogeneous density (kg/s), r_{hi}, is defined in Equation C.9.

$$r_{hi} = \left(\frac{x_i}{r_G} + \frac{1-x_i}{r_L}\right)^{-1} \qquad [C.9]$$

Hence, the two-phase multiplier becomes:

$$f^2 = \frac{r_L}{r_{h1}} \qquad [C.10]$$

The remaining term in Equation C.7 to evaluate is then the loss coefficient, k_{13}. Several authors have considered the evaluation of this term for regular (equal-diameter), square-edged T-junctions in terms of a quadratic equation in the form of Equation C.11.

$$k_{13} = A + BW_{31} + C^2W_{31} \qquad [C.11]$$

where, W_{31} is the mass flow ratio of gas and liquid diverted into the side-arm, given by Equation C.12.

$$W_{31} = \frac{WG_3 + WL_3}{WG_1 + WL_1} \qquad [C.12]$$

Different authors have suggested various, but very similar, values for the coefficients *A*, *B* and *C*. A selection of these are summarised in Table C.1. For this simple model approximate average values were assumed as $A = 1$, $B = -0.8$ and $C = 1$.

Table C.1: Constants for the loss coefficient equation for side-arm pressure drop for a regular sharp-edged T-junction

Source	A	B	C
Reimann and Seeger (1986)	1.0369	-0.9546	1.2123
Ballyk *et al.* (1988)	1.081	-0.914	1.05
Hwang and Lahey (1988)	1.0	-0.8285	0.6924

Equations C.1 and C.7 together with their ancillary equations form a complete description of the pressure drops around the junction. The final two pressure drops to be calculated are those associated with the control valves.

Control valve pressure drops (DP_{24}, DP_{35})

For the control valves a loss coefficient approach is used. So, for any valve the pressure drop can be represented by Equation C.13.

$$\Delta P_{ij} = \frac{k_{ij}\dot{m}_i^2 f_{Li}^2}{2r_L} \qquad [C.13]$$

where k_{ij} is the characteristics pressure loss coefficient for the valves and f^2_{Li} is the two-phase multiplier. For globe valves, as used here, ESDU (1989) recommended the equation proposed by Morris (1985) as defined in Equation C.14.

$$f_L^2 = \left[x_i \frac{r_L}{r_G} + K(1-x_i)\right]\left[x_i + \frac{(1-x_i)}{K}\left(1+\frac{(K-1)^2}{(r_L/r_G)-1}\right)\right] \qquad [C.14]$$

where K is a simple function of the phase density and quality as defined in Equation C.15.

$$K = \left[1 + x\left(\frac{r_L}{r_G} - 1\right)\right]^{1/2} \qquad [C.15]$$

For consistency the valve characteristic pressure loss coefficients, k_{ij}, were selected to be equivalent to the control valves on the experimental facility, as given in Appendix D. Thus, the quoted valve characteristics values (*Cv*) need to be converted into pressure loss coefficients. Equation C.13 can be rearranged in terms of a pseudo inlet velocity, *u*, as shown in Equation C.16.

$$u = \sqrt{\frac{2}{k_{ij} f}} \sqrt{\frac{\Delta P_{ij}}{r_L}} \qquad [C.16]$$

Multiplying Equation C.16 by the cross-sectional area of the pipe, *A*, and noting that the valve coefficient data is based on water, thus r_L = 1000 and f = 1, Equation C.17 is obtained.

$$Cv = uA = A\sqrt{\frac{2}{k_{ij}}} \sqrt{\frac{\Delta P_{ij}}{1000}} \qquad [C.17]$$

The valve data is calculated with pressure in the units of psi and flowrate in USgpm, (1 m^3/s is equivalent to 1.595×10^4 USgpm). So, assuming a maximum pressure drop of 1 bar across the control valves the final relationship between the pressure loss coefficient, k_{ij}, and *Cv* would be then given by Equation C.18.

$$k_{ij} = \frac{4513.85}{Cv^2} \qquad [C.18]$$

Thus, all the pressure drops can now be numerically defined for any specific valve setting.

Description of the Phase Split

Describing the pressure drops defines only half of the simulation model. The remaining information comes from knowledge of the gas-liquid flow split at the T-junction. There have been many models published for stratified (Shoham *et al.*, 1987, Hwang *et al.*, 1988, Hart *et al.*, 1991, Penmatcha *et al.*, 1996) and annular (Shoham *et al.*, 1987, Hwang *et al.*, 1988, Azzopardi *et al.*, 1988) flows dividing at a horizontal T-junction.

The initial choice was the well established prediction method of Shoham *et al.* (1987), who considered both stratified and annular flows arriving at the junction. Their model is based on the assumption of the presence of a dividing vertical streamline separating the flow that gets diverted into the side-arm from the flow that continues along the run. Hence, all the streamlines within the cross-sectional area bounded by this dividing line and the pipe wall get diverted into the branch, whilst those outside this area continue into the run. Simple geometrical descriptions modified to include centripetal forces acting on the liquid phase are then used to calculate the phase split. Further details, of course, can be found in the relevant reference.

The phase split data was implemented into the model by pre-calculating the mass flow split and associated side-arm quality over the full range of inlet gas and liquid flowrates, at regularly spaced intervals, and then interpolating the resultant data set into a regular matrix. This approach minimised the number of intermediate steps required during each calculation step of the simulation, reducing the computational overhead time required to solve the complex two-phase flow split models. This approach also added greater flexibility to the simulation, since the flow split data used for the interpolation could be changed easily without any additional changes to the main computer code.

Solution of Simulation Model

For both the main steady-state and the dynamic simulations the complete set of defining equations were then coded into Matlab®. The *fminsearch* function is then used to find the minimum of the *total pressure drop function*. This built-in Matlab command referred to as an unconstrained nonlinear optimization, starts with an initial estimate and finds the minimum of a scalar function consisting of several variables. A complete solution methodology is presented below for both cases, however, since the *total pressure drop function* is such an important common element it is explained separately.

Total pressure drop function

The *total pressure drop function* is the key element within the simulation model. It combines all the previously defined equations to provide a description of the pressure losses around the system. Remember that this function is minimised, using the *fminsearch* command, from within the steady-state and dynamic simulations for every calculation step. Below is a summary of the inputs and calculation steps and required to fully describe the pressure losses. (NB: Only the key equations are given for each pressure drop calculation, the requirement to use any required supplementary equations as described in the relevant sections above is explicitly implied.)

Step 1: Define gas and liquid densities and pipe cross-sectional area.

Step 2: Take constant inlet quality, x_1, and initial guesses for total inlet mass flowrate, W_1, and flow split, W_{31}, passed from steady-state/dynamic code and valve loss coefficients k_{24} and k_{35}.

Step 3: Calculate individual inlet gas and liquid mass flowrates and total mass flowrate in side-arm.

Step 4: Interpolate two-phase flow split model data to find side-arm quality.

Step 5: Calculate individual gas and liquid mass flowrates through the run and side-arm and run quality.

Step 6: Calculate run pressure drop, DP_{12}, using Equation C.1.

Step 7: Calculate side-arm pressure drop, DP_{13}, using Equation C.7.

Step 9: Calculate run and side-arm valves pressure drops, DP_{24}, DP_{35}, using Equation C.13.

Step 10: Determine *total pressure drop function*, DP_{total}, as:

$$\Delta P_{total} = \left(\Delta P_{12} + \Delta P_{24}\right)_{run} + \left(\Delta P_{13} + \Delta P_{35}\right)_{side-arm}$$

Step 11: For *fminsearch* the calculations repeat from Step 3 adjusting total mass flowrate, W_1, and flow split, W_{31}, as required but maintaining constant inlet quality, x_1.

Step 12: Output minimised values of total mass flowrate, W_1, and flow split, W_{31} (and side-arm quality, x_3, for dynamic simulation).

Steady-state case

The steady-state simulation utilises a simple loop procedure that steps through the calculations for the full range of valve setting combinations. There are essentially nine steps that are detailed below:

Step 1: Define constant inlet quality, x_1.

Step 2: Set nominal inlet total mass flowrate, W_1, and flow split, W_{31} (Equation C.12) as first guess to the solution.

Step 3: Set run valve fully open and determine k_{24} from known *Cv* data.

Step 4: Set side-arm valve fully open and determine k_{35} from known *Cv* data.

Step 5: Use *fminsearch* command to minimise the *total pressure drop function* by manipulating total inlet mass flowrate, W_1 and flow split, W_{31}, with constant inlet quality, x_1, and valve loss coefficients, k_{24} and k_{35}.

Step 6: Record output results based on new flow split, W_{31}, and valve settings:

(a) flow split, W_{31}
(b) total mass throughput, W_1
(c) Separation Factor, S_F, (defined in Equation 4.1)
(d) fraction of gas in side-arm
(e) fraction of liquid in run
(f) side-arm quality
(g) run quality

Step 7: Incrementally decrease the side-arm valve setting, recalculate k_{35} and repeat from Step 5, using previous W_1 and W_{31} as new first guess.

Step 8: Incrementally decrease the run valve setting, recalculate k_{24} and repeat from Step 4, using previous W_1 and W_{31} as new first guess.

Step 9: When total range of valve settings has been achieved stop.

Dynamic case

For the dynamic simulation, which was undertaken as a nominal exercise to investigate the valve interaction highlighted by the Relative Gain Array analysis, further information is required. Such analyses indicate that the best combinations are to control the total throughput by adjustment of the side-arm valve, with the side-arm quality then being controlled by the run valve. A conventional Single-Input-Single-Output control strategy is proposed coupled with two tomographic sensors, one measuring the feed conditions and controlling the side-arm valve and the other measuring the side-arm quality and controlling the run valve.

Dynamic effects are more difficult to quantify because of the effects of deadtime between the upstream measurement and application of action on the control valve. It is also likely that movement of the valves themselves will introduce other transient effects. It was felt unnecessary and impractical to attempt to allow for such unknown dynamic effects at this early stage. Thus, the dynamic model results presented in Chapter 4, Figure 4.9, considers only the dynamics attaching to the control valves themselves and time constants of 2 seconds have been assigned to the valve dynamics. This combined with the need for flow control implies the use of PI action as the underlying strategy. Since the desire here was just to explore the possibilities of valve interaction it was not thought necessary to fine tune these controllers at this time, although such a notion would be, of course, feasible. Simple tests highlighted suitable, but not necessarily perfect, PI values for the two control valves and these are presented in Table C.2 along with the selected set points.

Table C.2: Control valve PI values for the dynamic simulation

Valve	P	I	Set points
Run	2	0.25	$x_3 = 0.6$
Side-arm	-1	2	$W_1 = 0.07$

For any control system there needs to be a measure of the error between the set point and the actual measured value as defined in Equation C.19.

$$err_f(k) = f_{sp}(k) - f_{act}(k) \qquad [C.19]$$

where, err_f is the error, f_{sp} is the set point and f_{act} is the actual measured parameter at the current time period sample, *k*.

In a PI control strategy the response of the controller to the error is governed by Equation C.20.

$$X(k) = P\left[(err_f(k) - err_f(k-1) + \frac{err_f(k)T}{I}\right] + X(k-1) \qquad [C.20]$$

where *X(k)* is the calculated response at time period *k*, *P* is the Gain, *I* is the integral action, *T* is the discrete time sample period, $err_f(k)$ is the current measured error at time *k*, $err_f(k-1)$ is the last measured error within the previous time period, *(k-1)* and *X(k-1)* is the last calculated response.

As previously stated it must be remembered that the *total pressure drop function* is a common element that is still solved using the *fminsearch* function of Matlab. Like the steady-state case there are a number of steps that define the dynamic simulation procedure and these are outlined below:

Step 1: Define constant inlet quality, x_1.

Step 2: Define discrete time period, number of iterations/timescale and initial settings for the valves, Xv_{24} and Xv_{35}.

Step 3: Define control valve time constants, PI values and set points.

Step 4: Take initial guess for total mass flowrate, W_1, and flow split, W_{31}.

Step 5: Calculate valve loss coefficients, k_{24} and k_{35}, based on valve fraction open settings, Xv_{24} and Xv_{35}.

Step 6: Use *fminsearch* command to minimise the *total pressure drop function* by manipulating total inlet mass flowrate, W_1 and flow split, W_{31}, with constant inlet quality, x_1, and valve loss coefficients, k_{24} and k_{35}.

Step 7: Record output results based on new flow split, W_{31}, and valve settings:

(a) total mass throughput, W_1

(b) side-arm quality, x_3

Step 8: At set time period make the required change in conditions (For example, in Figure 4.9 the inlet quality is increased 1.5 times after 3 time periods and then decreased back to its original value after 50 time periods).

Step 9: Calculate current error from the set points, Equation C.19, and new valve settings, Xv_{24} and Xv_{35}, Equation C.20, remembering to allow for time constants.

Step 10: Use *fminsearch* command to minimise the *total pressure drop function* by manipulating total inlet mass flowrate, W_1 and flow split, W_{31}, with constant inlet quality, x_1, and new valve loss coefficients, k_{24} and k_{35}. Repeat from Step 7 for declared number of time periods.

Step 11: When time period is exceeded stop.

References

Azzopardi, B. J., Wagstaff, D., Patrick, L., Memory, S. B., and Dowling, J. (1988), "The split of two-phase flow at a horizontal T - Annular and stratified flow", UKAEA, Report AERE R 13059.

Ballyk, J.D., Shoukri, M. and Chan, A.M.C. (1988), "Steam-water annular flow in a horizontal dividing T-junction", *International Journal of Multiphase Flow*, Vol. 14, pp 265-285.

Chisholm, D. (1972), "An equation for velocity ratio in two-phase flow", N.E.L., Report No. 535.

Engineering Science Data Unit (ESDU) (1989), "Two-phase flow pressure losses in pipeline fittings", ESDU Item No. 89012.

Hart, J., Hamersma, P. J., and Fortuin, J. M. H. (1991), "A model for predicting liquid route preference during gas-liquid flow through horizontal branched pipelines", *Chemical Engineering Science*, Vol. 46, No. 7, pp. 1609-1622.

Hwang, S.T. and Lahey, R.T. (1988), "A study on single- and Two-phase pressure drop in branching conduits", *Experimental Thermal and Fluid Science*, Vol. 1, pp 111-125.

Hwang, S.T., Soliman, H.M. and Lahey, R.T. (1988), "Phase separation in dividing two-phase flow", *International Journal of Multiphase Flow*, Vol. 14, pp 439-458.

Morris, S. (1985), "Two-phase pressure drop across valves and orifice plates", *European Two-phase Flow Group Meeting*, Marchwood Engineering Laboratory, Southampton, UK.

Penmatcha, V.R., Ashton, P.J. and Shoham, O. (1996), "Two-phase stratified flow splitting at a T-junction with an inclined branch arm", *International Journal of Multiphase Flow*, Vol. 22, pp 1105-1122.

Reimann, J. and Seeger, W. (1986), "Two-phase flow in a T-junction with a horizontal inlet - Part II: pressure differences", *International Journal of Multiphase Flow*, Vol. 12, pp 587-608.

Reimann, J., Brinkmann, H. J., and Domanski, R. (1988), "Gas-Liquid flow in dividing T-junctions with a horizontal inlet and different branch orientations and diameters", Kernforschungszentrum Karlsruhe, Institut fur Reaktorbauelemente, Report KfK 4399.

Saba, N. and Lahey, R.T. (1984), "The analysis of phase separation phenomena in branched conduits", *International Journal of Multiphase Flow*, Vol. 10, pp 1-20.

Shoham, O., Brill, J.P. and Taitel, Y. (1987), "Two-phase flow splitting in a Tee junction – experiment and modelling", *Chemical Engineering Science.*, Vol. 42, pp 2667-2676.

APPENDIX D

Automatic Control System

This Appendix gives details of the control system, in terms of the control valve characteristics and the software implementation of control settings, as well as specific details about the simple optimisation performed on the automatic level control used in the down leg of the T-junction separator.

Control Valve

The control valves, (Baumann, linear, Model 24688) use a pneumatic actuator with an electrical input signal of 4-20 mA d.c. set by the control PC. The maximum rated flow coefficient was 4.00 and the complete characteristic curve for the valves is given in Figure D.1.

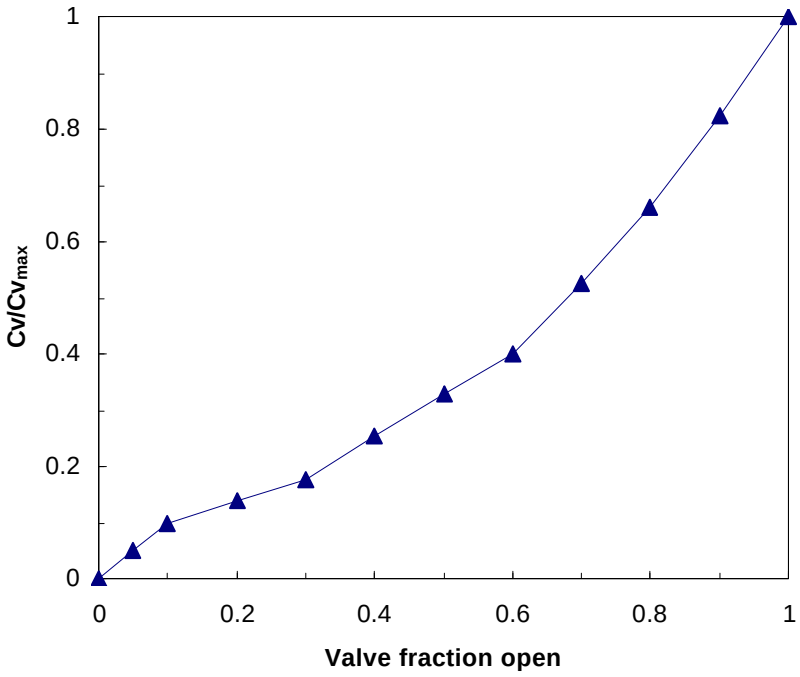

Figure D.1: Characteristics curve for the control valves (Baumann Model 24688, manufacturer's data)

Control Software

As detailed in Chapter 3, the control PC operated commercial data acquisition software, VisiDAQ®. This allowed instant access and modification to the liquid level set-point, the number of movements the valve could make per minute and the value of the proportional gain. Figure D.2 shows the screen visualisation of the T-junction facility used by the VisiDAQ software. The software allowed online manipulation of the control valves settings as well as the actuated cocks on the separation and measurement tanks and inlet transient feed lines. It also displayed the flowrates and pressures at all relevant points on the facility and indicated the liquid levels within all three separation tanks. Figure D.3 shows the interactive control box that allowed the *PID* settings for the automatic control valve to be manipulated. Remember for this case only the Gain Factor, *P*, needs to be used in a level control system.

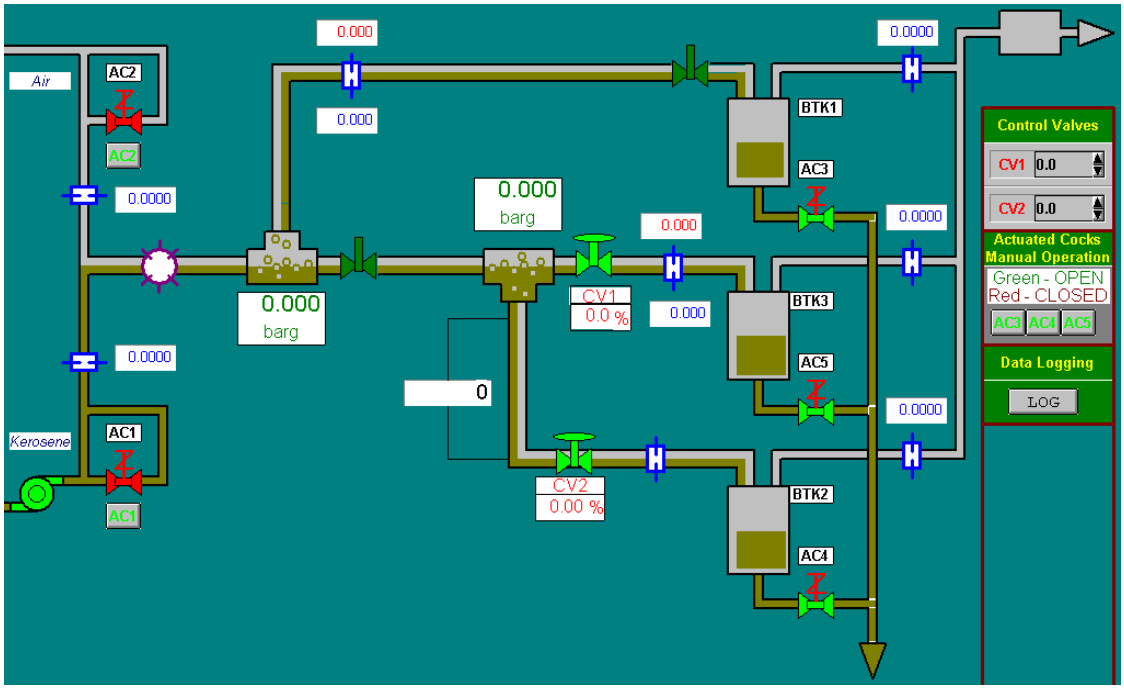

Figure D.2: VisiDAQ screen visualisation of the T-junction facility

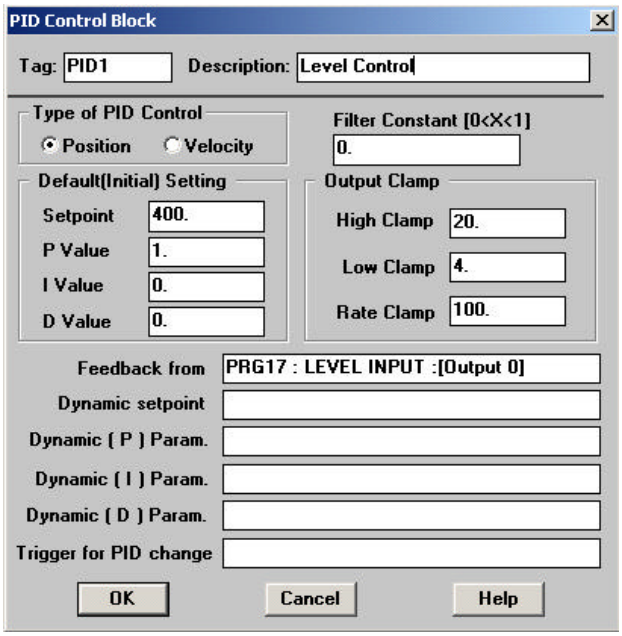

Figure D.3: VisiDAQ PID input box for setting automatic control valve

Level Control Optimisation

The aim for the level control optimisation was to perform a simple online assessment of the level control system suitable for the whole range of experimental inlet flowrates so that it delivers the best response to changes in the liquid height in the down leg. Thus, where it could be beneficial to conduct a wide range of experiments covering both stratified and slug flow it was decided, because of time restrictions, to limit the investigations to a representative flowrate and assume that the settings would apply throughout. As such, all these tuning experiments were conducted over a 120 second time period with a slug regime chosen with constant values of the gas and liquid superficial velocities, U_{gs} = 4.1 m/s and U_{ls} = 0.17 m/s. The set point was maintained at 400 mm and there were no other restrictions to the flow.

It was found that this approach, although not necessarily delivering the optimal level control for all conditions, maintained the liquid level in the down leg for the entire range of flow conditions. In theory, it could be beneficial to individually tune the system for the different flow regimes or even specific ranges of gas and liquid flowrates but that was beyond the scope of the present work.

Three different approaches were tested in an attempt to optimise the liquid level control. These were:

1. Change the proportional gain

2. Change the number of valve movements per minute

3. Use a damping function on the liquid height measurement

In all cases the objective was to maintain the liquid level as close to the set point as possible, while still having a system robust enough to cope with large fluctuations in the feed conditions. An evaluation of the results of these experiments is given below.

1. Proportional Gain

The proportional gain determines how hard the system will move the control valve setting in response to a deviation from the set point. If the gain is set too high the system may become unstable, switching between the two extreme of operation, i.e. fully open to fully closed. Conversely, if the gain is too low, the control valve will not respond enough and the liquid level will not be maintained. For the gain factors investigated, 0.5, 1 and 2, the liquid level was always maintained.

A method of determining the optimum gain to apply is to apply some simple statistical analysis of the level control data. Table D.1 gives the mean and standard deviation of the liquid level and the control valve setting for all three cases. Inspection of this data indicates that a gain of one, with the closest mean liquid level to the set point (400 mm) and the smallest standard deviation, would be the optimum value.

Table D.1: Statistical analysis of the affect of the proportional gain on the liquid level control

Proportional Gain	Valve setting (% open)		Liquid level (mm)	
	Mean	Standard deviation	Mean	Standard deviation
0.5	23.4	11.3	407	131
1	20.6	9.9	399	104
2	21.9	11.3	413	118

2. Valve Movements per Minute

By changing the number of movements the control system can apply to the valve over a set period of time the response will be dampened. Generally, this value should be set as high as possible so it does not become the determining step in the effective

operation of the level control. Limiting the number of movements to a very low value implies that the system cannot immediately respond to variations in the liquid level.

Table D.2 presents the same statistical analysis as the one carried out above. It shows that that the standard deviation in the valve setting increases as the allowed number of valve movements per minute increases. This is unsurprising, since the valve is allowed to move more frequently in an attempt to maintain the liquid level. However, the maintained liquid level results do not show the same trend. In this case a definite minimum standard deviation exists. Thus, in this case a better selection criterion is based only on the mean and standard deviation of the liquid level. This implies that the optimum number of valve movements per minute is 100.

Table D.2: Statistical analysis of the affect of the number of valve movements per minute on the liquid level control

Valve movements per minute	Valve setting (% open)		Liquid level (mm)	
	Mean	Standard deviation	Mean	Standard deviation
25	21.8	8.6	391	144
50	20.6	9.9	399	104
100	24.0	15.5	401	110
200	28.4	25.9	457	143
500	30.9	32.8	454	130

3. Damping Function

Similar to the case above, a damping function aims to reduce the noise of the control variable signal. The form of the damping function used here is given in Equation C.1.

$$L_H^*(i) = (1-a)L_H(i) + aL_H^*(i-1) \qquad [C.1]$$

where, $L_H^*(i)$ is the calculated damped liquid level at current time interval i, $L_H(i)$ is the actual liquid level at the current time interval i, $L_H^*(i-1)$ is the last calculated

damped liquid level, at time interval *i-1* and *a* is the damping coefficient. When *a* equals zero, the liquid level is uncorrected, as it approaches one the amount of damping increases.

Again a statistical analysis can be used to identify the affect of this damping on the performance of the level control. Table D.3 compares the four important parameters for a range of damping factors. In all cases the damping significantly decreases the effectiveness of the level control and was thus disregarded as a means to improve the level control performance.

Table D.3: Statistical analysis of the affect of the introduction of a damping factor on liquid level value on the liquid level control

Damping factor, *a*	Valve setting (% open)		Liquid level (mm)	
	Mean	Standard deviation	Mean	Standard deviation
No damping	24	15.5	401	110
0.1	23.9	17.6	423	137
0.9	30.8	26.9	460	185
0.95	24.8	26.3	448	200
0.99	34.5	36.1	453	268

Summary

The results of the investigation indicate that the optimum level control parameters were to set the proportional gain to 1 and to allow the valve to move 100 times per minute. These parameters were kept constant for all experimental investigations performed with the automatic level control in operation.

APPENDIX E

Steady-State Flow Split Results

This Appendix contains the tabulated data for the steady-state flow split results obtained for the various T-junction configurations. The stream numbers refer to Figure E1.

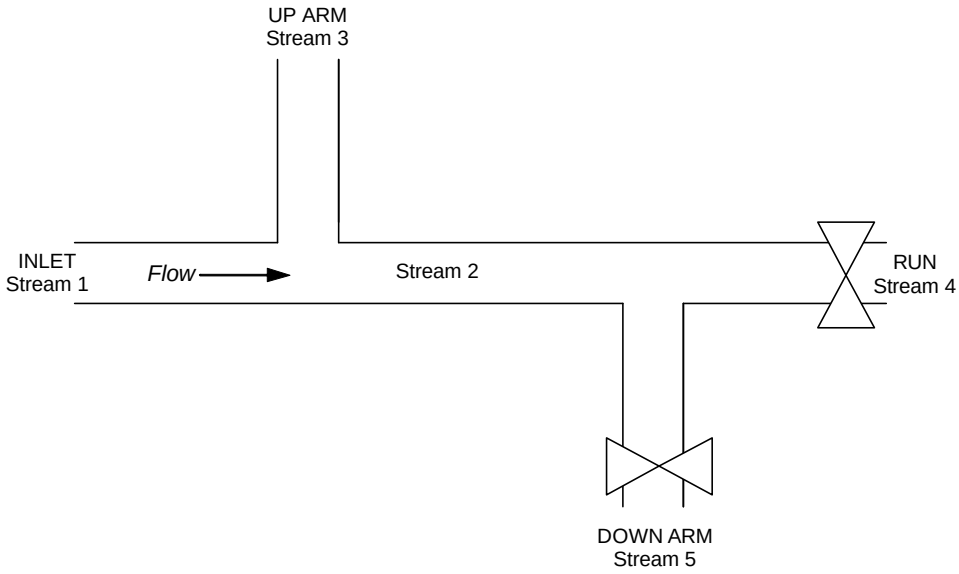

Figure E.1: Schematic of T-junctions showing stream numbering convention

Table E.1: Flow split at the vertically upwards side-arm only, U_{ls} = 0.07 m/s

Up valve setting (% open)	Run valve setting (% open)	Gas mass flow in stream (kg/s)			Liquid mass flow in stream (kg/s)		
		Inlet (1)	Up (3)	Run (4)	Inlet (1)	Up (3)	Run (4)
U_{gs} = 5.1 m/s							
100	**100**	0.0080	0.0063	0.0017	0.0606	0.0009	0.0597
100	**80**	0.0079	0.0058	0.0021	0.0602	0.0000	0.0602
100	**60**	0.0080	0.0043	0.0037	0.0617	0.0000	0.0617
100	**40**	0.0079	0.0030	0.0049	0.0585	0.0008	0.0577
100	**20**	0.0077	0.0014	0.0063	0.0604	0.0012	0.0592
100	**0**						
80	**100**	0.0079	0.0071	0.0008	0.0612	0.0005	0.0607
80	**80**	0.0083	0.0067	0.0016	0.0625	0.0003	0.0622
80	**60**	0.0081	0.0051	0.0030	0.0583	0.0001	0.0582
80	**40**	0.0080	0.0037	0.0043	0.0599	0.0007	0.0592
80	**20**	0.0076	0.0020	0.0056	0.0604	0.0005	0.0599
60	**100**	0.0082	0.0077	0.0005	0.0631	0.0099	0.0532
60	**80**	0.0080	0.0076	0.0004	0.0592	0.0000	0.0592
60	**60**	0.0076	0.0060	0.0016	0.0587	0.0000	0.0587
60	**40**	0.0077	0.0047	0.0030	0.0617	0.0000	0.0617
60	**20**	0.0077	0.0029	0.0048	0.0627	0.0000	0.0627
40	**100**	0.0082	0.0078	0.0004	0.0634	0.0235	0.0399
40	**80**	0.0080	0.0078	0.0002	0.0618	0.0133	0.0485
40	**60**	0.0080	0.0068	0.0012	0.0595	0.0013	0.0582
40	**40**	0.0077	0.0059	0.0018	0.0601	0.0004	0.0597
40	**20**						
20	**100**	0.0081	0.0077	0.0004	0.0625	0.0484	0.0141
20	**80**	0.0079	0.0076	0.0003	0.0588	0.0422	0.0166
20	**60**	0.0078	0.0072	0.0006	0.0625	0.0333	0.0292
20	**40**						
20	**20**						
0	**100**						

Table E.2: Flow split at the vertically upwards side-arm only, U_{ls} = 0.18 m/s

Up valve setting (% open)	Run valve setting (% open)	Gas mass flow in stream (kg/s)			Liquid mass flow in stream (kg/s)		
		Inlet (1)	Up (3)	Run (4)	Inlet (1)	Up (3)	Run (4)
U_{gs} = 3.3 m/s							
100	**100**	0.0053	0.0049	0.0004	0.1712	0.0514	0.1198
100	**80**	0.0052	0.0045	0.0007	0.1673	0.0285	0.1388
100	**60**	0.0053	0.0038	0.0015	0.1644	0.0162	0.1482
100	**40**	0.0056	0.0028	0.0028	0.1716	0.0174	0.1542
100	**20**	0.0054	0.0017	0.0037	0.1624	0.0057	0.1567
100	**0**						
80	**100**	0.0053	0.0048	0.0005	0.1711	0.0677	0.1034
80	**80**	0.0053	0.0046	0.0007	0.1652	0.0543	0.1109
80	**60**	0.0054	0.0042	0.0012	0.1639	0.0316	0.1323
80	**40**	0.0055	0.0031	0.0024	0.1701	0.0249	0.1452
80	**20**	0.0053	0.0022	0.0031	0.1653	0.0136	0.1517
60	**100**	0.0055	0.0049	0.0006	0.1663	0.1031	0.0632
60	**80**	0.0055	0.0048	0.0007	0.1636	0.0815	0.0821
60	**60**	0.0054	0.0044	0.0010	0.1624	0.0525	0.1099
60	**40**	0.0055	0.0039	0.0016	0.1625	0.0347	0.1278
60	**20**						
40	**100**	0.0054	0.0045	0.0009	0.1730	0.0507	0.1223
40	**80**	0.0053	0.0045	0.0008	0.1619	0.1027	0.0592
40	**60**	0.0053	0.0044	0.0009	0.1703	0.0763	0.0940
40	**40**	0.0052	0.0042	0.0010	0.1618	0.0678	0.0940
40	**20**						
20	**100**	0.0052	0.0047	0.0005	0.1710	0.1449	0.0261
20	**80**	0.0054	0.0045	0.0009	0.1705	0.1223	0.0482
20	**60**						
20	**40**						
20	**20**						
0	**100**						

Table E.3: Flow split at the vertically downwards side-arm only, U_{gs} = 0.3.3 m/s

Gas mass flow in stream (kg/s)				Liquid mass flow in stream (kg/s)			
Inlet (1)	**Up (3)**	**Run (4)**	**Down (5)**	**Inlet (1)**	**Up (3)**	**Run (4)**	**Down (5)**
U_{ls} = 0.12 m/s							
0.0050		0.0013	0.0037	0.1300		0.0150	0.1160
0.0052		0.0009	0.0044	0.1150		0.0128	0.1020
0.0052		0.0003	0.0049	0.1130		0.0060	0.1070
0.0053		0.0001	0.0052	0.1290		0.0090	0.1200
0.0052		0.0021	0.0031	0.1300		0.0200	0.1100
0.0050		0.0035	0.0015	0.1130		0.0220	0.0910
0.0048		0.0045	0.0004	0.1130		0.0260	0.0880
0.0053		0.0053	0.0000	0.1180		0.0610	0.0560
0.0051		0.0051	0.0000	0.1120		0.0310	0.0810
0.0050		0.0013	0.0037	0.1300		0.0150	0.1160
U_{ls} = 0.36 m/s							
0.0050		0.0009	0.0042	0.3320		0.0750	0.2570
0.0050		0.0005	0.0046	0.3340		0.0530	0.2800
0.0050		0.0002	0.0048	0.3410		0.0360	0.3060
0.0050		0.0001	0.0050	0.3400		0.0210	0.3170
0.0051		0.0000	0.0051	0.3300		0.0110	0.3200
0.0049		0.0011	0.0038	0.3320		0.0910	0.2410
0.0054		0.0042	0.0012	0.3210		0.1410	0.1800
0.0054		0.0054	0.0000	0.3030		0.1790	0.1240
0.0050		0.0050	0.0000	0.3330		0.2960	0.0370
0.0050		0.0050	0.0000	0.3300		0.1890	0.1410

Table E.4: Flow split at the vertically upwards side-arm with down leg valve 100% open, U_{ls} = 0.07 m/s

Up valve setting (% open)	Run valve setting (% open)	Gas mass flow in stream (kg/s)				Liquid mass flow in stream (kg/s)			
		Inlet (1)	Up (3)	Run (4)	Down (5)	Inlet (1)	Up (3)	Run (4)	Down (5)
U_{gs} = 5.1 m/s									
100	**100**	0.0078	0.0062	0.0013	0.0003	0.0630	0.0000	0.0111	0.0519
100	**80**	0.0081	0.0056	0.0017	0.0008	0.0626	0.0000	0.0136	0.0490
100	**60**	0.0086	0.0041	0.0025	0.0020	0.0619	0.0000	0.0053	0.0566
100	**40**	0.0084	0.0030	0.0029	0.0025	0.0635	0.0000	0.0043	0.0592
100	**20**	0.0082	0.0014	0.0037	0.0031	0.0612	0.0006	0.0057	0.0549
100	**0**	0.0081	0.0000	0.0044	0.0037	0.0623	0.0000	0.0033	0.0590
80	**100**	0.0082	0.0073	0.0008	0.0001	0.0633	0.0004	0.0047	0.0582
80	**80**	0.0083	0.0064	0.0014	0.0005	0.0643	0.0000	0.0114	0.0529
80	**60**	0.0084	0.0049	0.0020	0.0015	0.0621	0.0000	0.0105	0.0516
80	**40**	0.0081	0.0038	0.0022	0.0021	0.0626	0.0000	0.0076	0.0550
80	**20**	0.0083	0.0021	0.0033	0.0029	0.0598	0.0000	0.0082	0.0516
60	**100**	0.0080	0.0080	0.0000	0.0000	0.0625	0.0047	0.0000	0.0578
60	**80**	0.0081	0.0072	0.0007	0.0002	0.0624	0.0024	0.0043	0.0557
60	**60**	0.0084	0.0060	0.0014	0.0010	0.0626	0.0008	0.0075	0.0543
60	**40**	0.0080	0.0052	0.0013	0.0015	0.0600	0.0007	0.0125	0.0468
60	**20**	0.0080	0.0030	0.0026	0.0024	0.0601	0.0004	0.0105	0.0492
40	**100**	0.0082	0.0082	0.0000	0.0000	0.0633	0.0204	0.0000	0.0429
40	**80**	0.0086	0.0080	0.0001	0.0005	0.0608	0.0108	0.0000	0.0500
40	**60**	0.0081	0.0077	0.0001	0.0003	0.0600	0.0012	0.0037	0.0551
40	**40**	0.0080	0.0058	0.0012	0.0010	0.0612	0.0012	0.0083	0.0517
40	**20**								
20	**100**	0.0083	0.0083	0.0000	0.0000	0.0630	0.0439	0.0000	0.0191
20	**80**	0.0080	0.0080	0.0000	0.0000	0.0603	0.0341	0.0013	0.0249
20	**60**	0.0083	0.0080	0.0002	0.0001	0.0612	0.0214	0.0000	0.0398
20	**40**								
20	**20**								
0	**100**								

Table E.5: Flow split at the vertically upwards side-arm with down leg valve 100% open, U_{ls} = 0.18 m/s

Up valve setting (% open)	Run valve setting (% open)	Gas mass flow in stream (kg/s)				Liquid mass flow in stream (kg/s)			
		Inlet (1)	Up (3)	Run (4)	Down (5)	Inlet (1)	Up (3)	Run (4)	Down (5)
U_{gs} = 3.3 m/s									
100	**100**	0.0054	0.0045	0.0005	0.0004	0.1681	0.0286	0.0117	0.1278
100	**80**	0.0052	0.0038	0.0007	0.0007	0.1702	0.0253	0.0251	0.1198
100	**60**	0.0055	0.0031	0.0012	0.0012	0.1700	0.0138	0.0756	0.0806
100	**40**	0.0054	0.0029	0.0012	0.0013	0.1662	0.0059	0.0801	0.0802
100	**20**	0.0054	0.0014	0.0017	0.0023	0.1623	0.0039	0.0767	0.0817
100	**0**	0.0054	0.0000	0.0029	0.0025	0.1678	0.0000	0.0786	0.0892
80	**100**	0.0055	0.0045	0.0005	0.0005	0.1606	0.0476	0.0024	0.1106
80	**80**	0.0055	0.0041	0.0007	0.0007	0.1639	0.0378	0.0142	0.1119
80	**60**	0.0055	0.0039	0.0011	0.0005	0.1670	0.0241	0.0469	0.0960
80	**40**	0.0054	0.0035	0.0009	0.0010	0.1619	0.0031	0.0702	0.0886
80	**20**	0.0053	0.0019	0.0015	0.0019	0.1605	0.0102	0.0652	0.0851
60	**100**	0.0055	0.0040	0.0007	0.0008	0.1655	0.0851	0.0012	0.0792
60	**80**	0.0052	0.0043	0.0007	0.0002	0.1653	0.0704	0.0006	0.0943
60	**60**	0.0054	0.0046	0.0008	0.0000	0.1675	0.0516	0.0183	0.0976
60	**40**	0.0055	0.0038	0.0007	0.0010	0.1603	0.0214	0.0507	0.0882
60	**20**	0.0052	0.0026	0.0013	0.0013	0.1608	0.0208	0.0522	0.0878
40	**100**	0.0054	0.0054	0.0000	0.0000	0.1709	0.1184	0.0000	0.0525
40	**80**	0.0053	0.0051	0.0002	0.0000	0.1642	0.0919	0.0011	0.0712
40	**60**	0.0052	0.0049	0.0003	0.0000	0.1628	0.0553	0.0099	0.0976
40	**40**	0.0055	0.0048	0.0005	0.0002	0.1668	0.0480	0.0143	0.1045
40	**20**								
20	**100**	0.0051	0.0044	0.0005	0.0002	0.1654	0.1419	0.0025	0.0210
20	**80**	0.0053	0.0047	0.0004	0.0002	0.1637	0.1319	0.0012	0.0306
20	**60**	0.0053	0.0042	0.0006	0.0005	0.1627	0.1186	0.0000	0.0441
20	**40**								
20	**20**								
0	**100**								

Table E.6: Flow split at the vertically upwards side-arm with down leg valve 100% open, U_{ls} = 0.35 m/s

Up valve setting (% open)	Run valve setting (% open)	Gas mass flow in stream (kg/s)				Liquid mass flow in stream (kg/s)			
		Inlet (1)	Up (3)	Run (4)	Down (5)	Inlet (1)	Up (3)	Run (4)	Down (5)
U_{gs} = 3.3 m/s									
100	**100**	0.0051	0.0026	0.0004	0.0021	0.3271	0.0149	0.0574	0.2548
100	**80**	0.0052	0.0019	0.0004	0.0029	0.3239	0.0131	0.0579	0.2529
100	**60**	0.0051	0.0001	0.0009	0.0041	0.3235	0.0024	0.0624	0.2587
100	**40**	0.0051	0.0000	0.0007	0.0044	0.3315	0.0000	0.0669	0.2646
100	**20**	0.0052	0.0000	0.0008	0.0044	0.3386	0.0016	0.0724	0.2646
100	**0**	0.0055	0.0000	0.0008	0.0047	0.3366	0.0000	0.0739	0.2627
80	**100**	0.0053	0.0024	0.0003	0.0026	0.3362	0.0177	0.0402	0.2783
80	**80**	0.0052	0.0019	0.0003	0.0030	0.3218	0.0019	0.0435	0.2764
80	**60**	0.0053	0.0009	0.0003	0.0041	0.3281	0.0022	0.0534	0.2725
80	**40**	0.0052	0.0000	0.0005	0.0047	0.3268	0.0012	0.0473	0.2783
80	**20**	0.0051	0.0000	0.0005	0.0046	0.3405	0.0034	0.0529	0.2842
60	**100**	0.0054	0.0028	0.0001	0.0025	0.3193	0.0130	0.0280	0.2783
60	**80**	0.0055	0.0020	0.0001	0.0034	0.3292	0.0081	0.0271	0.2940
60	**60**	0.0052	0.0009	0.0001	0.0042	0.3316	0.0020	0.0356	0.2940
60	**40**	0.0051	0.0001	0.0002	0.0048	0.3269	0.0000	0.0270	0.2999
60	**20**	0.0051	0.0000	0.0002	0.0049	0.3411	0.0020	0.0353	0.3038
40	**100**	0.0053	0.0029	0.0000	0.0024	0.3280	0.0146	0.0096	0.3038
40	**80**	0.0054	0.0021	0.0000	0.0033	0.3387	0.0081	0.0150	0.3156
40	**60**	0.0053	0.0010	0.0000	0.0043	0.3281	0.0030	0.0173	0.3078
40	**40**	0.0051	0.0001	0.0001	0.0049	0.3432	0.0011	0.0285	0.3136
40	**20**								
20	**100**	0.0053	0.0031	0.0000	0.0022	0.3364	0.0162	0.0046	0.3156
20	**80**	0.0055	0.0021	0.0000	0.0034	0.3201	0.0093	0.0050	0.3058
20	**60**	0.0053	0.0009	0.0000	0.0044	0.3380	0.0060	0.0046	0.3274
20	**40**								
20	**20**								
0	**100**	0.0055	0.0029	0.0000	0.0026	0.3292	0.0136	0.0000	0.3156

Table E.7: Flow split with ay vertical upwards T-junction with down leg valve 50% open, U_{ls} = 0.35 m/s

Up valve setting (% open)	Run valve setting (% open)	Gas mass flow in stream (kg/s)				Liquid mass flow in stream (kg/s)			
		Inlet (1)	Up (3)	Run (4)	Down (5)	Inlet (1)	Up (3)	Run (4)	Down (5)
U_{gs} = 3.3 m/s									
100	**100**	0.0051	0.0050	0.0001	0.0000	0.3365	0.0249	0.0744	0.2372
100	**80**	0.0052	0.0038	0.0006	0.0008	0.3280	0.0158	0.0868	0.2254
100	**60**	0.0052	0.0022	0.0010	0.0020	0.3211	0.0092	0.0924	0.2195
100	**40**	0.0051	0.0004	0.0015	0.0032	0.3311	0.0009	0.1028	0.2274
100	**20**	0.0050	0.0000	0.0017	0.0033	0.3223	0.0014	0.0974	0.2235
100	**0**	0.0052	0.0000	0.0017	0.0035	0.3140	0.0000	0.1023	0.2117
80	**100**	0.0050	0.0043	0.0004	0.0003	0.3253	0.0278	0.0584	0.2391
80	**80**	0.0050	0.0036	0.0006	0.0008	0.3230	0.0155	0.0644	0.2431
80	**60**	0.0052	0.0023	0.0008	0.0021	0.3317	0.0119	0.0679	0.2519
80	**40**	0.0050	0.0009	0.0008	0.0033	0.3106	0.0000	0.0734	0.2372
80	**20**	0.0050	0.0000	0.0008	0.0042	0.3219	0.0033	0.0814	0.2372
60	**100**	0.0052	0.0046	0.0002	0.0004	0.3284	0.0257	0.0361	0.2666
60	**80**	0.0054	0.0041	0.0002	0.0011	0.3428	0.0214	0.0431	0.2783
60	**60**	0.0054	0.0027	0.0003	0.0024	0.3241	0.0069	0.0447	0.2725
60	**40**	0.0053	0.0012	0.0004	0.0037	0.3198	0.0037	0.0534	0.2627
60	**20**	0.0051	0.0002	0.0004	0.0045	0.3277	0.0003	0.0589	0.2685
40	**100**	0.0053	0.0048	0.0001	0.0004	0.3306	0.0280	0.0223	0.2803
40	**80**	0.0054	0.0042	0.0001	0.0011	0.3286	0.0200	0.0283	0.2803
40	**60**	0.0050	0.0026	0.0003	0.0021	0.3309	0.0129	0.0299	0.2881
40	**40**	0.0054	0.0012	0.0002	0.0040	0.3236	0.0028	0.0346	0.2862
40	**20**								
20	**100**	0.0053	0.0049	0.0000	0.0004	0.3287	0.0353	0.0092	0.2842
20	**80**	0.0053	0.0043	0.0000	0.0010	0.3313	0.0214	0.0100	0.2999
20	**60**	0.0051	0.0030	0.0000	0.0021	0.3236	0.0112	0.0105	0.3019
20	**40**								
20	**20**								
0	**100**	0.0053	0.0051	0.0000	0.0002	0.3352	0.0372	0.0000	0.2980

Table E.8: Flow split with constant liquid level in down leg, U_{ls} = 0.35 m/s

Up valve setting (% open)	Run valve setting (% open)	Gas mass flow in stream (kg/s)				Liquid mass flow in stream (kg/s)			
		Inlet (1)	Up (3)	Run (4)	Down (5)	Inlet (1)	Up (3)	Run (4)	Down (5)
U_{gs} = 3.3 m/s									
100	**100**	0.0051	0.0046	0.0005	0.0000	0.3242	0.0504	0.1203	0.1535
100	**80**	0.0050	0.0044	0.0006	0.0000	0.3303	0.0333	0.1388	0.1582
100	**60**	0.0050	0.0036	0.0014	0.0000	0.3087	0.0151	0.1503	0.1433
100	**40**	0.0051	0.0027	0.0024	0.0000	0.3182	0.0177	0.1752	0.1253
100	**20**	0.0053	0.0011	0.0042	0.0000	0.3251	0.0046	0.1982	0.1223
100	**0**	0.0052	0.0000	0.0052	0.0000	0.3283	0.0000	0.2087	0.1196
80	**100**	0.0051	0.0047	0.0004	0.0000	0.3211	0.0641	0.0929	0.1641
80	**80**	0.0051	0.0046	0.0005	0.0000	0.3147	0.0449	0.1048	0.1650
80	**60**	0.0049	0.0040	0.0009	0.0000	0.3232	0.0286	0.1268	0.1678
80	**40**	0.0049	0.0031	0.0018	0.0000	0.3168	0.0115	0.1648	0.1405
80	**20**	0.0050	0.0018	0.0032	0.0000	0.3091	0.0000	0.1787	0.1304
60	**100**	0.0051	0.0049	0.0002	0.0000	0.3292	0.0803	0.0654	0.1835
60	**80**	0.0051	0.0049	0.0002	0.0000	0.3113	0.0561	0.0784	0.1768
60	**60**	0.0049	0.0044	0.0005	0.0000	0.3205	0.0388	0.0994	0.1823
60	**40**	0.0051	0.0043	0.0008	0.0000	0.3132	0.0237	0.1258	0.1637
60	**20**	0.0052	0.0028	0.0024	0.0000	0.3075	0.0087	0.1598	0.1390
40	**100**	0.0052	0.0051	0.0001	0.0000	0.3182	0.0798	0.0345	0.2039
40	**80**	0.0052	0.0049	0.0003	0.0000	0.3202	0.0735	0.0487	0.1980
40	**60**	0.0050	0.0046	0.0004	0.0000	0.3149	0.0545	0.0659	0.1945
40	**40**	0.0051	0.0043	0.0008	0.0000	0.3246	0.0396	0.0954	0.1896
40	**20**								
20	**100**	0.0052	0.0051	0.0001	0.0000	0.3179	0.1006	0.0140	0.2033
20	**80**	0.0051	0.0050	0.0001	0.0000	0.3210	0.0911	0.0182	0.2117
20	**60**	0.0051	0.0049	0.0002	0.0000	0.3061	0.0612	0.0352	0.2097
20	**40**								
20	**20**								
0	**100**	0.0050	0.0048	0.0002	0.0000	0.3142	0.2097	0.0000	0.1045

Table E.9: Flow split with constant liquid level in down leg, U_{ls} = 0.08 m/s

Up valve setting (% open)	Run valve setting (% open)	Gas mass flow in stream (kg/s)				Liquid mass flow in stream (kg/s)			
		Inlet (1)	Up (3)	Run (4)	Down (5)	Inlet (1)	Up (3)	Run (4)	Down (5)
				U_{gs} = 5.1 m/s					
100	**100**	0.0079	0.0050	0.0029	0.0000	0.0686	0.0000	0.0180	0.0506
100	**80**	0.0082	0.0044	0.0038	0.0000	0.0690	0.0000	0.0200	0.0490
100	**60**	0.0082	0.0034	0.0048	0.0000	0.0664	0.0000	0.0182	0.0482
100	**40**	0.0078	0.0021	0.0057	0.0000	0.0692	0.0000	0.0196	0.0496
100	**20**	0.0081	0.0009	0.0072	0.0000	0.0688	0.0000	0.0159	0.0529
100	**0**	0.0080	0.0000	0.0080	0.0000	0.0668	0.0000	0.0145	0.0523
80	**100**	0.0076	0.0055	0.0021	0.0000	0.0683	0.0000	0.0136	0.0547
80	**80**	0.0081	0.0052	0.0029	0.0000	0.0699	0.0000	0.0170	0.0529
80	**60**	0.0082	0.0042	0.0040	0.0000	0.0687	0.0000	0.0197	0.0490
80	**40**	0.0083	0.0030	0.0053	0.0000	0.0697	0.0000	0.0212	0.0485
80	**20**	0.0076	0.0016	0.0060	0.0000	0.0686	0.0000	0.0235	0.0451
60	**100**	0.0080	0.0068	0.0012	0.0000	0.0671	0.0000	0.0077	0.0594
60	**80**	0.0079	0.0059	0.0020	0.0000	0.0704	0.0000	0.0145	0.0559
60	**60**	0.0081	0.0053	0.0028	0.0000	0.0711	0.0000	0.0195	0.0516
60	**40**	0.0082	0.0041	0.0041	0.0000	0.0710	0.0000	0.0210	0.0500
60	**20**	0.0081	0.0028	0.0053	0.0000	0.0673	0.0000	0.0216	0.0457
40	**100**	0.0076	0.0071	0.0005	0.0000	0.0675	0.0000	0.0073	0.0602
40	**80**	0.0076	0.0068	0.0008	0.0000	0.0694	0.0000	0.0096	0.0598
40	**60**	0.0077	0.0060	0.0017	0.0000	0.0692	0.0000	0.0124	0.0568
40	**40**	0.0082	0.0052	0.0030	0.0000	0.0665	0.0000	0.0155	0.0510
40	**20**								
20	**100**	0.0082	0.0081	0.0001	0.0000	0.0700	0.0028	0.0024	0.0648
20	**80**	0.0081	0.0079	0.0002	0.0000	0.0689	0.0000	0.0042	0.0647
20	**60**	0.0077	0.0071	0.0006	0.0000	0.0661	0.0000	0.0049	0.0612
20	**40**								
20	**20**								
0	**100**	0.0080	0.0080	0.0000	0.0000	0.0694	0.0337	0.0000	0.0357

Table E.10: Flow split with automatic level control on down leg, U_{ls} = 0.07 m/s

Run valve setting (% open)	Gas mass flow in stream (kg/s)				Liquid mass flow in stream (kg/s)			
	Inlet (1)	Up (3)	Run (4)	Down (5)	Inlet (1)	Up (3)	Run (4)	Down (5)
				U_{gs} = 3.3 m/s				
100	0.0051	0.0042	0.0009	0.0000	0.0644	0.0000	0.0115	0.0529
80	0.0050	0.0045	0.0005	0.0000	0.0643	0.0000	0.0094	0.0549
60	0.0052	0.0050	0.0002	0.0000	0.0623	0.0000	0.0035	0.0588
40	0.0052	0.0051	0.0001	0.0000	0.0618	0.0000	0.0030	0.0588
20	0.0052	0.0052	0.0000	0.0000	0.0635	0.0000	0.0008	0.0627
0	0.0053	0.0053	0.0000	0.0000	0.0608	0.0157	0.0000	0.0451
				U_{gs} = 5.1 m/s				
100	0.0077	0.0057	0.0020	0.0000	0.0585	0.0000	0.0075	0.0510
80	0.0079	0.0066	0.0013	0.0000	0.0619	0.0000	0.0090	0.0529
60	0.0078	0.0072	0.0006	0.0000	0.0614	0.0000	0.0085	0.0529
40	0.0081	0.0079	0.0002	0.0000	0.0607	0.0013	0.0045	0.0549
20	0.0080	0.0080	0.0000	0.0000	0.0603	0.0014	0.0001	0.0588
0	0.0081	0.0081	0.0000	0.0000	0.0608	0.0216	0.0000	0.0392
				U_{gs} = 7.0 m/s				
100	0.0110	0.0079	0.0031	0.0000	0.0604	0.0000	0.0075	0.0299
80	0.0109	0.0087	0.0022	0.0000	0.0607	0.0008	0.0050	0.0317
60	0.0109	0.0099	0.0010	0.0000	0.0618	0.0020	0.0034	0.0320
40	0.0109	0.0106	0.0003	0.0000	0.0598	0.0039	0.0010	0.0368
20	0.0113	0.0111	0.0002	0.0000	0.0594	0.0045	0.0000	0.0570
0	0.0115	0.0115	0.0000	0.0000	0.0617	0.0274	0.0000	0.0343
				U_{gs} = 8.5 m/s				
100	0.0147	0.0103	0.0044	0.0000	0.0639	0.0000	0.0120	0.0519
80	0.0147	0.0114	0.0033	0.0000	0.0605	0.0000	0.0115	0.0490
60	0.0141	0.0126	0.0015	0.0000	0.0654	0.0000	0.0125	0.0529
40	0.0139	0.0132	0.0007	0.0000	0.0637	0.0004	0.0025	0.0608
20	0.0139	0.0138	0.0001	0.0000	0.0605	0.0045	0.0027	0.0533
0	0.0143	0.0143	0.0000	0.0000	0.0607	0.0274	0.0000	0.0333
				U_{gs} = 9.6 m/s				
100	0.0177	0.0124	0.0053	0.0000	0.0645	0.0000	0.0135	0.0510
80	0.0177	0.0136	0.0041	0.0000	0.0625	0.0000	0.0155	0.0470
60	0.0169	0.0147	0.0022	0.0000	0.0639	0.0000	0.0110	0.0529
40	0.0169	0.0159	0.0010	0.0000	0.0665	0.0065	0.0051	0.0549
20	0.0170	0.0170	0.0000	0.0000	0.0618	0.0069	0.0000	0.0549
0	0.0170	0.0170	0.0000	0.0000	0.0627	0.0372	0.0000	0.0255

Table E.11: Flow split with automatic level control on down leg, U_{ls} = 0.17 m/s

Run valve setting (% open)	Gas mass flow in stream (kg/s)				Liquid mass flow in stream (kg/s)			
	Inlet (1)	Up (3)	Run (4)	Down (5)	Inlet (1)	Up (3)	Run (4)	Down (5)
				U_{gs} = 3.3 m/s				
100	0.0051	0.0048	0.0003	0.0000	0.1613	0.0043	0.0394	0.1176
80	0.0052	0.0049	0.0003	0.0000	0.1732	0.0069	0.0310	0.1256
60	0.0053	0.0051	0.0002	0.0000	0.1665	0.0171	0.0200	0.1294
40	0.0053	0.0052	0.0001	0.0000	0.1639	0.0372	0.0110	0.1647
20	0.0053	0.0053	0.0000	0.0000	0.1652	0.0392	0.0045	0.1215
0	0.0052	0.0052	0.0000	0.0000	0.1607	0.0784	0.0000	0.0823
				U_{gs} = 5.1 m/s				
100	0.0082	0.0071	0.0011	0.0000	0.1650	0.0009	0.0484	0.1157
80	0.0082	0.0076	0.0006	0.0000	0.1683	0.0039	0.0429	0.1215
60	0.0081	0.0080	0.0001	0.0000	0.1614	0.0149	0.0250	0.1215
40	0.0082	0.0082	0.0000	0.0000	0.1610	0.0171	0.0145	0.0863
20	0.0082	0.0082	0.0000	0.0000	0.1564	0.0451	0.0035	0.1078
0	0.0081	0.0081	0.0000	0.0000	0.1666	0.0745	0.0000	0.0921
				U_{gs} = 7.0 m/s				
100	0.0115	0.0099	0.0016	0.0000	0.1668	0.0039	0.0649	0.0980
80	0.0115	0.0104	0.0011	0.0000	0.1617	0.0080	0.0459	0.1078
60	0.0115	0.0111	0.0004	0.0000	0.1575	0.0094	0.0305	0.1176
40	0.0116	0.0114	0.0002	0.0000	0.1640	0.0314	0.0180	0.1137
20	0.0116	0.0116	0.0000	0.0000	0.1570	0.0451	0.0060	0.1059
0	0.0115	0.0115	0.0000	0.0000	0.1584	0.0763	0.0000	0.0821
				U_{gs} = 8.5 m/s				
100	0.0143	0.0116	0.0027	0.0000	0.1562	0.0000	0.0700	0.0862
80	0.0141	0.0123	0.0018	0.0000	0.1675	0.0035	0.0464	0.1176
60	0.0138	0.0130	0.0008	0.0000	0.1644	0.0098	0.0349	0.1457
40	0.0138	0.0135	0.0003	0.0000	0.1583	0.0098	0.0250	0.1235
20	0.0140	0.0140	0.0000	0.0000	0.1688	0.0255	0.0120	0.1058
0	0.0141	0.0141	0.0000	0.0000	0.1588	0.0706	0.0000	0.0882
				U_{gs} = 9.6 m/s				
100	0.0170	0.0136	0.0034	0.0000	0.1567	0.0006	0.0699	0.0862
80	0.0164	0.0145	0.0019	0.0000	0.1618	0.0098	0.0599	0.0921
60	0.0167	0.0158	0.0009	0.0000	0.1573	0.0037	0.0399	0.1137
50	0.0167	0.0163	0.0004	0.0000	0.1631	0.0027	0.0330	0.1274
40	0.0166	0.0163	0.0003	0.0000	0.1661	0.0039	0.0250	0.1372
20	0.0168	0.0167	0.0001	0.0000	0.1675	0.0061	0.0085	0.1529
10	0.0169	0.0169	0.0000	0.0000	0.1581	0.0353	0.0032	0.1196
0	0.0170	0.0170	0.0000	0.0000	0.1627	0.0647	0.0000	0.0980

Table E.12: Flow split with automatic level control on down leg, U_{ls} = 0.29 m/s

Run valve setting (% open)	Gas mass flow in stream (kg/s)				Liquid mass flow in stream (kg/s)			
	Inlet (1)	Up (3)	Run (4)	Down (5)	Inlet (1)	Up (3)	Run (4)	Down (5)
				U_{gs} = 3.3 m/s				
100	0.0048	0.0046	0.0002	0.0000	0.2679	0.0372	0.0700	0.1607
80	0.0050	0.0048	0.0002	0.0000	0.2600	0.0313	0.0464	0.1823
60	0.0050	0.0049	0.0001	0.0000	0.2680	0.0470	0.0250	0.1960
40	0.0050	0.0049	0.0001	0.0000	0.2737	0.0725	0.0150	0.2083
20	0.0050	0.0050	0.0000	0.0000	0.2559	0.0862	0.0050	0.1647
0	0.0050	0.0050	0.0000	0.0000	0.2607	0.1588	0.0000	0.1019
				U_{gs} = 5.1 m/s				
100	0.0076	0.0071	0.0005	0.0000	0.2770	0.0510	0.0849	0.1411
80	0.0079	0.0077	0.0002	0.0000	0.2620	0.0560	0.0649	0.1411
60	0.0081	0.0080	0.0001	0.0000	0.2703	0.0804	0.0409	0.1490
40	0.0083	0.0082	0.0001	0.0000	0.2611	0.0882	0.0220	0.1509
20	0.0082	0.0082	0.0000	0.0000	0.2615	0.1255	0.0125	0.1235
0	0.0082	0.0082	0.0000	0.0000	0.2587	0.1705	0.0000	0.0882
				U_{gs} = 7.0 m/s				
100	0.0114	0.0106	0.0008	0.0000	0.2674	0.0411	0.1048	0.1215
80	0.0114	0.0110	0.0004	0.0000	0.2682	0.0490	0.0800	0.1392
60	0.0115	0.0112	0.0003	0.0000	0.2586	0.0706	0.0449	0.1431
40	0.0115	0.0114	0.0001	0.0000	0.2582	0.0940	0.0250	0.1392
20	0.0114	0.0114	0.0000	0.0000	0.2604	0.1176	0.0115	0.1313
0	0.0115	0.0115	0.0000	0.0000	0.2568	0.1666	0.0000	0.0902
				U_{gs} = 8.5 m/s				
100	0.0138	0.0127	0.0011	0.0000	0.2570	0.0372	0.1198	0.1000
80	0.0138	0.0131	0.0007	0.0000	0.2586	0.0510	0.0900	0.1176
60	0.0137	0.0133	0.0004	0.0000	0.2637	0.0686	0.0500	0.1451
40	0.0139	0.0137	0.0002	0.0000	0.2554	0.0745	0.0300	0.1509
20	0.0142	0.0140	0.0002	0.0000	0.2664	0.1137	0.0194	0.1333
0	0.0142	0.0142	0.0000	0.0000	0.2685	0.1705	0.0000	0.0980
				U_{gs} = 9.6 m/s				
100	0.0173	0.0154	0.0019	0.0000	0.2681	0.0333	0.1348	0.1000
80	0.0170	0.0159	0.0011	0.0000	0.2686	0.0392	0.1098	0.1196
60	0.0169	0.0166	0.0003	0.0000	0.2670	0.0549	0.0749	0.1372
40	0.0169	0.0168	0.0001	0.0000	0.2609	0.0686	0.0394	0.1529
20	0.0170	0.0170	0.0000	0.0000	0.2620	0.1059	0.0130	0.1431
0	0.0171	0.0171	0.0000	0.0000	0.2647	0.1549	0.0000	0.1098

Table E.13: Flow split with automatic level control on down leg, U_{ls} = 0.40 m/s

Run valve setting (% open)	Gas mass flow in stream (kg/s)				Liquid mass flow in stream (kg/s)			
	Inlet (1)	Up (3)	Run (4)	Down (5)	Inlet (1)	Up (3)	Run (4)	Down (5)
				U_{gs} = 3.3 m/s				
100	0.0055	0.0052	0.0003	0.0000	0.3520	0.0900	0.0970	0.1650
80	0.0053	0.0052	0.0001	0.0000	0.3600	0.0980	0.0710	0.1910
60	0.0053	0.0052	0.0001	0.0000	0.3580	0.1220	0.0380	0.1980
40	0.0052	0.0052	0.0000	0.0000	0.3570	0.1410	0.0200	0.1960
20	0.0053	0.0053	0.0000	0.0000	0.3650	0.1680	0.0070	0.1900
0	0.0052	0.0052	0.0000	0.0000	0.3650	0.2410	0.0000	0.1240
				U_{gs} = 5.1 m/s				
100	0.0082	0.0079	0.0003	0.0000	0.3650	0.1100	0.1200	0.1350
80	0.0083	0.0082	0.0001	0.0000	0.3620	0.1240	0.0880	0.1500
60	0.0085	0.0084	0.0001	0.0000	0.3710	0.1290	0.0510	0.1910
40	0.0086	0.0086	0.0000	0.0000	0.3650	0.1630	0.0290	0.1730
20	0.0083	0.0083	0.0000	0.0000	0.3620	0.1930	0.0090	0.1600
0	0.0084	0.0084	0.0000	0.0000	0.3660	0.3550	0.0000	0.0110
				U_{gs} = 7.0 m/s				
100	0.0112	0.0105	0.0007	0.0000	0.3720	0.1078	0.1348	0.1294
80	0.0113	0.0110	0.0003	0.0000	0.3547	0.1006	0.0953	0.1588
60	0.0113	0.0112	0.0001	0.0000	0.3711	0.1388	0.0604	0.1719
40	0.0114	0.0113	0.0001	0.0000	0.3613	0.1698	0.0357	0.1558
20	0.0116	0.0116	0.0000	0.0000	0.3625	0.2019	0.0112	0.1494
0	0.0120	0.0120	0.0000	0.0000	0.3597	0.3489	0.0000	0.0108
				U_{gs} = 8.5 m/s				
100	0.0142	0.0135	0.0007	0.0000	0.3606	0.0804	0.1548	0.1254
80	0.0142	0.0138	0.0004	0.0000	0.3548	0.1078	0.1098	0.1372
60	0.0142	0.0140	0.0002	0.0000	0.3530	0.1313	0.0649	0.1568
40	0.0142	0.0141	0.0001	0.0000	0.3608	0.1509	0.0374	0.1725
20	0.0143	0.0143	0.0000	0.0000	0.3522	0.1941	0.0150	0.1431
0	0.0144	0.0144	0.0000	0.0000	0.3528	0.2548	0.0000	0.0980
				U_{gs} = 9.6 m/s				
100	0.0172	0.0159	0.0013	0.0000	0.3588	0.0725	0.1648	0.1215
80	0.0170	0.0165	0.0005	0.0000	0.3622	0.0921	0.1348	0.1353
60	0.0171	0.0168	0.0003	0.0000	0.3602	0.1235	0.0799	0.1568
40	0.0172	0.0170	0.0002	0.0000	0.3585	0.1568	0.0449	0.1568
20	0.0172	0.0171	0.0001	0.0000	0.3626	0.1882	0.0214	0.1530
0	0.0172	0.0172	0.0000	0.0000	0.3669	0.2687	0.0000	0.0982

Table E.14: Flow split with automatic level control on down leg, U_{ls} = 0.51 m/s

Run valve setting (% open)	Gas mass flow in stream (kg/s)				Liquid mass flow in stream (kg/s)			
	Inlet (1)	Up (3)	Run (4)	Down (5)	Inlet (1)	Up (3)	Run (4)	Down (5)
				U_{gs} = 3.3 m/s				
100	0.0052	0.0050	0.0002	0.0000	0.4567	0.1582	0.1323	0.1662
80	0.0052	0.0051	0.0001	0.0000	0.4628	0.1666	0.0884	0.2078
60	0.0053	0.0052	0.0001	0.0000	0.4583	0.1882	0.0466	0.2235
40	0.0054	0.0053	0.0001	0.0000	0.4684	0.2137	0.0254	0.2293
20	0.0054	0.0054	0.0000	0.0000	0.4697	0.2568	0.0110	0.2019
0	0.0053	0.0053	0.0000	0.0000	0.4567	0.3293	0.0000	0.1274
				U_{gs} = 5.1 m/s				
100	0.0082	0.0079	0.0003	0.0000	0.4542	0.1519	0.1423	0.1600
80	0.0084	0.0082	0.0002	0.0000	0.4560	0.1678	0.1063	0.1819
60	0.0084	0.0084	0.0000	0.0000	0.4603	0.1980	0.0584	0.2039
40	0.0085	0.0085	0.0000	0.0000	0.4647	0.2215	0.0354	0.2078
20	0.0084	0.0084	0.0000	0.0000	0.4707	0.2901	0.0140	0.1666
0	0.0082	0.0082	0.0000	0.0000	0.4567	0.3440	0.0000	0.1127
				U_{gs} = 7.0 m/s				
100	0.0112	0.0108	0.0004	0.0000	0.4580	0.1572	0.1508	0.1500
80	0.0115	0.0112	0.0003	0.0000	0.4651	0.1798	0.1148	0.1705
60	0.0116	0.0115	0.0001	0.0000	0.4646	0.2097	0.0734	0.1815
40	0.0116	0.0116	0.0000	0.0000	0.4671	0.2431	0.0437	0.1803
20	0.0117	0.0117	0.0000	0.0000	0.4631	0.2783	0.0154	0.1694
0	0.0120	0.0120	0.0000	0.0000	0.4469	0.3626	0.0000	0.0843
				U_{gs} = 8.5 m/s				
100	0.0144	0.0138	0.0006	0.0000	0.4537	0.1437	0.1767	0.1333
80	0.0144	0.0141	0.0003	0.0000	0.4538	0.1733	0.1388	0.1417
60	0.0144	0.0143	0.0001	0.0000	0.4631	0.1999	0.0809	0.1823
40	0.0145	0.0144	0.0001	0.0000	0.4516	0.2352	0.0400	0.1764
20	0.0145	0.0145	0.0000	0.0000	0.4604	0.2803	0.0213	0.1588
0	0.0145	0.0145	0.0000	0.0000	0.4587	0.3881	0.0000	0.0706

APPENDIX F

T-Junction Transient Flow Traces

This Appendix contains the individual trace plots for the transient responses through the T-junction system. The nominal inlet phase superficial velocities are outlined in Table F.1.

Table F.1: Steady-state gas and liquid superficial velocities and associated flow regimes used in transient studies

Cycle	U_{gs} (m/s)	U_{ls} (m/s)	U_{gs} (m/s)	U_{ls} (m/s)	U_{gs} (m/s)	U_{ls} (m/s)	U_{gs} (m/s)	U_{ls} (m/s)
1	2.4	0.06	8.0	0.06	8.0	0.35	2.4	0.35
2	3.4	0.06	9.0	0.06	9.0	0.22	3.4	0.22
3	3.4	0.06	9.0	0.06	9.0	0.35	3.4	0.35
4	3.4	0.06	5.5	0.06	5.5	0.35	3.4	0.35
5	5.5	0.06	9.0	0.06	9.0	0.35	5.5	0.35
6	3.4	0.06	9.0	0.06	9.0	0.14	3.4	0.14
Regime	**Stratified**		**Stratified**		**Slug**		**Slug**	

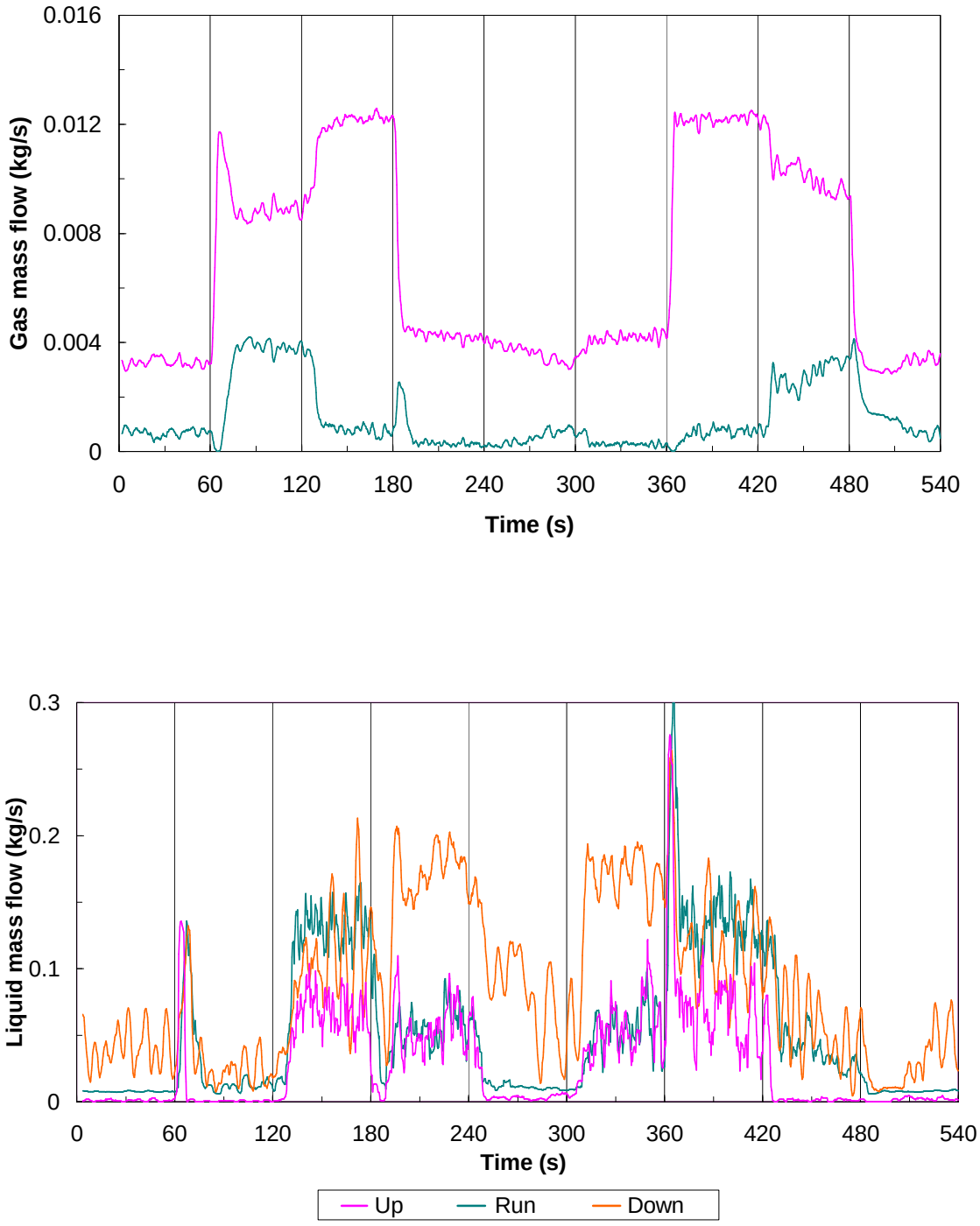

Figure F.1: Transient responses through the T-junctions for Cycle 1

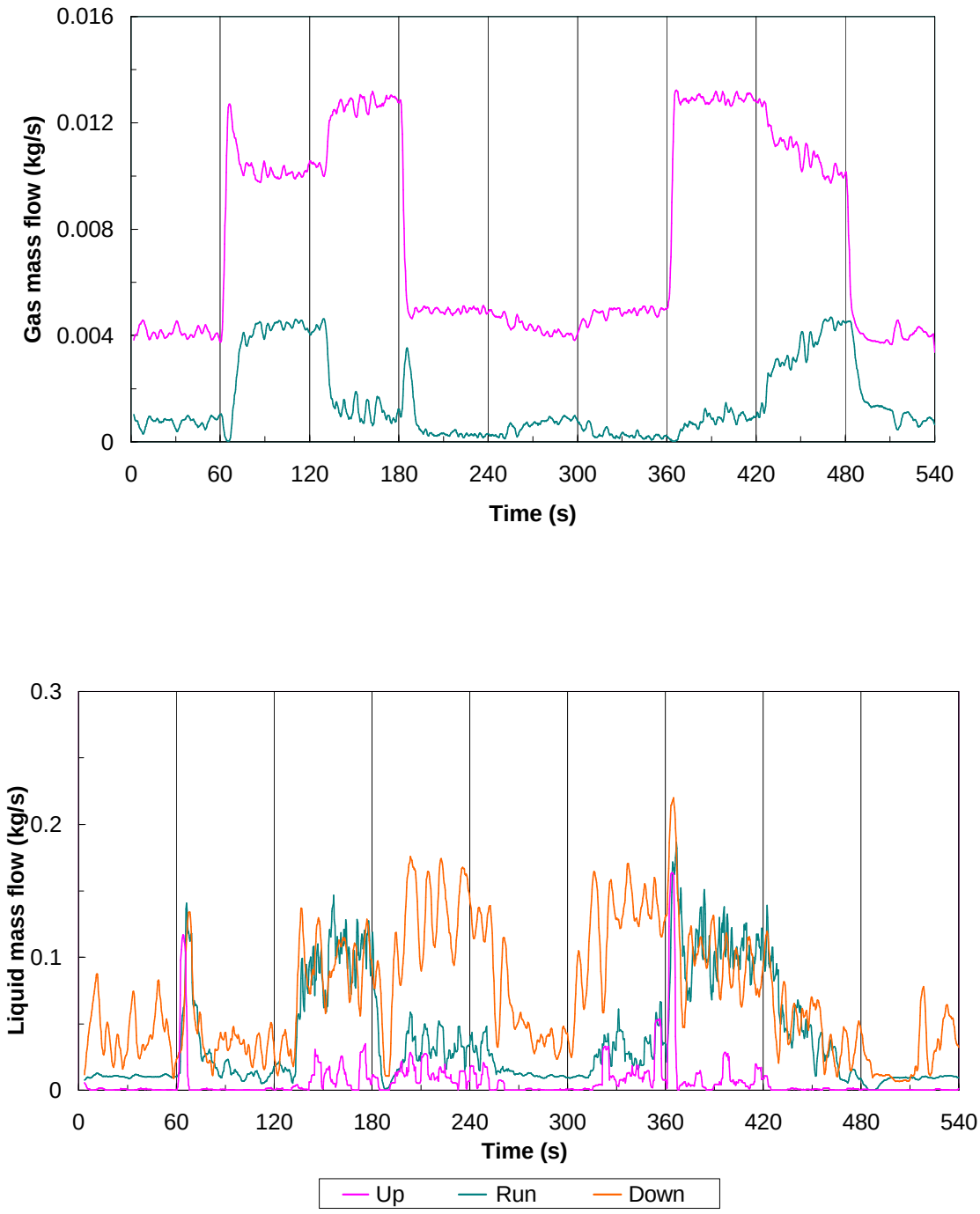

Figure F.2: Transient responses through the T-junctions for Cycle 2

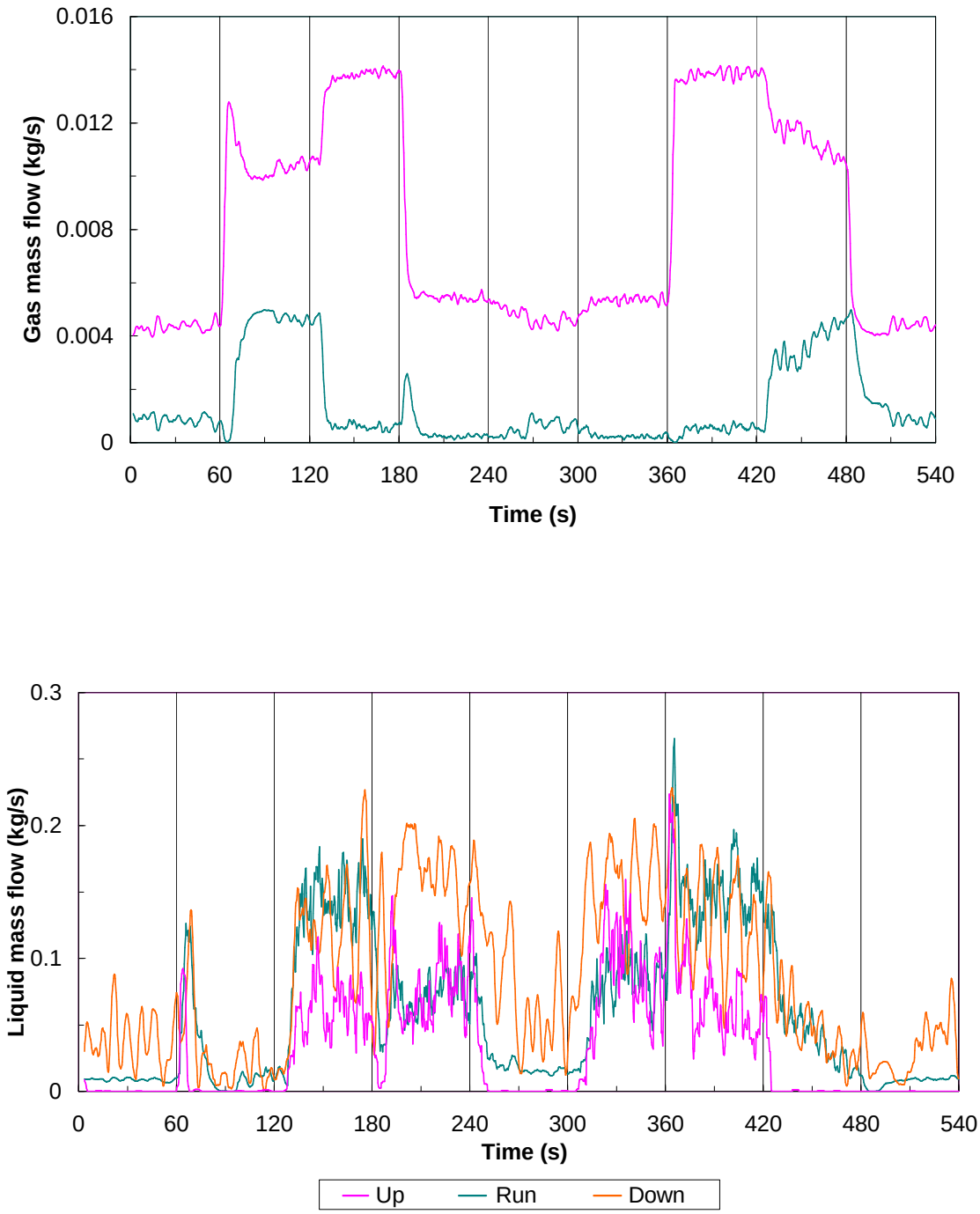

Figure F.3: Transient responses through the T-junctions for Cycle 3

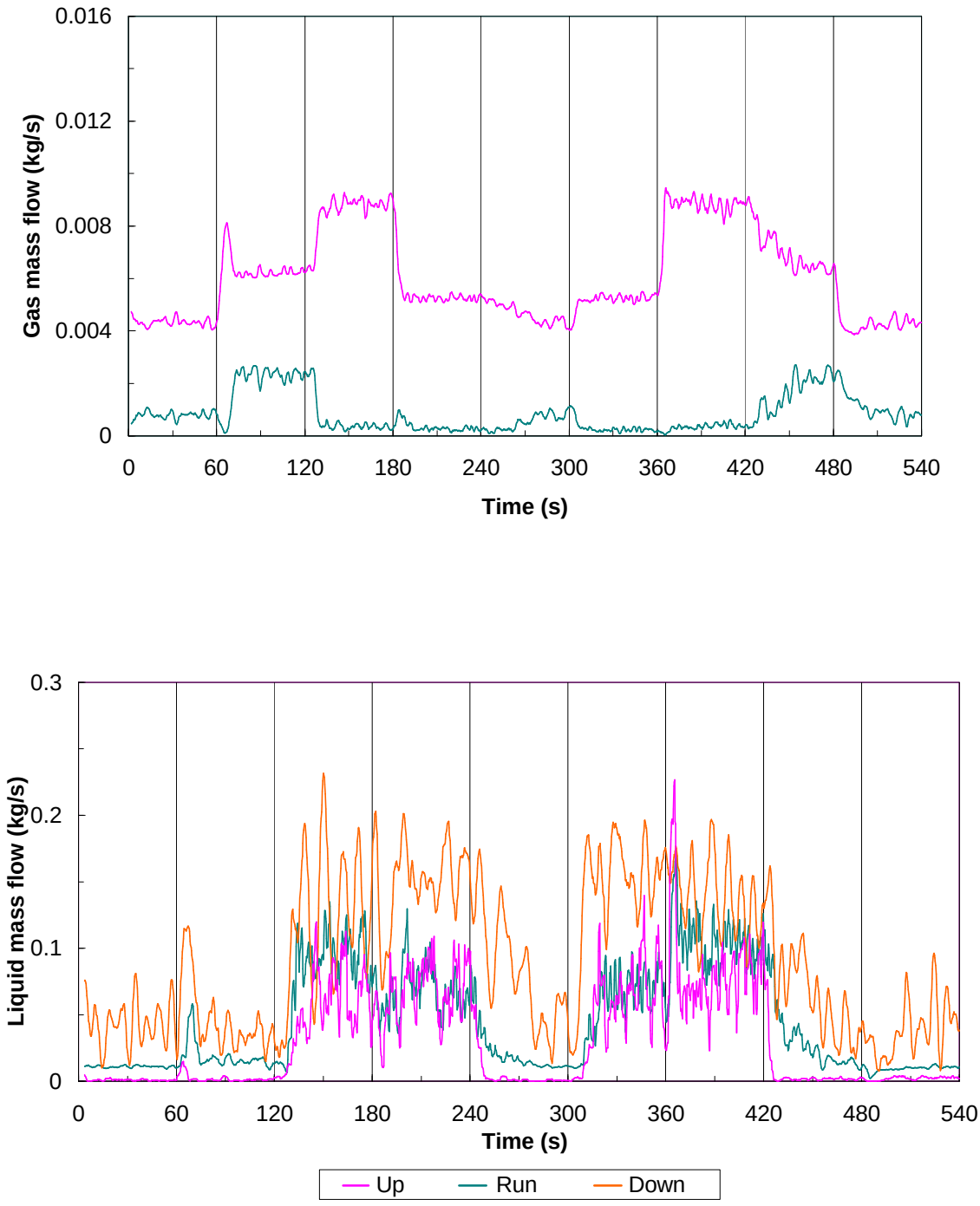

Figure F.4: Transient responses through the T-junctions for Cycle 4

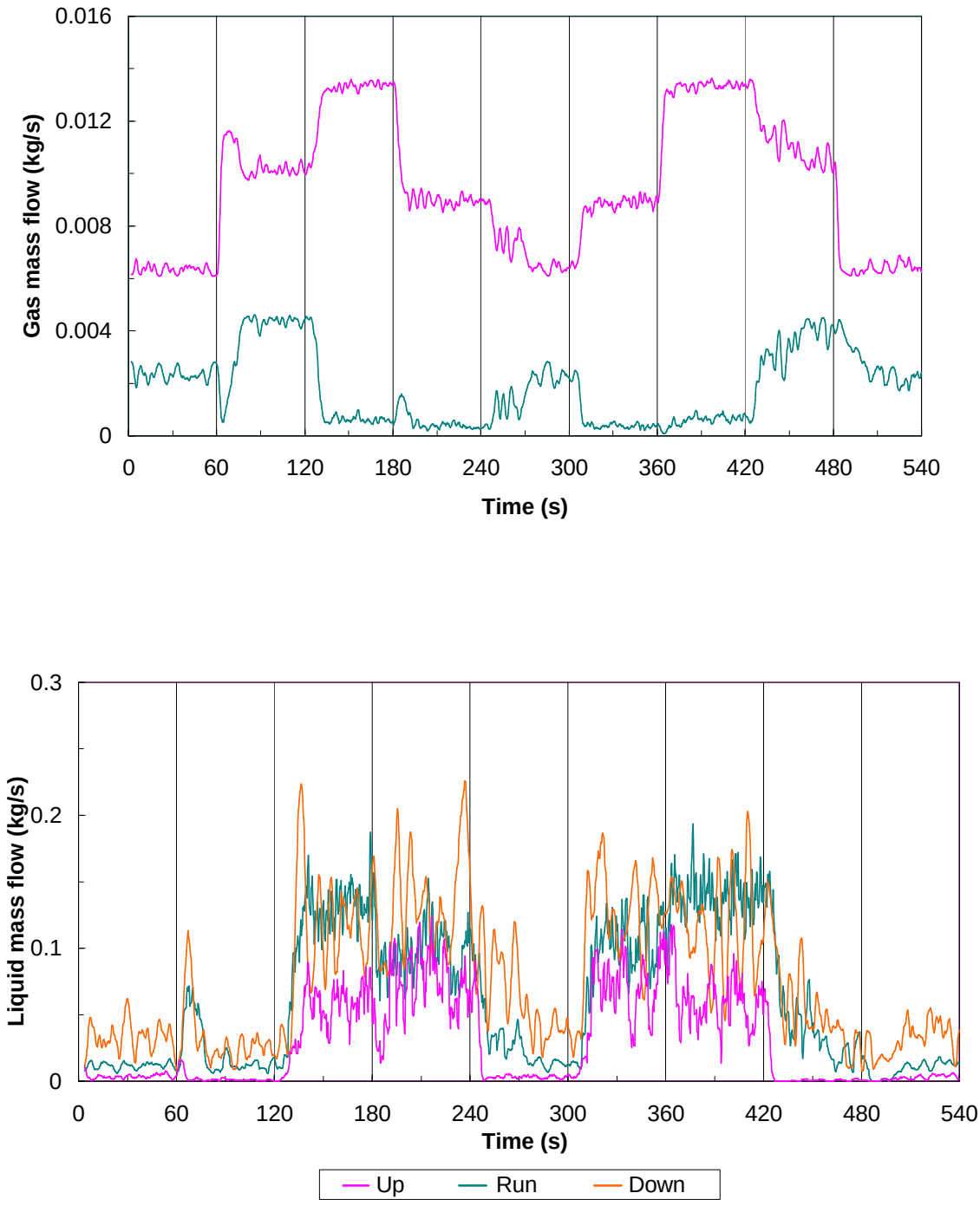

Figure F.5: Transient responses through the T-junctions for Cycle 5

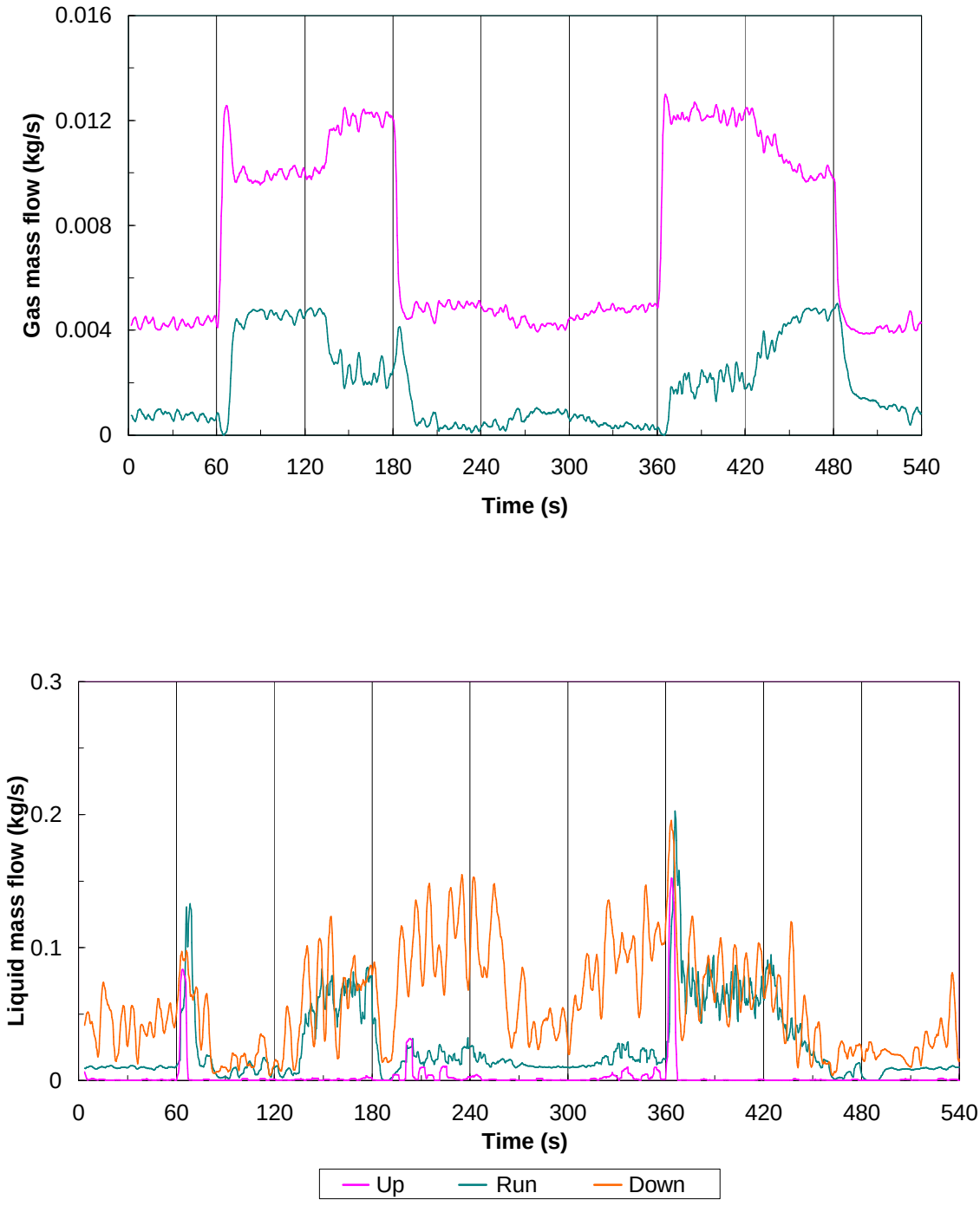

Figure F.6: Transient responses through the T-junctions for Cycle 6